Hochschule für Angewandte Wissenschaften Hamburg
Hamburg University of Applied Sciences

Bachelor Thesis

Department Automotive and Aeronautical Engineering

Balanced Field Length Calculation for a Learjet 35A/36A with Under-Wing Stores on a Wet Runway

Florian Ehrig

31. August 2012

Hochschule für Angewandte Wissenschaften Hamburg
Fakultät Technik und Informatik
Department Fahrzeugtechnik + Flugzeugbau
Berliner Tor 9
20099 Hamburg

In Cooperation with:

GFD Gesellschaft für Flugzieldarstellung mbH
An EADS Subsidiary
Flugplatz Hohn
24806 Hohn

Author: Florian Ehrig
Date of Examination: 31.08.2012

1st Examiner: Prof. Dr.-Ing. Dieter Scholz, MSME
2nd Examiner: Prof. Dr.-Ing. Hartmut Zingel

Industrial Supervising Tutor: Dipl.-Ing. Enrico Busse

Abstract

The Learjet 35A/36A is a twin-engine business jet. In a special configuration, it can be fitted with under-wing stores, a configuration for which no takeoff performance data on wet runways is currently available. This report outlines the creation of a numerical takeoff performance simulation for this specific aircraft on wet runways. The results shall be used to set up takeoff performance charts that can be used in daily flight operations.

To obtain Balanced Field Lengths and Decision Speeds according to EASA CS-25 certification specifications, the aircraft acceleration, takeoff and braking performance was determined. A comprehensive aircraft parameter estimation has been performed, permitting to consider the forces acting on the aircraft in various takeoff phases accurately in their dependency of time and speed.

A focus of the parameter investigation was put on the precipitation drag acting on the aircraft due to the wet runway conditions. A specific geometry-based investigation of the factors determining the amount of spray drag acting on the Learjet 35A/36A airframe with under-wing stores was performed. This permitted a conclusion on the additional drag due to water impingement on the aircraft in the special takeoff configuration.

The results of the simulation were set in relation with the existing aircraft performance data and a simplified calculation method. It was found that the simulation produces results of high accuracy and the results show consistent behavior with a variation in input parameters.

Hochschule für Angewandte Wissenschaften Hamburg
Hamburg University of Applied Sciences

DEPARTMENT FAHRZEUGTECHNIK UND FLUGZEUGBAU

Balanced Field Length Calculation for a Learjet 35A/36A with Under-Wing Stores on a Wet Runway

Task for a Bachelor Thesis according to University Regulations

Background

Eleven aircraft of type Learjet 35A and Learjet 36A are operated by the company GFD Gesellschaft für Flugzieldarstellung mbH based on the Military Airfield Hohn in the north of Germany. The GFD-owned aircraft can be operated as Special Mission Aircraft with stores mounted under each wing carrying external loads of up to 900 lbs (408 kg) on each side. Of interest is the calculation of the Takeoff Field Length (TOFL) of the GFD Learjets when operated with under-wing stores on a wet runway. The TOFL is the greater of the Balanced Field Length (BFL) and 115% of the All-Engines-Operative Takeoff Distance. The BFL is determined by the condition that the distance to continue a takeoff following a failure of an engine at a critical engine failure speed is equal to the distance required to abort it. It represents the worst case scenario, since a failure at a lower speed requires less distance to abort, whilst a failure at a higher speed requires less distance to continue the takeoff. V_1[1] during takeoff is the maximum speed at which the pilot is able to take the first action to stop the airplane (apply brakes) within the accelerate-stop distance and at the same time the minimum speed at which the takeoff can be continued to achieve the required height above the takeoff surface within the takeoff distance. The title of the project names specifically the BFL as it is usually the distance that determines the TOFL for aircraft with two engines.

[1] Critical Engine Failure Recognition Speed or Takeoff Decision Speed

Task

Set up a calculation / simulation based on the integration of the differential equation describing the aircraft motion under BFL conditions to output the BFL and V_1. The calculation should be done for a set of specified input data. The simulation should be compared to performance data from the Airplane Flight Manual (AFM).

Detailed tasks are:

- Literature review and description of operational hazards during takeoff on wet and contaminated runways.
- Collection of all required geometrical and performance data of the Learjet 35A/36A.
- Detailed review of certification rules related to takeoff performance calculations.
- Derivation of equations required for the calculation / simulation of the BFL.
- Literature review and extraction of key equations for the calculation of drag on a rolling aircraft caused by a wet or contaminated runway (in contrast to a dry runway).
- Investigation of further details for the performance calculation of the Learjet 35A/36A: Aircraft drag polar, drag due to spoilers, lift decrease due to spoilers, thrust decay with speed and air density, idle thrust, brake coefficients, braking capabilities, ...
- Set up, description, calibration and verification of the calculation / simulation.
- Calculation of BFL and V1 for a set of specified input data.
- Comparison of calculation results with simpler approaches (BFL from **Raymer 1989**; other TOFL estimation methods).

The report should be written in English based on German standards on report writing.

Declaration

I affirm that this report has been written entirely on my own, having used only the indicated references and tools. Where citations have been taken from other work than the present report, the source has been fully acknowledged and referenced.

Date Signature

Acknowledgements

I would like to express my sincere appreciation to all supervisors that have been accompanying me during the course of the project. Without the invaluable advice that only their experience and expertise could have provided, this work would not have been possible.

I am indebted to Prof. Dr.-Ing. Dieter Scholz, MSME, Dipl.-Ing. Enrico Busse and Dipl.-Ing. Svend Engemann for having given me the opportunity to elaborate my bachelor thesis on this exciting topic, and for their assistance and support provided in solving the challenges it involved.

My special gratitude goes to Mr. Enrico Busse, who took a lot of time to provide excellent advice, suggestions and help towards the creation of a sound report. His experience as certification engineer and Learjet pilot that he shared with me on numerous occasions has contributed greatly to my formation in becoming an aeronautical engineer.

Table of Contents

List of Figures

List of Tables

List of Symbols

a_0	Speed of sound in standard conditions(340.294 m/s)
a_n	Acceleration in z-axis of the aircraft during rotation
a	Acceleration
A_{eng}	Engine inlet area
A	Aspect ratio
$\Delta\alpha_0$	Zero lift angle of attack change due to flap deflection
$A_{tire,subm}$	Tire frontal area submerged in water
$A_{V,eff}$	Effective (aerodynamic) aspect ratio of the VTP
b	Wing span
b_V	VTP span
b_{eff}	Effective tire width
b_{fi}	Fuselage width at wing intersection
BPR	Bypass-Ratio of the engine
c_{out}	Outflow speed of the engine
c	Wing chord length
c_f	Flap segment chord length
c_t	Chord at Wing Tip
c_r	Chord at Wing Root
c_s	Chord of the Spoiler
C_D, c_D	Drag coefficient
$\Delta C_D, \Delta c_D$	Drag coefficient increment
C_L	Lift Coefficient Aircraft
c_L	Lift coefficient airfoil/section lift coefficient
C_L''	Lift coefficient per area
C_{L0}	Zero lift coefficient
$C_{L\alpha,W}$	Wing lift curve slope
$c_{L\alpha}$	Profile lift coefficient
$C_{L,H}\ i_h$	Lift contribution of the trimmed horizontal stabilizer
ΔC_L	Lift increment
$c_{L,\delta}$	VTP profile lift coefficient after rudder deflection
C_{Tci}	Specific engine temperature parameters
C_{fe}	Equivalent skin friction coefficient
D	Drag
D_F	Rim flange outer diameter
D_M	Mean overall tire diameter
d_{cont}	Contaminant depth
$d_{\%}$	Percental tire deflection,
d_i	Engine inlet diameter

E	Lift-to-Drag Ratio
E_{brake}	Brake Energy
e_{res}	Restitution Coefficient
e	Oswald factor
f	Correction/Adaption factor
F	Force
g	Gravity
G	Gas generator function
H	Pressure altitude in ft
h	Wing-to-ground distance
h_{SC}	Screen Height
h_{TR}	Transition Height
i_h	Incidence angle horizontal stabilizer
K'	Empirical correction factor for aerodynamic effectiveness
k_{angle}	Spray angle factor
K_{ff}	Lift interference factor
K_{store}	Store interference factor
K_Λ	Correction factor for VTP sweep
$\partial t/\partial H$	Temperature gradient with altitude
l	Length
M	Flight mach number
m	Mass
$\dot{m}$	Mass flow
N	Normal Force on Wheel Strut
n_{tire}	Number of tires
p	Barometric pressure
p_0	ISA standard ambient pressure
$r_{imp,\%}$	Ratio of total displaced water vs. water impinging on exposed area
R	Gas Constant
R_{LOF}	Radius of bow shaped rotation trajectory
S_G	Distance over ground
S	Geometrical reference area
SLR	Static Load Radius
T	Thrust
T_0	Static Thrust
t_0	ISA standard temperature
t_{true}	Temperature at test conditions
Δt_{ISA}	ISA temperature deviation
t_{wing}	Thickness of the wing
U	Ground lift coefficient estimate
u	Fluid particle velocity

v	Speed
V	V-Speed
V_N/V	Nozzle exit to inlet entry velocity ratio
$\dot{V}$	Volume flow
W_{tire}	Nominal tire width
W	Aircraft Weight

Greek Symbols

α_0	Profile zero angle of attack
$\alpha_{0,W}$	Zero Lift Angle, Wing
β	Reciprocal value of the Mach number correction
θ_{climb}	Initial liftoff climb angle
θ_{min}	Minimum second segment climb gradient
$\Delta\theta$	Difference of 2nd segment and initial climb gradient
θ	Temperature ratio
ρ_0	Air density at standard conditions (1,225 kg/m³)
ρ_{water}	Water density
ρ_{true}	Ambient air density
σ	Density Ratio
κ	Correction factor of the airfoil section lift curve slope
δ	Pressure ratio
δ_F	Flap deflection angle in radians
δ_{tire}	Deflection of the tire in m
δ_R	Rudder deflection
δ_S	Spoiler deflection angle
α_δ	Flap effectiveness parameter
ε_t	Wing twist angle tip to root in degrees, negative for washout
λ	Taper ratio of the wing
Λ_V	VTP Sweep
$\emptyset$	Ground effect factor
φ	Sweep angle Wing
μ	Runway surface friction coefficient
$\mu_{friction,brake}$	Braking friction coefficient
$\mu_{friction,dry}$	Dry rolling friction coefficient
$\mu_{friction,wet}$	Wet rolling friction coefficient
$\mu_{max,wet}$	Maximum Braking coefficient
γ	Runway Slope

Indices for Flight Phases

$(\ )_a$	Air distance
$(\ )_{acc}$	Acceleration
$(\ )_{ASD}$	Accelerate-Stop Distance
$(\ )_{climb}$	Climb
$(\ )_{cruise}$	in cruise condition
$(\ )_{LOF}$	At liftoff
$(\ )_{sc}$	Screen
$(\ )_{T/O}$	Takeoff
$(\ )_{TR}$	Transition
$(\ )_{TOD}$	Takeoff Distance

Indices for Aircraft Components

$(\ )_{DF}$	Dorsal Fin
$(\ )_E$	Engine
$(\ )_{EWM}$	Engine windmilling
$(\ )_{fuselage}$	Effect due to fuselage
$(\ )_{flap}$	Flap
$(\ )_{gear}$	Gear
$(\ )_H$	Horizontal stabilizer
$(\ )_S$	Spoiler influence
$(\ )_{skin}$	Skin
$(\ )_{spoiler}$	Spoiler
$(\ )_{store}$	Under-wing store
$(\ )_{TipTank}$	Tip Tank
$(\ )_V$	Vertical stabilizer/VTP
$(\ )_{VF}$	Ventral Fin
$(\ )_W$	Wing
$(\ )_{nose}$	Nose wheel, Nose wheel tire
$(\ )_N$	Nacelle
$(\ )_{main}$	Main wheel, Main wheel tire

Other Indices

$(\ )_{AEO}$	All Engines Operating
$(\ )_{AV}$	Average
$(\ )_{ASYM}$	Asymmetrical

$(\ )_{aquaplaning}$	Aquaplaning
$(\ )_{CL}$	Climb
$(\ )_{c}$	Compressibility influence
$(\ )_{corr}$	Correction
$(\ )_{CAS}$	Calibrated airspeed
$(\ )_{^\circ C}$	In degrees Celsius
$(\ )_{displ}$	Displacement
$(\ )_{dynamic}$	Dynamic
$(\ )_{ex}$	Excess
$(\ )_{exp}$	Exposed
$(\ )_{f}$	Friction
$(\ )_{GJE}$	Data from **GJE EXTGFD-003**
$(\ )_{G}$	Ground influence
$(\ )_{h}$	Horizontal
$(\ )_{IAS}$	Indicated Airspeed
$(\ )_{i}$	Induced
$(\ )_{imp}$	Impingement
$(\ )_{IDLE}$	Idle thrust
$(\ )_{K}$	In Kelvin
$(\ )_{Lecture}$	From academic reference
$(\ )_{load}$	Load factor
$(\ )_{max}$	Maximum
$(\ )_{min}$	Minimum
$(\ )_{MCG}$	Minimum Control Ground
$(\ )_{MCA}$	Minimum Control Air
$(\ )_{MBE}$	Maximum Brake Energy
$(\ )_{OEI}$	One Engine Inoperative
$(\ )_{P}$	Profile
$(\ )_{reflection}$	Reflection
$(\ )_{Rd}$	Rudder
$(\ )_{R}$	Rotation
$(\ )_{s}$	Stall
$(\ )_{semi}$	Half of the total value
$(\ )_{stop}$	stopping
$(\ )_{TAS}$	True Airspeed
$(\ )_{thrust}$	Thrust factor
$(\ )_{TOGA}$	Full Thrust
$(\ )_{total}$	total
$(\ )_{wet}$	Wetted area
$(\ )_{X}$	In X-Direction of the aircraft

List of Abbreviations

AFM	Airplane Flight Manual
AFMS	Airplane Flight Manual Supplement
AMC	Acceptable Mean of Compliance
AOA	Angle of Attack
ASD	Accelerate-Stop Distance
ASDA	Accelerate-Stop Distance Available
BFL	Balanced Field Length
BPR	Bypass Ratio
CAS	Calibrated Airspeed
CFD	Computational Fluid Dynamics
CG	Center of Gravity
EAS	Equivalent Airspeed
EPR	Engine Pressure Ratio
GFD	Gesellschaft für Flugzieldarstellung
IAS	Indicated Airspeed
ISA	International Standard Atmosphere
ITT	Interstage Turbine Temperature
KCAS	Knots Calibrated Airspeed
KIAS	Knots Indicated Airspeed
MAC	Mean Aerodynamic Chord
MSL	Mean Sea Level
NPA	Notice of Proposed Amendments
NPRM	Notices of Proposed Rule Making
OAT	Outside Air Temperature
PA	Pressure Altitude
PIC	Pilot in Command
PNF	Pilot Non Flying
QNH	Barometric Pressure Adjusted to Sea Level
RPM	Revolutions per Minute
RWY	Runway
SL	Sea Level
TAS	True Airspeed
TOD	Takeoff Distance
TODA	Takeoff Distance Available
TOFL	Takeoff Field Length
TOR	Takeoff Run
TORA	Takeoff Run Available
TOW	Takeoff Weight
VTP	Vertical Tailplane
ZFW	Zero Fuel Weight

1 Introduction

1.1 Motivation

The background of this project lies in the current certification status of the GFD fleet of Learjet 35A/36A. Flight operation in the special configuration with under-wing stores installed is currently only permitted for *dry runway conditions*.

In order to operate the aircraft with installed stores also in wet runway conditions, an addendum is required that extends the operational envelope for takeoff on *wet runways* with under-wing stores installed on the GFD fleet of Learjet 35A/36A. This report outlines the set-up of a numerical takeoff performance simulation for this configuration. Because the results of this report may be the basis of performance charts used in the daily flight operations, a focus has been put on the very accurate determination and modeling of aircraft parameters and certification requirements. This is also why a tendency to conservative approaches has been chosen in cases where assumptions had to be taken.

No operational experience is available to give an indication on the order of magnitude of additional spray impingement drag due to under-wing stores installation. Therefore, this effect has been a special area of investigation, since the certification requirements for wet and/or contaminated runways require the spray impingement drag to be considered, though without providing specific equations to determine this fraction of the total precipitation drag.

1.2 Definitions

Takeoff Distance (TOD)
According to **CS-25.113**, the Takeoff Distance (TOD) is the distance required for the aircraft to reach an obstacle height above the runway surface measured from the brake release point. The obstacle height to be cleared is 35 ft on a dry runway and 15 ft on a wet runway. The distinction between the All Engines Operative (AEO) and the One Engine Inoperative (OEI) takeoff configuration is made. The configuration leading to the more conservative result becomes limiting.

Accelerate-Stop Distance (ASD)
In case of an aborted takeoff, **CS-25.109** defines the Accelerate-Stop Distance (ASD) as the overall ground distance that includes both the acceleration up to the speed at which the decision to abort the takeoff is made and the braking distance required to bring the aircraft to a complete stop from this speed. Safety margins and pilot reaction times need to be considered.

Liftoff Distance
The Liftoff Distance is defined as the distance covered from the brake release point to the point at which the aircraft first becomes airborne. The speed at which this distance is covered is referred to as the Liftoff Speed, V_{LOF}.

Balanced Field Length (BFL)
The Balanced Field Length (BFL) is the distance resulting from a critical engine failure at the unique speed that leads to equal distances to either continue or abort the takeoff from this speed. The TOD and the ASD are equal at the Balanced Field Length. The Balanced Field Length therefore represents one possible limitation on the minimum runway length that needs to be available for the aircraft taking off.

Decision Speed V_1
The Decision Speed is the maximum speed to abort the takeoff and the minimum speed to continue the takeoff when the runway length available equals the Balanced Field Length. It therefore marks the critical engine failure recognition speed at which the any of the two decisions to either continue or abort the takeoff would lead to the same overall distance, the Balanced Field Length.

Takeoff Field Length
The TOFL is the greater of the Balanced Field Length and 115% of the All-Engines-Operative Takeoff Distance and determines the minimum field length that needs to be available for takeoff.

Wet Runway
According to **EU-OPS 1.480**, a runway is to be considered wet, when the runway surface is covered with precipitation of a depth of up to 3 mm, or when it is covered with precipitation such that it causes the surface to appear reflective, without significant areas of standing water.

Contaminated Runway
According to **EU-OPS 1.480**, a runway is to be considered contaminated when more than 25% of the runway surface area within the required length is covered by precipitation of a depth equivalent to 3 mm or more in water depth.

Indicated Airspeed (IAS)
The Indicated Airspeed is the speed value shown on the flight deck by the airspeed indicator. It may be calibrated for aircraft specific errors to yield the calibrated airspeed (CAS).

Calibrated Airspeed (CAS)
The Calibrated Airspeed is the Indicated Airspeed corrected for the aircraft specific errors. Without compressibility effects at high speeds, it is equal to the Equivalent Airspeed (EAS).

Equivalent Airspeed (EAS)
The Equivalent Airspeed is the speed at which the aircraft would have to fly at ISA, MSL conditions when the dynamic pressure experienced by the aircraft in the actual flight conditions was to equal the dynamic pressure at ISA, MSL.

True Airspeed (TAS)
The True Airspeed is the speed of the aircraft with respect to the surrounding mass of air. Without wind influence, the True Airspeed equals the ground speed.

Critical Engine
According to **CS-25** definitions, the critical engine is the one whose failure would most adversely affect the performance or handling qualities of an aircraft.

Bypass Ratio (BPR)
The Bypass Ratio is the ratio of the mass flow through the fan of a turbofan engine as compared to the mass flow through the core of the engine.

Flat Rating
The term Flat Rating refers to the fact that the maximum deliverable thrust of an engine is limited to a static maximum thrust rate for operation below a specific outside air temperature. Hence, the engine thrust does not vary with temperature at outside air temperatures below the *flat rate temperature*.

Precipitation Drag
Precipitation drag according to the **EASA AMC-25.1591** refers to the drag force experienced by an aircraft in wet or contaminated runway conditions. It consists of the *displacement drag* of the tires through a water pool, the *skin friction drag* of water particles along the fuselage and the *spray impingement drag* of water particles colliding with the exposed surfaces of the aircraft.

1.3 Project Objectives

In terms of project objectives, there were three major fields of interest that are covered in this report.

The *first objective* was to conduct a comprehensive investigation and determination of all relevant aircraft parameters necessary for a detailed basic modeling of the aircraft. Only limited aircraft performance data has been available, which is why the parameter determination was done in a general approach applicable to any type of airplane. An overview on the parameters required and applied either by certification or physical exigencies has been part of the analysis. This permits to compare with other possible approaches the approach and assumptions chosen for the performance simulation.

The *second objective* was to elaborate a simulation concept in a numerical computing environment that permits to accurately model the aircraft performance during the takeoff with regard to time- and speed dependant parameter variation. The numerical simulation method is expected to offer a precision benefit over simplified approaches based on averaged parameters. The numerical simulation shall be capable to deliver reliable charts for Balanced Field Length and the Decision Speed V_1 for a range of different airport environmental parameters.

The *third objective* the report discusses is an analytical consideration of the spray impingement drag exerted on the aircraft fuselage by precipitation on the runway. Focus of this investigation was put on the large under-wing stores. The findings made and the approach chosen can be of interest for other aircraft calculations.

1.4 Main Literature

Main assumptions and parameters for the report were taken from three major fields of reference data.

Since the results of the takeoff performance calculations shall be the baseline for actual aircraft operations, one focus was put on the certification requirements governing takeoff performance determination. The **CS-25** and passages from **EU-OPS 1** have been the basis for the analysis, complemented by **Acceptable Means of Compliance (AMC)** applicable to certain aspects of the discussed problems. This permitted to set up a basic simulation infrastructure that could be fed with specific performance characteristics of the Learjet 35A/36A.

As only limited performance data of the Learjet 35A/36A in the specific operator's configuration is available, **analytical approaches** to determine aircraft performance parameters based on geometry and other data available on the aircraft had to be investigated. Renowned literature from preliminary aircraft design was best suited for application in this purpose. Main sources are the "Synthesis of Subsonic Airplane Design" by E. Torenbeek, as well as the volume "Airplane Design" by J. Roskam. Furthermore, "Aircraft Design – A conceptual approach" from D. P. Raymer was used mainly to obtain estimates from simple equations as a means to validate the results obtained acc. to Roskam and Torenbeek. Also, "Fluid Dynamic Drag" by S. F. Hoerner was a valuable source used for parts of the drag coefficient estimation.

Wet runway operations are one of the most dangerous operation scenarios for an aircraft. Therefore, the effects of the wet runway conditions for the takeoff performance determination were considered thoroughly. In addition to the **certification documents**, a number of **research papers** investigating precipitation drag on a wet runway have therefore been analyzed. Most notable in this respect is the work of NASA on "Measurements of Flow Rate and Trajectory of Aircraft Tire-Generated Water Spray" as well as the ESDU document "Estimation of spray patterns generated from the sides of aircraft tyres running in water or slush". NLR investigations of the latter documents in a CFD spray simulation and a comparison with flight tested data has also proved to be of value for the analysis.

Also, three sources of aircraft performance data were used as a reference – the original **AFM** of the Learjet 35A/36A, the **AFMS 9702-2** Airplane Flight Manual Supplement as well as the **GJE EXTGFD-003** report.

The **GJE EXTGFD-003** report is the report that was used to create certified performance data for the aircraft with stores on a dry runway. It therefore serves as a good validation source for the parameters determined on academic approaches.

The greatest challenge due to the complexity of the investigations was to select the approach out of the many approaches proposed by the literature that was finally used in the performance simulation for this report. The report therefore also serves to compare different approaches from the literature, if applicable.

1.5 Structure of the Report

The report is structured in eight main chapters that are arranged in a consecutive order.

Chapter 2 serves the reader to enter the topic of wet runway takeoff performance calculations. It is outlined which main factors have to be considered for the takeoff performance determination specifically on wet runways, but also operational considerations are discussed.

Chapter 3 outlines the certification requirements and regulations that have been driving the performance simulation development. The theory behind the various distance, reaction time and speed definitions to be applied according to the certification documents is presented, which is building the baseline for the subsequent calculations.

Chapter 4 contains all numerical relationships necessary to set up a numerical takeoff performance simulation. It has been structured in a way that facilitates the distinction of the various phases during the takeoff, in order for the reader to be able to trace the specific set of parameters that is employed in each of these phases. Numerical equations and estimation approaches are presented in this chapter, without referring to any specific aircraft. This permits to neutrally describe model parameters without being influenced by specific characteristics, and can therefore serve as the point of reference for the specific parameter discussion for the Learjet 35A/36A performed in Chapter 6.

Chapter 5 outlines the investigation of additional drag force components due to the impingement of water droplets on the aircraft surface performed for the Learjet 35A/36A. This chapter takes into account a number of different research documents in order to analytically determine the amount of drag caused by the specific Learjet 35A/36A geometry.

Chapter 6 is the point of convergence of all aircraft related parameter estimations developed in Chapter 4 and shows the approaches selected from the literature in their application on the specific aircraft.

Chapter 7 presents the numerical takeoff performance simulation and gives an overview on the functional architecture as well as the calibration concept employed. The simulation integrates all relations outlined in the previous chapters of this report into a single program that autonomously performs the takeoff performance simulation. The results obtained by this simulation are then validated, compared and analyzed in chapters 8, 9 and 10.

Chapter 8 therefore presents the simulation results obtained from the calculations. This includes a comparison of the results to known data and a simpler calculation method.

Chapter 9 is then used to outline possible error sources and influences on the takeoff performance simulation. For that reason, a parameter variation analysis is presented that aims at validating the behavior of the simulation with a change in the input parameters.

Chapters 10 and 11 bring the report to a conclusion with concluding remarks on the calculation and parameter estimation approach as well as recommendations for possible further improvements of the takeoff performance simulation.

Detailed analysis or validation that would leave the common thread of a chapter or section is included in the Appendix of this report.

2 Operational Hazards

2.1 Hazards from Wind, Rain, Snow and Ice

The takeoff phase is one of the most challenging and dangerous phases in the complete flight. Many factors influence the safe conduct of a takeoff sequence. The presence of environmental factors such as wind, rain, snow and ice is crucially impacting the performance of the aircraft as compared to operation on a dry standard day.

Effect of Wind

The effect of *wind* on the performance determination is important to consider, as it can have a different effect on the aircraft depending on its direction. The most favorable condition possible is the wind coming from the direction in which the aircraft is about to take off. This *headwind component* will *reduce the takeoff distance* because the aircraft lifts off at a relative air speed. A headwind component therefore requires less energy and acceleration distance since a portion of the required liftoff speed is already imparted on the aircraft due to wind. In contrast to this, an adverse effect will be seen when the wind comes from behind the aircraft due to a reversal of the effect described above.

When the wind comes from a side angle (referred to as cross wind) to the runway, this will affect the directional stability of the aircraft (especially in slick runway conditions) due to the fact that a side force is acting on the aircraft as a whole, and a moment around the z axis is induced through the rudder area which represents an disproportionally big partial area of the fuselage side view. This represents a hazard because of the risk to slide sideways off the runway as well as through a yaw moment present as soon as ground contact is lost which leads to a bank angle and might result in wing tip contact to the ground or destabilized takeoff. Therefore, a maximum cross as well as tail wind speed needs to be predetermined.

Effect of Precipitation

Rain, snow and ice are having physical implications on the *airplane* itself as well as on the *runway surface conditions*. The role of precipitation as runway contaminants is of high importance for the takeoff distance and decision speed determination and is considered specifically in the upcoming sections. Snow and ice in this respect should be seen as to have the same effect as rain, except for the greater magnitude of their impact. Icing on wings, engine nacelles and control surfaces though is an effect does not occur in rain but poses a very considerable threat that needs to be taken into account. Also, the damage to the aircraft due to small stones contained in sputtered water or ice parts raised by the wheels being dashed against the fuselage poses a further hazard to the aircraft (**NLR-TP-2001-216**).

Even though jet engines are designed to ingest a certain amount of water while continuing to operate normally, deteriorated and high intensity ground water spray is not beneficial for the safe operation (risk of compressor stall, engine flame-out, and foreign object damage/FOD). Therefore, the precipitation spray may not directly be pointed towards the engine intake (**EASA AMC E 790**). Aircraft manufactures therefore foresee provisions to prevent the precipitation spray from being directed at sensitive areas. This consideration will be of importance in the later determination of the actual spray geometry of the Learjet 35A/36A.

Another factor to consider is the reduced visibility in adverse weather conditions, possibly increased by waft-back water or snow particles due to thrust reversing (**NLR-TP-2001-204**).

2.2 Definitions for Wet and Contaminated Runways

The calculations performed by means of the methods described in this report shall be done for *wet runway* conditions. This term needs to be differentiated from the term *contaminated runway* conditions.

The margin for standing water depth on the runway for the classification as a wet runway is 3 mm, beyond which the runway is to be considered contaminated. It is to be always considered contaminated when covered with snow, slush or ice.

EU-OPS 1.480

> *A runway is considered wet when the runway surface is covered with water or equivalent, [with a depth less than or equal to 3 mm], or when there is a sufficient moisture on the runway surface to cause it to appear reflective, but without significant areas of standing water."*
>
> (…)
>
> *A runway is considered to be contaminated when more than 25% of the runway surface area (whether in isolated areas or not) within the required length and width being used, is covered by –*
>
> *(a) surface water more than 1/8th inch (3mm) deep*
> (…)

According to **EU-OPS 1.475** (d), a wet runway may, as long as it refers to a concrete/asphalt covered runway, also be considered as dry in terms of performance parameters. However, a damp runway is closer to a wet runway in terms of braking action, which therefore must specifically be addressed in a wet runway condition. However, no precipitation effects other than the braking coefficient degradation are determined in the Certification Specification **CS-25.109**.

Normative literature or regulations such as **EASA AMC 25.1591** exists specifically for contaminated runway conditions. The latter does include specific equations that can be used in order to approximate specific physical precipitation effects upon the airplane. They will be discussed in detail in the performance parameters discussion.

2.3 Wet Runway Effects on Aircraft Performance

The performance on wet runways changes in some crucial factors for the operation of the aircraft. There are three major impacts on the aircraft performance that result from an operation on a wet runway:

- additional drag induced through the fluid-aircraft interaction
- reduced braking force due to significantly decreased braking coefficient
- Aquaplaning/Hydroplaning

These will be discussed in detail in the following sections.

2.3.1 Aquaplaning

According to **NASA-TN-D-2056**, aquaplaning occurs on smooth runways at a fluid depth of 2mm and more. For a wet runway with fluid depths of up to 3mm, it is therefore relevant to consider aquaplaning.

The aquaplaning speed is determined from **EASA AMC 25.1591** Section 7.1.1as

$$v_{aquaplaning} = 9\sqrt{p_{tire}} \quad \textbf{(1.1)}$$

With

p_{tire}	Tire pressure in lb/in²
$v_{aquaplaning}$	Aircraft aquaplaning ground speed in kts

Aquaplaning has three major effects that are of importance and have to be considered in the calculations.

Since the tire begins to float up, it subsequently loses contact to the runway surface (tarmac) and *directional control* through wheel to ground contact is *considerably reduced*.

This is of importance if the aircraft minimum control speed of the aircraft[2]on ground, V_{MCG}, is close to or even higher than the aquaplaning speed of the aircraft because then directional control of the aircraft is very limited.

Likewise, *braking forces*, applied in case of an aborted takeoff, are *reduced* due to the flotation of the tire.

A third factor of aquaplaning is the *reduction of drag due to aquaplaning*. As the tire starts to float, it displaces less water, which leads to a decrease in the displacement drag force. **EASA AMC 25.1591** provides an estimation for the effect of the drag reduction due to aquaplaning by application of an *aquaplaning factor*. As can be seen in figure 2.1, the aquaplaning factor decreases gradually beyond aquaplaning speed. It needs to be multiplied with the water induced drag forces in order to give a realistic estimation of the actual forces occurring beyond aquaplaning speed.

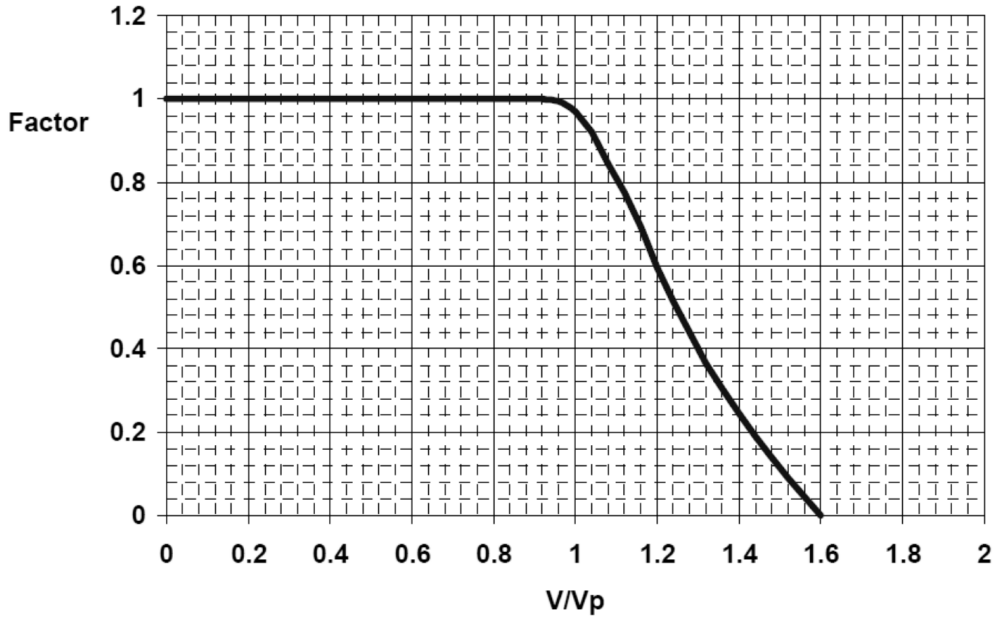

Fig. 2.1 Effect of Speed on Water Drag Coefficients (from **AMC 25.1591**)

According to Fig. 2.1, the aquaplaning factor can be approximated as follows:

For

$$1 < \frac{v}{v_P} < 1{,}6$$

$$f_{aquaplaning} = 1 - \left(\frac{1}{0{,}6}\right)\left(\frac{v}{v_{aquaplaning}} - 1\right) \qquad \textbf{(1.2)}$$

2 Minimum Control Speed is the calibrated airspeed, at which, when the critical engine is suddenly made inoperative, it is possible to maintain control of the airplane with that engine still inoperative, and maintain straight flight (**EASA CS-25.149**)

With

$f_{aquaplaning}$	Aquaplaning Factor
v	Aircraft Ground Speed
$v_{aquaplaning}$	Aircraft aquaplaning ground speed

2.3.2 Acceleration

The acceleration capability of the aircraft is impacted by the wet runway conditions by numerous factors. **NLR-TP-2001-204** and the **AMC 25.1591** outline 3 major precipitation drag components for Aircraft operation on wet runways which are also referred to as precipitation drag forces:

- Displacement Drag (Tires)
- Impingement/Collision Drag (direct collision on aircraft components)
- Skin Friction Drag

Also, the tire-to-ground rolling friction on a wet runway is impacted by the wet runway condition. The detailed equations for this component will be discussed in Section 4.1.9.

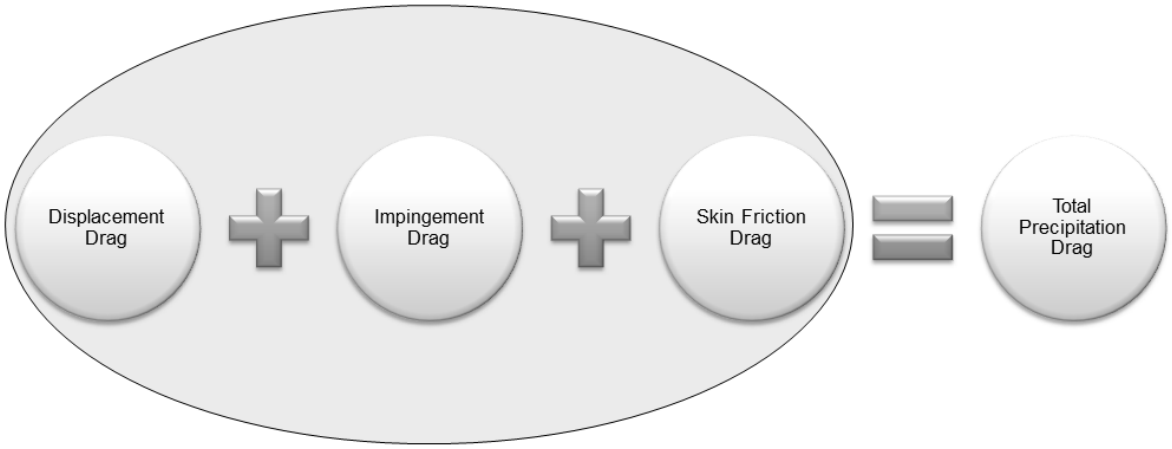

Fig. 2.2 Precipitation Drag Forces due to Contaminated Runway Conditions

All these force components impact the *acceleration capabilities* of the aircraft *negatively* and represent a drastic difference to a dry runway operation. According to **NLR-TP-2001-204**, they are also subject to piloting technique, because the pilot can reduce or increase the amount of drag by slight unloading/loading of the front wheel of the aircraft through elevator input during the ground roll. If applied correctly, this technique can reduce the precipitation drag during the acceleration, or increase the drag during the deceleration of the aircraft, as desired by the applicant.

Displacement Drag

The displacement drag is the drag force which results from the wheel contact to the runway surface. Below aquaplaning speed, the wheel is creating a “dry spot” at its runway-tire contact surface. Therefore, it has to displace the amount of water that was previously at this now dry spot which creates a drag force. The faster the tire moves, the more energy is incurred in the water bow wave that forms, until the surface tension of the water is overridden and a spray pattern emerges. This spray itself then creates new forms of precipitation drag which are spray collision (impingement) and skin friction drag.

Impingement Drag

As soon as the tire induced water wave emerges from the puddle, droplets may impinge on the aircraft components. Unfortunately, the **EASA AMC 25.1591** does not provide quantifiable information to determine the magnitude of this impingement drag force. Therefore, as part of the investigative objectives of this work, a special section is introduced to determine the actual amount of collision drag especially due to the installation of under-wing stores but also on other exposed surfaces of the airframe. The calculation of this retarding force requires to be considered in dependence of speed, due to the fact that the collision impulse magnitude of water droplets is speed-dependant. The drag reduction factor due to aquaplaning also needs to be considered.

Skin Friction Drag

The skin friction drag that is mainly caused by the water spray from the front wheel is conservatively considered through the simple equation provided in Section 7.1.3 b.2 of **EASA AMC 25.1591**. This equation determines a drag coefficient from the length of the wetted fuselage. The wetted fuselage is assumed to amount for 75% of the total length of the fuselage, since the top of the spray plume is expected to reach the fuselage behind the front wheel. The drag reduction factor due to aquaplaning needs to be considered.

Rolling Friction

The rolling friction on a wet runway is higher than the rolling friction on a dry runway. The determination of the friction force is requires the aircraft lift force as an input, because the weight of the aircraft and the lift force together determine the normal force acting on the wheels. This normal force then determines the retarding force component when multiplied with the rolling friction coefficient for a wet runway.

2.3.3 Deceleration

Deceleration is part of the takeoff performance calculation, because an aborted takeoff due to malfunction necessitates the aircraft to be brought to a halt on the runway. While the retarding forces described above will be maintained and assist the deceleration of the aircraft, a wet runway still has a negative impact on the deceleration capabilities of an aircraft. This is because the effect of higher drag forces is overridden by a major decrease in braking friction that results from an increased sleekness of the runway.

Braking coefficients for dry runways can best be obtained from flight test data. Clearly, the braking coefficient for a wet runway can never be higher than that for a dry runway.

This is confirmed by the relationship given in Fig. 2.3 which relates wet runway surface friction to the dry runway surface friction coefficient for grooved and smooth runway surfaces.

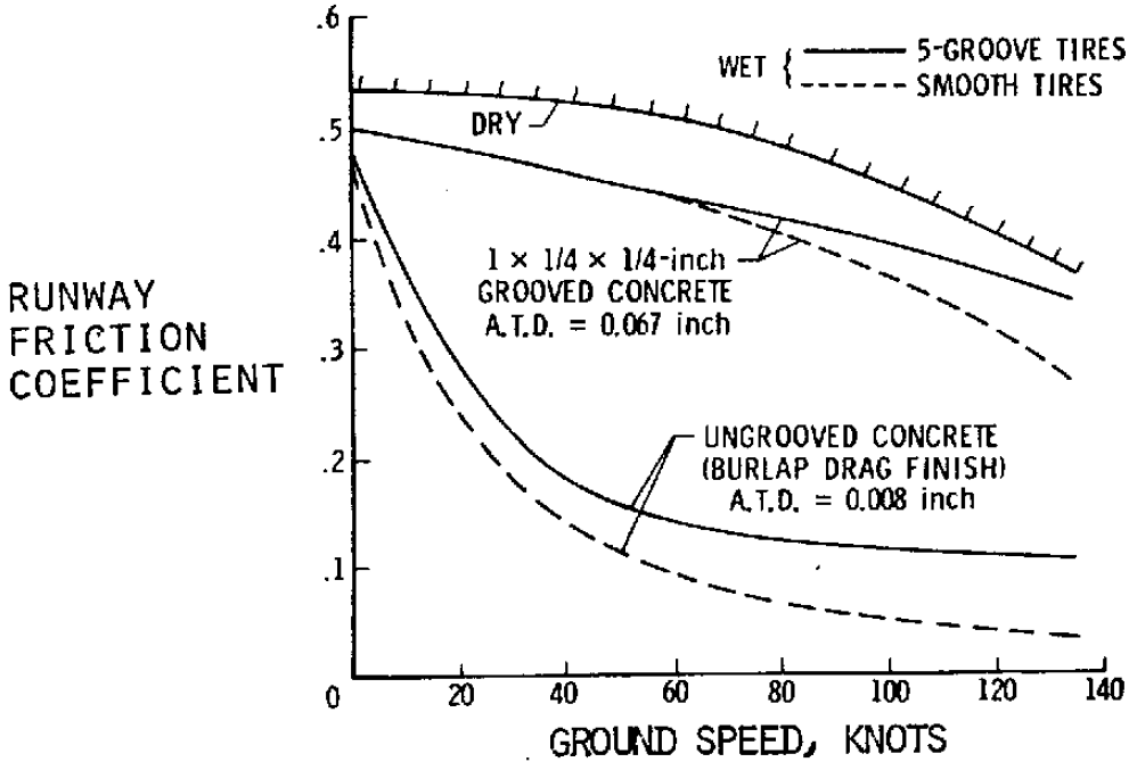

Fig. 2.3 Available Traction at Tire-Surface Interface (**NASA TM-X-72650**)

As can be seen clearly, the overall friction coefficient and hence the braking capability of the aircraft wet runway is roughly half that of the aircraft on a dry runway.

The reduced deceleration performance of the aircraft and the reduced acceleration performance of the aircraft combined result in higher Accelerate-Stop Distances for aborted takeoff runs. Since one major retardation device are the aircraft brakes, the speed at which a flight can safely be aborted and from which an aircraft can be brought to a complete stop on a runway of specific length will always be lower in wet condition as compared to dry conditions.

2.3.4 Directional Stability

The directional stability of the aircraft refers to its movement along the runway center line. Since the simulation as one of the project objectives outlined at the beginning of the report is being developed for a longitudinal motion, the directional stability determination is beyond the scope of this report. However, it is still an aspect influenced by the wet runway conditions, so it shall be briefly discussed.

The major force that is playing a role in terms of directional stability on wet runways is the sideways acting friction force of the tire. Similar to the linear motion friction, this force is being reduced by the adverse runway surface conditions. The aircraft can sustain less side force/momentum on slick surfaces, which is of relevance when the pilot is required to exert such a force in order to keep the aircraft on the runway center line during the takeoff run.

This effect is worsened by all factors that influence the momentum around the yaw-axis of the aircraft, such as the loss of an engine (differential thrust), side wind but also aileron deflection that might decrease the normal load on the critical tire and thus further reduce its sideway friction force. The effect is also worsened by uneven distribution of the surface contaminant, such as water or ice patches causing a braking action imbalance which may lead to the aircraft veering off the runway.

2.4 Responsibilities, Precautions and Airmanship

From a pilot's point of view, the variety of factors effecting aircraft performance and handling qualities plays a role in his overall flight condition assessment and the subsequent briefing. As part of the flight preparation, all of these factors need to be considered.

According to **EU-OPS 1.490** sections a) and b), the operator being the responsible pilot in command (PIC) has to consider the maximum takeoff mass and the takeoff distances/V_1 before taking off in his current configuration. The fact that these performance data are currently not available for the Learjet 35A/36A discussed in this report with under-wing stores installed in wet runway conditions motivates the investigations and calculations presented in this report.

When determining the maximum takeoff mass, the operator/pilot has to take account for headwind component, runway alignment distance, pressure altitude at aerodrome, ambient temperature at aerodrome, runway slope as well as runway surface type and condition. It is necessary for the flight crew to be prepared for a rejected takeoff during the takeoff roll, therefore the briefing needs to address specifically the rejected takeoff case and the speed up to which such an abort is still safe. The decision of whether to stop or to go is taken by the PIC, because this decision action has a significant impact on the flight safety. The PIC will therefore keep the hands on the thrust levers until the aircraft reaches the speed V_1, even when he is the pilot non-flying (PNF). If a malfunction or problem occurs during the takeoff roll, the captain will call out his decision to confirm whether the takeoff run will be continued or aborted[3].

Therefore, the appropriate performance charts representing the present conditions or a correction factor to be applied to values for standard conditions are to be used in the flight preparation. These are contained in the AFM or the AFMS. Because the aerodynamic qualities of the aircraft (influencing V_s, V_{MCG}, V_R, V_{MCA}, V_2) do not change for wet runway operations, none of the aerodynamically derived aircraft speeds changes. Only V_1 is impacted by the degraded runway conditions, as discussed in Section 2.3.3.

3 The procedures described here are the standard procedures acc. to**FAA AC 120-62**. They can, however, vary depending on the operator specific AFM procedures given for the respective flight crews.

3 Certification Regulations

3.1 Overview of Regulations for the Takeoff

As for any other part of aviation, many regulatory requirements and definitions have been made to describe the takeoff phase of the aircraft. Those that are relevant to the determination of the takeoff distance and the abort speed shall be outlined in this paragraph.

The jet aircraft takeoff performance is being addressed in the Part 25 of both the Federal Aviation Regulations (FAR) of the FAA (Federal Aviation Authority, USA) and in their equivalent, the Certification Specifications CS-25 (former JAR-25) issued by the EASA (European Aviation Safety Agency) in Europe. As the regulations of EASA and FAA contents are almost similar to each other, the EASA CS-25 shall be the reference for further argumentations used in this report.

Generally, the relevant CS-25 sections are specifying the details to be available to the operator in terms of *aircraft performance information*, the *takeoff speeds*, *takeoff trajectory*, as well as providing definitions for the limiting *takeoff distances* necessary in two cases.

The distinction is made between the *Accelerate-Go* (Takeoff) and the *Accelerate-Stop* (Aborted Takeoff) Case. The respective distances are the *Takeoff Distance* (TOD) and the *Accelerate-Stop Distance* (ASD). Both of these cases distinguish again between an attempted takeoff with *All Engines Operating* (AEO) and with *One Engine Inoperative* (OEI), the less favorable, longer distance in either condition becomes limiting. In addition, there is other regulatory material complementing the CS-25 for certain detailed aspects of the takeoff performance calculations.

The regulation Section **CS-25.105** specifies the general takeoff data that needs to be available to execute a takeoff. It requires that takeoff speeds, distances and the takeoff path be determined for a selected aircraft configuration and runway condition as a function of weight, altitude and ambient temperature. Subsequently, the definitions for these requirements are given in the relevant sections of CS-25 listed below.

The takeoff speeds are defined in section **CS-25.107**, listing the definitions for V_{EF}, the critical engine failure speed, V_1, V_{MU}, V_R, V_{LOF}, V_2 and V_{FTO}. All speeds except for V_{EF} and V_1 are determined from aerodynamic performance data of an aircraft.

When these aerodynamically derived speeds are already known for an aircraft configuration, the speed V_1 and its associated V_{EF} are therefore the only unknown parameters that need to be determined with the new environmental conditions and effects outlined in Chapter 2. This is the case for the calculation performed in this report for the Learjet 35A/36A, and the V_1 speed is derived from the Balanced Field Length Calculation discussed in Section 3.6.

The distance covered during an aborted takeoff is the Accelerate-Stop Distance (ASD), whose definition is regulated by Section **CS-25.109**. It is applied for the case that the decision to abort the takeoff run occurs before or at the takeoff decision speed V_1. Both the AEO and the OEI conditions are to be considered to determine the limiting condition. CS-25.109also specifies basic braking friction values for wet runways as a function of tire pressure. These values may be used if no more detailed test data for the specific aircraft are available.

The takeoff path is regulated in Section **CS-25.111** and specifies the procedure from the point at which the standing aircraft initiates the takeoff until transition to en-route configuration or a point 1500 feet above ground and considers the case of an engine failure at V_{EF}. It is of high relevance for the takeoff calculations performed in this report, as it specifies the takeoff path and procedure the aircraft needs to be able to follow when an engine failure occurs after V_1. It equally specifies minimum climb gradients during the takeoff path, which will play a role in the validation of the final calculation results at the end of this report.

Section **CS-25.113** defines the takeoff distance and the takeoff run. It differentiates the AEO and the OEI conditions. For the OEI condition, a takeoff with assumed engine failure in accordance to CS-25.111 needs to be considered. For the AEO condition, a safety factor of 1,15 needs to be applied to the takeoff distance. The higher resulting distance from both methods becomes limiting. Both conditions have been considered in this report.

Both takeoff and landing are the maneuvers associated with the highest risk during the flight. In the history of the FAR/CS-25, many amendments have therefore been made to the original certification requirements in order to account for lessons learned from previous incidents and to improve the overall safety of aviation. These Amendments are proposed through *JAA Notice for Proposed Amendments (NPA)* and/or *FAA Notices of Proposed Rule Making (NPRM)* and then introduced as FAR or CS Amendments. Of importance for this report is especially the **FAR Amendment 25-92** which includes the requirement to include specific considerations for wet runway conditions in the takeoff performance calculations. Notable for this report are also the **FAR Amendment 25-42** in combination with the **EASA AMC 25.101(h)(3)** with respect to the different pilot recognition and reaction times to be considered in the Accelerate-Stop Distance calculation.

In order to assist the practical application of the regulatory Certification Specifications (CS), the EASA also issues Acceptable Means of Compliance (AMC) documents. These AMC provide qualified technical interpretative material that may, but does not have to be used, in order to comply with certification requirements set by the CS. Acceptable Means of Compliance documents have therefore been used in this report. The most important document used is the **EASA AMC 25.1591**, which specifies equations and calculation approaches to assess the takeoff performance on contaminated runways.

Due to the nature of frequently updated regulations, it is of importance to make a judgment on the applicability of certain regulatory requirements when developing supplementary certifiable calculations or design for a specific aircraft. Due to a "grandfathering clause"[4] it can, but does not have to be the most current version of the regulatory requirements that is applicable to the existing aircraft.

3.2 Aircraft Speeds during Takeoff

For the aircraft, characteristic speeds are denominated with a capital V entailed by a subscript, they are referred to as V-Speeds. V-Speeds are provided to the operator in Indicated Air Speed (IAS) or Calibrated Air Speed (CAS), according to the speed displayed on his speed indicator. During the takeoff roll in normal, AEO conditions, there are four major V-Speeds that need to be considered for the performance calculation. These are the Takeoff Decision Speed V_1, the Rotation Speed V_R, the Liftoff Speed V_{LOF} and the safe climb speed V_2. In OEI conditions, the speed at which the engine fails, V_{EF}, is another very important parameter. V_1 is the highest speed at which a takeoff can still safely be aborted and represents one of the most important speeds in the takeoff performance determination.

There are a number of other relevant V-Speeds which are acting as limitations due to aerodynamic or mechanic properties of the aircraft. In fig: 3.1, they are indicated with a red band for the mechanical and with a blue band for the aerodynamically limiting speed regions.

4 This refers to the fact that older aircraft may still be certified under older regulatory requirements if the original aircraft has been certified according to older standards applicable at the time of initial certification.

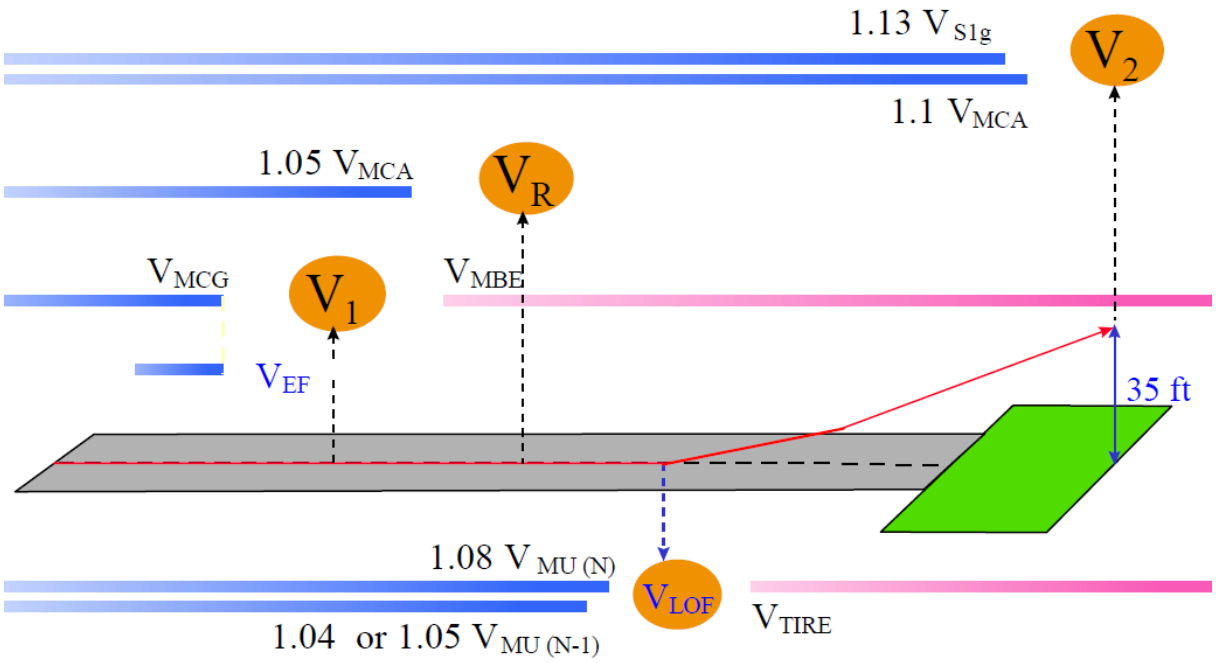

Fig. 3.1 Takeoff Speeds and ground distances in AEO condition (**Airbus 2002**)

From a mechanical point of view, one limiting speed is the maximum tire speed V_{TIRE}, justified from the maximum centrifugal forces on the aircraft tires. Another limitation is the Maximum Brake Energy Speed V_{MBE}. This is the takeoff mass dependent maximum speed up to which the aircraft brakes are able to dissipate the kinetic energy of the airplane in a stopping case. If the aircraft is faster and has kinetic energy higher than the maximum brake energy limit, the aircraft braking system cannot sustain sufficient braking action to bring the aircraft to a complete stop. As a consequence, the highest speed at which a takeoff could be aborted is V_{MBE}, an upper boundary for V_1. **CS-25.109** specifies that a flight test demonstration of the maximum brake kinetic energy accelerate-stop distance must be conducted with no more than 10% of the allowable brake wear range remaining on each of the wheel brakes.

Aerodynamically justified characteristic V-Speeds have to be flight-tested, they will be found in the AFM of a certified aircraft. They can be approximated as a function of the stall speed of the aircraft at 1g vertical acceleration, $V_{S,1g}$ or V_S. The estimation for V_{LOF} is presented according to **Roskam VII**, the V_R and V_2 estimations according to **GJE EXTGFD-003**.

$$V_R \approx 1{,}18\, V_S \quad \textbf{(3.1)}$$

$$V_{LOF} \approx 1{,}2\ V_S \quad \textbf{(3.2)}$$

$$V_2 \approx 1{,}23\, V_S \quad \textbf{(3.3)}$$

Also, the minimum control speeds have to be determined in flight test. **CS-25.149** specifies the V_{MC} as follows:

> *V_{MC} is the calibrated airspeed, at which, when the critical engine is suddenly made inoperative, it is possible to maintain control of the aeroplane with that engine still inoperative, and maintain straight flight with an angle of bank of not more than 5°.*

The stability properties of the aircraft and the means to stabilize the aircraft on the ground are different to those in the air; therefore there is a distinction between V_{MCG} (ground) and V_{MCA} (air). Due to this stability criterion, the rotation speed V_R can never be lower than V_{MCA}. Likewise, the decision speed V_1 can never be lower than V_{MCG}. The aircraft in an OEI condition would not be able to sustain stable conditions. This is of importance for the takeoff performance calculation when the V_1 and V_R speeds coincide with the V_{MC} requirements, usually for low takeoff masses.

The Minimum Unstick Speed V_{MU} shown in Fig. 3.1 is the lowest speed at which the aircraft can get airborne. However, due to the large Angle of Attack (AOA) necessary, the lift-to-drag ratio is unfavorable and not optimal to clear the obstacle height at minimum distance.

The following procedure describes a takeoff in **AEO conditions** as shown in Fig. 3.1. The aircraft will accelerate from the brake release point passing the Takeoff Decision Speed V_1 towards the rotation speed V_R. The nose of the aircraft is rotated (about 3°/s[5]) and the aircraft lifts off at liftoff attitude at the speed V_{LOF} and climbs out accelerated. The objective is to pass an obstacle at a specific height at the end of the runway at the safe climb speed V_2. In case of a wet runway, when the required obstacle clearance height is reduced to give a performance benefit, the V_2 can still be reached at the original obstacle clearance height defined for dry runways.

In **OEI conditions**, an engine is assumed to fail at a specific speed V_{EF} as defined in **CS-25.107**. Should this critical malfunction occur before the decision speed V_1, the pilot will take action to abort the takeoff run. Should the engine fail after passing V_1, the pilot will not abort the takeoff run because the remaining stopping distance would not be sufficient, and continue the takeoff under OEI conditions.

The following definition from **CS-25.107** serves as a baseline for the further discussions and calculations of the OEI condition in this report. It marks the difference between V_{EF} and V_1.

> *(a)(2) V1, in terms of calibrated airspeed, is selected by the applicant; however, V1 may not be less than V_{EF} plus the speed gained with the critical engine inoperative during the time interval between the instant at which the critical engine is failed, and the instant at which the pilot recognises and reacts to the engine failure, as indicated by the pilot's initiation of the first action (e.g. applying brakes, reducing thrust, deploying speed brakes) to stop the aeroplane during accelerate-stop tests.*

5 this pitch rate is a common orientation but may vary for specific aircraft and/or configurations

The most critical V_{EF} is so close before V_1 that the engine failure recognition occurs exactly at V_1. This is the most critical and highest speed, because at V_1 both GO or STOP decisions coincide and the aircraft will either have to accelerate with OEI from this lowest speed to proceed with a takeoff, or brake from this maximum reject speed down to a full stop. V_1therefore defines the boundary between the GO and the STOP case and its knowledge therefore is of major importance in the takeoff preparations and will be determined in this report. In contrast to the other speeds discussed, it is also dependent of the runway length available.

3.3 Distances in the Takeoff (Accelerate-Go) Case

The takeoff procedure of an aircraft can be divided into three major phases. The ground acceleration phase, the rotation phase and the airborne acceleration phase together constitute the *Takeoff Distance* (TOD). During the acceleration from brake release point to the point at which V_{LOF} is reached and runway contact is lost, the corresponding *Liftoff Distance* is covered. After liftoff during climb-out to screen height, the *Air Distance* is covered. The Liftoff Distance also includes the Rotation Distance between the rotation point at V_R and the liftoff point. At the rotation point, the nose gear of the aircraft is raised from the runway to liftoff AOA, while contact to the runway surface is sustained by the main gear.

Due to the requirement that a critical failure during the takeoff phase always has to be considered as discussed in Section 3.1, the AEO and the OEI conditions have to be calculated individually to determine the limiting total TOD. When determining the takeoff performance in an OEI condition, the '*critical engine*' needs to be assumed to fail, which the **CS-25** specifies as the one *that would most adversely affect the performance or handling qualities of an aircraft*.

Fig. 3.2 gives an overview on the discussed takeoff sequence for a takeoff in OEI conditions. TOGA is the takeoff/go-around thrust, while N is the number of engines. This subscript is used to distinguish the AEO (N) and OEI (N-1) conditions.

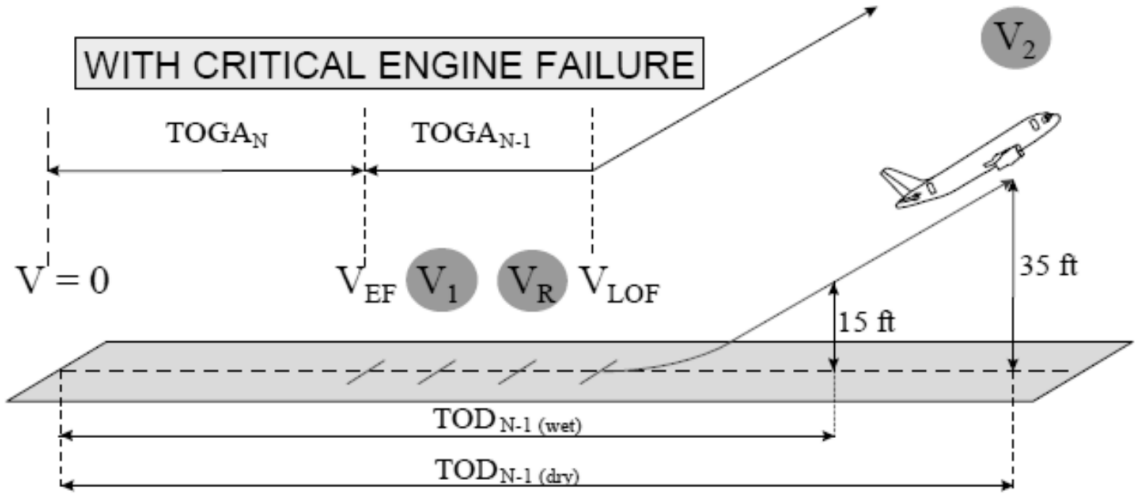

Fig. 3.2 Takeoff in OEI Conditions (**Airbus 2002**)

The most important change between the certification requirements of the TOD of a wet runway compared to a dry runway is the reduction of the screen height from 35 ft to 15 ft as can be seen in Fig. 3.2. This screen height is an assumed obstacle which the aircraft has to be able to clear at the end of the Air Distance. **CS-25.113** defines the Takeoff Distance as follows:

*a) The takeoff distance on a **dry runway** is the greater of the following values:*
- *TOD OEI dry as the Distance covered from the brake release to a point at which the aircraft is 35 feet above the takeoff surface, assuming the failure of the critical engine at V_{EF} and recognition at V1,*
- *1.15 factored TOD AEO dry equals 115% of the distance covered from brake release to a point at which the aircraft is 35 feet above the takeoff surface, assuming all engines operating.*

*b) The takeoff distance on a **wet runway** is the greater of the following values:*
- *The take-off distance on a dry runway determined in accordance withCS-25.113 a)*
- *TOD OEI wet as the Distance covered from brake release to a point at which the aircraft is at 15 feet above the takeoff surface, ensuring the V2 speed to be achieved before the airplane is 35 feet above the takeoff surface, assuming failure of the critical engine at V_{EF} and recognition at V1.*

According to the above statement, the TOD on a *dry* runway, according to CS-25.113 b), can also become limiting for the *wet* runway TOD. This seemingly redundant distinction is relevant for aircraft that have a Thrust-to-Weight ratio so high that the reduced screen height of a wet runway would lead to a smaller TOD than was needed on a dry runway.

In the TOD calculation, the Air Distance does not necessarily have to be covered above the actual runway surface. It can also be covered above a *clearway*, referring to a surface that does not count as a part of the actual runway length, but is suitably shaped to allow the aircraft to climb out to screen height, e.g. a grassy area at the end of the runway. It is beneficial to consider the existence of a clearway, because it implies a performance benefit in the determination of the runway length required for takeoff.

In the case that a clearway is present, it is therefore necessary to distinguish between Takeoff Distance and *Takeoff Run* (TOR). The TOR is related to the actual runway length that is used for the acceleration to liftoff speed and may be smaller as the TOD because it takes into account the existence of a clearway to cover the Air Distance, as shown in Fig. 3.3.

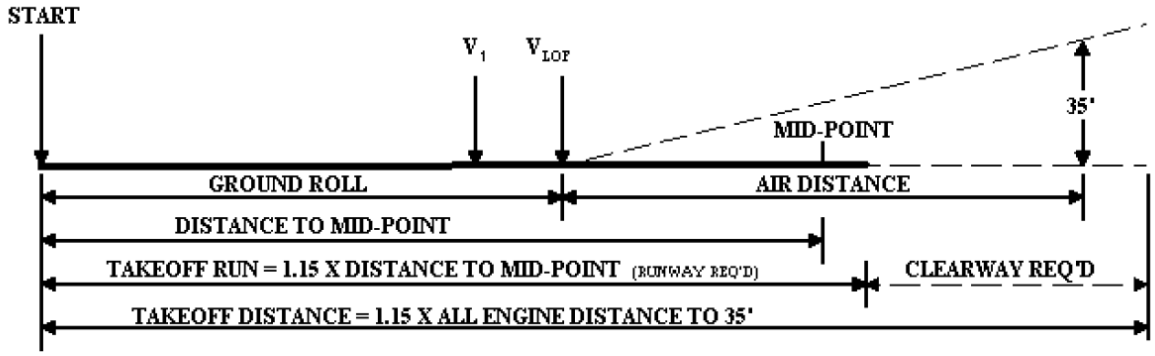

Fig. 3.3 Takeoff Run and Takeoff Distance with Clearway considered (**FAA AC 25-7B**)

For a runway with clearway, **CS 25.113** defines the Takeoff Run as follows:

*a) The takeoff run on a **dry runway** is the greater of the following values*

- *TOR OEI dry as the Distance covered from brake release to a point equidistant between the point at which V_{LOF} is reached and the point at which the aircraft is 35 feet above the takeoff surface, assuming failure of the critical engine at V_{EF} and its recognition at V1,*
- *115% of the TOR AEO dry as the distance covered from brake release to a point equidistant between the point at which V_{LOF} is reached and the point at which the aircraft is 35 feet above the takeoff surface, assuming all engines operating.*

*b) The takeoff run on a **wet runway** is the greater of the following values:*

- *TOR OEI wet as the Distance covered from the brake release to a point at which the aircraft is at 15ft above the takeoff surface, ensuring the V2 speed to be achieved before the airplane is 35 feet above the takeoff surface, assuming the failure of the critical engine at V_{EF} and its recognition at V1.*
- *115% of the TOR AEO wet as the distance covered from brake release to a point equidistant between the point at which V_{LOF} is reached and the point at which the aircraft is 35 feet above the takeoff surface, assuming all engines operating.*

According to CS-25.113, the TOD equals the TOR when no clearway is present. Without a clear- or stopway available, a *Balanced Field Length* (BFL) can be determined. Consequently, when a Balanced Field Length shall be determined such as in this report, the Takeoff Run does not have to be considered separately and all relevant distances must be covered on or above the runway surface.

For the purpose of flight planning, the pilot must match the Takeoff Distance (TOD) with the Takeoff Distance Available at the airport (TODA), respectively the Takeoff Run (TOR) with the Takeoff Run Available (TORA) when a clearway shall and may be considered. The Accelerate Stop Distance Available (ASDA) is relevant for a rejected takeoff and is discussed in Section 3.4. Fig. 3.4 shows a graphical representation of the relationships.

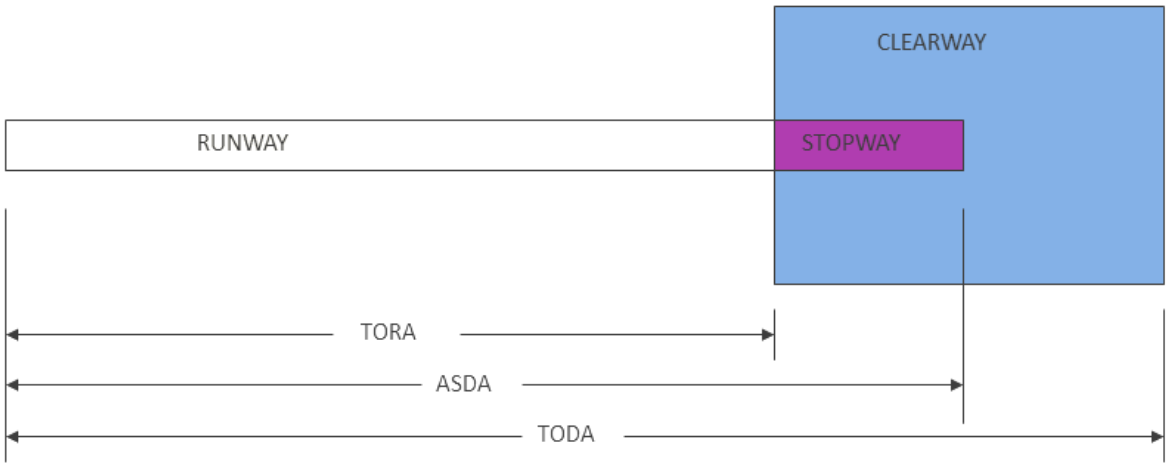

Fig. 3.4 TORA, ASDA and TODA with Clear- and Stopway available (**Airbus 2002**)

3.4 Distances in the Accelerate-Stop Case

As opposed to the continuation of the takeoff after a critical failure such as the loss of an engine, the pilot may also opt to bring the aircraft to a complete stop at or before V_1 is reached. Instead of further accelerating the aircraft, the pilot applies all available means of braking. The overall ground distance that includes both the acceleration and the braking distance is then referred to as the *Accelerate Stop Distance* (ASD).

Summarized according to **CS-25.109**, the ASD is defined as the sum of the distances to:

- Accelerate the airplane with all engines operating to V_{EVENT},
- Accelerate from V_{EVENT} to V1 assuming the event motivating the rejection of the takeoff occurs at V_{EVENT} and the pilot takes the first action to reject the takeoff at V_1
- Come to a full stop
- Plus a safety margin distance equivalent to 2 seconds at constant V_1 speed

According to CS-25.109, the distinction between the AEO and the OEI case needs to be made, the larger resulting Accelerate-Stop Distance of which condition becomes limiting. In the OEI case, the trigger event is the engine failure occurring at V_{EF}, and the aircraft is brought to a stop with one inoperative engine. In the AEO case, the takeoff is rejected due to an event which did not lead to the loss of an engine. Usually, the ASD under AEO conditions is larger than under OEI conditions, as the failed engine produces a drag increment facilitating the deceleration.

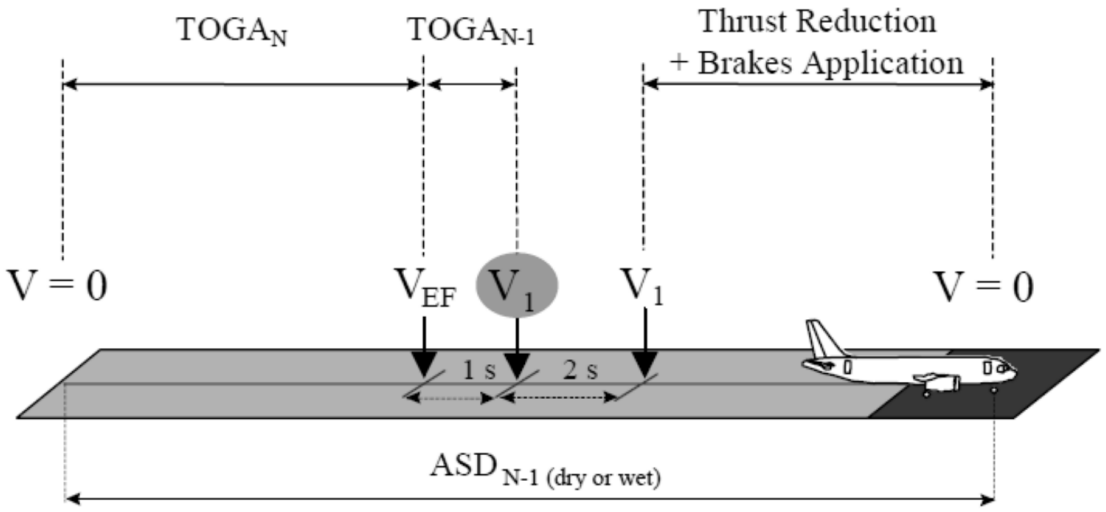

Fig. 3.5 Aborted Takeoff with Critical Engine Failure (**Airbus 2002**)

If a stopway is available, in equivalence to the clearway philosophy this field may be used as a performance benefit. The pilot may account for it in the Accelerate-Stop-Distance Available (ASDA) when he compares this to the ASD for his operating conditions.

On wet runways, the reduced braking capacity needs to be taken into account for. CS-25.109 provides special braking friction coefficients for different surface and operating conditions for wet runways.

3.5 Reaction Times after Critical Failure

When an engine of the aircraft fails or another event necessitates a rejected takeoff, the pilots are required to react in a specified way in order to maintain control. The human reaction times to activate the braking devices need to be taken into account for in the ASD by adding the distance equivalent to two seconds at V_1 to the ASD. For a more detailed determination of these reaction times, **AMC 25.101 (h)(3)** specifies the time steps to be considered between the activation of the retarding devices, while the two second distance shall be seen as a safety margin to account for operational variability in the activation of braking devices.

As in the course of the report, a time-step based calculation method for the takeoff distances will be shown, taking the detailed application sequence of braking devices into account is possible. However, in the pace of historical development the CS/FAR-25 specification, there have been a number of amendments with differing time step definitions. It is important to determine if the original regulations valid at the time of first flight of the aircraft are to be taken into consideration (grandfathering clause), or if the current regulatory basis should be applied.

According to **Airbus 2002**, the history of Amendments can be roughly divided into three phases: before, within and after the CS/FAR Amendment 25-42 from March 1, 1978. The pre-Amendment 25-42 CS/FAR 25 valid at first flight of the Learjet 35A/36A required *no reaction time distance* to be added to the ASD. The CS/FAR Amendment 25-42 then required *two seconds* of *continued acceleration* after V_1 to add to the ASD. This was considered to be too strict and the NPA 244 and NPRM 93-08 were incorporated into the CS-25.109 in 2000/1998.

This current version of the **CS-25.109** requires adding two seconds *at V_1 speed* to the total distance instead of considering a continued acceleration. In turn it requires that the runway surface condition is taken into account for (dry/wet), and specifies specific brake energy testing requirements.

For the deployment of braking means, FAA Advisory Circular **AC 2025-7 (**Chapter 2, section 2**)** specifies that the time delay between the activation of the second and third braking devices is to be amounted for with one second each. This complies to **AMC-25.101 (h)(3)** which states that the activation time delays must be validated with the operator and the demonstrated time delays must be expanded as shown in Fig. 3.6.

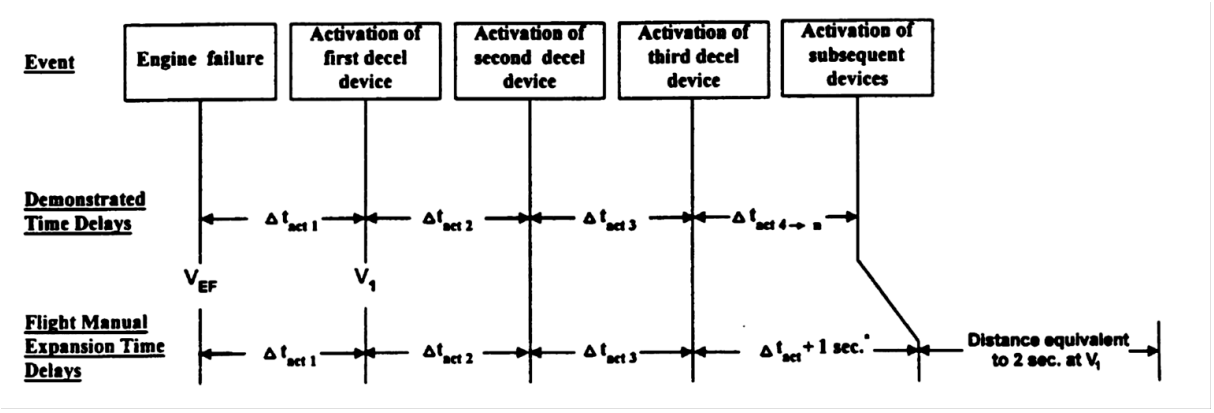

Fig. 3.6 V1 and V_{EF} Interdependence and Time Delay for Retardation Device Activation (**AMC-25.101 (h)(3)**)

In the case of the Learjet 35A/36A, applying the grandfathering clause in order to not consider the two seconds reaction time distance in the ASD would not be conservative. It would also require additional certification effort for the operator, because according to **Airbus 1998** the authorization to operate under the grandfathering clause must be obtained by the operator and cannot be applied to an aircraft automatically.

Hence, for the calculations performed for the ASD in this report, the reaction times according to Fig. 3.6 and **AMC-25.101 (h)(3)** are used, considering specific reaction times and a 2-second equivalent distance margin at constant V_1 speed.

3.6 Balanced Field Length

As was pointed out in the previous sections, the decision speed V_1 plays an important role in the takeoff performance calculations. It requires considering the Takeoff as well as the Accelerate-Stop cases and their respective TOD and ASD. There is one single V_1, at which rejecting the takeoff would lead to the same required distance as a continued takeoff. Rejecting the takeoff after passing V_1 would lead to a longer stopping distance and overall ASD than if the takeoff was continued. The opposite is true for the TOD. Hence, the *Balanced Field Length* (BFL) is the distance at which the *TOD and the ASD are equal*, as shown in Fig. 3.7. The BFL therefore also represents a limitation to the *minimum runway length* that needs to be available for the aircraft taking off, when no clear- or stopways are taken into account for.

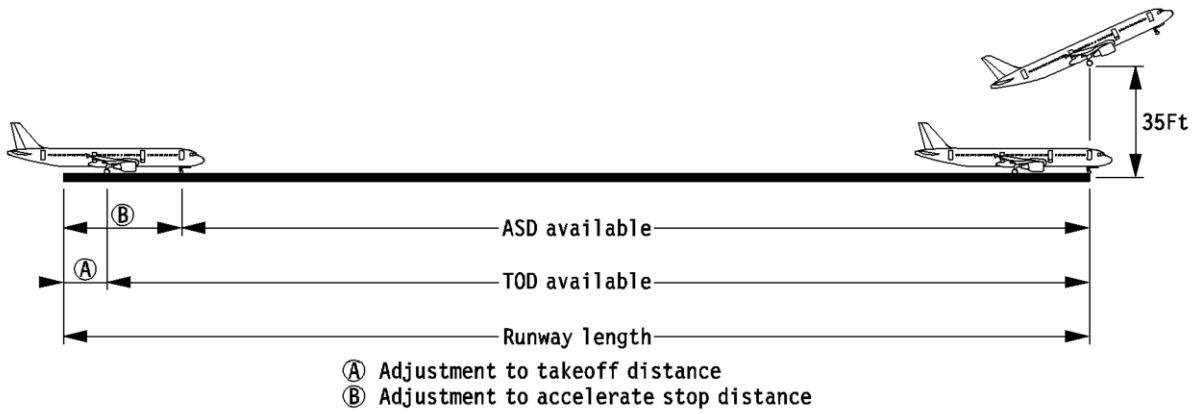

Fig. 3.7 Balanced Field length as Equal Distance of ASD and TOD (**Airbus 2002**)

Considering a fixed takeoff-weight while varying the speed at which an engine is assumed to fail, the following observations can be made for the TOD/ASD calculations:

If the assumed engine failure speed is increased gradually, the TOD required shrinks, since the acceleration phase with all engines operating is longer. The same screen height at the end of the airborne phase can be reached at a shorter overall distance.

At the same time, increasing V_{EF} also increases the ASD, since both the distances due to the reaction time delay as well as the total deceleration distance are becoming larger since more kinetic energy is to be decelerated.

This means that the resulting distances TOD and ASD are essentially a function of V_{EF}. If the assumed engine failure speed is increased incrementally for the ASD and the TOD calculation in the OEI case, two converging graphs are resulting.

They are forming an intersection point at the BFL and the associated balanced V_1. Figure 3.8 provides an example that was actually produced by the simulation developed and presented in this report.

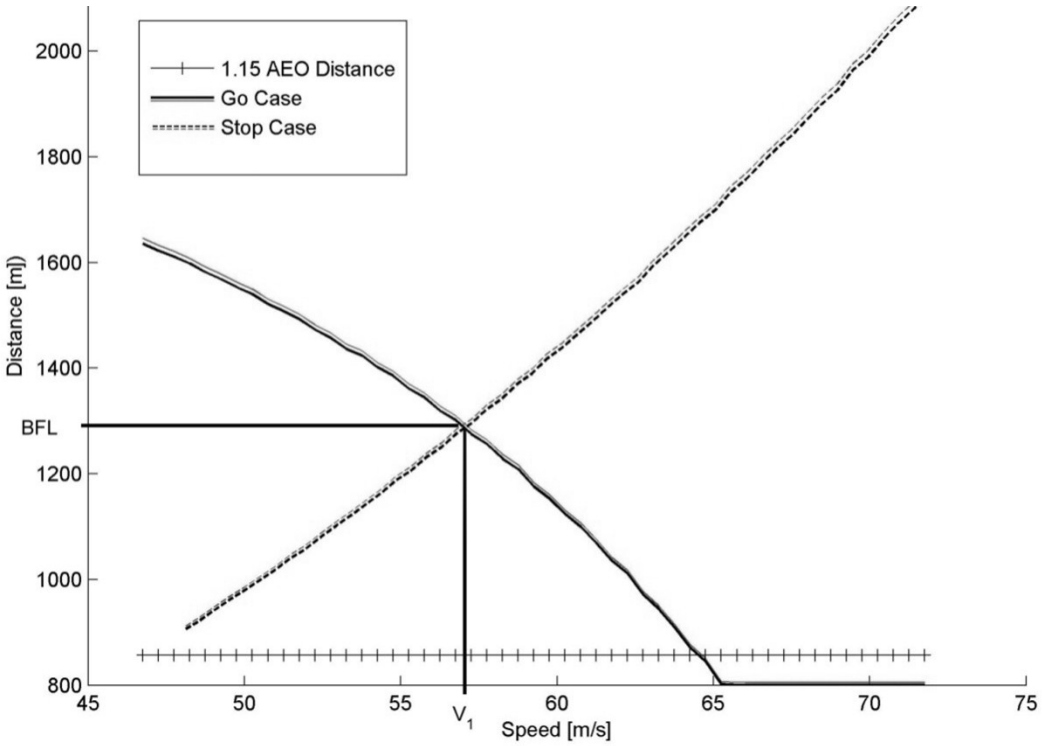

Fig. 3.8 Example Balanced Field Length – TOD and ASD Curve Intersection

As the *Takeoff Distance* (TOD) and *Accelerate Stop Distance* (ASD) definitions make a distinction between *All Engines Operative* (AEO) and *One Engine Inoperative* (OEI) conditions, it is important to determine which one of the two possible conditions becomes then limiting for the Balanced Field Length. Naturally, both ASD and TOD used in one Balanced Field Length calculation need to be determined in the same assumed condition, either AEO or OEI.

An AEO Takeoff Distance constant is shown in Fig. 3.8 for comparison with an OEI Takeoff Distance curve. When the Takeoff Distance with All Engines Operating is smaller than the Takeoff Distance with One Engine Inoperative, as is usually the case for 2-engine aircraft, any possible intersection point with an ASD curve would lead to non-conservative, smaller Balanced Field Lengths. Hence, if the Takeoff Distance in All Engines Operative conditions can be shown to be smaller than in One Engine Inoperative conditions, the latter becomes limiting and represents the baseline for the BFL determination.

3.7 Takeoff Field Length

After a number of definitions and descriptions for possible cases and distances covered in an attempted or executed takeoff have been provided, the Takeoff Field Length (TOFL) refers to the one that becomes limiting for the aircraft taking off. This distance can be:

- 115% of the TOD in AEO conditions
- The TOD in an OEI condition
- The ASD in either condition

The latter two points combined constitute the BFL, by definition as shown in Section 3.6. Therefore, the TOFL definition can be simplified to being the limiting, greater distance of the Balanced Field Length (BFL) and 115% of the All Engines Operative Takeoff Distance.

Because the TOFL is designed to accommodate the worst case, assuming a possible engine failure, it is the minimum field length the takeoff runway must have for the taking off aircraft, if no stop- or clearways are taken into account. As has been shown by calculation, for the Learjet 35A/36A considered in this report, it is always the BFL that becomes limiting.

The knowledge of the pairs of data, Balanced Field Length and balanced V1 for each set of environmental and aircraft configurations is necessary for the flight preparation and is different for each variation of the influencing parameters. As this project shall provide preliminary performance data to be used to develop operating charts for the actual operation of the aircraft, the calculation of the BFL is performed for a range of varying density altitudes.

3.8 Consideration of Precipitation Drag on a Wet Runway

The consideration of the takeoff performance on a *wet runway* is best done by developing a numerical simulation that evaluates the equation of motion for a BFL on a wet runway. However, as outlined in Section 3.1, the **CS-25.109** regulations do not consider any degradation to the aircraft environment other than the reduced braking coefficient. The equations to estimate precipitation drag components are provided in **EASA AMC25.1591**, a document that applies to *contaminated runways*.

It is clear that by not considering precipitation drag effects on a wet runway, an error towards less conservative takeoff performance results will be made, especially at the upper boundary of the wet runway definition. Additional drag will necessarily occur not only on contaminated but also wet runways, which by definition can be contaminated with up to 3 mm of precipitation. The application of the **EASA AMC 25.1591** for a water depth of 3 mm consequently considers the critical boundary for a wet runway in a conservative and reliable manner. It also allows considering additional impingement drag effects due to the installation of under-wing stores. The determination of this effect was also one of the investigation objectives of this report.

When the precise method of using a numerical simulation of the takeoff performance is available, it allows accounting for this additional drag component. Consequently, the precipitation drag should and has been considered in the numerical takeoff performance simulation.

4 Performance Calculation

The chapter is providing the input necessary to set up the performance calculation as a set of functions grouped by the takeoff phase. The aircraft parameters change in each of these phases; therefore this chapter is structured by takeoff phases, subdivided into the equations valid for each phase. As the parameters are also structured by takeoff phase in the performance calculation, this allows quick retrieval of the equations used for each of these phases.

4.1 Liftoff Distance

The Liftoff Distance as defined in the previous chapter is the distance that the aircraft covers on the ground until it lifts off. Four main forces act on the aircraft, just as in the flight condition. Thrust, Drag, Lift and Weight in their combination produce an acceleration of the aircraft during the ground roll.

During stable flight condition, the engine will provide thrust such as to balance the aircraft drag. During the takeoff procedure, the engine must provide additional thrust to accelerate the aircraft.

The thrust T and the drag D are force components in opposite directions and also vector quantities having an associated magnitude and direction. The thrust reduced by the drag of the aircraft is the excess thrust that accelerates the aircraft and is a vector quantity itself.

4.1.1 Equation of Motion – Derivation

According to Newton's second axiom, the law of motion, mass m multiplied by the acceleration a equals the external force F on an object in the direction of the acceleration.

$$F = m \cdot a \tag{4.1}$$

For the horizontal discussion of an aircraft such as in the takeoff phase, the horizontal net force F_h is equal to the *excess thrust* F_{ex}.

$$F_{ex} = F_h = T - D = m \cdot a \tag{4.2}$$

Consequently, the *acceleration* of the aircraft is the obtained by dividing the *excess thrust* by the *aircraft mass*. Aircraft with a high excess thrust can accelerate faster than aircraft with low excess thrust.

$$a = \frac{(T - D)}{m} \tag{4.3}$$

The drag force of the aircraft is not the only component countering the thrust force. Additionally, a *ground friction force* and a *runway slope related weight component* reduce the excess thrust and add to the drag force *D* from equation 4.3. This leads to:

$$a = \frac{T - D - F_f - m \cdot g \cdot sin\gamma}{m} \tag{4.4}$$

With

γ	Runway Slope
F_f	Friction Force
g	Gravity

Should excess thrust and mass of the aircraft remain constant, the basic equation of motion is solved for speed and distance covered as a function of time. However, this equation can only be used in the case that the forces (and subsequently the acceleration) are constant. However, all components from equation 4.4 are speed dependant. The speed dependency will be discussed with equations in sections 4.1.6 for Thrust, 4.1.7 for Lift, 4.1.8 for Drag and 4.1.9 for Rolling Friction and Gravity component.

Therefore, in order to solve the equation of motion for an aircraft, it is therefore necessary to integrate the velocity divided by acceleration. This is shown in equation 4.5.

$$S_G = \int_{v_i}^{v_f} \frac{v}{a} dv \tag{4.5}$$

With

v_i	Initial Speed
v_f	Final Speed

The acceleration a for the aircraft taking off is provided by equation 4.4. Combining equations 4.4 and 4.5 into an overall equation for the ground roll distance leads to the ground roll distance presented in equation 4.6.

$$S_G = \; m \cdot \int_0^{v_{LOF}-v_{wind}} \frac{v_G}{T - D - F_f - m \cdot g \cdot \sin\gamma} dv_G \tag{4.6}$$

The same equation can not only be used for the acceleration distance determination of the aircraft – when a negative acceleration due to braking device deployment is obtained, equation 4.6 permits likewise to determine the stopping distance. In this case, the initial speed v_i is the speed at which the retardation of the aircraft is initiated, and the final speed v_f is zero.

4.1.2 Equation of Motion – Integration for Hand Calculations

For usage of equation 4.6 for quick calculations without a computer, the integral needs to be simplified. This is done assuming that the excess thrust is constant. In the above equation, the *initial speed* is set to *brake release*, and the *final speed* of the takeoff run is the *liftoff speed*, at which the aircraft leaves the runway.

A distance covered on the ground implies that the speeds used for the calculation are ground speeds.

For the liftoff speed in the distance calculation equation, true air speed (TAS) has therefore to be used. The *wind speed* v_{wind} is then subtracted from v_{LOF}, which yields the liftoff ground speed.

The simplification yields:

$$S_G = \frac{1}{2} \cdot m \cdot \frac{(v_{LOF} - v_{wind})^2}{T - D - F_f - m \cdot g \cdot \sin\gamma} \tag{4.7}$$

With

$$D = \frac{1}{2}\rho \cdot S_W \cdot c_D \cdot v_{av}^2 \tag{4.8}$$

$$L = \frac{1}{2}\rho \cdot S_W \cdot c_L \cdot v_{av}^2 \tag{4.9}$$

$$F_f = \mu \cdot (m \cdot g - L) \tag{4.10}$$

And

c_D	Drag coefficient, to be determined acc. to Sect. 4.1.7
c_L	Lift coefficient, to be determined acc. to Sect. 4.1.8
S_W	Wing reference area
ρ	Air density
v_{av}	Average speed during the takeoff run

As Thrust, Lift and Drag actually vary with velocity, this velocity must be approximated and an average constant speed for each of them determined. It is not sufficient to assume the forces at the level at the beginning or the end of the takeoff run phase. The speed at which the average forces have to be determined according to **Scholz 1999** is calculated from Eq. 4.11.

$$\frac{v_{av}}{v_{LOF}} = \sqrt{\frac{1}{2}\left(1 + \left(\frac{v_{wind}}{v_{LOF}}\right)\right)^2} \tag{4.11}$$

In still wind, this reduces to

$$v_{av} = 0{,}707 \cdot v_{LOF} \tag{4.12}$$

When the stall speed$v_s$of the aircraft is known, V_{LOF} can be determined according to **Roskam VII** as

$$v_{LOF} = 1{,}2 \cdot v_s \tag{4.13}$$

In Non-ISA environmental conditions, it is very important to consider the difference between the ground speed and the speed indicated on board the aircraft, the format in which also the reference speeds are given. This is discussed in Section 4.1.5.

4.1.3 Influence of Parameter Variation on Liftoff Distance

When the basic parameters of the Liftoff Distance are changed, the Liftoff Distance changes as a function of these variations. In order to prepare the validation of the results of the takeoff performance calculation in Chapter 9, the expected variation of the Liftoff Distance shall be discussed. This allows predicting expected trends to the Liftoff Distance when certain parameters are varied.

In order to show the effect of parameter variation on the Liftoff Distance (and therefore in analogy on the Accelerate-Stop-Distance), the relationship presented in equation 4.7 shall be presented in expanded form. For simplification reason during parameter impact assessment, the Takeoff Distance shall be assumed proportional to the Liftoff Distance.

$$S_G = \frac{\frac{m}{2} \cdot (v_{LOF}(\rho) - v_{wind})^2}{T\,(\rho, v, f_{thrust}) - D(v, \rho, S_W, c_D) - F_f(v, L(v, \rho, S_W, c_L), m, \mu) - m \cdot g \cdot \sin\gamma} \tag{4.14}$$

Equation 4.14 is very suitable to show the dependency of S_G from the basic input parameters which themselves again depend from a number of other variables. The factors that need to be considered are:

Basic Parameters

- Thrust T
- Drag D
- Lift L
- Friction F_f
- Aircraft Mass m
- Liftoff Ground Speed v_{LOF}

Variables influencing the Basic Parameters

- Air Density ρ
- Wind Component v_w
- Wing Reference Area S_W
- Aircraft Lift Coefficient c_L
- Aircraft Drag Coefficient c_D
- Runway surface friction coefficient μ
- Runway slope γ
- Thrust Factor (Engine Specific Behavior Characteristics) f_{thrust}

Dependency of the Liftoff Distance from Basic Parameters

As can clearly be seen from the basic Liftoff Distance equation, the distance is inversely related to the aircraft thrust. When the above equation was reduced to contain only the thrust in the nominator, the following expression would be true.

$$S_G \propto \frac{1}{T} \tag{4.15}$$

The *higher the thrust*, the *shorter is the expected Liftoff Distance*. When thrust is reduced, the distance is expected to rise. Due to the existence of other impacting forces, this relationship however is not directly inversely proportional. For the consideration of the thrust force, an engine dependent thrust factor may be considered, which accounts for specific characteristics of the engine in certain conditions, such as for example a decrease in thrust due to an active air conditioning system, or flat rating characteristics. This is further specified in Section 4.1.6.

The drag and friction force are acting in the same direction; therefore their impact shall be summarized with the letter *R* for resistance, denoting either *D* or F_f.

$$S_G \propto \frac{1}{F - R} \tag{4.16}$$

The *higher the resistance force*, the *smaller is the excess thrust* as difference between thrust and resistance. Consequently, the *Liftoff Distance rises* with rising resistance, either through drag force or through friction force.

The lift force plays only a secondary role in the horizontal force calculation, because it is contained in the determination of the friction force.

$$F_f = \mu \cdot (m \cdot g - L) \tag{4.17}$$

In analogy to the above statement, the *lower the lift force* is, the higher will the friction force become, which in turns *increases the Liftoff Distance*.

The aircraft mass is an interesting factor, because it is contained in both the denominator and the nominator. The biggest influence has its presence in the denominator, because an increase in aircraft mass has a direct influence on the Liftoff Distance when no runway slope is considered. Its influence is further increased by the fact that the aircraft mass is also contained in the friction force equation. The *higher the aircraft mass*, the *higher the friction force*, with the described consequences.

$$S_G \propto m \tag{4.18}$$

Overall, a rising aircraft mass therefore has a *rising impact on the Liftoff Distance*. With runway slope consideration however, the aircraft mass can also have an *inverse effect*, if a downward sloping runway is considered. The nominator term $-(m \cdot g \cdot \sin\gamma)$makes that, in case γ becomes negative, a force in the direction of the thrust force is created. This actually increases the excess thrust, with the effects considered above. Inversely, an upward sloping runway has the opposite effect and increases Liftoff Distance.

The Liftoff Ground Speed is a very important factor to consider, because it depends from the wind component and the true liftoff air speed. As outlined in Section 4.1.5, the true liftoff air speed varies as a function of air density. The lower the air density, the higher is the true air speed at constant calibrated or equivalent air speed.

$$S_G \propto v_{LOF,G}^2 \tag{4.19}$$

This relationship indicates that the *higher the liftoff ground speed*, the *higher the Liftoff Distance* becomes.

Influence of the Air Density on the Liftoff Distance

The Air density is the variable that is contained in most of the basic parameters used to determine the Liftoff Distance. It is dependent from air pressure and temperature, as outlined in Section 4.1.5.

When the air density decreases, the following variables change: The liftoff ground speed increases, the thrust decreases, the drag force decreases and the lift decreases whereby the friction force increases. For an explanation of the density influence on these basic parameters, refer to sections 4.1.6, 4.1.7 and 4.1.8. From a decrease in density follows that the only favorable effect for the overall Liftoff Distance is the decrease in drag force. Consequently, with *decreasing air density*, an *increase in Liftoff Distance* can be expected.

Influence of the Wind Component on the Liftoff Distance

The necessity of the use of ground speeds for the determination of the Liftoff Distance has already been outlined in Section 4.1.4. Because an aircraft lifts off not at a specific ground speed, but at a specific relative equivalent air speed, the wind component needs to be considered in the distance evaluation. A *headwind component reduces the liftoff ground speed* and thereby the Liftoff Distance, while a *tailwind component has the inverse effect*.

Influence of Wing Surface, Aircraft Lift and Drag components

The above factors are determining the aerodynamic properties of the aircraft. As the wing surface is the reference area for lift and drag coefficients, the aerodynamic forces increase with an increase in wing area, when the coefficients remain constant. An increase of the aerodynamic coefficients for lift or drag of course also leads to an increase in both lift and drag forces with the respective effects on the Takeoff Distance as described above.

Runway Surface Friction Coefficient

The runway surface friction coefficient plays a very important role because of its direct influence on the friction force. Naturally, a *higher friction coefficient* induces a higher friction force, with a resulting *increase in Liftoff Distance*. This is the main reason why a takeoff on a wet runway is expected to require a longer Liftoff Distance than a takeoff on a dry runway. More detailed considerations on the friction coefficient and other friction forces due to precipitation on the runway will be outlined in sections 4.1.9 and 4.1.10.

Impact of Parameter Variation on the Accelerate-Stop-Distance

The impact a parameter change has on the overall Accelerate-Stop Distance is *inverse* to the impact it has on the Liftoff Distance. In the braking case, the objective of creating forces acting on the aircraft is inverted, because the aircraft needs to create as much negative excessive thrust through braking as possible in order to bring the aircraft to a stop. Therefore, the effects that negatively influence the Liftoff Distance are beneficial for the Accelerate-Stop Distance.

4.1.4 Equation of Motion – Usage for Numerical Integration

The assumption of an average speed for the takeoff roll is a good method in order to get an easy equation that is suitable to estimate the magnitude of the Takeoff Distances of an aircraft. However, with rising speed, the acceleration usually decreases, especially in case of an assumed engine failure. Therefore, a numerical method that integrates the distances time-step-wise with regard to the changes in the acceleration at different speeds provides greatly improved precision in the Takeoff Distance determination. A time step is the difference between the times at each point at which aircraft parameters are evaluated, the time starts to count at brake release.

There are various integration methods that permit time-step wise integration. A time-step-wise integration is an *iterative method*, because variables are evaluated for specific increments of the time parameter.

The general principle about how an iterative method works is described in this section. The difference between the iterative integration methods is the way in which the intervals are evaluated, leading to different levels of precision. The Euler method is the easiest integration method, and not specifically adapted to solving differential equations. In contrast to this, the *Runge-Kutta integration method* offers the advantage to be especially conceived for evaluating a *differential equation* with regard to time. It was therefore applied to the calculation method used in this report. As its specific operating principle is heavily linked to the set-up of the calculation program used for this report, it will be described in more detail in Section 7.4.2.

The Takeoff Distance determination by a time-step method is a differential equation, since the speed of a specific interval is determining the acceleration valid for this interval, which in turn is the input for the next interval. In the subsequent step, a new speed is calculated as a function of the time step and the acceleration experienced during the previous step. This is shown in Eq. 4.20.

$$v_{G,n+1} = v_{G,n} + \Delta t \cdot a_n(t_n, v_{G,n}) \tag{4.20}$$

With

$$a_n = \frac{1}{m}(T_n - D_n - F_{f,n}) - g \cdot sin\gamma \tag{4.21}$$

Equation 4.20 shows how the acceleration and the time step t of each interval determine the speed that is considered in the upcoming interval. From this relationship, it is possible to determine the distance increment by a principle similar to the one shown in Eq. 4.22.

$$S_{n+1} = S_n + \Delta t \cdot v_{G,n}(t) \tag{4.22}$$

Due to the iterative methodology, the accuracy of the final speeds and distances depends heavily on the time step between each evaluation. **Yechout 2003** suggests to use a time step no larger than 0,1 seconds.

By applying the above approach, a relationship between speed and distance can be obtained from the equation of motion. Plotting the distance S_n with regard to the speed v_G for each time step increment yields the relationship represented in Fig. 4.1. This figure originates from the performance simulation presented in this report and displays an OEI acceleration case. As a result of the engine failure, a_n is reduced after V_{EF} and the decreased slope of the graph in Fig. 4.1 reflects this clearly.

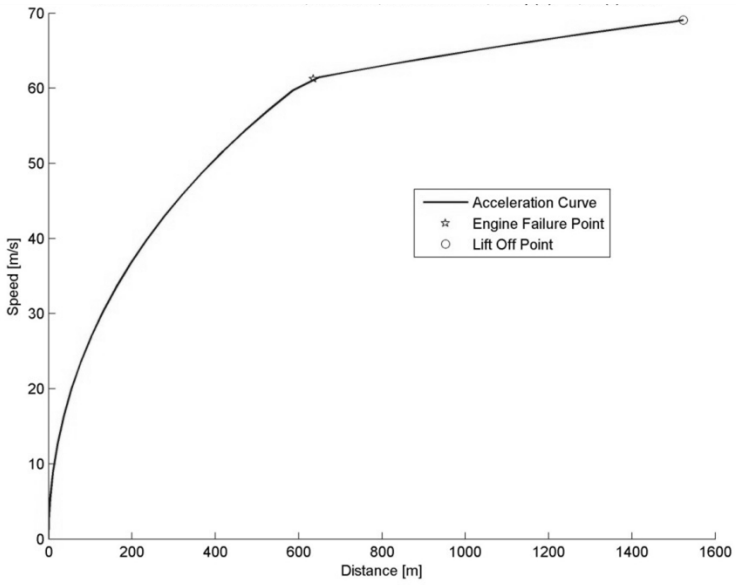

Fig. 4.1 Distance and Velocity for Acceleration with Decreasing Excess Thrust

Any correlation between a speed and a distance can be obtained from this figure. Characteristic speeds are V_{EF} and V_{LOF}. The plot of the liftoff speed directly shows the distance that has been covered until this speed has been reached, which is the Liftoff Distance.

For a braking aircraft, the same equation of motion and integration remains valid, with the difference that the acceleration becomes negative as the aircraft brakes, leading to an inversion of the graph shown above. In this case, the speed and distance at each time interval are smaller than at the previous interval. This case is represented in Fig. 4.2 and originates as well from the performance calculation presented in this report.

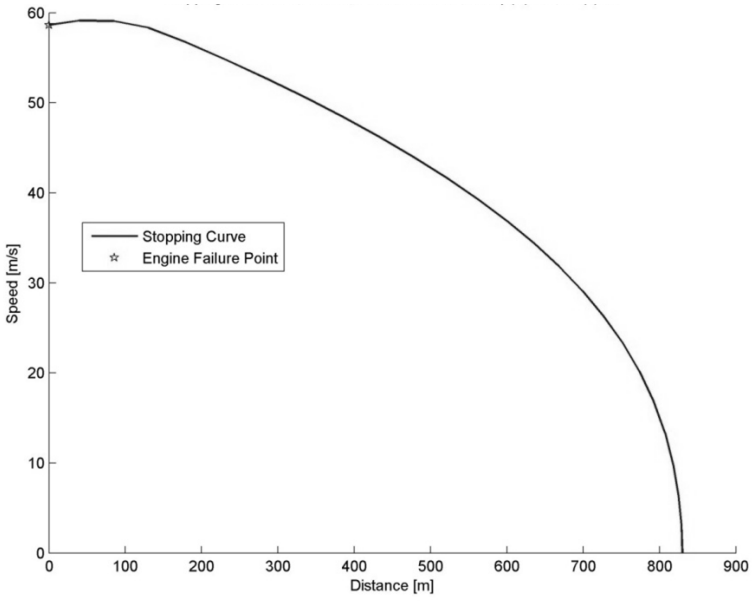

Fig. 4.2 Distance and Velocity for Deceleration with Negative Excess Thrust and delayed Retardation Device Activation

4.1.5 Density, Pressure and Reference Speeds in Non-Standard Atmosphere

The takeoff distance and speed charts need to reflect a range of different environmental conditions if they shall be used in flight operations. Environmental parameters such as pressure, density and temperature, are interdependent. This necessitates deciding which parameter variations need to be reflected in the actual takeoff performance charts.

Since the pilot will always be given the QNH of the aerodrome by means of the weather information system, he will be able to determine the pressure altitude of the aircraft easily. Furthermore, he will have a readout of the total air temperature on the airfield through onboard devices.

Therefore, the parameter variations that will need to be reflected in the takeoff performance charts are Required Takeoff Field Length and V_1 as a function of Pressure Altitude (PA) and Outside Air Temperature (OAT).

The first step to calculate the parameters of a Non-ISA environment is to calculate the difference between the actual Outside Air Temperature t_{true} and the standard temperature t_0 that would be present in ISA conditions at the selected pressure altitude. The standard ISA temperature in K is calculated according to **Scholz 1999** by

$$t_0 = 288{,}15\ [\mathrm{K}] - \frac{\partial t}{\partial H} \cdot H \tag{4.23}$$

With

$\partial t/\partial H$	Temperature gradient (1.981210^{-3}/ft)
H	Pressure altitude in ft

Secondly, the true outside temperature in Kelvin needs to be known. It is converted from degrees Celsius to Kelvin by the following equation.

$$t_{true,K} = t_{true,°C} + 273{,}15\ [\mathrm{K}] \tag{4.24}$$

This can then be used to determine the temperature ratio ϴ from

$$\theta = \frac{t_{true,K}}{t_0} \tag{4.25}$$

The difference in Kelvin between both temperatures is called Δt_{ISA}.

$$\Delta t_{ISA} = t_{true,K} - t_0 \tag{4.26}$$

For various parameters, the pressure p_{true} at the current pressure altitude must be known. It can be determined without the need to take into account any other ISA deviations at this point, because pressure altitudes shall be the input values to the performance chart. The pressure ratio δ can then be obtained as well.

$$p_{true} = p_0 \left(1 - \frac{L}{T_0} \cdot H\right)^{5.25588} \tag{4.27}$$

$$\delta = \frac{p_{true}}{p_0} \tag{4.28}$$

With

p_0 Standard ISA pressure (101325 Pa)

From the temperature ratio Θ, the speed of sound a can be determined according to the following equation:

$$a = a_0 \sqrt{\theta} \tag{4.29}$$

With

a_0 Speed of sound in standard conditions (340.294 m/s)

For the density ρ_{true} and the density ratio σ, the following equations are valid (from **Young 2001**)

$$\rho_{true} = \rho_0 \cdot \frac{\delta}{\theta} \tag{4.30}$$

$$\sigma = \frac{\rho_{true}}{\rho_0} \tag{4.31}$$

With

ρ_0 Density at standard conditions (1,225 kg/m³)

This allows determining the density at the considered environmental conditions in order to calculate many depending factors such as the Lift and Drag forces.

Reference Speeds in Non-ISA Conditions

Reference speeds for the operator of an aircraft are usually given in Calibrated Airspeed (CAS) or Indicated Airspeed (IAS). In case a calibration is necessary to convert IAS into CAS, the aircraft manufacturer will provide calibration charts. The CAS reflects the speed that determines the aerodynamic properties (in incompressible flow), while the IAS is displayed on the flight deck of the aircraft; they are independent of changes in air density.

Compressibility corrections are necessary only for flight speeds greater than M=0.3 according to **Roskam, Lau 1997**. Therefore, the CAS can be considered equal to Equivalent Air Speed (EAS) during the takeoff phase.

What this means is that in Non-ISA conditions, the True Air Speed (TAS) will vary with a change in environmental conditions, while CAS/EAS remain constant. It was pointed out that for the determination of a distance over ground, it is necessary to consider ground speeds for characteristic points such as the liftoff speed, signifying the Liftoff Distance. If the AFM values were not corrected to TAS, the overall distances calculations were erroneous.

Hence, a conversion of CAS (or EAS) in TAS becomes necessary, to be applied when AFM values are used to determine a ground distance. Vice versa, ground speeds must be corrected to EAS when aerodynamic forces at a specific ground speed shall be considered.

$$v_{TAS} = \frac{v_{CAS}}{\sqrt{\frac{\rho_{true}}{\rho_0}}} \tag{4.32}$$

4.1.6 Thrust and Thrust Lapse

The thrust of an aircraft varies considerably with a change in the parameters speed, air pressure and outside air temperature. An analysis of the thermodynamic cycle of a specific engine would yield the most accurate results. The influence on the thrust with variation of the impacting parameters is shown in Fig. 4.3.

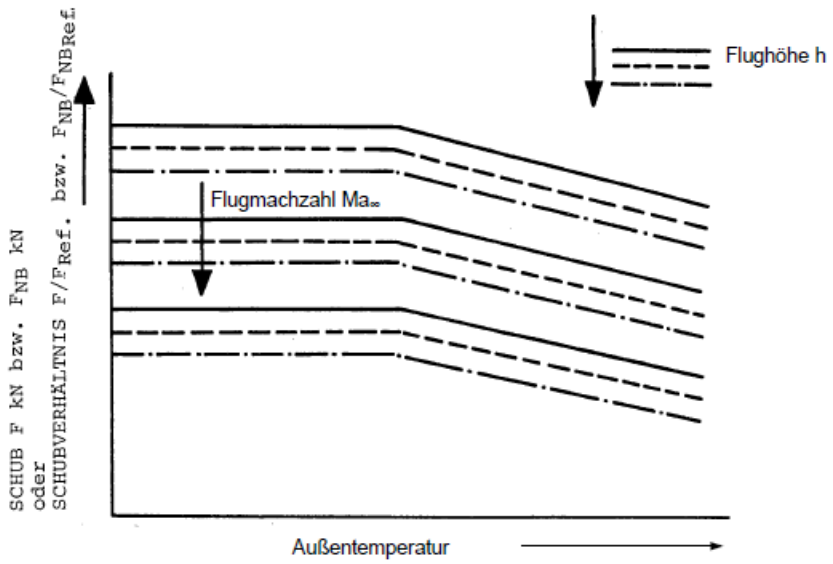

Fig. 4.3 Thrust Variation with Pressure Altitude, Mach Number and OAT, flat rated (**AT21100.01**)

The thrust of a jet engine is derived from the basic equation acc. to **Bräunling 2004**:

$$F = \dot{m}\,(c_{out} - v) \tag{4.33}$$

With

c_{out}	Outflow speed of the engine
v	Flight speed
$\dot{m}$	Mass flow through the engine

and

$$\dot{m} = \rho \cdot c_0 \cdot A_{eng} \tag{4.34}$$

With

A_{eng}	Engine inlet area
ρ	Air density

The density of the air is related to the temperature t and air pressure p by the equation

$$\rho = \frac{p}{R\,t} \tag{4.35}$$

With

R Gas Constant (287,04 J kg^{-1} K^{-1} for dry air)

Because of the relationship from Eq. 4.35, increasing the pressure altitude (lowering the air pressure) and increasing the Outside Air Temperature will lead to a decrease in thrust available. The thrust also decreases respectively when the flight Mach number is increased, since as a result the velocity differential ($c_{out} - c_0$) will decrease.

In order to calculate the complete thermodynamic cycle of the engine of the considered aircraft, a complex engine parameter determination would be necessary, leaving the scope of this work. Furthermore, only limited information on the aircraft to be considered in this calculation is available. Therefore, a number of simplified approaches need to be used. However, there are fairly accurate estimation methods that achieve an approximation of the thrust variation with the parameter variation based on the initial thrust the engine delivers at flight mach number M=0.

Installed Thrust

The initial thrust of the engine as provided by the engine manufacturer considers the engine in ideal test conditions. In order to determine the actual thrust it delivers when installed on an aircraft, the installation losses need to be considered. The remaining thrust acting on the airframe is referred to as installed thrust. According to **Roskam VI**, major causes of thrust reduction due to installation losses are the inlet pressure loss and the power extraction due to engine utilities, such as the electrical generators or bleed air.

When no comprehensive information to detail these installation losses are available, **LTH AT21000.06** specifies the installation loss to account for approx. 3% of the engine's net uninstalled thrust.

Thrust Variation with Mach Number and Pressure Altitude

The installed initial thrust T_0 can then be varied according to the simplified approaches available to reflect the parameter influence on available thrust. The most commonly used models are from **Bartel & Young 2007**, as well as **Brüning, Hafer, Sachs 1993** and **Torenbeek 1982.** They all share a common structure where the following variables are used:

$$T = T_0 \, (A - k_1 \, M + k_2 \, M^2) \tag{4.36}$$

With

T_0 Static thrust at M=0

A, k_1 and k_2 are the parameters to vary the thrust output. The approaches use different methods to determine these parameters, leading to different levels of accuracy when compared to test data.

A short overview on the different methods and models shall be given below.

Brüning, Hafer, Sachs 1993

$$T = T_0(1 - k_1 \, v + k_2 v^2) = T_0(1 - k_1' M + k_2' M^2) \tag{4.37}$$

With

$$k_1 = (2{,}44 \cdot 10^{-4} \cdot BPR + 1{,}66 \cdot 10^{-3}) \left(\frac{m}{s}\right)^{-1} \tag{4.38}$$

$$k_2 = (6{,}16 \cdot 10^{-7} \cdot BPR + 4{,}08 \cdot 10^{-6}) \left(\frac{m}{s}\right)^{-1} \tag{4.39}$$

$$k_1' = a \cdot k_1 \tag{4.40}$$

$$k_2' = a \cdot k_2 \tag{4.41}$$

BPR Bypass-Ratio of the Engine

Torenbeek 1982

$$T = T_0\left(1 - \frac{0{,}45\ (1 + BPR)}{\sqrt{(1 + 0{,}75\ BPR)G}} \cdot M + \left(0{,}6 + \frac{0{,}11\ \sqrt{BPR}}{G}\right) \cdot M^2\right) \quad \textbf{(4.42)}$$

With

G Gas generator function

G = 0.9 for low BPR
G = 1.1 for high BPR

Bartel & Young 2007

$$T = T_0\left(A - \frac{0{,}377\ (1 + BPR)}{\sqrt{(1 + 0{,}82\ BPR)G}} \cdot Z \cdot \frac{p_{true}}{p_0} \cdot M + \left(0{,}23 + 0{,}19\ \sqrt{BPR}\right) \cdot X \cdot \frac{p_{true}}{p_0} \cdot M^2\right) \quad \textbf{(4.43)}$$

With

G Gas generator function

G = 0.9 for low BPR
G = 1.1 for high BPR

And

$$A = -0{,}4327\left(\frac{p_{true}}{p_0}\right)^2 + 1{,}3855\left(\frac{p_{true}}{p_0}\right) + 0{,}0472 \quad \textbf{(4.44)}$$

$$X = 0{,}1377\left(\frac{p_{true}}{p_0}\right)^2 - 0{,}4374\left(\frac{p_{true}}{p_0}\right) + 1{,}3003 \quad \textbf{(4.45)}$$

$$Z = 0{,}9106\left(\frac{p_{true}}{p_0}\right)^2 - 1{,}7736\left(\frac{p_{true}}{p_0}\right) + 1{,}8697 \quad \textbf{(4.46)}$$

Comparing these three approaches for the thrust variation due to Mach number from the plot in Fig. 4.4, the slopes of thrust decay with Mach number increase show that compatible results are obtained. For these plots, an installed initial thrust at brake release of 3400 lbs has been selected.

Furthermore, as the approach according to **Bartel & Young 2007** is the only one to include pressure altitude deviations in the basic equation, for demonstration the pressure altitude deviations have been plotted as well in Fig. 4.4.

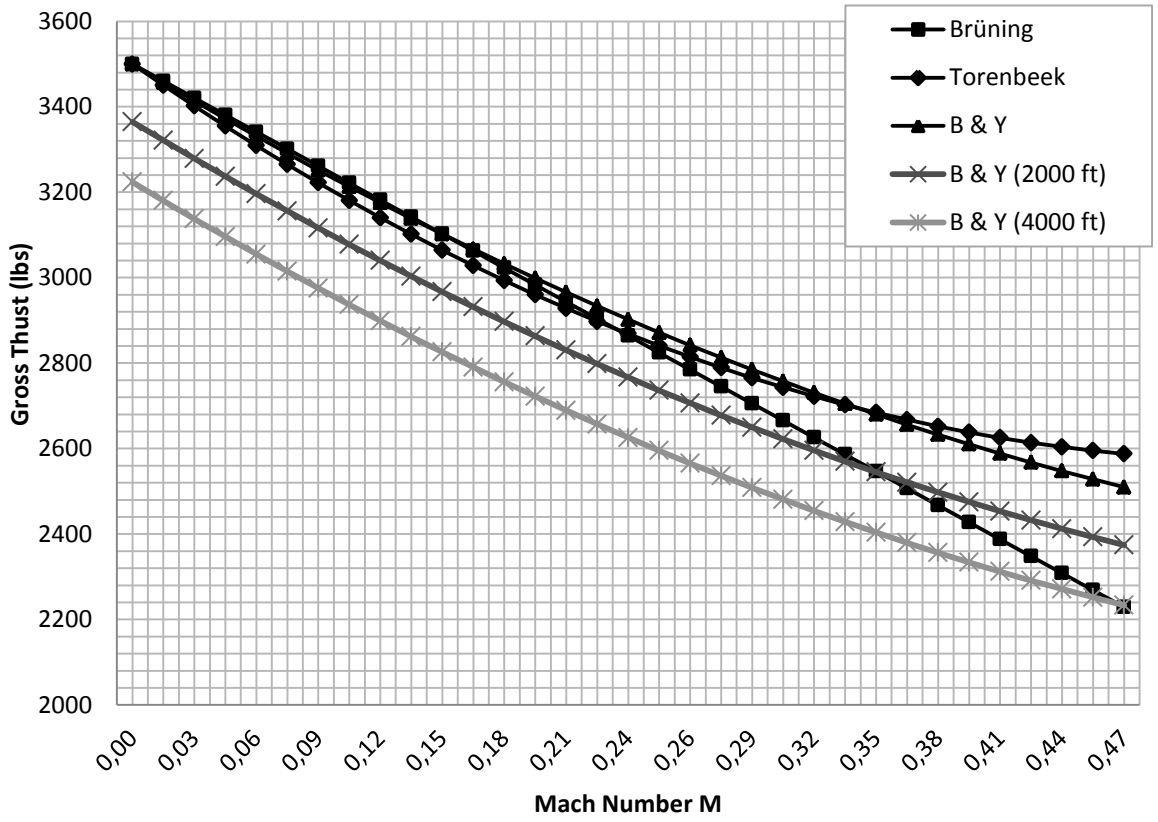

Fig. 4.4 Different Approaches to compare Mach Number Dependency of Thrust
(Baseline: Uninstalled Thrust TFE-731-2B-2 Engine)

As can be seen clearly in this figure, for the considered speed band up to M = 0,3 during the takeoff phase, the three approaches deliver values for thrust are in close agreement with each other. However, Torenbeek and Brüning do not describe the variation of thrust in dependence of the pressure altitude. Therefore, for means of this report, the Bartel & Young 2007 approach was selected as the most accurate model to consider both Mach number and pressure altitude corrections.

Temperature Correction

Concerning the temperature correction, the engine would have to be numerically simulated including pressure and temperature ratios between the different stages inside the engine. Another special concern is the flat-rate temperature of the engine, a concept that is outlined in the following paragraphs.

Roskam VI suggests to have detailed manufacturer information at hand for the thrust lapse due to temperature determination. When no detailed engine data is available, an estimation based on generic approaches is necessary. This is generally done by a thrust lapse factor that is multiplied with the difference to the reference temperature at which thrust data T_0 is available. Approaches from **EUROCONTROL 2009** and **Raymer 1989** can be used to determine this thrust lapse rate.

According to **EUROCONTROL 2009**, the thrust T_{true} at Non-ISA conditions is determined from Eq. 4.47.

$$T_{true} = T_0\left(1 - C_{Tc5}(\Delta t_{ISA} - C_{Tc4})\right) \tag{4.47}$$

With

Δt_{ISA}	Temperature difference between OAT and the reference ISA value
T_0	Nominal Thrust without temperature correction
C_{Tci}	Specific aircraft parameters

The coefficients C_{Tc5} and C_{Tc4} are provided for specific aircraft that do not reflect the aircraft considered in this report. Furthermore, simplified flat rate temperature considerations through the Δt_{ISA} increment are already included in this equation, which can be determined more accurately if certain information is available from the AFM. As the AFM is available for the aircraft considered in this report and permits detailed flat rate temperature considerations, the EUROCONTROL approach shall not be applied.

Raymer 1989 states that thrust can be corrected as shown in Eq. 4.48:

$$T_{true} = T_0(1 - 0.0075 \cdot \Delta t_{ISA}) \tag{4.48}$$

With

Δt_{ISA}	Temperature difference between OAT and the reference ISA value
T_0	Nominal thrust without temperature correction

Engine Flat Rate Characteristics

The flat-rate OAT is a temperature at which the engine has been flat-rated, which means that in order to preserve the engine's durability and lifetime, the engine is de-rated from its maximum level of thrust for the respective environmental conditions.

Thrust decays with rising outside air temperature as can be seen in equation 4.35. However, this would imply that a jet engine which is operated at lower temperatures than its respective design point would consequently produce a higher thrust rating. Clearly though, this higher thrust rate would increase the wear on the engine. The Interstage Turbine Temperature (ITT) and max Revolutions per Minute (RPM) limits[6] constitute the envelope for maximum thrust at different altitudes and outside air temperatures.

According to **Bräunling 2004**, these temperature limits are a function of the pressure altitude. A flat-rated engine produces thrust below its flat-rate temperature only at its flat-rate Engine Pressure Ratio (EPR). The thrust limiting flat-rate temperature is also referred to as T_{REF}. What this means is that the density correction for the engine due to temperature influence as outlined in the previous section is only applied for OAT greater than the flat rate temperature limit. Below this limit, the thrust remains constant and varies only with pressure altitude and Mach Number, as can be approximated by **Bartel & Young 2007**.

This relationship results in the thrust-to-OAT relationship shown in Fig. 4.5 which was derived from the simulation and Learjet 35A/36A data presented in this report.

6 See Appendix D for Learjet TFE-731-2 ITT and RPM limit envelope chart

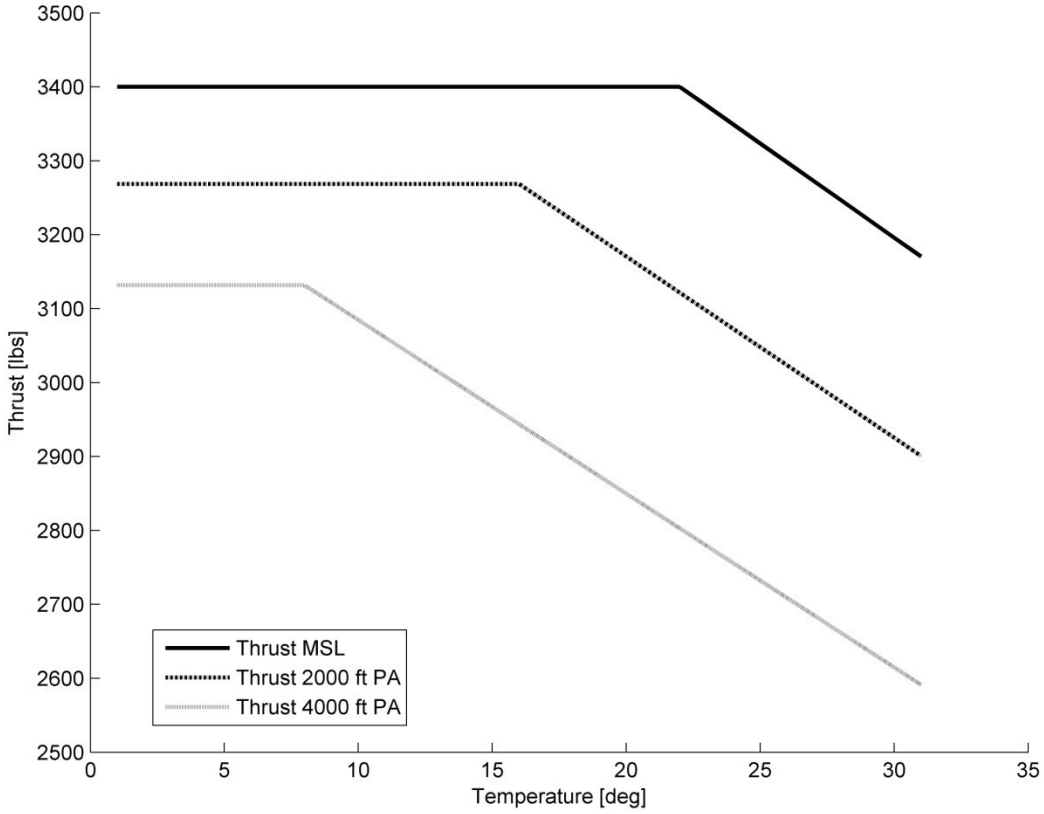

Fig. 4.5 Thrust Flat Rating for different Pressure Altitudes, TFE-731-2 Turbofan Engine
Baseline: Installed Thrust on Learjet 35A/36A

The flat rate temperature limit is determined from the N1 RPM to OAT chart such as the one attached in Appendix D of this report exemplarily for the Learjet 35A/36A. According to **Bräunling 2004**, the flat rate temperature is reached at the OAT at which the N1 RPM for the appropriate pressure altitude reaches its maximum. A detailed discussion on the flat rate temperature limit determination of the exemplary Learjet 35A/36A engine from the ITT/RPM limit chart is done in Section 6.7.

To conclude the thrust variation discussion, a consideration of *installed vs. uninstalled thrust*, a *flat-rated engine performance determination* according to OAT flat rate limit and a *Mach number/pressure altitude correction* according to **Bartel & Young 2007** in combination with *Non-ISA Temperature Variation Corrections* above the flat rate temperature will provide the most reliable results. A validation against actual thrust data from flight test results will follow in the parameter discussion to show that the theoretical assumptions also match the reality.

4.1.7 Aerodynamic Lift on Ground

The Lift force on ground plays an important role when determining the drag force due to rolling or braking resistance, as the wheel load which is needed for the determination of the friction force is dependant from the lift.

The Lift in general can be obtained from equation 4.49:

$$L = \frac{\rho}{2} v^2 \, C_{L,G} S_W \tag{4.49}$$

With

$C_{L,G}$	Lift coefficient on ground
v	Aircraft speed (CAS/EAS for the takeoff phase)
S_W	Wing reference area

The Lift Coefficient on ground $C_{L,G}$ describes the lift coefficient for the complete aircraft. It needs to be broken down into the contributing components of the aircraft, notably the wings, horizontal tailplane and fuselage.

For the overall aircraft lift coefficient, equation 4.50 applies:

$$C_{L,G} = C_{L0} + C_{L\alpha,W} \, \alpha + C_{L,H} \, i_h + \Delta C_{L,F} + \Delta C_{L,fuselage} \tag{4.50}$$

With

$C_{L,G}$	Overall aircraft lift coefficient on ground
C_{L0}	Zero lift coefficient
$C_{L\alpha,W}$	Wing lift curve slope
α	Wing Angle of Attack (AOA), on runway equals wing incidence angle
$C_{L,H} \, i_h$	Lift contribution of the trimmed horizontal stabilizer
$\Delta C_{L,F}$	Lift increment due to flap extension
$\Delta C_{L,fuselage}$	Lift increment due to fuselage

Zero Lift and Wing Lift Coefficients

The wing lift coefficient consists of two parts, the zero lift coefficient of the wing and the lift due to an incidence angle of the airfoil.

$$C_{L,W} = C_{L0} + C_{L\alpha,W}\,\alpha \tag{4.51}$$

With

$C_{L,W}$ Wing Lift Coefficient

The wing lift coefficient estimation is made according to the approaches outlined in **DATCOM 1978.** The estimation methods in this source are approximations derived from numerous tests. The estimations do not consider boundary layer disturbances through surface roughness, curvatures, heat transfer and pressure gradients, but will be of adequate precision for means of this report.

The **Wing Lift Curve Slope** $C_{L\alpha,W}$ is determined from equation 4.52

$$C_{L\alpha,W} = \frac{2\pi A}{2 + \sqrt{\frac{A^2\beta^2}{\kappa^2}\left(1 + \frac{\tan^2\varphi_{50}}{\beta^2} - M^2\right) + 4}} \tag{4.52}$$

With

$$\beta = \sqrt{1 - M^2} \tag{4.53}$$

And

A	Aspect ratio of the wing
β	Reciprocal value of the Mach number correction
κ	Correction factor of the airfoil section lift curve slope
φ_{50}	Sweep angle at 50% cord

It is possible to reduce the correction factor κ of the airfoil section to 1, also the Mach number correction factor may be set to 1 due to the fact that the takeoff phase as outlined in section 4.1.5 is situated in a low Mach number region.

Hence, Eq. 4.53 simplifies to

$$C_{L\alpha,W} = \frac{2\pi A}{2 + \sqrt{A^2(1 + \tan^2 \varphi_{50} - M^2) + 4}} \tag{4.54}$$

In order to correct the sweep angle, a conversion according to **Scholz 1999** is used.

$$tan\varphi_n = tan\varphi_m - \frac{4}{A}\left(\frac{n-m}{100} \cdot \frac{1-\lambda}{1+\lambda}\right) \tag{4.55}$$

With

n	Chord location at which sweep angle is desired
m	Chord location at which sweep angle is known
λ	Taper ratio of the wing

For the **Zero Lift Coefficient**, the Eq. 4.56 applies, using the Wing Lift curve Slope from Eq. 4.54:

$$C_{L0} = C_{L\alpha,W}\alpha_{0,W} \tag{4.56}$$

According to **DATCOM1978**, where the zero-lift angle of attack$\alpha_{0,W}$ of the wing can be determined from Eq. 4.57. A linear spanwise twist distribution is assumed.

$$\alpha_{0,W} = \alpha_0 + \frac{\Delta\alpha_0}{\varepsilon_t}\varepsilon_t \frac{\alpha_{0,M\ true}}{\alpha_{0,M=0,3}} \tag{4.57}$$

With

α_0	Profile zero angle of attack (between -2° and -4°, **Anderson 2007**) For NACA 64A airfoils, values are provided in Fig. 4.8
ε_t	Wing twist angle tip to root in degrees, negative for washout
$\frac{\alpha_{0,M\ true}}{\alpha_{0,M=0,3}}$	Mach Number correction acc. to Fig. 4.6
$\frac{\Delta\alpha_0}{\varepsilon_t}$	Change in zero lift angle of attack due to wing twist acc. to Fig. 4.7

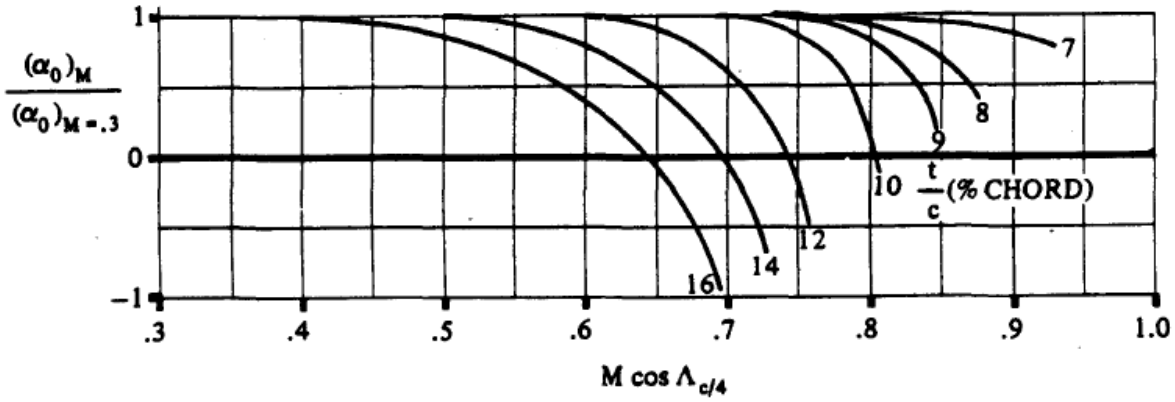

Fig. 4.6 Determination of the Mach Correction Factor for Zero Lift Angle of Attack (**DATCOM 1978**)

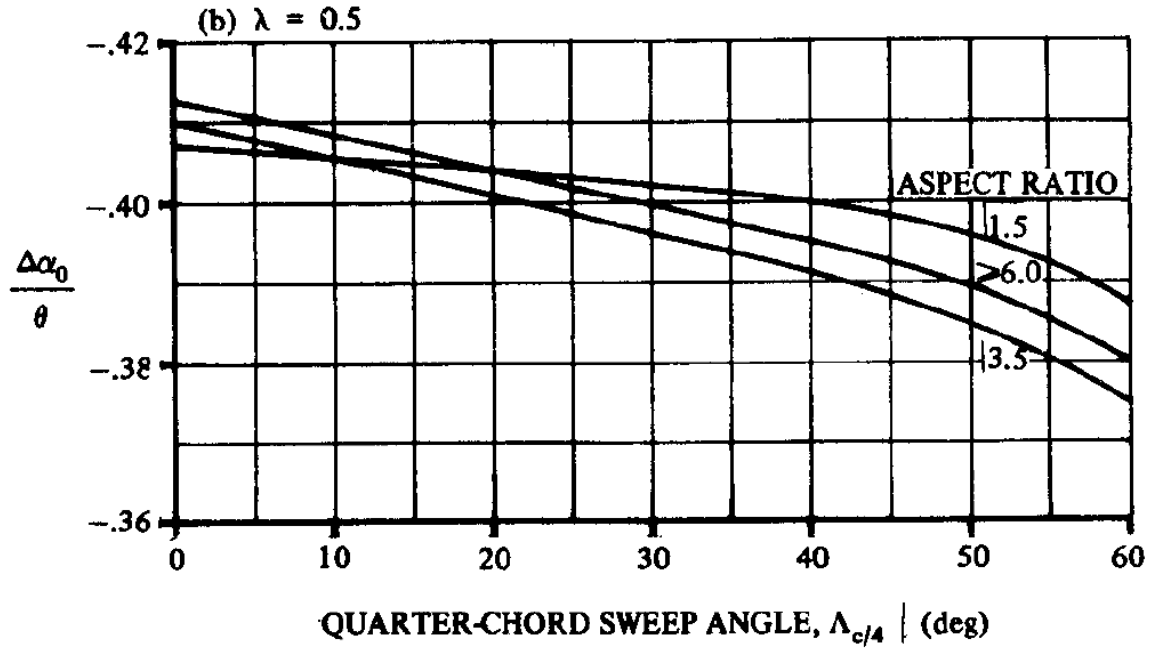

Fig. 4.7 Determination of the Wing Twist to Zero Lift Angle of Attack Ratio (**DATCOM 1978**)

As the Wing Lift Curve Slope $C_{L\alpha,W}$ is dependent from the Mach number, the lift coefficient varies slightly with Mach number. If a time-step wise calculation method can be applied, the lift coefficient should therefore be calculated for the appropriate velocity at that time. For simplification, as the AOA does not change while the aircraft is on the runway, it can also be assumed constant.

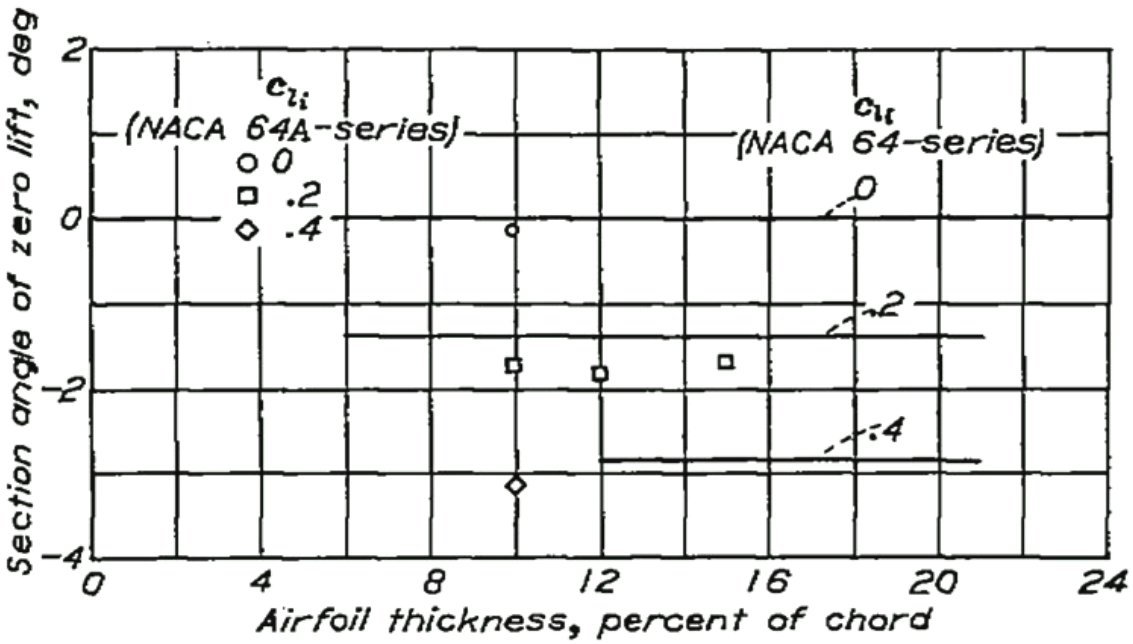

Fig. 4.8 Section Angle of Zero Lift for NACA 64A profiles (**NACA Report 903**)

Lift Coefficient Increment due to Flaps

The flaps on the wing are acting as a lift augmentation device; therefore the lift coefficient of the aircraft wing is increased as shown in Eq. 4.50. The lift coefficient increment $\Delta C_{L,F}$ is calculated from the section lift coefficient $c_{L,F}$ with flap influence as shown in Eq. 4.58

$$\Delta C_{L,F} = c_{L,F} \cdot K' \cdot \frac{S_{flap}}{S_W} \tag{4.58}$$

With

K'_{flap}	Empirical correction factor for flap effectiveness acc. to Fig. 4.9
$c_{L,F}$	Section lift coefficient with flap influence acc. to Eq. 4.59
S_W	Wing area
S_{flap}	"Flapped" area along the wing chord acc. to Fig. 4.10

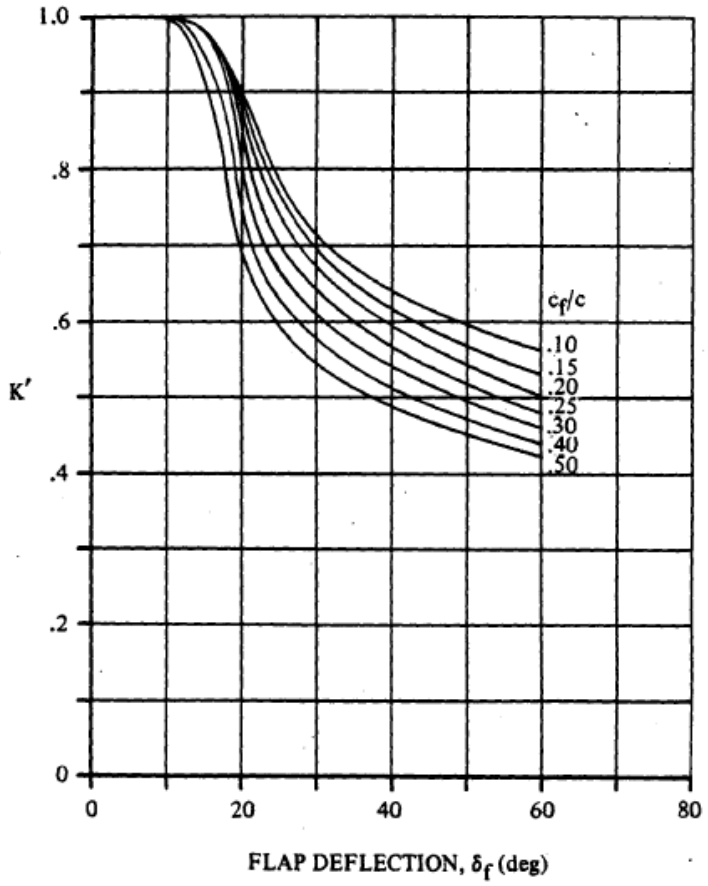

Fig. 4.9 Empirical correction Factor for Flap Effectiveness (**DATCOM 1978**)

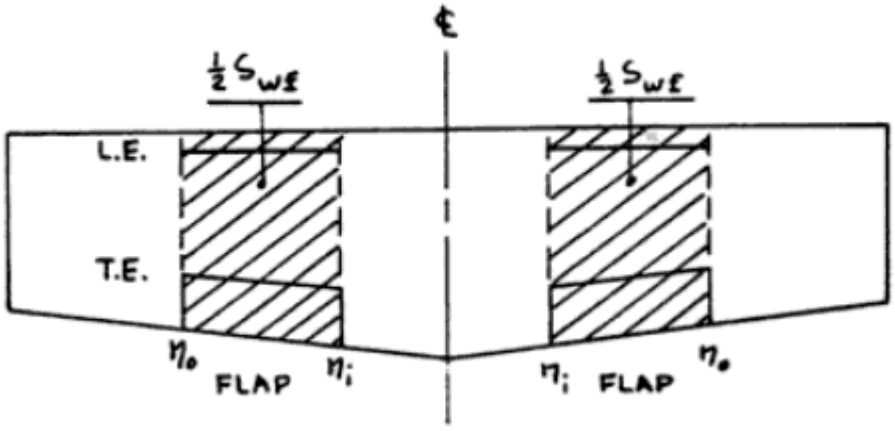

Fig. 4.10 Flapped Area of the Wing along the Chord Line(**Roskam VI**)

The section lift coefficient with flap influence as applicable for a single slotted flap is given by Eq. 4.59 in accordance to **DATCOM 1978**.

$$c_{L,FLAP} = c_{L\alpha} \cdot \alpha_\delta \cdot \delta_F \tag{4.59}$$

With

α_δ	Flap Lift effectiveness parameter acc. to Fig. 4.11
δ_F	Flap deflection angle in radians
$c_{L\alpha}$	Profile lift coefficient

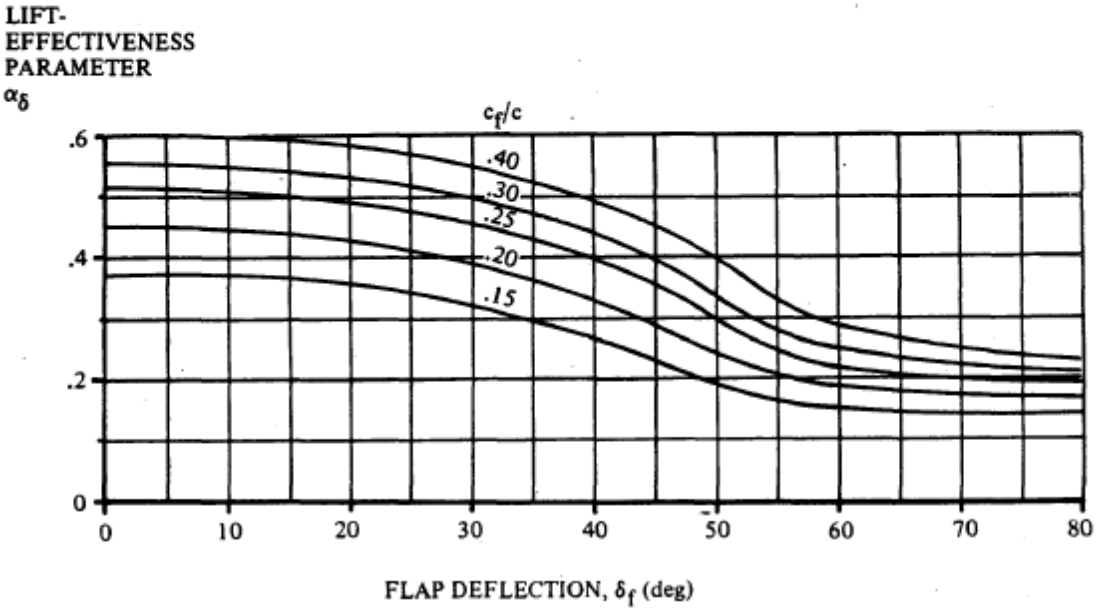

Fig. 4.11 Lift Effectiveness Parameter by Flap Deflection Angle (**DATCOM 1978**)

The flap extension does not only have an effect in terms of lift coefficient increment, the flap extension also reduces the zero lift angle of attack due to the increased camber of the airfoil section. According to the empirical equation provided by **DATCOM 1965**, the zero lift angle increment in degrees can be estimated from the flap deflection angle.

$$\Delta\alpha_0 \approx -1{,}15 \frac{c_f}{c} \delta_F \tag{4.60}$$

With

$\Delta\alpha_0$	Zero lift angle of attack change due to flap deflection
c_f	Flap segment chord length
c	Wing chord length

Lift Coefficient Increment due to Fuselage Carryover

The lift coefficient of the aircraft as shown in Eq. 4.50 accounts for the lift contribution of the horizontal stabilizer. By the presence of the fuselage, an interaction between the lift created by the wing alone is also created. This effect shall be examined first, as it is related to the lift increment due to flap extension.

According to **Torenbeek 1982**, it has to be considered that the lift distribution across the wing is disturbed by the fuselage and reduced.

The easiest assumption would be to assume that the fuselage does not create any lift during takeoff, which may be true for large flap deflections when a large gap between the flaps and the fuselage exists. In this case it is valid that

$$S_{exp} = S_W - S_{fuselage} \tag{4.61}$$

With

S_{exp}	Exposed wing area
S_W	Reference wing area
$S_{fuselage}$	Fuselage area intersecting with the wing reference area

If this case shall be applied, in the lift force equation(see equation 4.49) the reference wing areaS_W should be set as the net wing area S_{exp}.

If a more elaborated approach is chosen, **Torenbeek 1982** suggests the lift carry-over by the fuselage to be estimated from the lift generated by the wing center section if it was assumed to be extended to the aircraft centerline.

Thus, the lift coefficient increment due to fuselage interference $\Delta C_{L,fuselage}$ would be calculated from Eq. 4.62.

$$\Delta C_{L,fuselage} = K_{ff} \cdot \frac{2}{1+\lambda} \cdot \frac{b_{fi}}{b} \cdot C_{L0} \tag{4.62}$$

With

K_{ff}	Lift interference factor ($0 < K_{ff} < 2/3$) according to **Torenbeek 1982**
b_{fi}	Fuselage width at wing intersection
b	Wing span

As a lift increment to the overall aircraft lift coefficient is added, even though the overall wing lift is disturbed by the fuselage, it is obvious that also in this case, the wing reference area in Eq. 4.50 needs to be substituted by the exposed wing area as shown for Eq. 4.61. In this case however, by using the $\Delta C_{L,fuselage}$ increment, the lift over the fuselage is not assumed to be zero.

Other lift increments due to the fuselage, such as the lift created by the cylindrical body, are assumed to be zero, as the aircraft accelerating on the runway does not incur a fuselage angle of attack.

Lift force on the Horizontal Tailplane

For the horizontal tailplane, two major effects need to be considered for the takeoff run. These are the downwash created by the main wing, and the trim setting of the horizontal stabilizer for the takeoff.

In case of a variable incidence horizontal stabilizer that pivots around its rear spar, as is the case for the Learjet 35A/36A, the angle of attack of the complete horizontal stabilizer is altered for trim setting. For takeoff, the trim setting should be set such that the elevator forces necessary for the rotation are acceptable and the aircraft is trimmed out for the initial climb. The more aft the Center of Gravity (CG) of the aircraft is located, the less nose-up force needs to be created. For the engine-out analysis, the most aft CG is the most conservative assumption that should be taken into account for the takeoff performance calculation. Hence, the necessary trim force is reduced or may even be resulting in a slight nose-down trim setting as for the Learjet 35A/36A.

The downwash effect on the horizontal stabilizer refers to the fact that the free stream velocity vector on the horizontal tail plane is changed by the flow over the main wing. This leads to the air flow acting on the horizontal stabilizer to come from a slight upward angle, reducing the effective incidence angle of the horizontal stabilizer. This effect would therefore induce a slight nose-up pitch moment. However, if the aircraft is equipped with a T-tail such as the Learjet 35A/36A, according to **Torenbeek 1982** the downwash effect on the horizontal stabilizer is very small and can be neglected.

For means of this performance calculation, both effects are expected to be acting in opposite directions and be of small magnitude, and have subsequently been considered negligible.

4.1.8 Aerodynamic Drag on Ground

The drag force of the aircraft as shown in the equation of motion is a direct contributor to the Takeoff Distance. As a result, the accurate determination of the drag coefficient is of high importance for the set of parameters to be developed for the performance calculation.

The Drag in general can be obtained from equation 4.63:

$$D = \frac{\rho}{2} v^2 \, C_D S_W \tag{4.63}$$

With

C_D	Drag coefficient
v	Aircraft speed (CAS/EAS for the takeoff phase)
S_W	Wing reference area

The Drag Coefficient on ground C_D describes the drag coefficient for the complete aircraft. It needs to be broken down into the contributing components of the aircraft, notably the drag due to lift, profile drag and additional drag force contributors.

For the overall aircraft drag coefficient, equation 4.64 applies:

$$C_D = C_{D,P} + C_{D,i} + C_{D,c} \tag{4.64}$$

With

$C_{D,P}$	Profile drag coefficient
$C_{D,i}$	Induced drag coefficient due to lift
$C_{D,c}$	Compressibility drag coefficient, negligible below M=0,3

The compressibility effect as outlined before is assumed to be zero due to the small flight speeds experienced by the aircraft in the considered phase. The induced drag coefficient and the profile drag coefficient are therefore the remaining drag coefficient contributors.

Induced Drag Coefficient

For the induced drag coefficient on ground $C_{D,i,G}$, equation 4.65 applies.

$$C_{D,i,G} = \emptyset \frac{{C_L}^2}{\pi A e_{T/O}} \tag{4.65}$$

With

$e_{T/O}$	Oswald efficiency factor during takeoff run
$\emptyset$	Ground effect factor

The ground effect factor is determined as the runway surface influences the lift and especially vortex generation around the wing. The ground effect reduces the drag due to lift.

$$\emptyset = \frac{\left(16\frac{h}{b}\right)^2}{1 + \left(16\frac{h}{b}\right)^2} \tag{4.66}$$

With

h	Wing-to-ground distance
b	Wing span

Oswald Efficiency Factor

In order to correctly determine the induced drag coefficient, it is necessary to know the Oswald efficiency factor, taking in account any deviations from the optimal, elliptical lift distribution on the wing. It can be determined in two ways.

According to **Nita, Scholz 2012**, the Oswald efficiency factor can be approximatively estimated as a function of leading edge sweep angle and aspect ratio if no other aircraft data are available, as shown in Eq. 4.67a with Eq. 4.67b.

$$e = \frac{\left(1 - 2\left(\frac{d_{fuselage}}{b}\right)^2\right)\left(-0{,}0015213\left(\frac{M}{0{,}3} - 1\right)^{10{,}8209489} + 1\right) k_{e,D0}}{1 + \left(0{,}0524\,{\lambda_f}^4 - 0{,}15\,{\lambda_f}^3 + 0{,}1659\,{\lambda_f}^2 - 0{,}0706\,\lambda_f + 0{,}0119\right) A} \tag{4.67a}$$

Where

$$\lambda_f = \lambda - 0{,}45\,\mathrm{e}^{0{,}0375\,\varphi_{25}} + 0{,}357 \tag{4.67b}$$

With

e	Oswald efficiency factor
$d_{fuselage}$	Fuselage diameter
b	Wing span
$k_{e,D0}$	Statistical correction factor, Businessjet: $k_{e,D0} = 0{,}864$ (**Nita, Scholz 2012**)
A	Aspect ratio of the wing
e	Euler's Number
φ_{25}	Quarter chord sweep angle

However, the Oswald efficiency factor is degraded in takeoff configuration due to the extension of flaps which further make the lift distribution deviate from optimal conditions. Therefore, an alternative approach is presented to obtain *e* during the ground roll from known data of the aircraft in flight.

In reversal of Eq. 4.65 and assuming literature values for e from **Scholz 1999**, the following relationships can be found and used with existing aircraft data.

$$e_{cruise} = \frac{C_L^2}{\pi \cdot A \cdot C_{D,induced,cruise}} \tag{4.68}$$

This assumes that the induced drag coefficient in cruise is known, along with the corresponding lift coefficient in cruise. With these parameters known, the Oswald efficiency factor can be obtained by a relation to literature values.

$$e_{T/O} = e_{T/O,Lecture}\left(\frac{e_{cruise}}{e_{cruise,Lecture}}\right) \tag{4.69}$$

With

$e_{cruise,Lecture}$ Oswald factor for cruise from **Scholz 1999** lecture notes
Assumed: $e_{cruise,Lecture} = 0.85$

$e_{T/O,Lecture}$ Oswald factor for takeoff from **Scholz 1999** lecture notes
Assumed: $e_{T/O,Lecture} = 0.7$

Profile Drag Coefficient

The profile drag coefficient of the aircraft is constituted from the zero lift drag coefficient and the sum of all drag coefficient increments due to additional contributors, such as flaps, extended gear, under-wing stores.

$$C_{D,P} = c_{D,0} + \sum \Delta c_D \tag{4.70}$$

Estimation of the Zero Lift Drag Coefficient

The first step in the profile drag coefficient estimation is the determination of the zero lift drag coefficient $c_{D,0}$ of the aircraft.

The aircraft moving in the airflow creates various forms of drag through interference with the air flow. Friction on the surfaces of the aircraft areas wetted by the air flow is the main contributor to the zero drag coefficient.
According to **Raymer 1989**, it is estimated by applying an equivalent skin friction coefficient, C_{fe} to the ratio of wing reference area S_W to the total wetted area S_{wet} of the aircraft.

$$c_{D,0} = C_{fe} \frac{S_{wet}}{S_W} \tag{4.71}$$

With

S_{wet}	Area of the aircraft wetted by the air flow around all aircraft parts
C_{fe}	Equivalent skin friction coefficient acc. to **Raymer 1989**
	$C_{fe} = 0{,}003 \ldots 0{,}004$ for civil jet aircraft

The equivalent skin friction coefficient can be augmented by 5% accounting for additional drag creating items such as antennas, trim drag, interference drag, control surface gaps etc.

The wetted area of the aircraft is to be determined by making an analysis of the aircraft based on geometrical surfaces that are measureable, the exposed areas S_{exp}. A set of specific equations permits to calculate the wetted areas from the exposed areas, these are provided in appendix E of this report along with an example for the Learjet 35A/36A.

Drag Increment due to Flap Extension

The drag increment due to the extension of the aircraft flaps is twofold. The first contribution is the amount of drag the flaps create in the induced drag coefficient by augmenting the lift coefficient for the aircraft.

This is approximated by using the lift coefficient including the lift due to flap increment for the induced drag determination. Additionally, a profile drag coefficient is to be applied due to flap extension.

According to **Roskam VI**, the profile drag coefficient for extended flaps augments with the angle of flap deflection as a function of the relation between wing and flap chord line, which appears reasonable. According to this approach, the relationship shown in Fig. 4.12 is obtained.

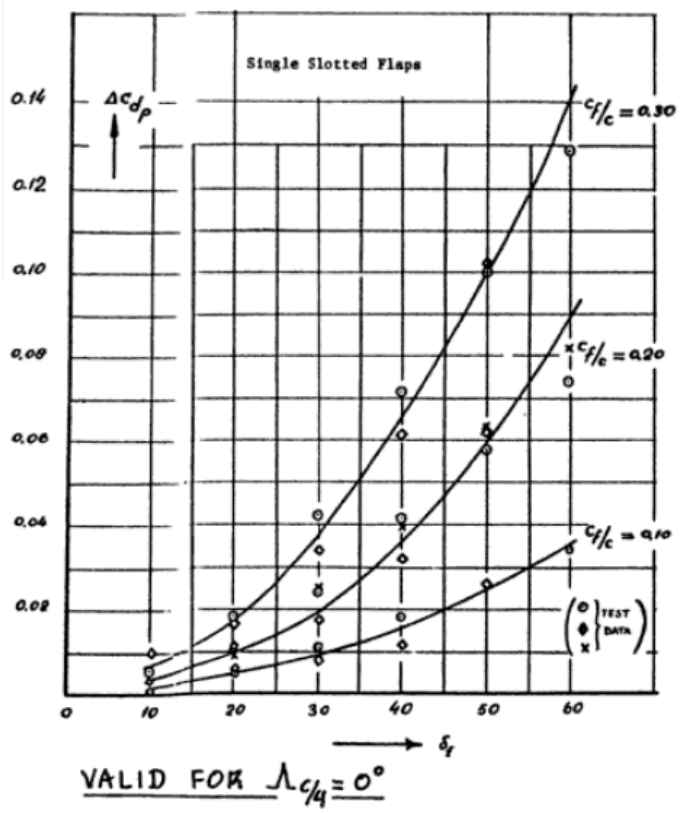

Fig. 4.12 Profile Drag Increment due to Flap Deflection (**Roskam VI**)

Even though Fig. 4.12 provides values for zero sweep angle, it can be seen that for very small flap deflection angles such as to be expected during the takeoff phase, the flap induced drag coefficient increment is very small, in the region of $\Delta c_{D,flap} = 0{,}005$ for 8° flap deflection, with the influence of the chord line ratios c_f/c diminishing.

Therefore, the approach proposed by **Loftin 1980** appears to be of sufficient precision for the performance calculation during the takeoff phase. It is valid for $C_L \geq 1.1$, will therefore be of relevance in the flight phase after liftoff.

$$\Delta c_{D,flap} = 0.05\, C_L - 0.055 \qquad \textbf{(4.72)}$$

Drag Increment due to Gear Extension

The drag increment due to gear extension can be determined based on many different methods. Generally, according to **Roskam, Lan 1997**, the gear drag is connected to the lift of the aircraft wing due to downwash and vortex effects influencing the direction of the air flow directed towards the gear. Fig. 4.13 shows this relationship directly as a function of the flap deflection angle.

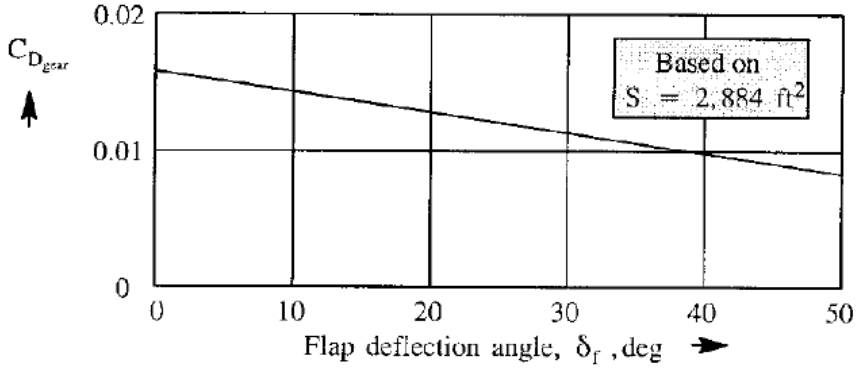

Fig. 4.13 Gear Drag Coefficient as a Function of the Flap Deflection Angle (**Roskam, Lan 1997**)

Roskam I provides estimates for the gear drag coefficient increment in the range of

$$\Delta c_{D,gear} = 0{,}015 \ldots 0{,}025$$

but declares this as a first, rough estimate.

Torenbeek 1982 provides two methods to determine the undercarriage drag coefficient increment. The application of the first method, which is considering local flow conditions (but not considering fuselage or wing gear bay openings), leads to a strongly airplane lift coefficient dependant gear drag coefficient increment in the range of:

$$\Delta c_{D,gear} = 0{,}0149 \left(\text{for } C_{L,G} \sim 0{,}138\right) \ldots 0{,}0107 \left(\text{for } C_{L,LOF} \sim 1{,}318\right)$$

A more accurate gear drag determination for a retractable gear configuration including drag through gear bay openings is done according to the approach given by **Hoerner 1965**, based on the gear frontal area.

$$\Delta C_{D,gear} = c_{D,gear} \frac{S_{gear}}{S_W} \tag{4.73}$$

With

S_{gear}	Gear frontal area
$c_{D,gear}$	Gear drag coefficient with reference to the gear frontal area acc. to Fig. 4.14

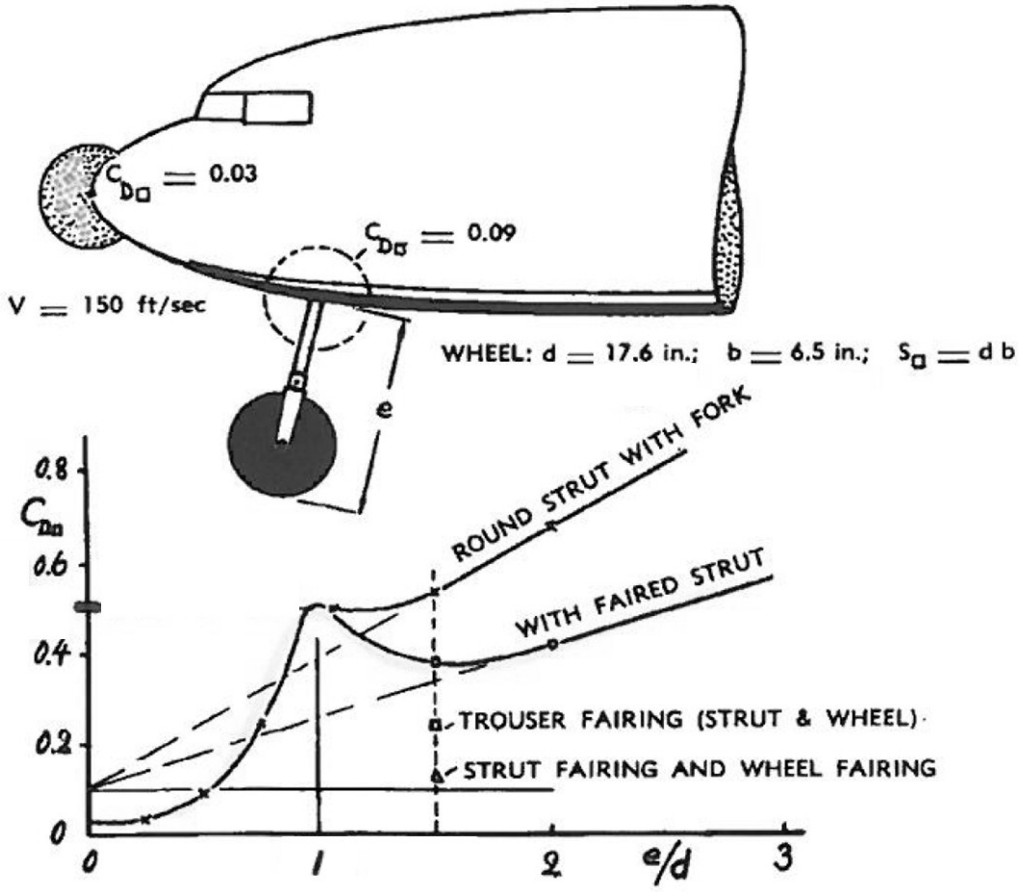

Fig. 4.14 Drag Coefficient of a Retractable Gear or Wheel Configuration (**Hoerner 1965**)

According to **Hoerner 1965**, the drag coefficient acc. to Fig. 4.14 is proportionally applicable on the wheel or the total gear area, yielding the respective drag coefficient increment for either a single wheel-strut combination or the total retractable landing gear configuration. For the takeoff performance calculation, it is necessary to consider the total gear drag coefficient increment, therefore the total gear drag area should be used as a reference area.

Drag Increment due to Under-Wing Stores Installation

The installation of additional items on the airframe has of course an impact on the overall profile drag coefficient of the aircraft as well. As the aircraft considered in this report shall be considered to be equipped with under-wing stores installed on racks under the wing, it is necessary to estimate this drag increment.

According to **Roskam VI**, the store may be considered like a small fuselage section, with the equivalent skin friction coefficient applied to the wetted area of the store surface. In an altered form that relates the store drag coefficient directly to the total aircraft drag coefficient, the approach yields:

$$\Delta C_{D,store} = \sum_i K_{store} c_{fe,store} \left(\frac{S_{wet,store}}{S_W}\right) S_{wet,store} \tag{4.74}$$

With

K_{store} Store interference factor acc. to **Roskam VI**
$K_{store} = 1{,}3$ in configuration shown in Fig. 4.15

$c_{fe,store}$ Equivalent skin friction coefficient of the store, analog to a fuselage

$S_{wet,store}$ Wetted area of the store considered

$\frac{S_{wet,store}}{S_W}$ Ratio to refer store equivalent skin friction coefficient to complete aircraft

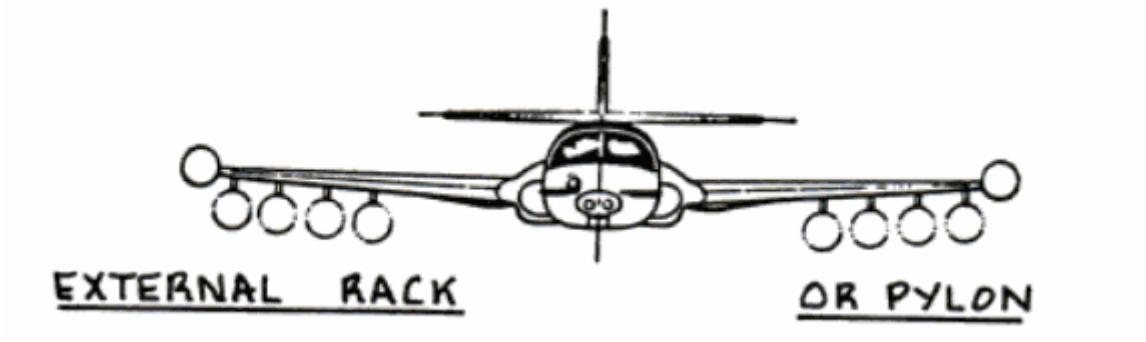

Fig. 4.15 Stores Configuration in External Rack or on Pylon (**Roskam VI**)

Plausibility Check of Lift to Drag Ratio

In order to validate the zero lift drag coefficient and the Oswald factor, a plausibility check through the determination of the maximum Lift-to-Drag Ratio E_{max} can be carried out when the required parameters are developed. This is in particular very useful due to the fact that for the Oswald efficiency factor and the zero lift drag coefficient a number of assumptions had to be taken.

For different aircraft configurations, it is therefore possible to determine E_{max} by Eq. 4.75 and compare it to usual values or glide distance data from the AFM.

$$E_{max} = \left(\frac{L}{D}\right)_{max} = \frac{1}{2}\sqrt{\frac{\pi\, A\, e}{C_{D,0}}} \tag{4.75}$$

If reasonable values for this glide ratio are obtained, the parameters determined for the zero lift drag coefficient and the Oswald efficiency factor can be judged to be reasonable as well in their combination.

4.1.9 Rolling Friction and Gravity

Aircraft mass, gravity and runway friction force in combination with a runway slope are closely related to each other. The runway friction F_f is determined from the normal force of the tires on the runway surface and the friction coefficient, the downhill or uphill force depends only on the aircraft mass and the runway slope. The general relationships are shown in Fig. 4.16.

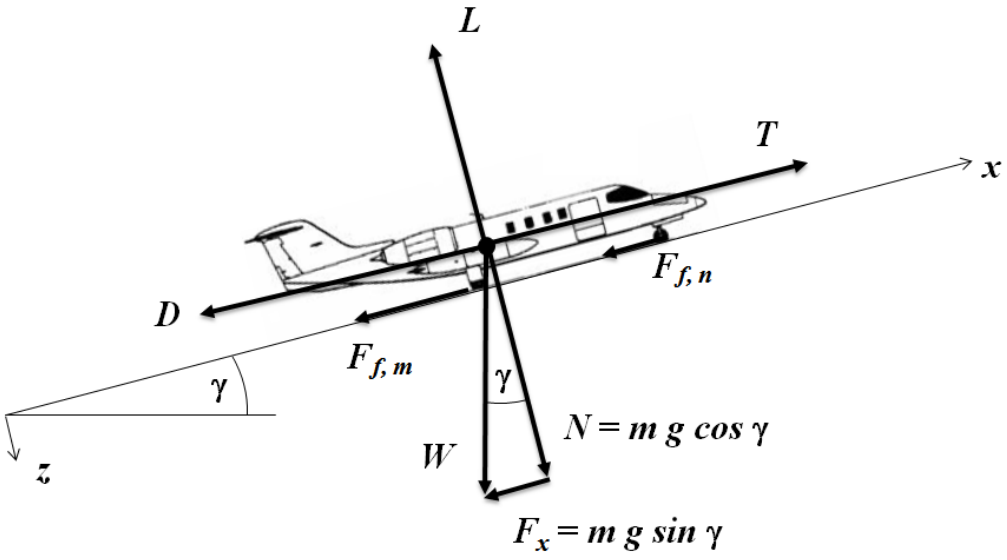

Fig. 4.16 Runway Slope, Friction and Downhill Force in their Relation to each other

The weight of the aircraft and the lift force together determine the vertical force acting on the wheel. This resulting force acting normal to the runway surface is then multiplied with the rolling friction coefficient to yield the *friction force component* due to friction of the tire and the runway.

If the friction coefficient can be assumed equal for the nose and the main wheel, the normal forces acting on each of the wheels can be added up and yield the total aircraft mass. The friction forces $F_{f,m}$ and $F_{f,n}$ then simplify to the relation shown in Eq. 4.76.

$$F_{friction} = \mu_{friction} (N - L) \tag{4.76}$$

With

$$N = m \cdot g \cdot \cos\gamma \tag{4.77}$$

And

L	Lift force of the Aircraft
γ	Runway Slope
m	Aircraft mass

When the runway slope is not zero, the weight of the aircraft itself needs to be considered as well due to the downhill force or the grade resistance, depending whether the runway is upward or downward sloping.

$$F_X = m \cdot g \cdot \sin\gamma \tag{4.77}$$

Together, the above equations determine the complete force due to aircraft mass and runway friction in consideration of a runway slope.

$$F_{retardation} = \mu_{friction}(m \cdot g \cdot \cos\gamma - L) + m \cdot g \cdot \sin\gamma \tag{4.78}$$

In order to determine the friction force, it is necessary to determine the surface rolling friction coefficients. According to **Scholz 1999**, there are different assumptions on the rolling friction to be found in the literature.

Table 4.1 Static Surface Rolling Friction Coefficients, from **Scholz 1999**

Surface	**Kohlman 1992**	**Currey 1988**	**Torenbeek 1988**
$\mu_{friction}$ *Concrete or Tarmac, wet and dry*	0,02 ~ 0,05	0,008 ~ 0,02	0,02

According to Table 4.1, there is a wide spread from 0.02 to 0.05, furthermore no distinction between wet and dry rolling friction is being made explicitly.

According to **NASA TP-D2770**, the rolling friction (as well as the braking friction) varies with speed. The time-step wise calculation method applied in this report permits using a variable friction coefficient. Therefore, the data Fig. 4.17 is used. It shows a diagram derived from flight test data with a Cessna Citation, a business jet of comparable size to a Learjet 35A/36A.

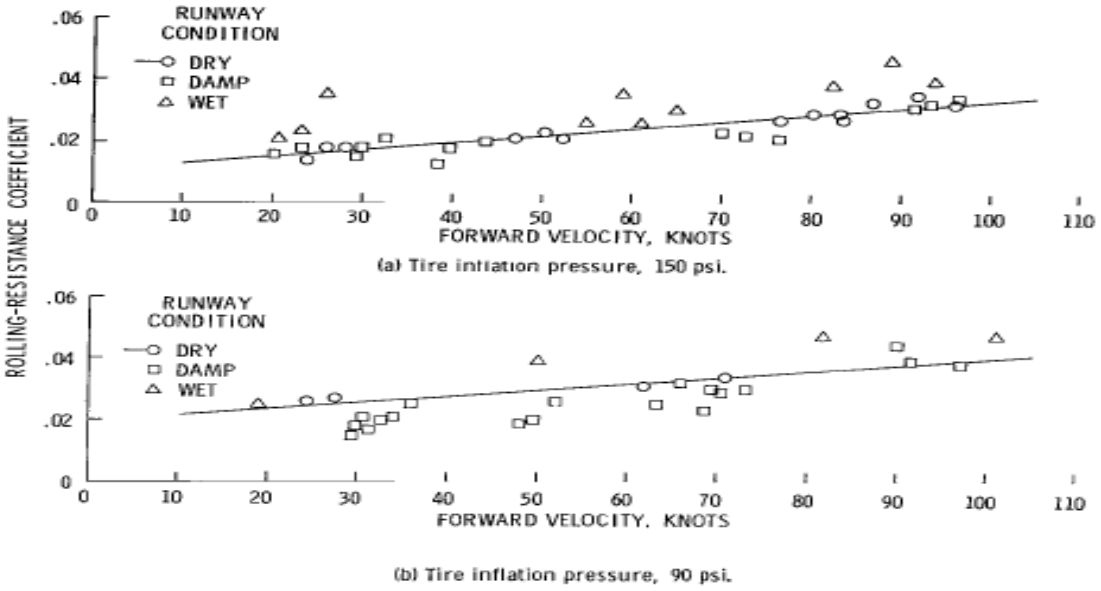

Fig. 4.17 Dynamic Surface Rolling Coefficients for a Small Business Jet (**NASA TP-2770**)

Based on Fig. 4.17, the surface rolling friction coefficient was read from the diagram for various speeds and approximated linearly in order to obtain a equation that can be integrated in a time-step wise takeoff performance simulation. The drag reduction factor due to aquaplaning is not considered.

For the dry runway, the friction-coefficient to velocity equation was linearly approximated as:

$$\mu_{friction,dry} = 0{,}0002\ v_{aircraft} + 0{,}0135 \tag{4.79}$$

For the wet runway, the friction-coefficient to velocity equation was linearly approximated as:

$$\mu_{friction,wet} = 0{,}0002\ v_{aircraft} + 0{,}0165 \tag{4.80}$$

With

$v_{aircraft}$ Aircraft ground speed in knots

As can be seen from Eq. 4.79 and 4.80, the resulting rolling friction coefficients are in the same order of magnitude as the constant friction coefficients provided in Table 4.1, with the advantage of greater precision for the performance calculation.

4.1.10 Displacement, Collision and Skin Friction Drag due to Water Spray

As outlined in Chapter 2, there are different components of drag force which are acting on the aircraft on a wet runway due to precipitation. This section shall now provide the equations provided as acceptable means of compliance by **EASA AMC 25.1591**.

Displacement Drag of the Tires

In accordance to Section 7.1.2 of **EASA AMC 25.1591**,the displacement drag of the tires is calculated from Eq. 4.81.

$$D_{displ} = n_{tire}\, c_{D,displ} \cdot \frac{1}{2} \cdot \rho_{water} \cdot v_{ground}^2 \cdot A_{tire,subm} \tag{4.81}$$

With

D_{displ}	Tire water displacement drag component
$c_{D,displ}$	Displacement drag coefficient, $c_{D,displ}$ = 0,75 with reference to the tire frontal area A_{tire}
ρ_{water}	Water density
n_{tire}	Number of wheels

And $A_{tire,subm}$ as the tire frontal area submerged in water, to be calculated acc. to Eq. 4.82:

$$A_{tire,subm} = b_{eff} \cdot d_{cont} \tag{4.82}$$

With

b_{eff}	Effective tire width
d_{cont}	Contaminant depth (water depth on the runway)

The drag determined like this for one wheel is then multiplied by the total number of wheels on the aircraft if no differentiation between different tires or tire pressures needs to be made. The drag reduction factor due to aquaplaning needs to be considered.

Determination of the Effective Tire Width

The effective tire width according to **EASA AMC 25.1591** needs to take into account the deflection of the loaded tire.

$$b = 2W_{tire}\left[\left(\frac{d_{cont}+\delta_{tire}}{W_{tire}}\right)-\left(\frac{d_{cont}+\delta_{tire}}{W_{tire}}\right)^2\right]^{\frac{1}{2}} \tag{4.83}$$

With

W_{tire}	Nominal tire width
δ_{tire}	Deflection of the tire in m, to be obtained by manufacturer data

In order to calculate the tire deflection δ in m as required by Eq. 4.83, it is necessary to know the geometry of the tire. According to **Goodyear 2002**, the normal deflection rate of an aircraft tire lies between 31% and 35% of the nominal tire diameter for the static load case. By knowing this deflection rate, it is possible to recalculate the actual deflection in absolute values by Eq. 4.84 from **Goodyear 2002**.

$$SLR = \frac{D_M}{2} - d_{\%}\left(\frac{(D_M - D_F)}{2}\right) \tag{4.84}$$

With

SLR	Static Load Radius
D_M	Mean overall tire diameter
D_F	Rim flange outer diameter
$d_{\%}$	Percental tire deflection, $d_{\%} = 32\% \ldots 35\%$ acc. to **Goodyear 2002**

The nominal deflection δ then results from the difference between the mean overall tire diameter and the Static Load Radius.

$$\delta_{tire} \;=\; SLR - \frac{D_M}{2} \;=\; d_{\%}\left(\frac{(D_M - D_F)}{2}\right) \tag{4.85}$$

Fig. 4.18 is used to visualize the relations set up in Eq. 4.84 and 4.85.

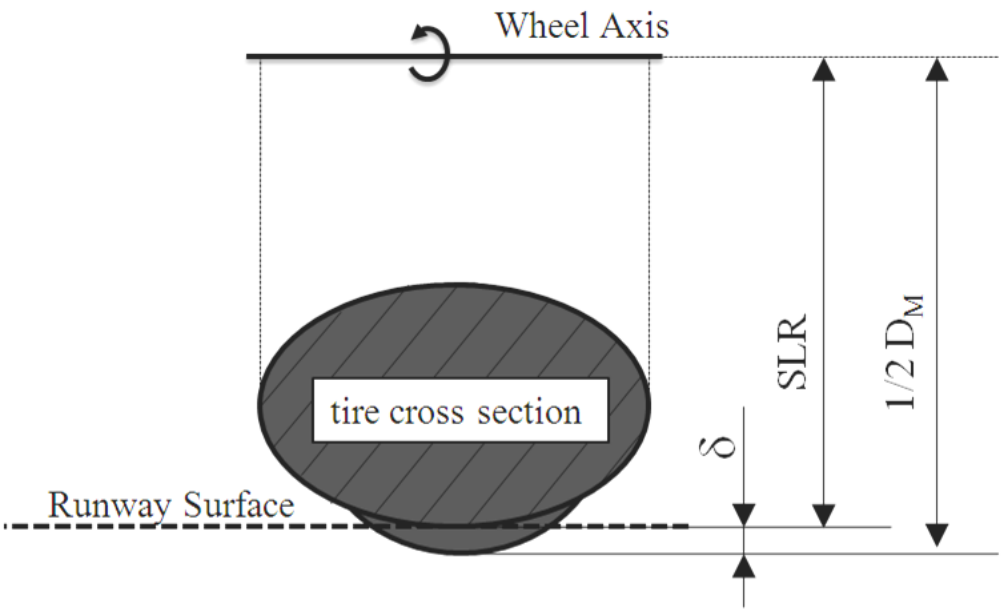

Fig. 4.18 Tire Deflection, Static Load Radius and Mean Overall Diameter

Skin Friction Drag

The skin friction drag can be determined according to Section 7.1.3 b.2 of **EASA AMC 25.109**. A skin friction drag coefficient due to water spray is to be applied to the length of the wetted fuselage. The wetted fuselage length L_{wetted} is assumed to amount for 75% of the total length of the fuselage, $L_{fuselage}$. This is an assumption as to where the top of the spray plume is expected to impinge on the airframe. The drag reduction factor due to aquaplaning needs to be considered.

$$D_{skin} = \frac{1}{2} c_{D,skin} \cdot \rho_{water} \cdot v^2{}_{ground} \cdot A_{tire,subm} \tag{4.86}$$

With

$$c_{D,skin} = 8 \cdot l_{wetted} \cdot 0{,}0025 \tag{4.87}$$

$$l_{wetted} = 0{,}75 \cdot l_{fuselage} \tag{4.88}$$

And

$l_{fuselage}$ Nominal length of the fuselage in ft

Spray Impingement Drag

In contrast to the skin friction drag, there is no specific equation given for the impingement drag in **EASA AMC 25.1591** or **EASA AMC 25.109**, because this drag is highly dependent on the aircraft geometry.

The impingement drag therefore varies from aircraft to aircraft, which is why Chapter 5 of this report is dedicated to the water spray impingement drag determination. Chapter 5 will therefore show a method to estimate the impingement drag as a function of geometry specific properties of the Learjet 35A/36A. The approach could also be generalized and applied to other aircraft, taking into account a changed aircraft geometry.

4.2 Air Distance

The previous sections discussed the aircraft accelerating on the runway, covering the Liftoff Distance. After the Liftoff Distance has been covered and the aircraft has reached V_{LOF}, the aircraft will have to cover a certain distance in the air until passing the obstacle or screen height. In the case of a BFL determination, the Air Distance is always part of the runway field length required and needs to be considered.

A simplified approach not taking into account the acceleration of the aircraft between V_{LOF} and V_2 is outlined in this section. This simplification can be made as the screen height is significantly reduced on a wet runway, and the aircraft under this condition does not have to reach V_2 when clearing the reduced screen height of 15 feet on a wet runway. This has been discussed in Section 3.3.

The method to determine the Air Distance is based on a simplified Roskam 1997 method from **Scholz 1999**. This approach divides the aircraft trajectory after liftoff into two separate trajectories, the bow-shaped *rotation phase trajectory* and the linear *climb phase trajectory* at a constant climb angle as shown in Fig. 4.19.

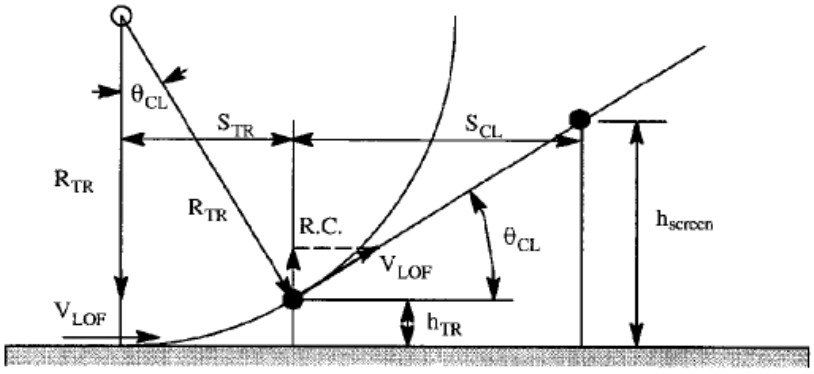

Fig. 4.19 Climb out to Obstacle Height method (**Roskam, Lan 1997**)

As the incidence angle of the aircraft changes and multiple effects influence the lift force acting on the aircraft, the lift coefficient in flight differs from the lift coefficient on ground. It is a sufficiently accurate method as proposed by **Scholz 1999** to assume that the lift at the liftoff point needs to balance the weight of the aircraft. It bases on the assumption that the aircraft rotates to a new attitude where the aircraft lift equals its weight.

At small climb angles, it can be assumed that $cos\theta_{climb} = \theta_{climb}$. This leads to the assumption that

$$L_{LOF} = W$$

or

$$\frac{1}{2}\rho \cdot v_{LOF}^2 \cdot C_{L,LOF} \cdot S_W = m \cdot g \tag{4.89}$$

With

L_{LOF}	Lift force on the aircraft at liftoff
W	Weight force of the aircraft due to its mass m
$C_{L,LOF}$	Lift coefficient at liftoff
g	Earth gravity

By transformation of Eq. 4.89, the lift coefficient of the aircraft at liftoff yields:

$$C_{L,LOF} = \frac{2 \cdot m \cdot g}{\rho \cdot v_{LOF}^2 \cdot S_W} \tag{4.90}$$

As shown in equation 4.13 from Section 4.1.2, the liftoff speed v_{LOF} can be estimated from the stall speed of the aircraft as provided by the AFM.

4.2.1 Rotation and Climb Trajectory

During the bow shaped flight phase, the aircraft experiences an *augmented g-load* along its z axis (yaw axis). The lift during the rotation phase must therefore balance the weight of the aircraft augmented by the centrifugal acceleration a_N which is greater than earth gravity. In analogy to Eq. 4.89, the following assumption is made.

$$L - W = m \cdot a_N \tag{4.91}$$

Substituting the acceleration a_N and aircraft mass m yields

$$L - W = \frac{W}{g} \cdot \frac{v_{LOF}^2}{R} \tag{4.92}$$

With

m	Aircraft mass
a_N	Acceleration in z-axis of the aircraft during rotation
R_{LOF}	Radius of bow shaped rotation trajectory

Load Factor during Rotation Phase

In order to determine the radius of the bow shaped rotation trajectory, the load factor n needs to be determined. It results from the acceleration experienced by the aircraft in the z-axis.

$$\frac{L}{W} = n \quad \rightarrow \quad L = n \cdot W \tag{4.93}$$

From Eq. 4.93 follows through substitution:

$$n = \frac{L}{W} = \frac{\frac{1}{2}\rho\, v_{LOF}^2 \cdot C_{L,LOF} \cdot S}{\frac{1}{2}\rho\, v_S^2 \cdot C_{L,max} \cdot S} = \left(\frac{v_{LOF}}{v_S}\right)^2 \cdot \frac{C_{L,LOF}}{C_{L,max}} = 1{,}2^2 \cdot \frac{C_{L,LOF}}{C_{L,max}} \tag{4.94}$$

It can be assumed that the ratio of lift coefficients according to **Scholz 1999** is in the order of:

$$\frac{C_{L,LOF}}{C_{L,max}} \approx 0{,}8 \tag{4.95}$$

This yields an estimation for the load factor n experienced by the aircraft during the bow shaped rotation trajectory.

$n \approx 1{,}15$

Rotation Trajectory Bow Radius

Introducing the relation for L from Eq. 4.93 into equation 4.92 yields:

$$n \cdot W - W = W(n-1) = \frac{W}{g} \cdot \frac{v_{LOF}^2}{R} \tag{4.96}$$

This permits to determine the radius R by transformation of Eq. 4.96.

$$R = \frac{v_{LOF}^2}{g(n-1)} \tag{4.97}$$

The bow radius R can now be calculated by using the estimation for the load factor $n \approx 1{,}15$.

Transition Height

With R being known, the transition height h_{TR} between the bow shaped rotation phase and the linear climb phase can be determined. The transition height takes place at the point where the aircraft trajectory reaches the maximum constant climb angle possible for the aircraft configuration. This means that the aircraft cannot further increase its climb angle and will follow a linear climb trajectory from the transition height on.

From Fig. 4.19, the transition height can be determined geometrically to be:

$$h_{TR} = R - R \cdot \cos\theta_{climb} = R\,(1 - \cos\theta_{climb}) \tag{4.98}$$

With

h_{TR} Transition Height

The climb angle θ_{climb} the aircraft is able to assume during the climb phase is a function of the aircraft thrust, weight, lift and drag.

For small angles of θ_{climb}, it can be assumed that $W \approx L$. This yields:

$$\sin\theta_{climb} = \frac{T-D}{W} \approx \frac{T}{W} - \frac{D}{L} \tag{4.99}$$

Thus

$$\theta_{climb} = \arcsin\left(\frac{T}{W} - \frac{1}{E}\right) \tag{4.100}$$

4.2.2 Rotation and Climb Distances over Ground

For the rotation phase and the linear climb phase, two cases need to be distinguished:

A) The screen height has already been cleared when the transition height is reached

$$h_{SC} \leq h_{TR}$$

B) The screen height has not been cleared when the transition height is reached

$$h_{SC} > h_{TR}$$

Case A – Screen Height Cleared when Transition Height Reached

In this case, the Air Distance is determined from the rotation trajectory radius R intersection with the screen height h_{SC}:

$$S_a = \sqrt{R^2 - (R - h_{SC})^2} \tag{4.101}$$

With

h_{SC} Screen Height

This can be further simplified if $R \gg h_{SC}$, the single summand allowing to simplify with $h_{SC} \approx 0$ to:

$$S_a = \sqrt{2 \cdot R \cdot h_{SC}} \tag{4.102}$$

Case B – Screen height not Cleared when Transition Height Reached

If the screen height is not yet cleared when the bow shaped rotation phase trajectory blends into the climb phase trajectory, the distance over ground covered at constant climb angle has to be considered until the screen height is passed.

In this case, the climb phase distance needs to be added to the rotation phase distance.

For the distance covered over ground until reaching the transition height:

$$S_{TR} = R \sin \theta_{climb} \tag{4.103}$$

For the distance covered over ground in a linear climb trajectory at θ_{climb}:

$$S_{CL} = \frac{h_{SC} - h_{TR}}{\tan \theta_{climb}} \tag{4.104}$$

The total Air Distance is then calculated from the sum of the rotation phase distance and the climb distance.

$$S_a = S_{TR} + S_{CL} \tag{4.105}$$

4.3 Takeoff Distance – All Engines Operative

When all engines are operative and no other malfunction occurs that would require the pilot to abort the takeoff before V1, the takeoff will be executed as planned. The takeoff distance AEO will actually be less than the minimum TOFL values provided by the AFM charts, since the aircraft can take off using its full installed thrust.

The equations discussed in the previous sections of this chapter will be governing the takeoff performance calculation.

Depending on the runway condition, the different forces (Thrust and Drag with elements of the Drag determined through Lift and Weight) acting on the aircraft need to be considered within the equation of motion until V_{LOF} has been reached. This will determine the acceleration distance. Then the Air Distance as outlined above is added to the acceleration distance. The total Takeoff Distance S_{TOD}(disregarding any clear- or stopways) is the sum of the Liftoff and the Air Distances.

$$S_{TOD} = S_{LOF} + S_a \tag{4.106}$$

4.4 Takeoff Distance – One Engine Inoperative

As opposed to the AEO takeoff case, should an engine fail during the takeoff phase, there are major changes in the thrust and drag force balance that determines both acceleration and Air Distance. Both distances will, as a result, become larger. The Takeoff Distance is determined acc. to e. 4.106 but with changes in the parameter set of the aircraft.

As a primary consequence of an engine failure, the thrust-to-weight ratio declines. As it declines, the climb angle of the aircraft equally declines, as expressed by Eq. 4.100. This means that at an airport at which a limited field length is available, the weight of the aircraft becomes a limiting factor in the takeoff preparations.

This section shall outline the equations applying to the calculation of an OEI case. The parameters discussed in the following sections will have to be applied to the baseline equations outlined in the previous sections.

4.4.1 Engine Failure Speed

An engine failure can occur at any point during the flight. Even though an engine failure always represents a critical malfunction, the criticality of the incident depends on the speed the aircraft has at the point at which the engine fails.

The later the engine fails, the more critical it becomes for the braking distance (see Accelerate-Stop Distance section) but the less critical it becomes for the takeoff distance. The aircraft can accelerate longer with both engines and the failed engine does not influence the acceleration distance but for a smaller section. The concept of the BFL has been presented, from this concept it becomes clear that the most critical engine failure speed is the one so close before V_1 that the first pilot action occurs exactly at V_1. This critical engine failure speed is used as a baseline to calculate both the Takeoff Distance as well as the Accelerate-Stop Distance in the OEI conditions.

4.4.2 Thrust and Drag after Engine Failure

When an engine fails and a thrust differential develops, the aircraft experiences a series of unfavorable changes to elementary flight mechanical parameters. As the most evident consequence the available thrust is reduced by the thrust originally produced by the failed engine. Through the differential thrust conditions, the aircraft is subjected to a moment around the yaw axis towards the inoperative engine which needs to be compensated by the pilot. In takeoff power settings, the thrust differential caused by a failed engine is maximized. Additionally, the failed engine produces a considerable drag force, referred to as windmilling drag. The yaw moment caused by the engine failure also leads to an asymmetrical flight condition, and a high rudder deflection is necessary to maintain straight flight. Therefore, a windmilling and an asymmetrical flight condition drag increment needs to be added to the overall drag coefficient of the aircraft and the available thrust reduced.

This means, that in a continued takeoff under OEI conditions, the takeoff performance is drastically degraded. In the air, the aircraft will not only yaw, but also bank by a maximum of 5 degrees[7] to the side of the failed engine. This roll-yaw coupling creates a sideslip angle, but reduces the rudder deflection necessary for balancing the asymmetrical flight condition. According to **Torenbeek 1982**, the wings level condition as shown in Fig. 4.20 is the worst case scenario in terms of asymmetrical drag due to the very large rudder deflection necessary.

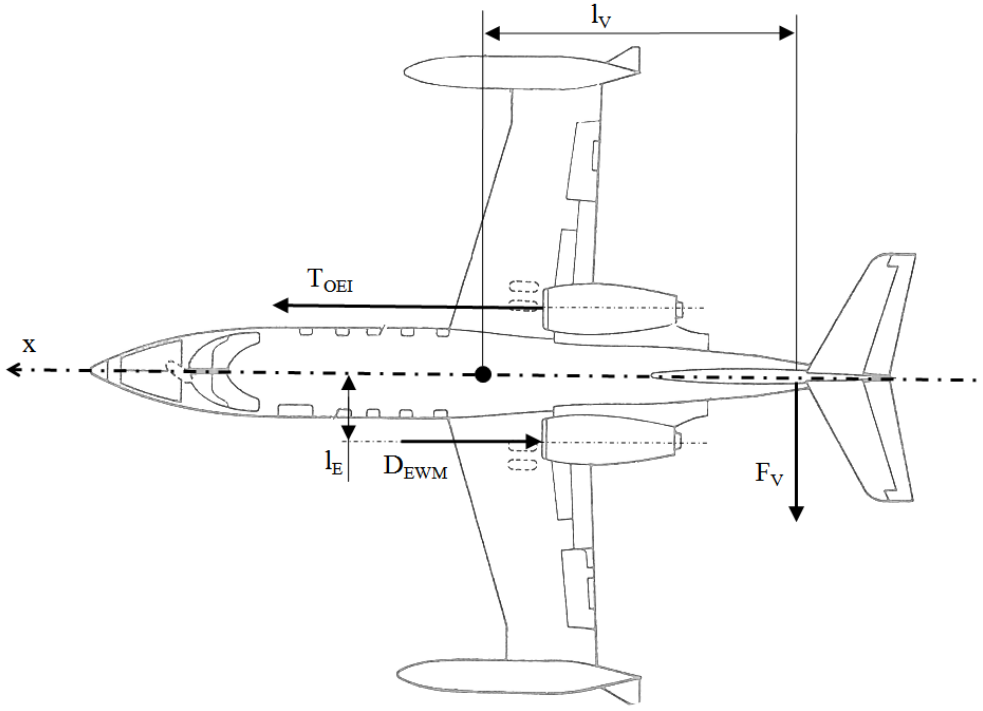

Fig. 4.20 Forces acting on the Aircraft in Engine Failure Case, Wings Leveled

7 The maximum roll angle in OEI condition is limited to 5° by CS 25.149

Windmilling Drag

For the approaches presented in this section, the engine is assumed to fail in a way that windmilling of the engine[8] is still possible, in contrast to a locked rotor engine failure.

According to **Scholz 1999**, the drag force of a windmilling engine lies between 15% (low BPR) and 25% (high BPR) of the net thrust rating of the engine. This assumption can be used for a preliminary sizing of the vertical tailplane (VTP) but is of limited precision for the take-off performance calculation.

According to **Torenbeek 1982**, the drag force of a failed engine can also be determined according to geometrical and engine specific parameters. It takes into account the spillage of the inlet and the internal drag due to air flow through the windmilling engine.

$$D_{EWM} = \frac{1}{2}\rho\, v^2 \cdot S_W \cdot C_{D,EWM} \tag{4.108}$$

The windmilling drag coefficient $\Delta C_{D,EWM}$ according to **Torenbeek 1982** is referenced to the engine inlet area, and has been re-referenced to the aircraft reference area S_W.

$$\Delta C_{D,EWM} = \left(0{,}1 + \frac{2}{1 + 0{,}16\, M^2} \cdot \frac{V_N}{V}\left(1 - \frac{V_N}{V}\right)\right) \cdot \frac{\frac{\pi}{4} \cdot d_i^2}{S_W} \tag{4.109}$$

With

d_i	Engine inlet diameter
M	Flight mach number
V_N/V	Nozzle exit to inlet entry velocity ratio $V_N/V \approx 0{,}42$ for low bypass engines (**Torenbeek 1982**)

Asymmetrical Flight Condition Drag Increment

The inoperative engine develops a yaw moment which depends on the distance between the thrust vector and the Center of Gravity (CG). The pilot counteracts by using the rudder. In a simplified and conservative approach, it shall be assumed that the complete yaw moment shall be balanced by rudder deflection alone, as suggested by **Torenbeek 1982**. This leaves aside the role of the wheel side force component on the runway and a possible sideslip angle in flight, but spares to perform a complete yaw moment analysis. The chosen approach will be of adequate precision and conservatism for means of the takeoff performance calculation.

8 Windmilling refers to the condition that the engine shaft and rotors can still turn and air can pass through the blades rotated by the free-stream velocity

Taking into account the equilibrium of momentum around the yaw axis of the aircraft, a relation between the forces from figure 4.20 can be obtained for a twin engine aircraft. This is done to show the origins of the equation finally used for the drag increment calculation based on **Torenbeek 1982**.

$$l_E(T_{OEI} + D_{EWM}) = F_V \cdot l_V \tag{4.110}$$

With

T_{OEI}	Thrust produced by the remaining engine
D_{EWM}	Windmilling drag produced by the engine
l_E	Engine to CG distance
l_V	VTP to CG distance
F_V	Force from VTP due to Rudder

For a given aircraft power plant architecture, the required rudder force F_V can be determined in this way.

In order to determine the drag due to the rudder, the necessary rudder deflection could be determined based on a **DATCOM 1978** method.

$$F_V = \frac{1}{2}\rho\, v^2 \cdot\ \delta_{Rd} \cdot c_{L,\delta} \cdot K' \cdot K_\Lambda \cdot S_V \tag{4.111}$$

With

δ_{Rd}	Rudder deflection
$c_{L,\delta}$	VTP profile lift coefficient after rudder deflection
K'_{Rd}	Rudder efficiency factor
K_Λ	Correction factor for VTP sweep
S_V	VTP area

However, this equation cannot easily be solved for the rudder deflection δ_{Rd} due to the fact that the rudder efficiency factor changes with the HTP lift slope gradient, yielding an equation with two unknown variables. Therefore, another approach from **Torenbeek 1982** may be used to estimate the profile drag increment due to rudder deflection directly. The equation from Torenbeek adapted to a jet aircraft is given by Eq. 4.112.

$$\Delta C_{D,ASYM} = K_{ASYM}\left(\frac{T_{OE}}{\frac{1}{2}\,\rho\, v^2} + \Delta C_{D,EWM}\right)^2 \tag{4.112}$$

Where

$$K_{ASYM} = \left(\frac{l_E}{l_V}\right)^2 \frac{1}{S_V} \frac{1}{\pi\, A_{V,eff}} \left(1 + 2{,}3 \sqrt{\frac{S_r}{S_V}} \left(\frac{A_{V,eff}}{cos\Lambda_V}\right)^{-1/3}\right) \tag{4.113}$$

With

$A_{V,eff}$	Effective (aerodynamic) aspect ratio of the VTP acc. to Fig. 4.21
S_{Rd}	Rudder surface
S_V	VTP area
l_E	Engine to CG distance
l_V	VTP 25% MAC to CG distance

It should be pointed out that the most adverse condition for the asymmetrical flight condition is the one where the lever arm from CG to rudder is minimized. This is why the most conservative approach is to consider the aircraft it its max aft CG configuration.

Furthermore, as the dynamic pressure is contained within the equation for a drag coefficient, it should not be included dynamically in a time-step wise calculation. Otherwise, the drag coefficient would rise incongruently with decreasing flight speed in a stopping motion. In reality, the increasing available tire side force to balance the yaw moment at low speeds would rather lead to a reduction in the required rudder deflection. It shall therefore be recommended to determine an asymmetrical drag coefficient increment constant at a suitable flight speed, e.g. at V_1.

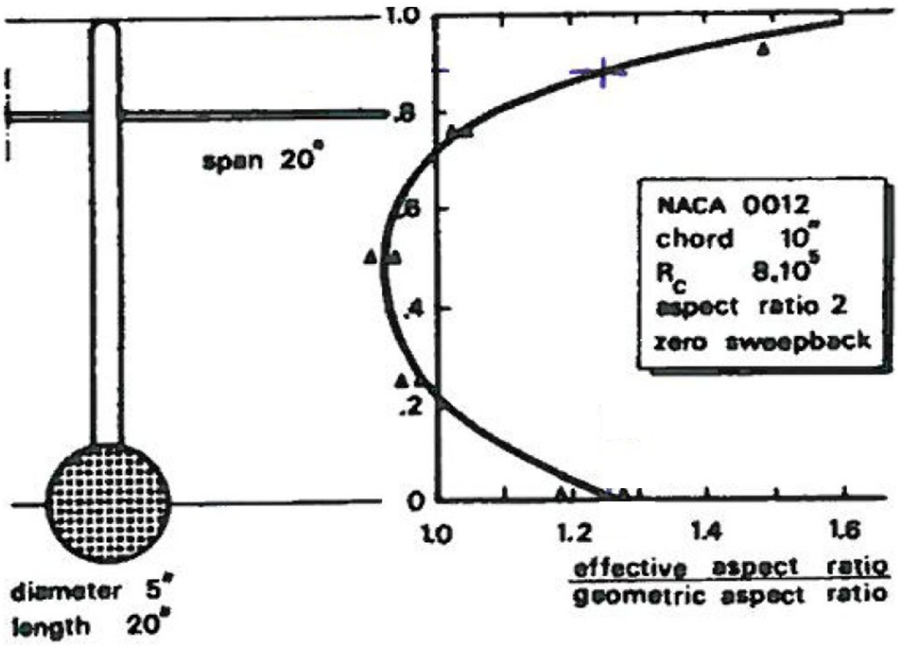

Fig. 4.21 Effective VTP Aspect Ratio of the Fin for a T-tail configuration (**Torenbeek 1982**)

4.5 Accelerate-Stop Distance

Should the pilot opt to abort the takeoff due to an engine failure or another serious malfunction, he can choose to do so until reaching the decision or safe abort speed V1. The Accelerate-Stop Distance is therefore divided into the acceleration phase and the deceleration phase, at whose end the aircraft will have been brought to a complete stop.

$$S_{ASD} = S_{acc} + S_{stop} \tag{4.114}$$

According to the CS-25.109 requirement to take pilot reaction times into consideration, the pilot will activate the first available means of braking at an interval of 1 second after engine failure recognition.

In this case, as the aircraft does not leave the ground, the equation of motion can be applied for both the acceleration as well as the deceleration phase. This has already been shown in Section 4.1.4. As all means of braking are deployed, instead of a positive acceleration now a negative acceleration should be achieved. Braking is initiated at V_{EF} plus the speed gained until pilot recognition as soon as he takes measures for an aborted takeoff, yielding negative acceleration.

4.5.1 Braking Force

The primary means of braking in the Accelerate-Stop Case are the brakes, no thrust reverse is considered as the aircraft considered in this report is not equipped with such a system. The deceleration performance on a wet runway is degraded in comparison to a dry runway due to increased sleekness.

The equation used to calculate the braking force is similar to the one used for the determination of the rolling friction force, the same concept applies. However, it is necessary to consider only the braking wheels to exert a friction force to the runway, therefore the normal load acting on the braking wheels cannot be considered equal to the complete aircraft weight anymore. Also, a moment of inertia around the CG due to braking must be taken into account for.

As a consequence, Eq. 4.115 includes a gear load factor to account for said effects.

$$F_{friction,brake} = \mu_{friction,brake} \left(m \cdot g \cdot cos(\gamma) \cdot f_{load,gear} - L\right) \quad \textbf{(4.115)}$$

With

$\mu_{friction,brake}$	Braking friction coefficient
m	Aircraft Mass
g	Gravity
γ	Runway slope
$f_{load,gear}$	Gear load factor

The gear load factor is essentially the percentage of the aircraft weight actually acting as a normal force on the braked wheels. In order to consider only the braking wheels of the main gear, a weight record of the empty aircraft can be used. For the Learjet 35A/36A, an exemplary weight record is shown in appendix G. Considering the empty aircraft weight record leads to conservative results, as the fuel in the wings for takeoff is not considered. This may account for compensation of the amount the moment of inertia further decreases the load on the main gear. This conservative assumption hence spares an analysis of the momentum balance around the aircraft pitch axis.

Two different approaches to determine the braking friction are provided by **CS-25.109** and **EASA AMC 25.109** to determine a speed-dependent braking friction coefficient. It is difficult to determine an exact value for the braking friction, due to the fact that the sleekness of the runway depends on many factors such as the macro- and micro-texture and tire residue on the runway surface. Therefore, in flight operations, an effective runway braking action measured by a friction tester can be made available to the operator.

However, the friction coefficient necessarily differs between the friction measurement device and the actual aircraft and a prediction of actual braking coefficients is difficult. Therefore, the equations provided by the certification specifications have been used, as no specific flight tested data is available.

The equations from **CS-25.109** provide values for braking coefficients with regard to speed and tire pressure.

Table 4.2 Maximum Braking Friction Coefficients on Wet Runways (**CS-25.109**)

Tire Pressure (psi)	Maximum Braking Coefficient (tire-to-ground)
50	$\mu_{max,wet} = -0{,}0350\left(\frac{v}{100}\right)^3 + 0{,}306\left(\frac{v}{100}\right)^2 - 0{,}851\left(\frac{v}{100}\right) + 0{,}883$
100	$\mu_{max,wet} = -0{,}0437\left(\frac{v}{100}\right)^3 + 0{,}320\left(\frac{v}{100}\right)^2 - 0{,}805\left(\frac{v}{100}\right) + 0{,}804$
200	$\mu_{max,wet} = -0{,}0331\left(\frac{v}{100}\right)^3 + 0{,}252\left(\frac{v}{100}\right)^2 - 0{,}658\left(\frac{v}{100}\right) + 0{,}692$
300	$\mu_{max,wet} = -0{,}0401\left(\frac{v}{100}\right)^3 + 0{,}263\left(\frac{v}{100}\right)^2 - 0{,}611\left(\frac{v}{100}\right) + 0{,}614$
	(4.116)

The equations above must be corrected to account for an anti-skid system efficiency factor for wet runways. The efficiency of the anti-skid system depends on the modulation capability. Table 4.3 provides the reference values to take into account according to **CS-25.109**.

Table 4.3 Anti-Skid System Efficiency on Wet Runway (**CS-25.109**)

Type of anti-skid system	Efficiency value
On-Off	0.30
Quasi-Modulating	0.50
Fully Modulating	0.80

The relation of anti-skid and locked-wheel braking coefficient is shown is Fig. 4.22 in order to underline the importance of the consideration of an anti-skid system efficiency factor to apply to the maximum braking friction values provided in Table 4.2.

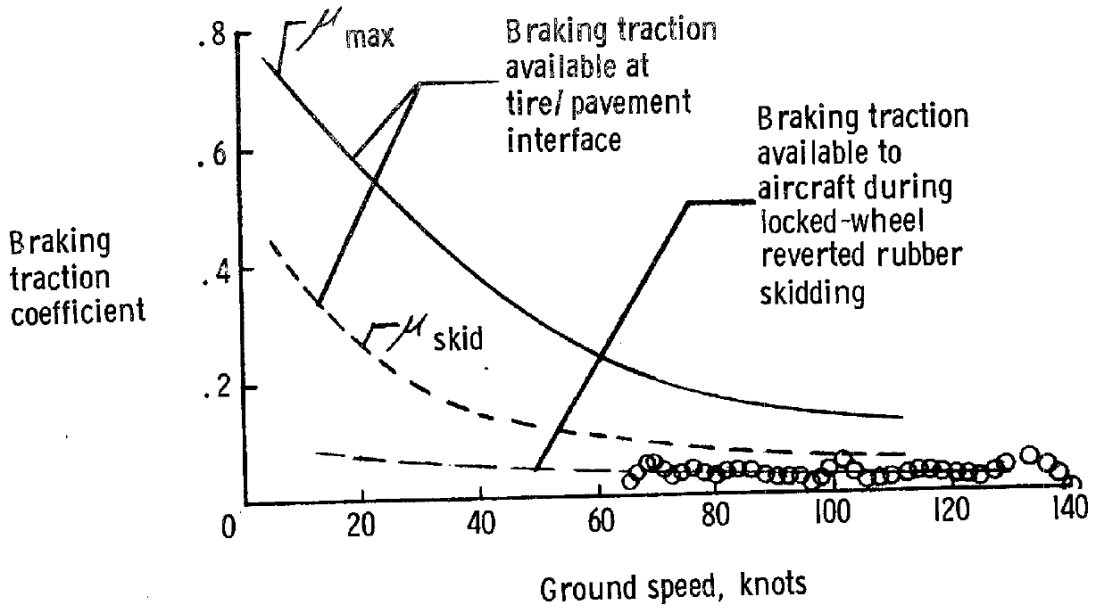

Fig. 4.22 Braking Friction Coefficient on Wet Runway, Maximum, Anti-Skid and Locked Wheel (**NASA TM-X-72650**)

It is necessary to review the equations 4.116 from **CS-25.109** with caution, since at low speeds, the equations suggest a braking coefficient which is quite high. There is a chance that the braking coefficient determined in accordance with above equations would lead to higher braking coefficients for a wet runway than could be achieved even on a dry runway.

EASA AMC 25.109 is considering a different equation for the braking coefficient variation with regard to speed. However, this document guides the estimation of influential factors on a contaminated runway, and the braking friction coefficients may be too conservative for application on a wet runway.

$$\mu_{max,wet} = -0{,}0632\left(\frac{v}{100}\right)^3 + 0{,}2683\left(\frac{v}{100}\right)^2 - 0{,}4321\left(\frac{v}{100}\right) + 0{,}3485 \qquad \textbf{(4.117)}$$

According to the document, Eq. 4.117 shall be used for the determination of the braking friction coefficient up to aquaplaning speed. Above aquaplaning speed, a constant aquaplaning braking coefficient of 0,05 shall be used.

In order to have an appreciation of the different braking friction coefficient calculation approaches presented in this section, a plot showing them in relation to each other is shown in Fig. 4.23. The **CS-25.109** data is not including any correction factors due to anti-skid efficiency acc. to Tab. 4.3.

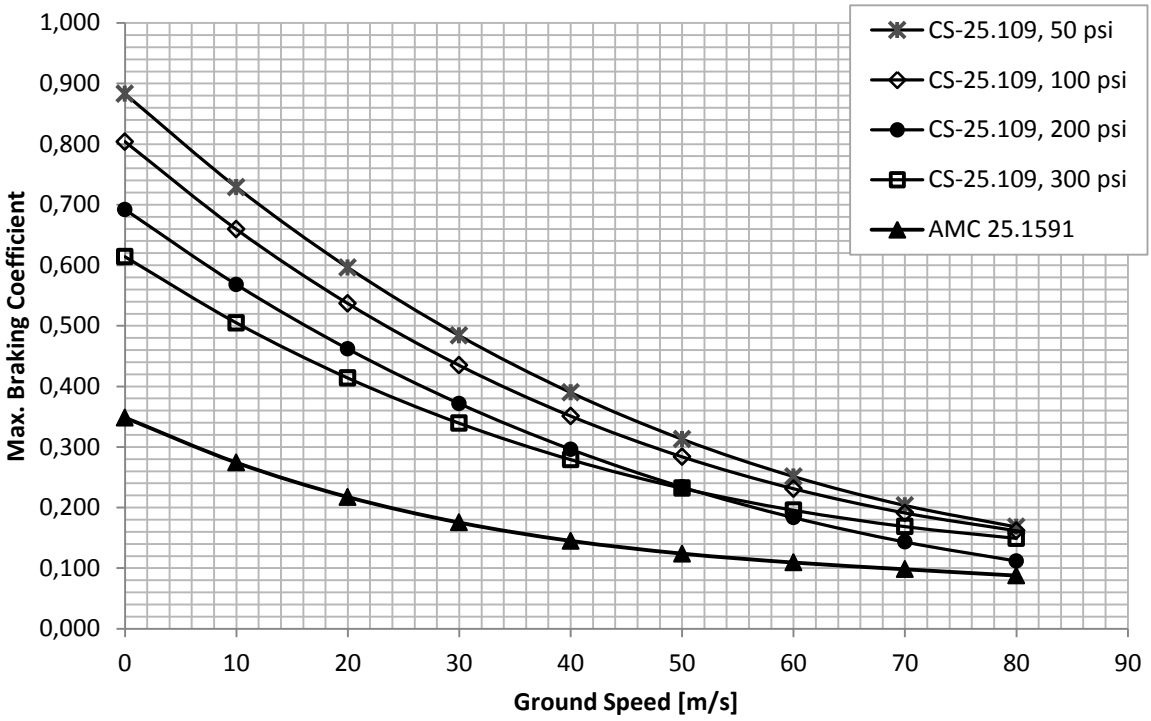

Fig. 4.23 Basic Braking Coefficients for Wet Runways, **CS-25.109** and **EASA AMC-25.1591**

It is important to note that due to the spoiler deployment (refer to Section 4.5.2), a large portion of the Lift force is depleted with the goal to increase the wheel load and thus the available friction force when braking.

4.5.2 Drag and Lift Coefficients after Spoiler Deflection

As a means to assist the retardation of the aircraft, the spoilers may be extended from the wings. Spoiler deflection has two effects: A disturbance of the air flow over the wings leads to a large portion of the lift being lost, and the extended surface of the spoiler also exerts a drag force on the aircraft.

Lift Coefficient with Turbulent Flow behind Spoiler Hinge Line

An approach based on **Scholz 1999** is used to determine the lift coefficient after spoiler deflection. For the lift coefficient reduction, it is assumed that the wing has the same lift load per area over the whole wing area. Thus, the lift coefficient C_L which has been determined for the wing without spoiler deflection can be converted into a lift coefficient per area C_L''.

$$C_L'' = \frac{C_L}{S_W} \tag{4.118}$$

It is assumed that the hinge line where the spoiler is extended into the air stream is the boundary behind which the wing does not produce any more lift due to flow separation, as shown in Fig. 4.24. For the determination of the lift coefficient after spoiler deployment, the complete area behind the spoiler in the direction of the trailing edge along the spoiler hinge line therefore considered as lost as reference area for the lift coefficient of the wing. The area behind the spoiler hinge line is referred to as the wetted spoiler area S_{SW} and needs to be determined based on the actual wing geometry.

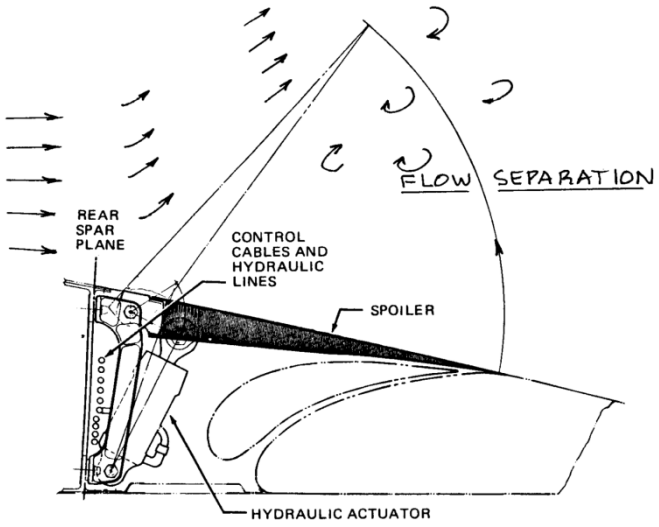

Fig. 4.24 Turbulent Flow behind a deflected Spoiler (**Roskam III**)

With this area being known, the new lift coefficient for the wing with extended spoilers $C_{L,S}$ can be determined from equation 4.119.

$$C_{L,S} = (S_W - S_{SW}) \cdot C_L'' = \left(1 - \frac{S_{SW}}{S_W}\right) \cdot C_L \tag{4.119}$$

With

$C_{L,S}$	Lift coefficient after spoiler deflection
S_{SW}	Wetted area of the wing behind the spoiler hinge line
C_L''	Lift coefficient per area assuming equally distributed lift load

Drag Coefficient Increment based on Flat Plate Drag Coefficient

The drag force evaluation equations for the spoiler when activated are taken from **LTH BM 21 600-01** and consist of the literature drag coefficient value for a flat plate, deployed at an angle of δ_S. The flow condition and force resultant are shown in Fig. 4.25.

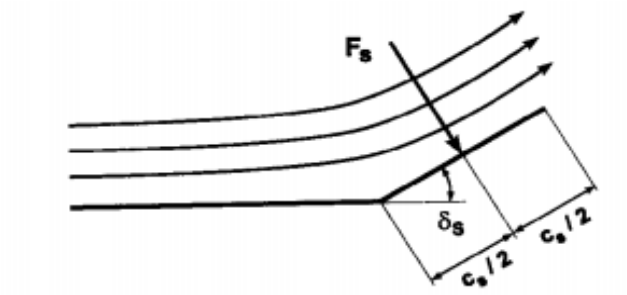

Fig. 4.25 Extended Spoiler Geometry Upper Wing (**Scholz 1997**)

Eq. 4.120 provides the drag increment due to spoiler deflection directly with reference to the aircraft.

$$\Delta c_{D,spoiler} = 1.8 \cdot \cos(\delta_S) \cdot K' \cdot \frac{S_S}{S_W} \tag{4.120}$$

With

S_S	Spoiler area, projected in flight direction for swept wings
δ_S	Spoiler deflection angle
K'_S	Spoiler efficiency factor

For upper wing flow, **Scholz 1997** suggests to use $K' = 1{,}3$ due to the increased local flow velocity on the upper surface of the wing. For means of the performance calculation placed in a relatively low speed environment, a conservative efficiency factor of $K' = 1{,}0$ will be used.

Both effects of the spoiler deflection need to be taken into consideration in the Lift and Drag determination of the aircraft after spoiler deflection. This has a direct influence on the equation of motion.

4.6 Balanced Field Length

With all of the parameters shown in the previous sections of this chapter, it is possible to model the aircraft performance for calculation of the AEO Takeoff Distance, the OEI Takeoff Distance and the Accelerate-Stop-Distance. As has been outlined also in Section 3.5, the ASD will need to be determined under OEI conditions.

From the Balanced Field Length determination, the most critical engine failure speed can also be determined. The equations of motion for acceleration and deceleration phase as well as the Air Distance need to be fed into a performance simulation and will provide the intersection point of TOD and ASD.

The iterative numerical integration method applied in this report to determine the BFL is presented in Chapter 7. All parameters and considerations outlined in chapters 3 and 4 have entered the functional architecture of this simulation.

An empirical equation to calculate the BFL is given by **Torenbeek 1982**. This handbook method is based on average accelerations and decelerations, and may be used to get an indication of the order of magnitude of the BFL. However, due to its empirical nature, it is only applicable to *dry runways*.

$$BFL = \frac{0{,}863}{1 + 2{,}3\,\Delta\theta}\left(\frac{\frac{W}{S_W}}{\rho_{true}\; g\; C_{L,LOF}} + h_{sc}\right)\left(\frac{1}{\frac{T_{AV}}{W} - U} + 2{,}7\right) + \left(655/\sqrt{\frac{\rho_{true}}{\rho_0}}\right) \tag{4.121}$$

With

BFL	Balanced Field Length in ft
$\Delta\theta$	Difference of 2nd segment and initial climb gradient acc. to Eq. 4.123
W	Aircraft Takeoff Weight (TOW)
S_W	Wing reference area
ρ_{true}	Ambient air density acc. to Eq. 4.30
ρ_0	Standard ISA air density
g	Gravity
$C_{L,LOF}$	Lift coefficient at liftoff, acc. to Eq. 4.90, in OEI configuration
h_{sc}	Screen Height in ft
T_{AV}	Average thrust acc. to Eq. 4.122 from **Torenbeek 1982**
U	Ground lift coefficient acc. to Eq. 4.124 from **Torenbeek 1982**

The following equations are needed to determine input parameters needed for Eq. 4.121.

$$T_{AV} = 0{,}75\, T_0 \left(\frac{5 + BPR}{4 + BPR}\right) \tag{4.122}$$

With

BPR Engine Bypass Ratio

$$\Delta\theta = \theta_{climb} - \theta_{min} \tag{4.123}$$

With

θ_{min} Minimum second segment climb angle acc. to **CS-25.111**
$\theta_{min} = 0{,}024\, rad$ for twin engine aircraft

θ_{climb} Initial liftoff climb angle acc. to Eq. 4.125

Ground Lift Coefficient approximation for BFL determination according to **Torenbeek 1982**:

$$U = 0{,}01\, C_{L,LOF} + 0{,}02 \tag{4.124}$$

In order to obtain correct results, it is important to used consistent units throughout the equation. Imperial units are used for the BFL and the screen height by **Torenbeek 1982**, therefore SI units may be only be used in all terms where they are used as ratios.

3.7 Takeoff Field Length

After a number of definitions and descriptions for possible cases and distances covered in an attempted or executed takeoff have been provided, the Takeoff Field Length (TOFL) refers to the one that becomes limiting for the aircraft taking off. This distance can be:

- 115% of the TOD in AEO conditions
- The TOD in an OEI condition
- The ASD in either condition

The latter two points combined constitute the BFL, by definition as shown in Section 3.6. Therefore, the TOFL definition can be simplified to being the limiting, greater distance of the Balanced Field Length (BFL) and 115% of the All Engines Operative Takeoff Distance.

Because the TOFL is designed to accommodate the worst case, assuming a possible engine failure, it is the minimum field length the takeoff runway must have for the taking off aircraft, if no stop- or clearways are taken into account. As has been shown by calculation, for the Learjet 35A/36A considered in this report, it is always the BFL that becomes limiting.

The knowledge of the pairs of data, Balanced Field Length and balanced V1 for each set of environmental and aircraft configurations is necessary for the flight preparation and is different for each variation of the influencing parameters. As this project shall provide preliminary performance data to be used to develop operating charts for the actual operation of the aircraft, the calculation of the BFL is performed for a range of varying density altitudes.

4.8 Climb Weight Limit

A limit to the takeoff performance of an aircraft is not only imposed through the available length of the runway, but also through requirements originating from later phases of the takeoff along the takeoff path described by **CS-25.111**.

Once the screen height has been passed, the aircraft is required to maintain a continuous climb gradient. Under certain OEI conditions, this climb gradient may become limiting to the ability of the aircraft to safely perform a takeoff, even though the screen height could be cleared.

CS-25.111 specifies the minimum continuous climb gradient an aircraft has to be able to achieve along the takeoff path. Depending on the number of engines, a specific minimum climb gradient is required in different takeoff phases order to perform the takeoff procedure according to regulatory requirements. Tab. 4.4 displays the minimum climb gradients required for the continuous climb phase

Table 4.4 Minimum Climb Gradients specified by **CS-25**

Number of Engines	**2**	**3**	**4**
Initial Climb Gradient OEI	>0%	0,3%	0,5%
Second Segment Climb Gradient OEI	2,4%	2,7%	3,0%
Continuous Final Climb Gradient	1,2%	1,5%	1,7%

The Thrust-to-Weight Ratio of an aircraft is the determining factor that decides on the climb angle θ_{climb} and respectively on the climb gradient that is achievable after takeoff. The higher the aircraft weight or the smaller the aircraft thrust, the smaller the achievable climb angle. Equation 8.1.1 provides the numerical evidence of this relationship.

$$\theta_{climb} = \arcsin\left(\frac{T}{W} - \frac{1}{E}\right) \tag{4.125}$$

Resulting from this requirement, for an aircraft with a given excess thrust output, the only variable that can be adapted to ensure meeting the certification requirement is to impose a weight limit for the aircraft in a given configuration. This limit is referred to as climb weight limit and is a result of airborne flight characteristics. The climb weight limit is independent of runway conditions. Whenever a takeoff performance calculation for the ground and initial climb phase up to screen height is performed, a cross check with the climb weight limit therefore has to follow up in order to ensure that the aircraft performance is also sufficient for the subsequent phases along the takeoff path.

Climb Weight Limit Charts consider this fact and have been used in the evaluation of the calculated takeoff performance data of the Learjet 35A/36A.

5 Water Spray Impingement Drag

It was outlined in Section 4.1.10 that the water spray plume displaced by the tires and impinging on the fuselage creates a drag force. No generic equations can be provided by certification specifications, as the aircraft surface that is exposed to direct spray impact depends largely on the aircraft geometry and the tires used. The impingement forces occur at those parts of the aircraft structure where a significant spray density is expected to impact on the surface at a normal or non-oblique angle. Otherwise it would be considered in the skin friction drag force component. The momentum loss of the mass of fluid when colliding with the aircraft is creating the drag force. According to **EASA AMC-25.1591**, this resulting drag forces must be taken into account.

Due to specific tire geometry resulting in specific spray plume shapes and specific structural geometries of the aircraft need to be taken into consideration. Therefore, in this section, specific parameters for the considered Learjet 35A/36A shall be investigated. However, the methodology and references used may be applicable to other specific aircraft as well.

For the Learjet 35A/36A considered in this report, the impingement drag force determination is of special interest due to the installation of under-wing stores. It has not been clear to what extend the water spray from the tires will interact with the stores, motivating an extensive investigation.

As will be shown further on in this section, the stores may be subjected to a significant amount of impinging spray due to their location under the wings. This is where the maximum spray density is expected resulting from a specific front wheel tire geometry. The spray impingement calculation however is done for the complete aircraft surface subjected to the spray impingement, not only the stores are located in the potential spray plume.

Fig. 5.1 MTR-101 Pod installed under the wing of a Learjet 35A/36A

5.1 Literature Review

The most accurate method to determine the impingement drag and especially the location of the spray impingement is the actual flight test analysis. This method is applied for initial certification of any larger civil aircraft. It allows pinpointing dangerous effects due to the water spray such as engine ingestion of water spray or impingement on control surfaces or flaps.

If flight test data for the specific aircraft are not available, test data from generic tire and geometry combinations can provide valuable information for the estimation of the generated forces and spray angles. Most notable in this regard are **NASA TP2718** providing actual flow density information for a range of different aircraft tires and tire speeds. Furthermore, **NLR-TP-2001-490** relates analytical estimation based on a spray flow simulation to actual flight test results. Test data from **Barrett 1970** has been used to investigate the effect of spray angle deviation due to chined tires.

For a purely analytical investigation of the spray impingement drag, one of two notable sources used in this report is **ESDU 83042** for an analysis of spray angles resulting from the tire geometry. Further data has been taken from **NLR-TP-2001-204** for analytical results developed with a spray flow simulation. It provides valuable information on restitution coefficient and impingement behavior of water droplets.

5.2 Spray Wave Types of Main and Front Wheels

Each of the wheels of the aircraft is creating a spray of water particles in specific trajectories that impinge on the aircraft. **NLR-TP-2001-204** outlines two different types of waves formed when an aircraft tire is running through a water pool, side wave and bow wave. The type of spray to be considered in the calculations must be known in order to estimate angles and force components.

The *side wave* is formed by a spray plume directed sideways from the tire and forming a spray envelope as shown in Fig. 5.2. The side wave is created on each side of a tire, its height and angle depending on the velocity imparted on a fluid particle through the rolling tire. The *bow wave* is created only between a dual-wheel gear setup. It could be seen as the merging of both side wave plumes directed inwards of the dual-wheel, resulting in an out-canceling of sideways directed velocity components.

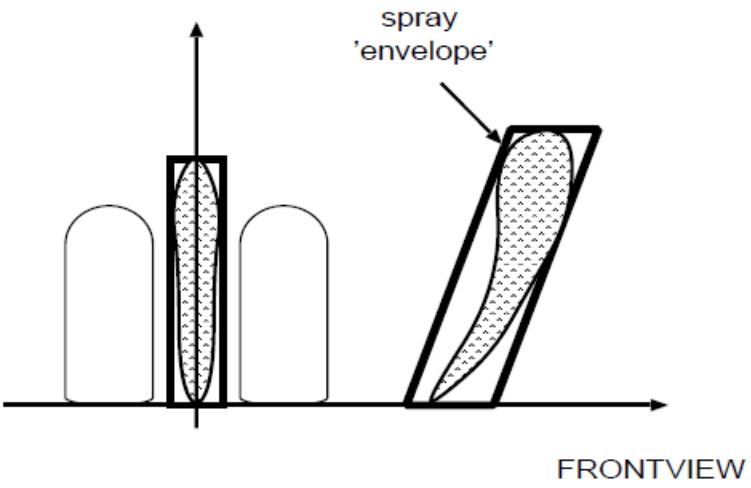

Fig. 5.2 Bow and side wave of spray plume(**NLR-TP-2001-204**)

The aircraft tire causing the largest amount of water droplet impingement on the aircraft structure is the front wheel tire. The main gear spray is created below the wing and sideways of the fuselage on either side. The only considerable amount of impingement drag through main wheel spray could be created when the spray is colliding with the trailing edge of the wing flaps at large deflections.

On the Learjet 35A/36A, due to the installation of under-wing stores, the flap deflection is limited to 8° which is why this drag component is not considered in detail. For that reason, the spray drag created by the front wheel and impinging on the aircraft fuselage in turn will be considered conservatively.

5.3 Spray Angle Assumptions

In order to evaluate the amount of drag created by the front wheel tire spray, it is important to know the angle at which the water is displaced sideways. The spray angle is defined between the main axis of the spray and the tire z-axis as seen from the front.

Many assumptions on the spray angle are made by the different sources listed in Section 5.1. Because the spray geometry relies very much on the tire configuration and the aircraft speed, there is no generic angle provided for a generic tire as a function of aircraft speed.

In addition to this, the tire used for the Learjet 35A/36A is chined[9], further rendering generic spray angle estimations difficult.

9 A chined tire has an extension at either side of the profile that acts as a deflector and reduces the spray angle

According to **ESDU 83042**, the effect of spray deflectors to a large extend depends on the leg load and the water depth the chine has been designed and tested for.
However, not only the angle of the spray but also the source point of the sideways directed water spray needs to be investigated. As can be seen in Fig. 5.2, the side wave does not form at the tire-to-ground contact area. A source point estimation is outlined in **ESDU 83042**.

Therefore, the spray angle assumption used for this report relies on test data from other aircraft, the **ESDU 83042** spray angle estimations for non-chined tires and an assumption for the chine influence based on the actual tire geometry of the Learjet 35A/36A.

An estimation of the spray angle with regard to aircraft speed is shown in Fig. 5.3. As can be seen, the spray angle rises with rising aircraft speed until the aquaplaning speed has been reached. The reduction of displaced water[10] due to aquaplaning then results in a reduction of the spray angle.

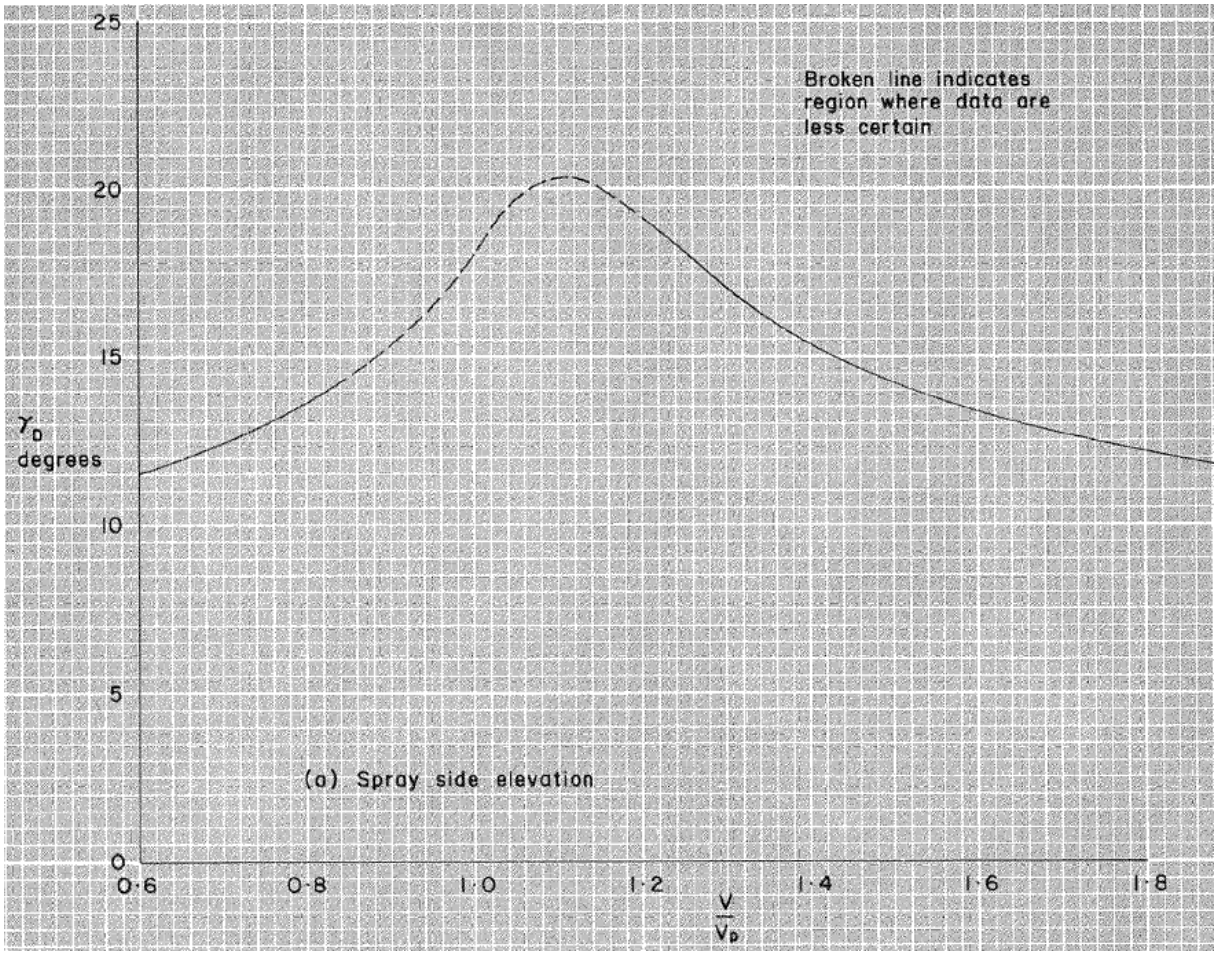

Fig. 5.3 Spray Angle with regard to Aircraft and Aquaplaning Speed (**ESDU 83042**)

10 See section 2.3 for the water displacement and aquaplaning speed relationship

Based on **ESDU 83042**, the spray deflection angle of the front tire seems to be around 20° at aquaplaning speed, which matches with the spray angle amplitude given in **NASA TP2718**.

The graph from Fig. 5.3 gives reason to assume that the amount of drag created by the water spay is influenced by two factors. The first factor is the aquaplaning factor which has been outlined in Section 2.3, reducing the amount of water displaced above aquaplaning speed. The second factor is the dependency and variation of the spray angle with tire speed. This angle is key to an assumption on the amount of exposed airframe surface. At low speeds, the angle and therefore the amount of spray impingement can be assumed to be negligible. It is rising to a maximum at aquaplaning speed. Expressed in an equation, this relationship leads to the assumption of a correction factor k_{angle} applicable to the maximum expected amount of drag.

$$D_{imp,dynamic} = k_{angle} \cdot D_{imp,max} \tag{5.1}$$

With

$D_{imp,dynamic}$	Speed dependant impingement drag
$D_{imp,max}$	Static amount of impingement drag at aquaplaning speed (maximum)

And

For $v_{aircraft} < v_{aquaplaning}$

$$k_{angle} = \frac{v_{aircraft}}{v_{aquaplaning}} \tag{5.2}$$

For $v_{aircraft} > v_{aquaplaning}$, the aquaplaning factor to be applied to precipitation drag forces above aquaplaning is assumed to account for the subsequent reduction in impingement drag force.

Concerning the effects of the chines, a study based on test data is used to investigate the behavior of the spray envelope deflected by tire shines. **Barrett 1970** determines that chines comparable to those installed on the Learjet 35A/36A (chine type 4) yield a spray envelope boundary of 27° measured from the ground, as shown in Fig. 5.4. It must be noted that, in disagreement with the other sources used, **Barrett 1970** defines the spray deflection angle from the ground upwards.

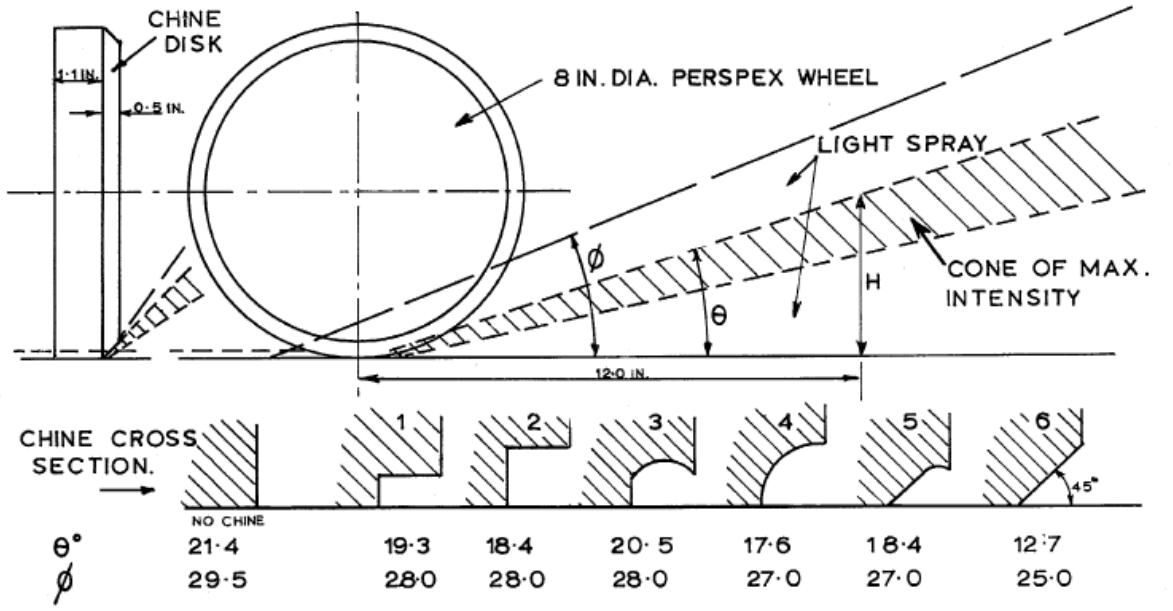

Fig. 5.4 Chined Tire Deflection Spray Angle (**Barrett 1970**)

The task of the shines is to deflect the water spray towards a lower spray angle. As will be shown in Fig. 5.6 and Fig. 5.7, the chines on the Learjet 35A/36A clearly have the task to prevent water spray from being directed in the area of the engine inlets.

A picture of the considered nose wheel tire is given in Fig. 5.5. Geometrical relations and angles are indicated by straight lines. The basic tire spray deflection angle without shines is assumed to amount to 20° as of **ESDU 83042**. Added to this basic tire spray deflection angle is then an assumed chine deflection angle of 30°.

When measured from the ground as in the definition used by **Barrett 1970**, the main axis of the spray would then be directed upwards from the runway surface at an angle of approximately 30°. This matches closely with the spray envelope boundary of 27° degrees from **Barrett 1970** as shown in Fig. 5.4. This can be seen as a validation of the assumed spray angle based on basic tire and shine geometry.

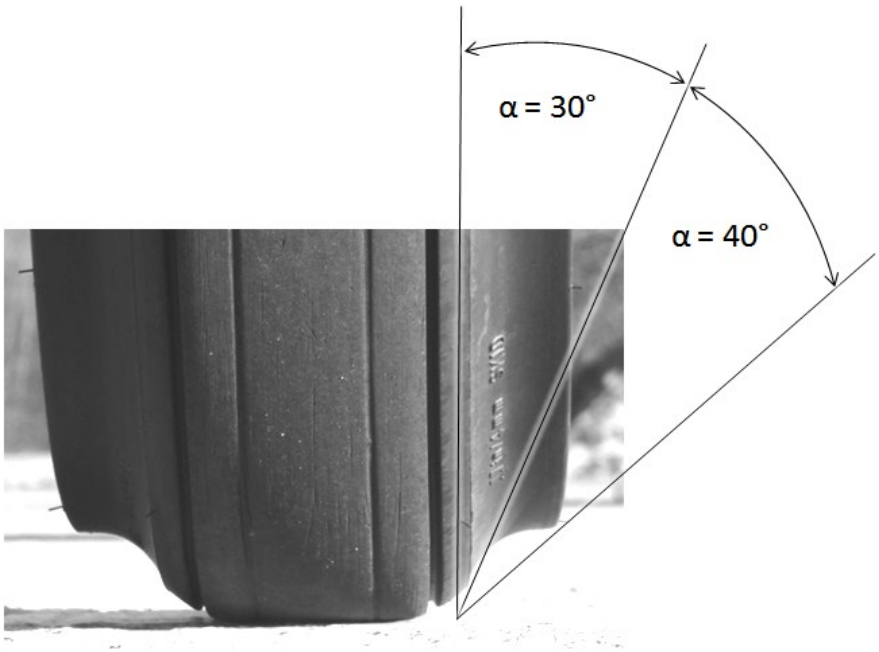

Fig. 5.5 Learjet 35A/36A GFD configuration front wheel tire with shines

Flight tests performed by the NLR in a Citation II jet aircraft to validate the **NLR-TP-2001-204** study are shown in **NLR-TP-2001-490**. The NLR Citation II is equipped with the same tire type as the Learjet 35A/36A from this report[11], with the exception that the Citation II tires are not equipped with chines. In **NLR-TP-2001-204**, the spray flow simulation "CRspray" results developed for the NLR Citation II are provided in graphical form. Due to the similarity of aircraft tires and aircraft size, the "CRspray" simulation results can be applied to the Learjet 35A/36A with a certain degree of accuracy.

The spray envelopes shown in **NLR-TP-2001-204** have therefore been overlaid to scale with a frontal view of the Learjet 35A/36A due to the similarity of both aircraft. All spray envelopes have been determined using a cross-ply tire *without chines* at an inflation of 35 psi and a speed of 60 ft/s[12], a tire load of 500 lb and a pool depth of 0.6 inch. The effect of the chines on the Learjet 35A/36A tire is estimated by a further rotation of the spray envelope by 30° as shown in each figure.

Fig. 5.6 shows the graph obtained by "CRspray" overlaid with the Learjet 35A/36A geometry. Fig. 5.7 shows a spray envelope measured in Test Run 39 of **NASA TP2718** overlaid with the Learjet 35A/36A geometry.

11 Tire type installed on the NLR Citation II Jet has been verified in a communication with NLR
12 This aircraft velocity corresponds to about 70% of the hydroplaning velocity (**NLR-TP-2001-204**)

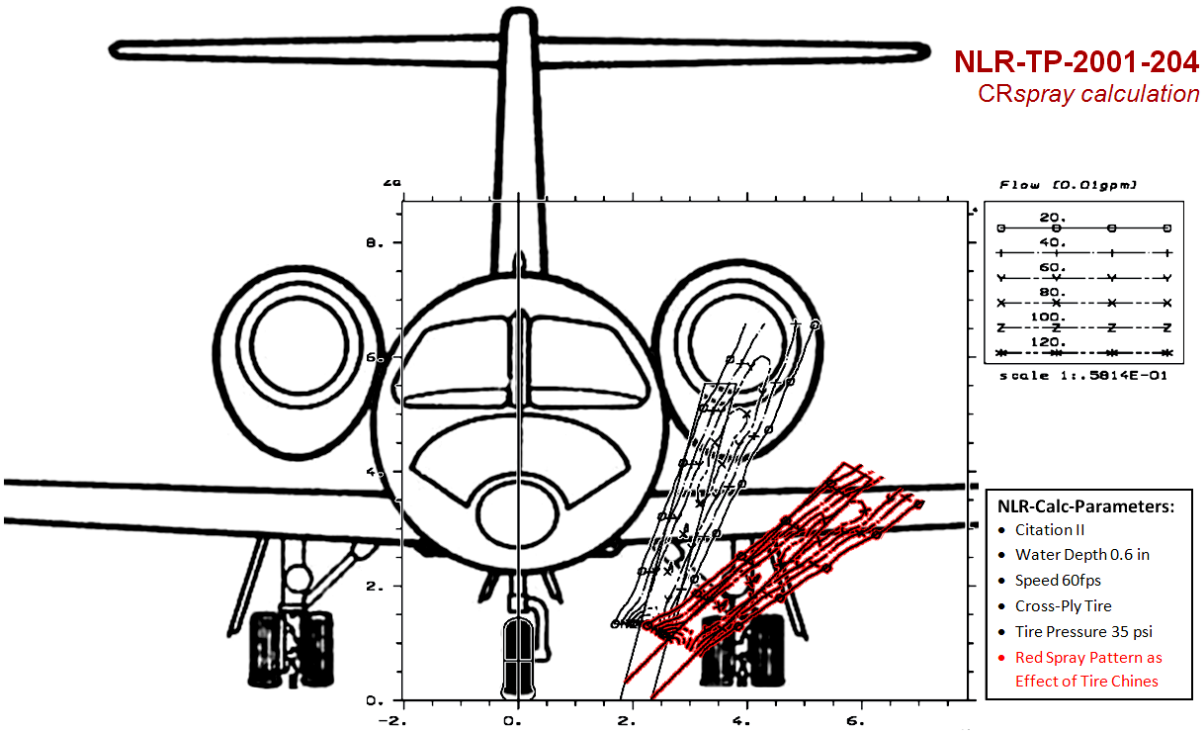

Fig. 5.6 Overlay "CRspray" Calculation and Learjet 35A/36A (based on **NLR-TP-2001-204**)

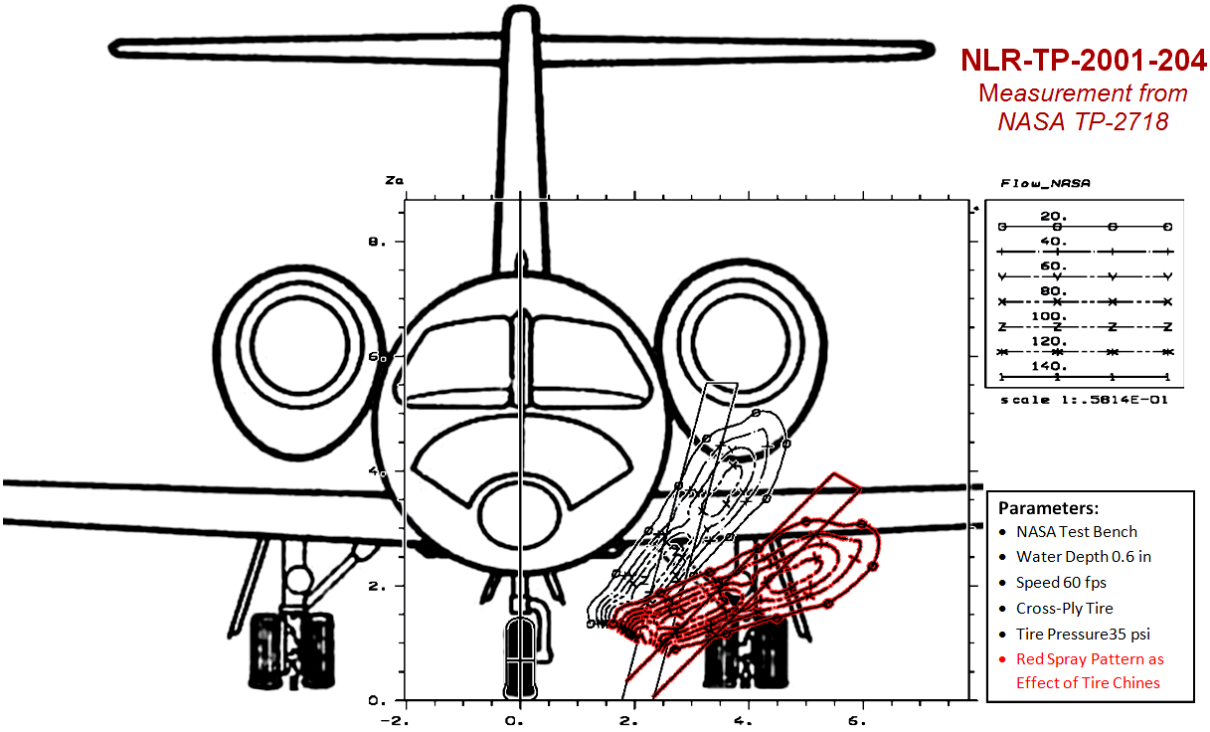

Fig. 5.7 Overlay NASA TP-2718 Test Run and Learjet 35A/36A (based on **NLR-TP-2001-204**)

As can be seen clearly, the spray plume rises from the ground towards the aircraft structure and the spray plume extends towards the engine ingestion area. With chines assumed and the spray plume deflected by 30°, the engine ingestion area is not targeted by the spray. This can be seen as a further validation of the assumption for the chine induced spray deflection.

However, the spray plume at 30° deflection is directed towards the area of the store attachment points under the wings. This means that impinging spray could hit the stores frontally at the maximum spray density. Since the approach to consider the chines is relatively simple, a large conservatism may be applicable. The *worst case scenario* to consider would therefore be the center of the spray plume to be targeted directly in the direction of the stores, with its maximum density at the location of the stores.

In addition, it can be seen that also a section of the wing and the main landing gear is in the trajectory of the spray wave. The exposed airframe due to water spray is therefore assumed to consist of the *under-wing store* frontal area, the *wing frontal section* above the stores as well as the *main landing gear* area on each side of the nose wheel.

5.4 Areas of the Aircraft Exposed to Water Spray

After the spray angle determination has been carried out and the impacted exposed parts of the aircraft been found, the sum of the exposed area has to be determined.

For the determination of the exposed aircraft surface due to under-wing stores installed, the largest stores certified for installation on the aircraft, MTR-101, have been taken as a baseline. The MTR-101 dimensions are taken from Fig. 5.8.

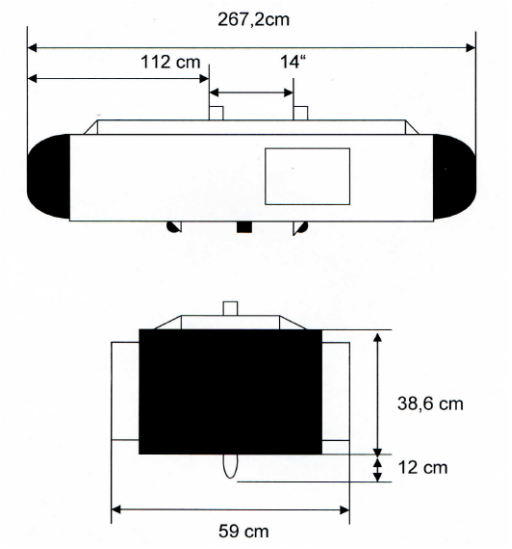

Fig. 5.8 Under-Wing Store MTR-101 Dimensions

Fig. 5.8 yields a frontal area of $A_{frontal,store} = 0{,}23\ m^2$. The store also has a total wetted area of $S_{wet,store} = 5{,}22\ m^2$.

The wing section at the location of the store shall be assumed to be impacted by the spray as well. As the aircraft is equipped with a NACA 64A-109 airfoil, the thickness t_{wing} of the wing amounts for 9% of the chord length[13]. The root chord c_t is 2,74 m long. Thus:

$$t_{wing} = 0{,}09 \cdot 2{,}74\ m = 0{,}24\ m$$

For the frontal area of this wing section, the width of a store is used to determine the dimensions along the y-axis of the aircraft. This yields $A_{frontal,wing\ section} = 0{,}14\ m^2$.

For the main gear area, the measurements from Fig. 5.9 have been used.

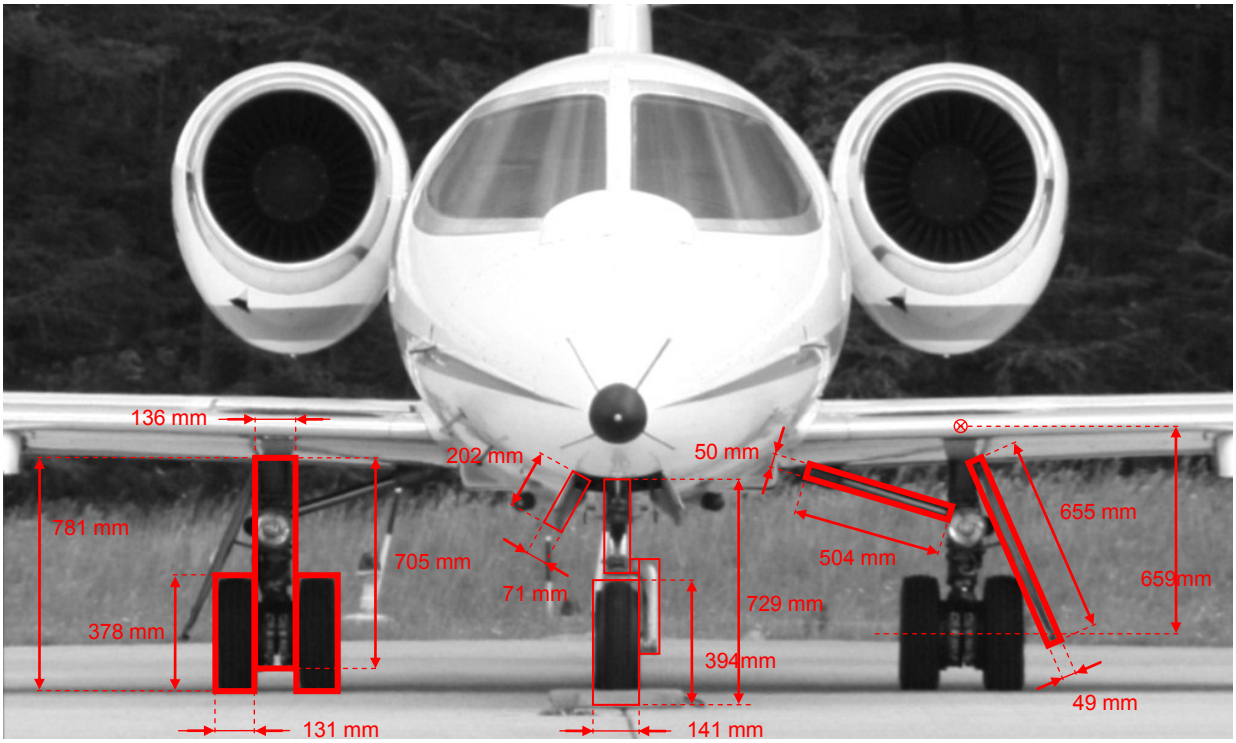

Fig. 5.9 Gear Geometry Front View Learjet 35A/36A, Measurements taken from the Aircraft

For the main gear, this yields a total frontal area of $A_{frontal,main\ gear} = 0{,}25\ m^2$.

In total, this yields a total exposed area the Learjet 35A/36A of $A_{exp} = 0{,}62\ m^2$.

13 According to standard NACA nomenclature, the last two digits of the code number give the thickness in percent of the chord length.

5.5 Water Impingement Drag Force Determination

For the estimation of the actual momentum loss induced drag force of the water impingement, the **NASA TP2718** research results were taken into account as the most valuable source of specific data.

NASA conducted research for the **NASA TP2718** with a range of different tire loadings, types, deflections and speeds behind a dummy fuselage, as shown in Fig. 5.10. The form of a typical side wave can also be seen in this figure. Water quantities were measured with a rack of test tubes that would ingest the water quantities measured at the test location. Since there are no test runs whose parameters would completely match the actual parameters used for this report, all possible combinations that were tested by NASA were evaluated. The run that was found to reflect the Learjet 35A/36A conditions most appropriately in terms of tire deflection, speed and measurement location of the measurement board was then selected. The test run selected was run 33 due to water depth, tire speed and especially the test rack measurement location in the area of the under-wing stores. Focus of the investigation was the under-wing store area, as the amount of impingement drag and its repercussion on the takeoff performance has been the most unclear.

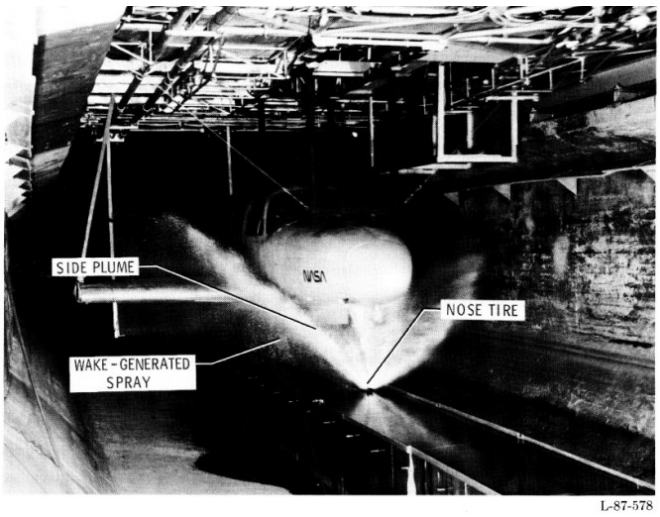

Fig. 5.10 NASA Spray Test Vehicle (**NASA TP2718**)

This allowed analysis of the chart from **NASA TP2718** providing the water masses ingested by each of the tubes of the test rack. Each tube location is signified by a small square, containing the amount of water ingested by it. As the test conditions used by NASA do not match the parameters to be considered in this report completely, the study was used to estimate a relation between the total water mass displaced by the tire, and the water mass that is targeted at the exposed area of the aircraft.

Identification of the area of highest spray intensity equally determines the worst case placement of an object placed in the water flow. This area is highlighted in Fig. 5.11.

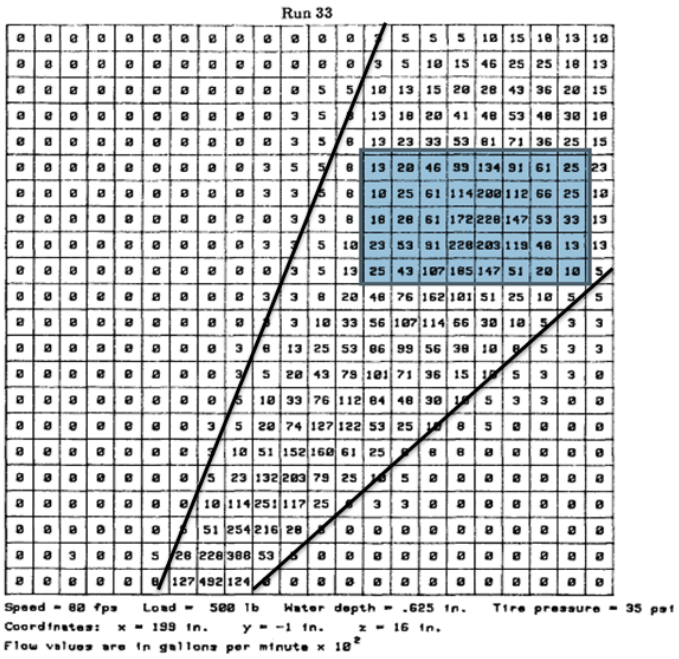

Fig. 5.11 NASA Spray Pattern of Test Run 33, Identification of Maximum Spray Intensity Area (**NASA TP2718**)

The blue square in Fig. 5.11 represents the sum of all areas exposed to the spray identified according to the Learjet 35A/36A geometry. As the blue box is located where the maximum density of the spray is obtained, the worst case scenario is covered by assuming that the exposed areas are subjected to the highest spray intensity.

The absolute amount of water that was measured by all test tubes in total was counted by summing up all values for each test tube in the whole chart. Then, summing up the amount of water contained in the blue box alone led to the determination of a ratio between water outside and inside the blue box. This ratio reveals which amount of water compared to the total displaced water will hit the exposed areas of the aircraft in a worst-case assumption.

It was found that the amount of water in this area of highest density accounts for 20-30% of the total water masses displaced by the tires, also in other test runs. Consequently, for the following calculations, a ratio of 30% is assumed for the amount of water that actually impinges on the exposed areas, compared to the total water mass displaced by the tires.

The following equations derive a relation for the impingement drag force with regard to aircraft speed and water depth. The total water mass displaced $\dot{m}_{displ,total}$ is given by Eq. 5.3

$$\dot{m}_{displ,total} = \dot{V}_{displ,total} \cdot \rho_{water} \tag{5.3}$$

With

$\dot{m}_{displ,total}$	Total mass flow displaced by a tire
$\dot{V}_{displ,total}$	Total volume flow displaced by a tire
ρ_{water}	Density of water, $\rho_{water} = 1000\ \mathrm{kg/m^3}$

And

$$\dot{V}_{displ,total} = A_{tire,subm} \cdot v_{aircraft} \tag{5.4}$$

$A_{tire,subm}$	Frontal area of tire submerged in the runway contaminant, see Sect.
$v_{aircraft}$	Aircraft Speed

The actual quantity of water impinging against the exposed areas of the aircraft is found from Eq. 5.5. It gives the water mass flow on either side of the fuselage as $\dot{m}_{imp,semi}$. It is assumed that no bow wave is formed, which is a valid and conservative approximation for a single nose wheel tire such as the one installed on the Learjet 35A/36A.

$$\dot{m}_{imp,semi} = r_{imp,\%} \cdot \frac{\dot{m}_{displ,total}}{2} \tag{5.5}$$

With

$\dot{m}_{imp,semi}$	Water mass flow against exposed area on either side of the fuselage
$r_{imp,\%}$	Ratio of total displaced water vs. water impinging on exposed area

For the Learjet 35A/36A geometry, a value of $r_{imp,\%} \approx 0{,}3$ was determined.

From the water mass flow against the exposed areas of the aircraft, the resulting drag force can be calculated based on a simplified **NLR-TP-2001-204** method.

Boundary layer assumptions can and need to be neglected. Also, **NLR-TP-2001-204** suggests a restitution coefficient of 0.2, which reflects the energy dissipated in the inelastic collision of water particles with the stores surface.

This yields:

$$D_{imp} = 2\,\dot{m}_{imp,semi} \cdot (u_{particle} - e_{res} \cdot u_{reflection} - (1 - e_{res}) \cdot u_{fluid}) \tag{5.6}$$

With

e_{res}	Restitution Coefficient, e_{res} = 0.2 acc. to **NLR-TP-2001-204**
$u_{reflection}$	Velocity of fluid particles reflected from impingement surface
$u_{particle}$	Velocity of a fluid particle after impingement
u_{fluid}	Initial velocity of a fluid particle

Since the side wave directs the spay displaced by the frontal tire of the aircraft sideways, the fluid particles are assumed to incur no acceleration along the runway centerline. Therefore, the relative fluid particle velocity of a side wave spray droplet is assumed to be:

$$u_{fluid} = v_{aircraft}$$

Furthermore, the exposed area of the aircraft is measured from a frontal view and assumed flat, so it is plane and normal to the free stream direction. Therefore, the fluid particles are assumed to not be reflected by the impingement surface perpendicular to the free stream direction. The relative speed between aircraft and fluid particle is assumed to be zero after collision. This yields:

$$u_{reflection} = u_{particle} = 0$$

Resulting from these simplifications, Eq. 5.6 reduces to:

$$D_{imp} = 2\,\dot{m}_{imp,semi} \cdot (1 - e_{res}) \cdot v_{aircraft} \tag{5.7}$$

The spray angle correction factor k_{angle} may also be applied to Eq. 5.7 below aquaplaning speed, yielding

$$D_{imp} = k_{angle} \cdot 2\,\dot{m}_{imp,semi} \cdot (1 - e_{res}) \cdot v_{aircraft} \tag{5.8}$$

In the time-stepwise calculation method, this drag can be calculated for each aircraft speed. For reference, it is also possible to convert the impingement drag force back to a drag coefficient increment due to water spray with reference to the complete aircraft as shown in Eq. 5.9.

Determination of the Maximum Collision Drag Force

The equation derived for the collision drag needs to be validated, this shall be done for the configuration of the Learjet 35A/36A.

The aquaplaning speed according to Eq. 1.1 is 92,2 kts for the nose wheel tire of the Learjet 35A/36A, inflated at 105 psi. The highest impingement drag will be measured at the aquaplaning speed of $v_{aircraft} = v_{aquaplaning} = 47{,}4\ m/s$.

For the nose wheel and contaminant depth, the following data is used.

$$b_{eff} = 0{,}101 \text{ m}$$
$$d_{cont} = 0{,}003 \text{ m}$$

The total water mass flow displaced is obtained from equation 5.3 and 5.4 as:

$$\dot{m}_{displ,total} = 14{,}36 \text{ kg/s}$$

With $r_{imp,\%} = 0{,}3$, the amount of water mass flow to hit the exposed areas of the Learjet 35A/36A would be:

$$\dot{m}_{imp,semi} = 2{,}15 \text{ kg/s}$$

With the assumptions taken for the impingement drag, Eq. 5.8 yields

$$D_{imp} = 163{,}4 \text{ N}$$

As can be seen, both the drag increment and the drag force are very small compared to other contributors, even though a worst case with focus on the under-wing stores has been considered. It should be noted that the impact of deflected water from the underside of the wing and potential interference effects have not been considered. This could be determined in a CFD calculation.

For comparison, at equal conditions as the ones used for the impingement drag calculation for the Learjet 35A/36A, a skin friction drag of $D_{skin} = 46\,N$ is determined according to Eq. 4.86. This takes into account the complete skin friction drag for the aircraft fuselage.

Backed by this figure, the relatively low impingement drag force determined by Eq. 5.8 does seem to produce relatively coherent and plausible magnitudes for the drag force.

It should also be noted that the drag force data determined by flight test and CRspray simulation from **NLR-TP-2001-204**, considering the Citation II of the NLR at a *water depth of 12 mm*, cannot be compared by linear scaling to the drag force values determined above for the Learjet 35A/36A at *3 mm*.

This is pointed out in **NLR-TP-2001-490**, comparing flight test results for precipitation drag of a Dassault Falcon at a water depth of 20 mm to a Citation II at a water depth of 10 mm. The doubling of the water depth increased the precipitation drag by a factor of 10.

6 Aircraft Parameters

The takeoff performance calculation, notably the Balanced Field Length determination, is based on the equations outlined in chapters 4 and 5. Chapter 6 serves to apply them to the specific aircraft to be considered in the simulation. The input parameters used for this simulation are clustered by flight mechanical forces. When applicable, the specific parameters shown for the Learjet 35A/36A are validated with flight test data, literature values and references from the AFM and AFMS.

6.1 General

The Learjet 35A and 36A versions shown in Fig. 6.1 are light twin-turbofan business jets manufactured by Learjet Inc., a subsidiary of Bombardier Inc.

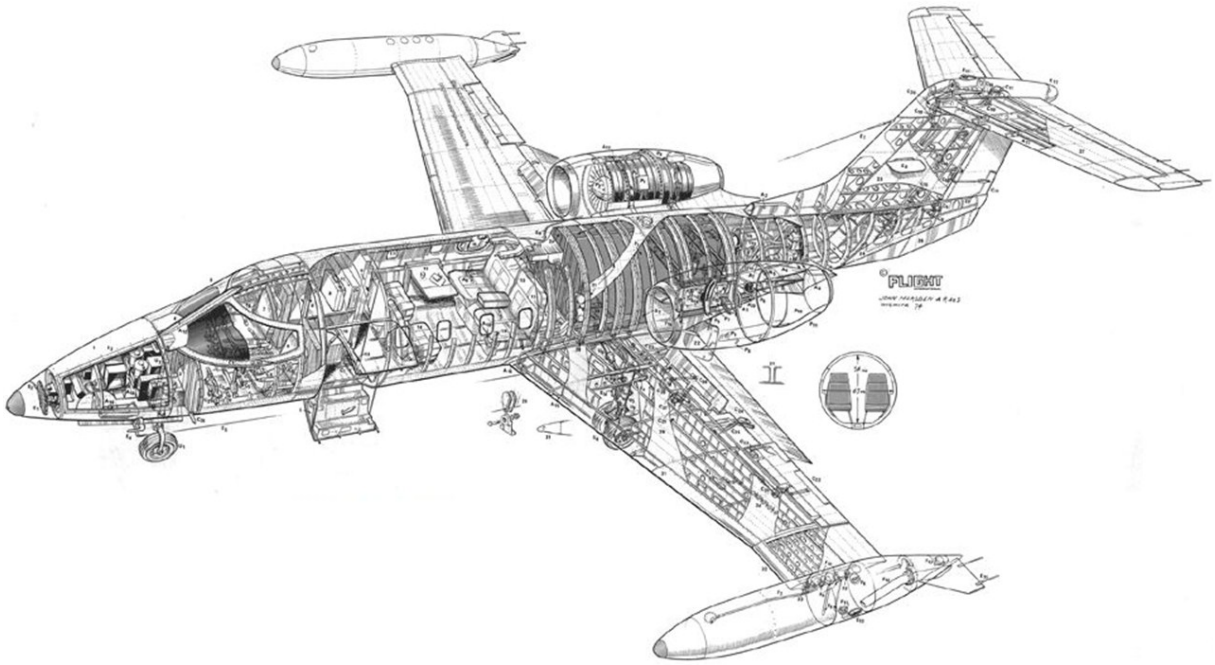

Fig. 6.1 Cutaway Picture of the Gates Learjet 35A/36A (**Flightglobal**)

The specific configuration of the operator GFD that operates the Learjet 35A/36A with underwing stores is referred to as EXTGFD configuration. This is the configuration considered in this report. A report that was used to determine dry runway takeoff performance AFMS data for the aircraft is available, and referred to as **GJE EXTGFD-003**.

The Learjet 35A/36A is equipped with two Garret TFE731-2-2B turbofans, each rated at 15,6 kN, pod-mounted on the sides of the rear fuselage. The aircraft is capable of reaching a maximum ceiling of 45,000 ft and obtains a maximum level speed of 471 knots at 25,000 ft. The gear is a retractable tricycle type, with twin wheels on each main unit and a single steerable nose wheel. The wing section is a NACA 64A109 profile with a modified leading-edge. The wing has a dihedral angle of 2°30', is mounted at an incidence angle of 1° and swept back at quarter chord angle of 13° (**Janes 1999**).

The Learjet 35A/36A empty weight (equipped) of 10,119 lbs relates to its maximum takeoff weight of 18,300 lbs in standard configuration and increased to 19,600 lbs in the configuration with extended wingtips according to the Aircraft Flight Manual Supplement **AFMS 9702-2**.

The GFD fleet of Learjet 35A/36A considered for this report is equipped with Avcon delta fins, extended tip tanks, under-wing store pylons and all aircraft are certified for the increased takeoff weight up to 19,600 lbs.

6.2 Geometry

All geometrical parameters that are being used in the simulation have been obtained from 3-view drawings from the **Learjet 30 Series Pilot Training Manual**, measurements taken from the actual aircraft and references from **Janes 1999**.

The Wing Surface and Reference Area S_W, wing span and aspect ratio are input parameters of major importance for the further discussions.

Wing Surface	S_W	23,53 m²
Wing Span	b	11,61 m (not over vane)
Aspect Ratio	A	5.7

The Aspect Ratio which is referenced in **Janes 1999** has been cross checked with the values obtained from the drawings.

The breakdown of surfaces from **Appendix F** yields a wetted surface of the aircraft of:

S_{wet}	154,65 m²	Wetted Area (Learjet 35A/36A)

The following geometric parameters will be used for subsequent calculations of parameters shown in this chapter or are needed as input data for equations from Chapter 4.

Table 6.1 Wing Parameters for Aerodynamic Analysis

Parameter	Symbol	Value	Unit
Wing Span over Tip Tank (not over vane)	b	11.61	m
Chord at Wing Tip	c_t	1.55	m
Chord at Wing Root	c_r	2.74	m
Chord of the Spoiler	c_s	0.3	m
Distance of the Wing to the Ground	h	1.0	m
Wing Reference	S_W	23.53	m²
Exposed Wing Area	S_{exp}	18,826	m²
"Flapped" Wing Surface, influenced by Flaps	S_{flap}	8.86	m²
Wetted Area of the Wing due to Spoiler Deflection	S_{SW}	1.3	m²
Wing Sweep at λ/4	φ_{25}	13,00	°
Taper Ratio	λ	0,57	-
Wing Twist	ε_t	-3	°
Incidence Angle	$\alpha 0$	1	°
Angle of Attack during takeoff roll	$\alpha 0$	1	°
Engine to CG Distance along pitch axis	l_E	1,24	m
VTP 25% MAC to CG Distance	l_V	4,97	m
VTP Area, total	S_V	3,73	m
VTP Span	b_V	1,81	m
VTP Sweep	Λ_V	36°	°

6.3 Mass

The mass of the aircraft is to be varied according to the requirement to provide a takeoff performance chart for various takeoff masses. When comparing the aircraft without stores to the aircraft with stores, the aircraft mass is assumed to be constant.

The operation procedure of GFD when under-wing stores are installed is to compensate the Zero Fuel Weight (ZFW) increment of the stores by taking less fuel on board. This means that no specific weight variation needs to be applied for the aircraft with and without under-wing stores.

6.4 Thrust

The Learjet 35A/36A power plant TFE-731-2-2B has the characteristics shown in Tab. 4.2 acc. to the **HONEYWELL TFE 731 Pilot Handbook**.

Table6.2 Honeywell TFE-731-2-2B Engine Characteristics

Parameter	Symbol	Value	Unit
By-pass-ratio	BPR	2,51	-
Thrust per engine	T_0	3500	lbs
Idle thrust per engine	$T_{0,idle}$	250	lbs

With an installation loss of 3% according to **LTH AT21000.06**, the net thrust per engine on the Learjet 35A/36A (Anti-Ice OFF) is:

$$T_{0,net} = 3395\ lbs$$

Limited test data for the TFE-731-2-B engine is available from **GJE EXTGFD-003**. The installed initial thrust $T_{0,net}$ at MSL, ISA can be validated with the respective graph for ISA, MSL from figure 6.2 suggesting a $T_{0,net}$ of 3400 lbs at M=0.

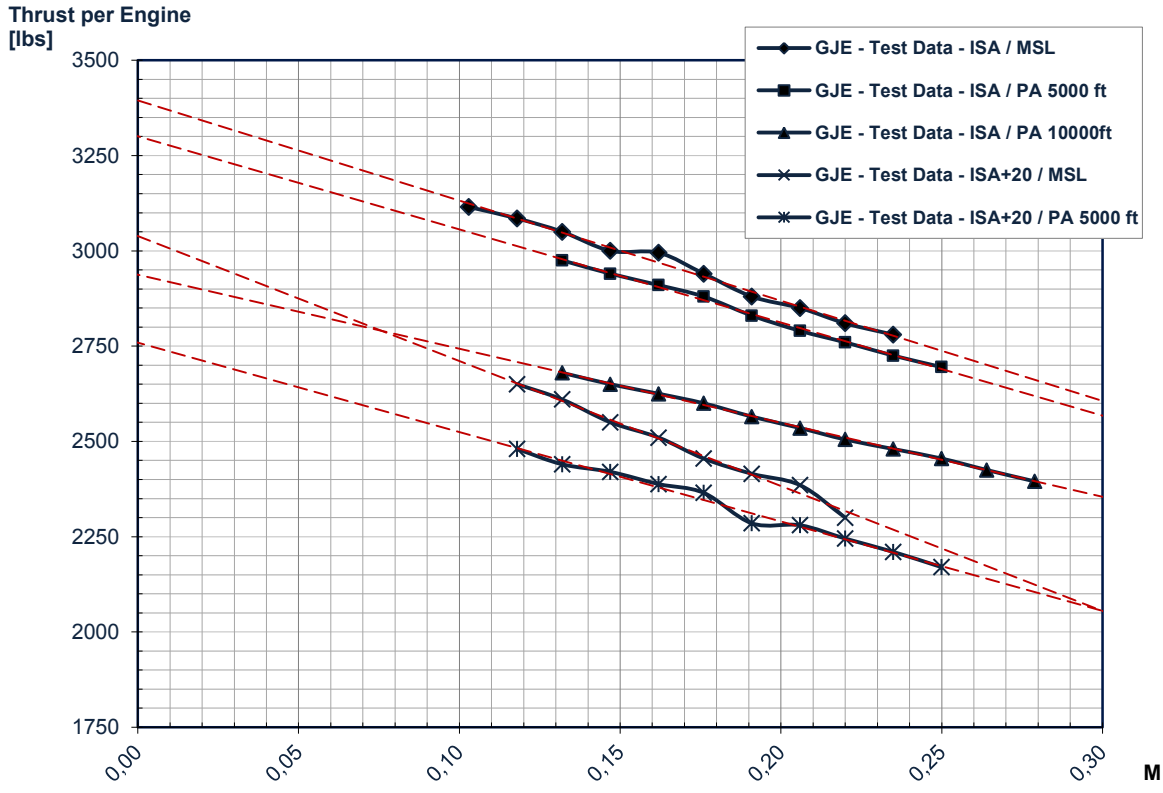

Fig. 6.2 **Installed Thrust** Variations with Pressure Altitude and OAT for TFE731-2B-2 Engine
*Linear Extrapolation of Test Data from **GJE EXTGFD-003***

As can be seen by the intersection of thrust slopes for different environmental parameters, the GJE test data might be influenced by inaccuracies. The thrust gradient with regard to Mach number should be constant. However, Fig. 6.2 represents the best available data for the installed engine.

Thrust Variation with Mach Number and Pressure Altitude

The **GJE EXTGFD-003** report test data shown in Fig. 6.2 does not represent the environmental conditions that shall be considered in this report. Therefore, the thrust data used for the report had to be calculated based on an academic approach.

For the determination of the thrust variation, the analysis from Section 4.1.6 was used to make the decision to model the thrust according to **Bartel & Young 2007** for pressure altitude and Mach number. Furthermore, the temperature correction acc. to **Raymer 1989** at temperatures above the flat rate temperature limit was used.

The academic thrust model was then used to determine the thrust at the test conditions provided by **GJE EXTGFD-003** shown in Fig. 6.2 in order to estimate the accuracy of the model. The validation plots are included in Appendix B. The test data is matched excellently by the academic approach at MSL, ISA. The academic thrust model matches with the test data, but for all non-ISA conditions provides conservative results by an amount of approximately 10%.

In order to obtain realistic thrust data for the simulation, correction factors for certain variables in the academic approach that are used to calculate the thrust according to **Bartel & Young 2007** had to be found. Two variables proved to be especially useful to control and adapt the academic thrust model. The Gas Generator Function G controls the slope of the thrust decay graph with regard to Mach number, without changing the amount of static thrust. The pressure ratio related term A given by Eq. 4.44 controls the offset of the graph along the thrust axis, which allows it to scale thrust data to desired values.

The correction factors necessary to match the test data have been derived empirically from the comparison between the graphs given in Appendix B. The correction aims at reducing the excessive conservatism that results from the application of the academic model. Correction factors used for G and A in each of the test cases are indicated for each figure. It was found that the slope of the thrust decay had to be corrected as a function of Delta-ISA. It can also be seen in Fig. 6.2 that the slope of the graph for ISA+20 thrust data differs to that of the thrust data at ISA conditions. Furthermore, the correction for the pressure ratio related term A was found to be a linear function of the pressure altitude. A plot showing the linear variation of A with pressure altitude is shown in Fig. B.7.

The determination of the necessary corrections resulted in two corrected equations for *G* and *A* used as a replacement in the original **Bartel & Young 2007** approach.

$$G = -0{,}01\,\Delta t_{ISA} + 0{,}9 \tag{6.1}$$

With

Δt_{ISA} Delta-ISA Temperature difference in K acc. to Eq. 4.26

For ISA conditions, Eq. 6.1 yields $G = 0{,}9$ as given as a reference for small By-Pass Ratios (BPR) in the thrust decay approximation.

For the pressure ratio related term *A* from Eq. 4.44, a correction factor $f_{corr,A}$ is used.

$$A = \left(-0{,}4327\left(\frac{p_{true}}{p_0}\right)^2 + 1{,}3855\left(\frac{p_{true}}{p_0}\right) + 0{,}0472\right) \cdot f_{corr,A} \tag{6.2}$$

With $f_{corr,A}$ derived from the corrections necessary to match the graphs

$$f_{corr,A} = 8 \cdot 10^{-6} \cdot H + 1 \tag{6.3}$$

And

H Pressure Altitude in ft

As a result of the corrections, the academic thrust model may be assumed to be of acceptable accuracy for the takeoff performance determination. Due to the fact that the actual environmental parameters to be used in this report differ far less from the ISA conditions than the thrust validation data, less correction of the thrust model is required and good matching with the test data is expected.

Flat Rate Characteristics

According to the **HONEYWELL TFE 731 Pilot Handbook**, the engine is flat rated at 22°C OAT at MSL, ISA. However, as outlined in Section 4.1.6, the flat rate temperature limit varies with pressure altitude, so that a relation between pressure altitude and flat rate limit has to be determined.

According to **Bräunling 2004**, the temperature at which the flat rate temperature limit is reached is the temperature where a maximum RPM as percentage of N1 speed is obtained. The Max RPM/ITT Limit Chart from the Learjet 35A/36A flight manual[14] was used to determine this relation as a function of pressure altitudes and the OAT.

The resulting graph that shows the max RPM/ITT limit OAT, signifying the flat rate temperature, with regard to pressure altitude, is given in Fig. 6.3.

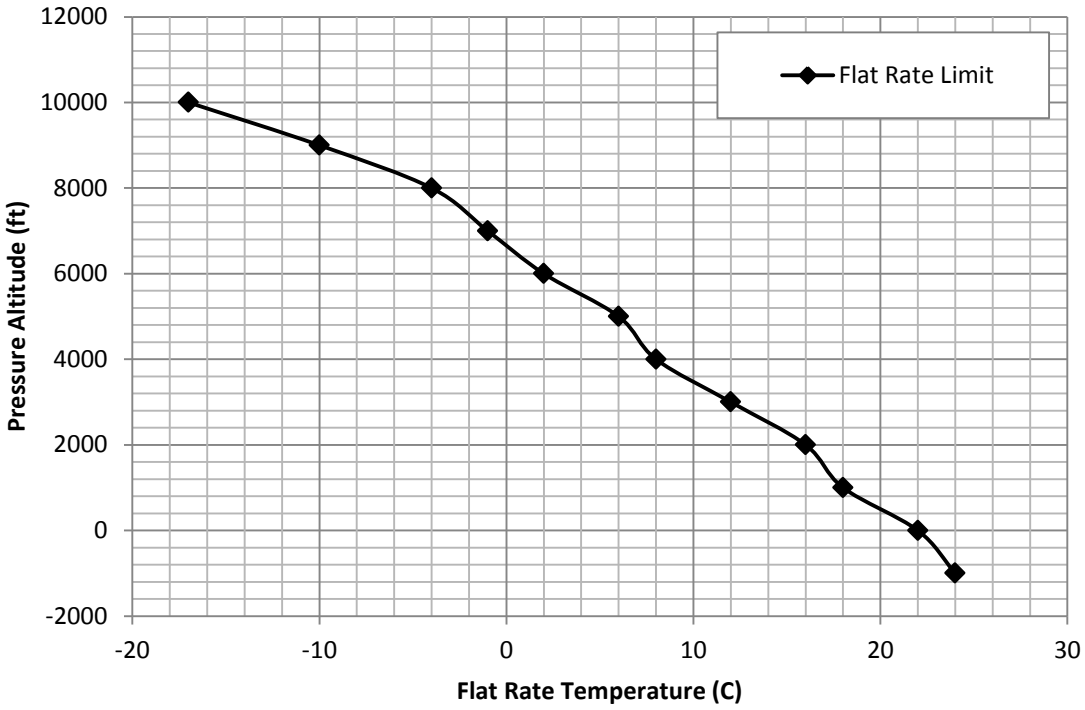

Fig. 6.3 Flat Rate Temperature Limit with Regard to Pressure Altitude,
Based on Learjet TFE-731-2 Thrust Setting Chart, Appendix D

From Fig. 6.3, the flat rate limit temperature of the engine can be determined for each pressure altitude. For example, at MSL, a flat rate temperature of 22°C OAT is achieved. This matches with the data from the **HONEYWELL TFE 731 Pilot Handbook**. The flat rate temperature limit then decays with rising pressure altitude.

14 See Appendix D

The flat rate temperature limits from Fig. 6.3 are used in the thrust model of the performance calculation. Fig. 4.5 shows the thrust decay with OAT under consideration of the flat rate temperature limit.

The failed engine produces windmilling drag, the resulting drag coefficient increment is determined in Section 6.5.

6.5 Lift Coefficient

All following data are determined for the takeoff configuration with flaps deflected at 8°. The lift-coefficient during the ground roll is determined speed-dependent from the equations of Section 4.1.7.

For the determination of the ground lift coefficient $C_{L,G}$, the lift coefficient components given in Tab. 6.3 have been determined.

Table 6.3 Lift Coefficient and Lift Coefficient Components, Ground, Flaps 8°, ISA, MSL (ISA, MSL, weight 19600 lbs, Flaps 8°, 120 kts)

Parameter	Symbol	Value	Equation
Lift Coefficient, Ground	$C_{L,G}$	0,243	Eq. 4.50
Lift Coefficient, Ground with Spoiler impact	$C_{L,Spoiler}$	0,223	Eq. 4.119
Lift Coefficient, Wing, without flaps	$C_{L,W}$	0,215	Eq. 4.51
Lift Coefficient, Aircraft, without flaps (for comparison)	-	0,178	-
Zero Lift Coefficient	$C_{L,0}$	0,138	Eq. 4.56
Flap Lift Increment	$\Delta C_{L,F}$	0,08	Eq. 4.58
Fuselage Carryover Lift Increment	$\Delta C_{L,Fuselage}$	0,0081	Eq. 4.62

Fig. 6.4 provides the plot of the parameters from Tab. 6.3 with regard to speed. As can be seen, the variation with speed is not very large.

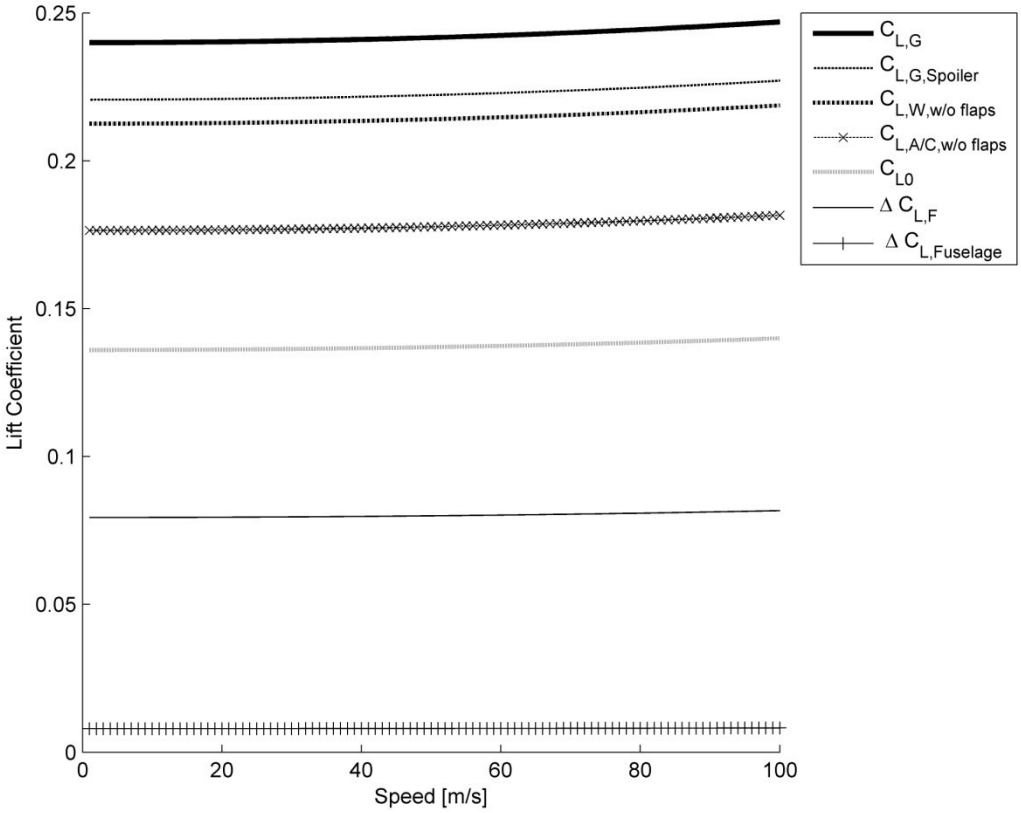

Fig. 6.4 Plot of Lift Coefficients and Components used for the numerical calculation (ISA, MSL, weight 19600 lbs, Flaps 8°)

For the calculation of the values from Tab. 6.3, the input parameters from Tab. 6.4 have been used.

For the Air Distance, $C_{L,LOF}$ has been calculated based on the Lift-to-Weight balance assumption according to Eq. 4.90. This lift coefficient in the performance calculation is therefore varying with liftoff speed and takeoff weight for each aircraft configuration. For the maximum takeoff weight of 196000 lbs, at V_{LOF} = 75 m/s, and with the parameters from Tab. 6.4, this yielded an exemplary $C_{L,LOF}$ of:

$$C_{L,LOF} = 1{,}318$$

Table 6.4 Input Parameters for Lift Coefficient Component Determination, Ground (ISA, MSL, weight 19600 lbs, Flaps 8°, 60 m/s)

Parameter	Symbol	Value	Equation/Source
Angle of Attack, On ground = Incidence Angle	α	1°	**Janes 1999**
Zero Lift Angle, Wing	$\alpha_{0,W}$	-1,78°	Eq. 4.57
Zero Lift Angle, Profile	α_0	-1,5°	Fig. 4.8
Wing Twist Angle	ε	-3°	**Janes 1999**
Mach Number Correction	-	1	Fig. 4.6
Wing Twist Correction	-	-0,408	Fig: 4.7
Profile Zero Lift Angle Change, Flaps	$\Delta\alpha_0$	-1,5°	Eq. 4.60
Flap Segment Chord Length	c_f	0,45 m	**NASA TN D-6573**
Wing Segment Chord Length	c	2,74 m	**NASA TN D-6573**
Flap Deflection Angle	δ	8°	**AFMS 9702-2**
Wing Lift Curve Slope	$C_{L\propto,W}$	4,43/rad	Eq. 5.52
Sweep Angle at 50% Chord	φ_{50}	12,697°	Eq. 4.55
Sweep Angle	φ_{25}	13°	**Janes 1999**
Flap Effectiveness Parameter	K'_{flap}	0,98	Fig. 4.9
Wing Area	S_W	23,53 m²	**Janes 1999**
"Flapped Area"	S_{flap}	8,86 m²	Measurement
Section Lift Coefficient with Flap Influence	$c_{L,Flap}$	0,235	Eq. 4.59
Flap Effectiveness Parameter	α_δ	0,38	Fig. 4.11
Lift Interference Factor Fuselage	K_{ff}	1/3	**Torenbeek 1982**
Wing Span	b	11,61 m	**Janes 1999**
Fuselage Width at Wing Intersection	b_{fi}	1,6 m	Measurement
Spoiler Wetted Area	S_{SW}	1,3 m²	Fig. F.4

Validation with GJE EXTGFD-003 Data

For a validation of the lift data, the **GJE EXTGFD-003** report was used. The input parameters for that report are based on a different calculation method and may be seen as an indication of the order of magnitude of the lift coefficient determined by the equations outlined in this report.

Table 6.5 Lift Coefficients given by **GJE EXTGFD-003** (ISA, MSL, weight 19600 lbs, Flaps 8°)

Parameter	Symbol	Value
Maximum Lift Coefficient	$C_{L,max,GJE}$	1,537 (MSL, ISA, 19600 lbs)
Lift Coefficient Taxi, Flaps 8°	$C_{L,taxi,GJE}$	0,185 (MSL, ISA, 19600 lbs)

It can be assumed that the takeoff will be performed not at the maximum lift coefficient but at the $C_{L,LOF}$. According to **Scholz 1999**, it can be estimated from Eq. 6.4.

$$C_{L,LOF} = 0{,}8 \cdot C_{L,max} \tag{6.4}$$

For the Maximum Lift Coefficient given in Tab. 6.5, this yields:

$$C_{L,LOF,GJE} = 1{,}23$$

Comparing this to the $C_{L,LOF} = 1{,}318$ used for the numerical calculation of this report estimated from the lift-to-weight balance, it can be concluded that both values lie in the same order of magnitude, with a 6% deviation. The same is true for the ground lift coefficient, while the deviation here is even larger. However, according **NLR-TP-2001-490**, the ground lift coefficient of a Citation II during ground roll lies in the region of $C_{L,G} = 0{,}4$. In the light of the detailed lift coefficient estimation, this can be seen as an indication that the lift coefficient assumed for the ground roll by **GJE EXTGFD-003** is indeed too small.

To conclude, the lift coefficients used in the simulation are in the expected order of magnitude. The lift force however has only an indirect impact on the takeoff performance via the normal load on the tires and resulting friction forces. Even the impact of a larger deviation of the lift coefficient would, as is shown in Section 9.2.2, have only a reduced impact on the overall BFL distance calculation.

6.6 Drag Coefficient

In contrast to the lift force, the drag force does directly influence the equation of motion in longitudinal direction. For the drag coefficient, a careful inspection of the parameters used for the drag coefficient determination is therefore necessary. Tab. 6.6 contains all drag coefficients used for the simulation.

Table 6.6 Drag Coefficients used in Takeoff Performance Simulation, Stores installed (ISA, MSL, weight 19600 lbs, Flaps 8°, 60 m/s)

Parameter	Symbol	Value	Equation
Overall Aircraft Drag Coefficient, AEO	$C_{D,TO,AEO}$	0,0606	Eq. 4.64
Overall Aircraft Drag Coefficient, Takeoff with OEI	$C_{D,TO,OEI}$	0,0797	Eq. 4.64
Overall Aircraft Drag Coefficient, Stop with OEI	$C_{D,AS,OEI}$	0,0979	Eq. 4.64
Induced Drag Coefficient, at 60 m/s	$C_{D,i}$	0,0031	Eq. 4.65
Profile Drag Coefficient	$C_{D,P,AEO}$	0,0575	Eq. 4.70
Zero Lift Drag Coefficient	$C_{D,0}$	0,0249	Eq. 4.71
Store Drag Increment, 2 MTR-101 installed	$\Delta C_{D,Store}$	0,0136	Eq. 4.74
Gear Drag Coefficient Increment	$\Delta C_{D,Gear}$	0,0190	Eq. 4.73
Flap Drag Increment *after Liftoff*	$\Delta C_{D,flap}$	0,0108	Eq. 4.72
Windmilling Drag Coefficient Increment	$\Delta C_{D,EWM}$	0,0100	Eq. 4.109
Asymmetrical Flight Condition Drag Increment, Full Thrust	$\Delta C_{D,ASYM,TOGA}$	0,0091	Eq. 4.112
Asymmetrical Flight Condition Drag Increment, Idle	$\Delta C_{D,ASYM,IDLE}$	0,0020	Eq. 4.112
Spoiler Drag Increment	$\Delta C_{D,Spoiler}$	0,0253	Eq. 4.120

For both the takeoff and the accelerate-stop conditions, a plot of the resulting drag coefficients with an assumed engine failure at 60 m/s has been created from the takeoff performance simulation, shown in Fig. 6.5 and Fig. 6.6.

These plots are not considering the reaction times and are just shown to evaluate the magnitude of the drag coefficient changes after engine failure.

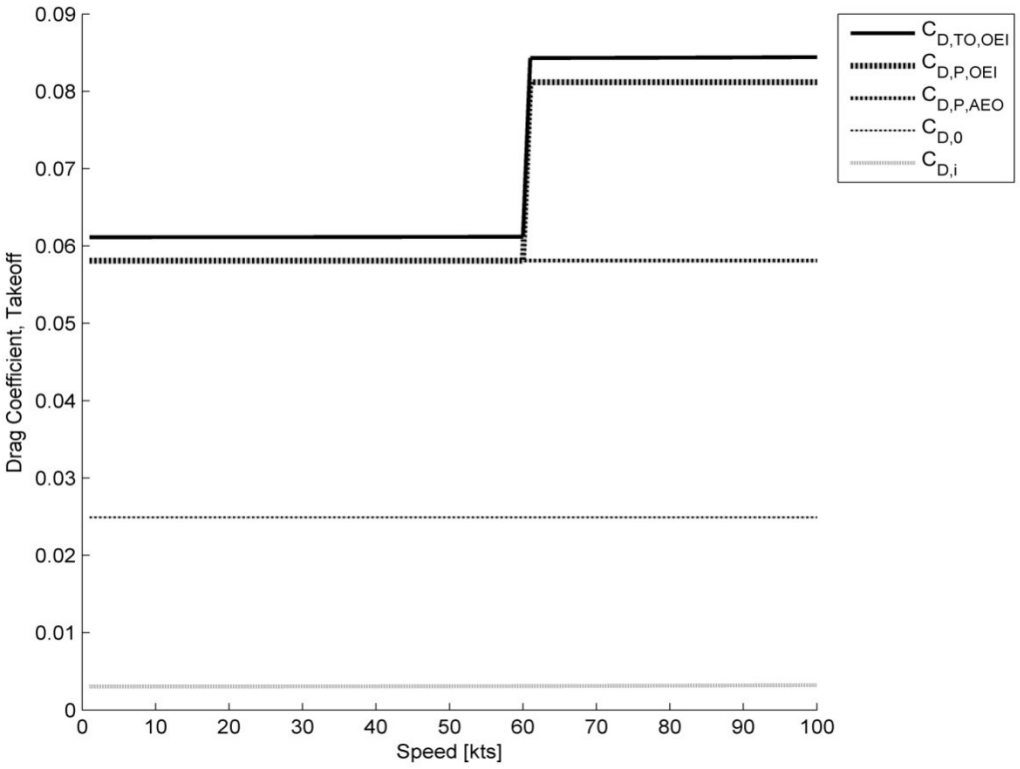

Fig. 6.5 Drag Coefficients Simulation for Learjet 35A/36A with Stores, Takeoff Case (Transition from AEO to OEI conditions shown exemplarily at 60 kts)

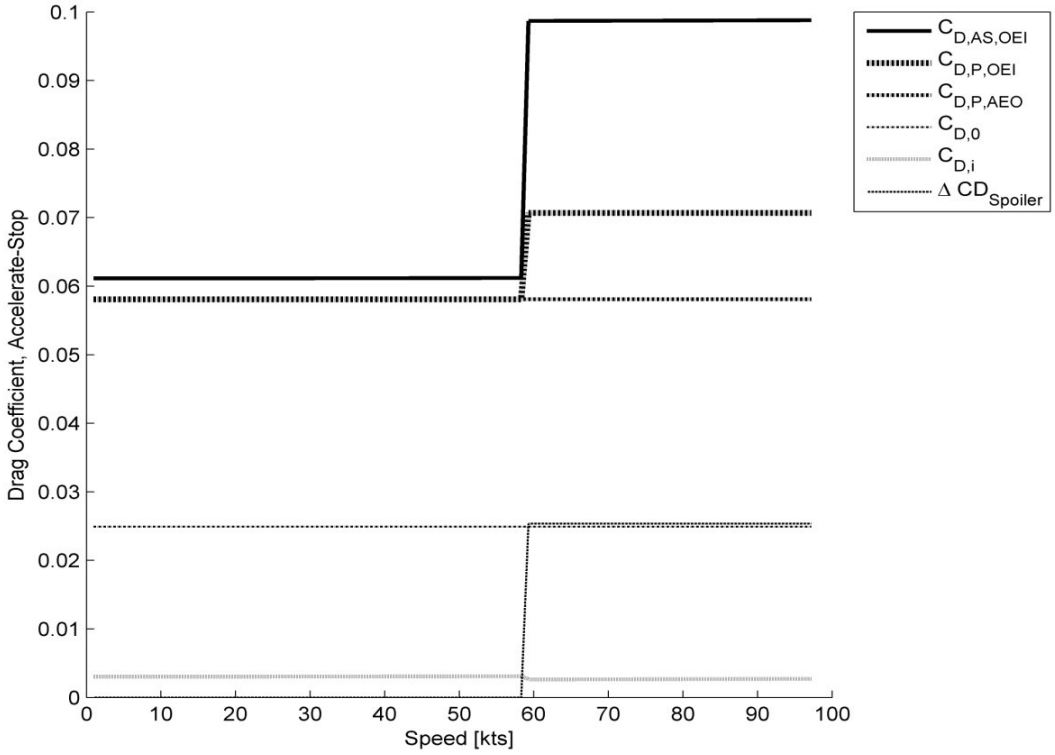

Fig. 6.6 Drag Coefficients Simulation for Learjet 35A/36A with Stores, Accelerate-Stop Case (Transition from AEO to OEI conditions shown exemplarily at 60 kts)

The calculation parameters used to determine the values from Tab. 6.6 shall now be outlined in detail for those drag coefficients and drag coefficient increments, where a more detailed analysis was necessary.

Zero Lift Drag Coefficient

For the zero lift drag coefficient, the equivalent skin friction drag coefficient approach by **Raymer 1989** from Eq. 4.71 was used. For the determination of the wetted area of the aircraft, a complete analysis of the Learjet 35A/36A based on geometrical measurements and other data was performed. The analysis is included in Appendix F of this report, and yielded a wetted area of $S_{wet} = 154{,}65\ \mathrm{m}^2$. With a $C_{fe} = 0{,}003$ and a 5% increase covering antennas, trim drag, interference drag, control surface gaps etc., this yielded a value for $C_{D,0}$.

$$C_{D,0,skin} = 0{,}0242$$

For the special GFD operation configuration (EXTGFD), the extended tip tanks have to be considered especially. According to the **AFMS 9702-2**, the extended tip tanks drag coefficient increment amounts to $\Delta C_{D,0} = 0{,}0007$. This was added to the $C_{D,0,skin}$ and yielded the zero lift coefficient used in the simulation.

$$C_{D,0} = 0{,}0249$$

Interestingly, this value relates very well to **Roskam 1989** who provides the drag coefficient breakdown for a Learjet 25 flying at Mach number $M = 0{,}75$, at $C_L = 0{,}336$.

Table 6.7 Profile Drag Coefficient Breakdown according to **Roskam 1989**

Parameter	**Value**	**% of total**
Basic Skin Friction drag	0,0180	53,25
Profile Drag Variation with Lift	0,0007	2,07
Interference Drag	0,0031	9,17
Roughness and Gap Drag	0,0015	4,44
(Induced Drag	*0,0072*	*21,30)*
(Compressibility Drag	*0,0028*	*8,28)*
(Trim drag	*0,0005*	*1,48)*
Total Drag Coefficient	**0,0338**	**100**
Total Lift Coefficient	**0,336**	**-**

The italic values in brackets do not apply for the takeoff speed range or are calculated by other methods as shown in this report. Compressibility and trim drag coefficient needs to be disregarded as well as the induced drag which is calculated independently according to Eq.4.65. This reduces the total drag breakdown of **Roskam 1989** to $C_{D,0} = 0{,}0238$ which is very close to the$C_{D,0} = 0{,}0242$ calculated via the equivalent skin friction coefficient.

Induced Drag Coefficient

The induced drag coefficient varies with the lift coefficient, as seen in Eq. 4.65. During the ground roll, the angle of attack is assumed constant, which leads to an almost constant induced drag coefficient as seen in Fig. 6.5 and 6.6. However, due to the lift coefficient reduction after spoiler deflection, the induced drag coefficient drops as a consequence, as can be seen in Fig. 6.6.

For a validation, the overall drag coefficient has been determined at a static speed at a lift coefficient of$C_{L,G} = 0{,}246$as experienced by the aircraft at 60 m/s.

$$C_{D,i} = 0{,}0031$$

The parameters from Tab. 6.8 were used to determine this drag coefficient acc. to Eq. 4.65. In order to do this, the drag coefficient for the aircraft in cruise configuration needed to be known. This has been done by using the lift and drag breakdown provided by **Raymer 1989** as shown in Tab. 6.7.

Table 6.8 Induced Drag Coefficient Calculation Parameters (ISA, MSL, weight 19600 lbs, Flaps 8°, 60 m/s)

Parameter	Symbol	Value	Equation/Source
Ground Effect Factor	$\emptyset$	0,65508	Eq. 4.66
Wing to Ground Distance	h	1 m	Measurement
Wing Span	b	11,61 m	**Janes 1999**
Oswald Efficiency Factor	e	0,72	Eq. 4.69
Literature Value e for Cruise	$e_{cruise,Lecture}$	0,85	**Scholz 1999**
Literature Value e for Takeoff	$e_{T/O,Lecture}$	0,7	**Scholz 1999**
Oswald Factor, Cruise, Learjet	e_{cruise}	0,876	Eq. 4.68
Lift Coefficient Cruise	$C_{L,Cruise}$	0,336	Tab. 6.7, **Raymer 1989**
Ind. Drag Coefficient Cruise	$C_{D,i,Cruise}$	0,0072	Tab. 6.7, **Raymer 1989**
Aspect Ratio	A	5,7	**Janes 1999**

Under-Wing Store Drag Coefficient Increment

The under-wing stores used by GFD are variable in shape and size. The largest under-wing store MTR-101 has already been described in Section 5.4. **GJE EXTGFD-003** provides the drag coefficient increment of a single MTR-101 store as:

$$\Delta C_{D,Store} = 0{,}0068$$

The approach proposed by **Roskam VI** was used to validate this store drag, but the certified data from **GJE EXTGFD-003** was used for the performance simulation as it has been certified.

According to Eq. 4.74 with the parameters from Tab. 6.9, one store yielded a total drag increment of:

$$\Delta C_{D,Store,Roskam} = 0{,}0067$$

It can be seen that this estimation is very close to the value given by **GJE EXTGFD-003** and can be assumed as validated.

Table 6.9 Store Drag Coefficient Increment Calculation Parameters, Approach **Roskam VI**

Parameter	Symbol	Value	Equation/Source
Store Interference Factor	K	1,3	**Roskam VI**
Equivalent Skin Friction Coefficient, Store	c_{fe}	0,0045	Estimation
Wetted Area of the Store	$S_{wet,store}$	5,22 m²	Measurement
Wing Area	S_W	23,53 m²	**Janes 1999**

Gear Drag Coefficient Increment

It was chosen to use the approach by **Hoerner 1965**, as it promised the most accurate estimation of the gear drag coefficient based on the specific Learjet 35A/36A configuration.

The calculation acc. to Eq. 4.73 yielded a value for the gear drag coefficient increment of:

$$\Delta C_{D,gear} = 0{,}0190$$

It can be seen that this gear drag coefficient is in the proximity of the expected value from Fig. 4.13 and also close to the value proposed by **Roskam I** and **Torenbeek 1982**. The data from Tab. 6.10 has been used to determine the parameters needed for Eq. 7.73.

Table 6.10 Gear Drag Coefficient Increment Calculation Parameters, Approach **Hoerner 1965**

Parameter	Symbol	Value	Equation/Source
Gear Strut Length to Wheel Diameter Ratio	e/d	2	Fig. 5.9
Gear Drag Coefficient based on Gear Area	$c_{D,gear}$	0,70	Fig. 4.14
Frontal Gear Area (total)	S_{wheel}	0,64 m²	Fig. 5.9
Wing Area	S_W	23,53 m²	**Janes 1999**

Engine Windmilling Drag Coefficient Increment

According to **Torenbeek 1982**, the windmilling drag of the engine can be determined from geometrical and engine specific characteristics. According to Eq. 4.109, the windmilling drag coefficient in the speed region of $M = 0{,}1 \ldots 0{,}2$ was determined to be:

$$\Delta C_{D,EWM} = 0{,}0100$$

The input data from Tab. 6.11 was used to perform a variation of windmilling drag with Mach Number as shown in Fig. 6.7.

Table 6.11 Windmilling Drag Coefficient Increment Calculation Parameters

Parameter	Symbol	Value	Equation/Source
Engine Inlet Diameter	d_i	0,716 m	Measurement
Nozzle Exit to Inlet Entry Velocity Ratio	V_N/V	0,42	**Torenbeek 1982**
Wing Area	S_W	23,53 m²	**Janes 1999**
Mach Number	M	Varied	See Fig. 6.7

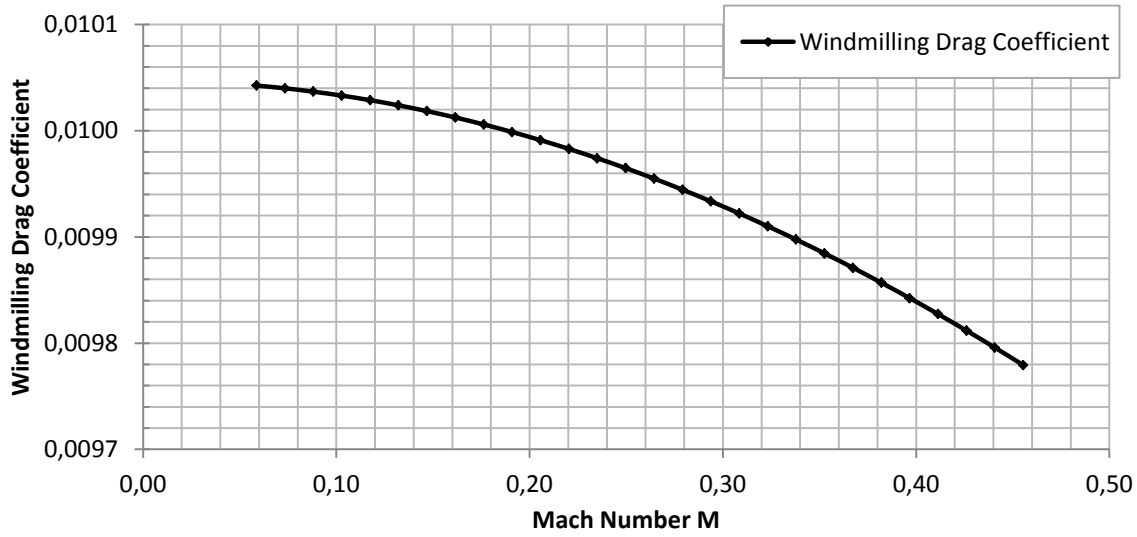

Fig. 6.7 Variation of Windmilling Drag with Mach Number

As can be seen, the windmilling drag varies very little with the Mach number. Therefore, a static value could be selected maintaining a good level of precision.

Asymmetrical Flight Condition Drag Coefficient Increment

As outlined in Section 4.4.2, the assumption of the windmilling induced yaw moment entirely by rudder deflection as proposed by **Torenbeek 1982** is a conservative assumption, not taking into account any bank and sideslip angles or tire side forces on the runway. However, banking of the aircraft while maintaining runway contact and shortly after takeoff is not possible, and the tire side forces are expected to be low due to the slippery wet runway conditions. Therefore, the approach presented in Eq. 4.112 to determine the asymmetry drag coefficient according to **Torenbeek 1982** was selected.

The determination of the asymmetry drag was already expected to be problematic due to the fact that the dynamic pressure is part of the equation of the asymmetry drag coefficient increment. This leads to the fact that for small speeds, the asymmetry drag tends to become infinitely large, because Eq. 4.112 is not designed for these very small speed regions.

The reason is that in theory, the rudder deflection required at low speeds is so large, that the maximum rudder travel is reached and a wings-level flight cannot be maintained by the aircraft. The equation however is designed to calculate a wings-level condition drag coefficient increment. As can be seen in Fig. 6.8, in accordance with this theoretical reflection, the drag coefficient below minimum control speed is rising towards unrealistic values.

Fig. 6.8 shows the variation of the asymmetrical drag coefficient according to **Torenbeek 1982** with flight speed. With lower density, the drag coefficient rises. The thrust variation with flight speed was done acc. to Sect. 6.4.

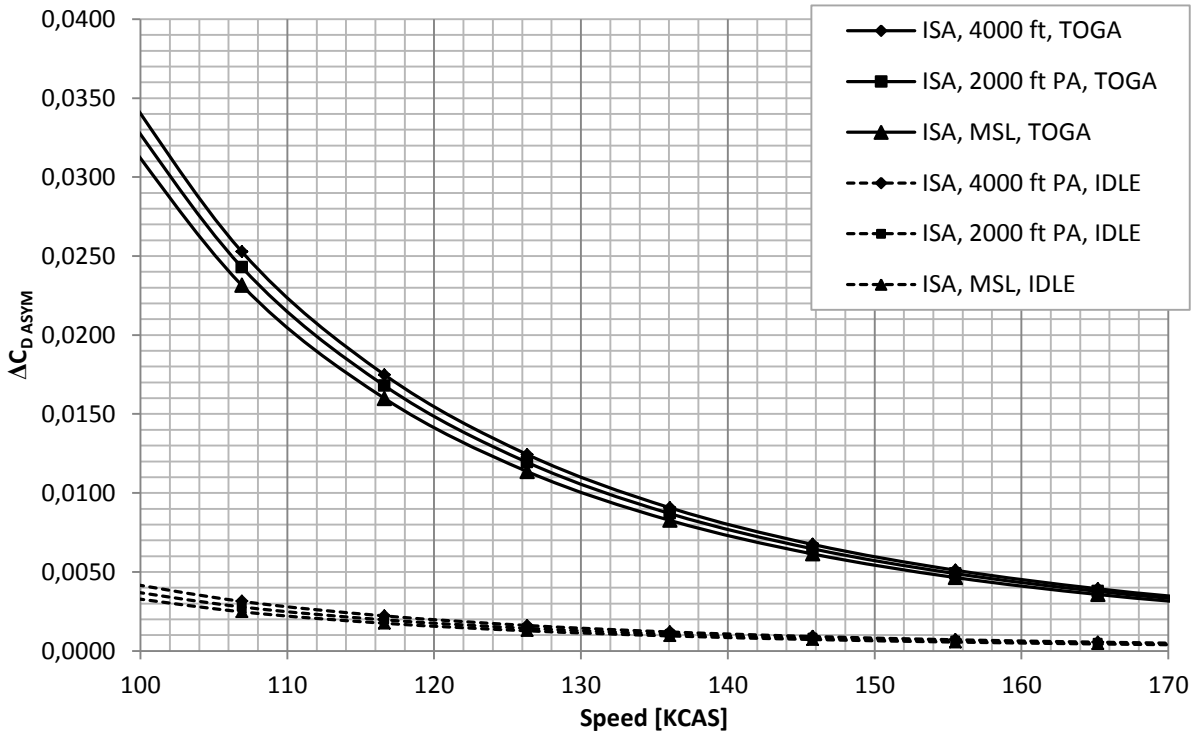

Fig. 6.8 Variation of Drag Coefficient due to Asymmetrical Flight Condition with Speed

Due to the strong dependency of this drag coefficient from speed, it could not be implemented dynamically and speed dependent into the time-step wise calculation, especially in the stop case. This would have led to very large, thus for the deceleration non-conservative drag coefficients, even when the thrust reduction to idle thrust is considered.

Consequently, a reasonable Minimum-Maximum-Average Calculation was performed for the speed range to be considered in the takeoff performance calculation. For the Learjet 35A/36A, the minimum control speed ground, V_{MCG}, is at 109 kts[15], and the maximum brake energy speed V_{MB} at 154 kts[16]. This marked the minimum and maximum speeds considered in the estimation of the average drag coefficient increment due to asymmetrical flight conditions.

15 See **AFMS 9702-2**
16 See Appendix A for Maximum Brake Energy Chart of the Learjet 35A/36A

With the parameters from Tab. 6.12, this yielded average drag increments for a range of ISA/MSL variations of:

$\Delta C_{D,ASYM,TOGA} = 0{,}0091$ At full takeoff thrust on remaining engine

$\Delta C_{D,ASYM,IDLE} = 0{,}0020$ At idle thrust on remaining engine

Table 6.12 Asymmetrical Flight Condition Drag Coefficient Increment Calculation Parameters

Parameter	Symbol	Value	Equation/Source
Engine Windmilling Drag Coefficient	$\Delta C_{D,EWM}$	0,0100	Eq. 4.109, Tab. 6.11
Minimum Speed	v_{min}	109 kts	V_{MCG}
Maximum Speed	v_{max}	154 kts	V_{MB}
Asymmetrical Geometry Coefficient	K_{ASYM}	0,100	Eq. 4.113
Engine to CG Distance	l_e	1,24 m	Measurement
VTP 25% MAC to CG Distance	l_V	4,97 m	Measurement, max aft CG
VTP Area, total	S_V	3,73 m²	Measurement
Effective VTP Aspect Ratio	$A_{V,eff}$	1,08	*see below*
Geometric VTP Aspect Ratio	$A_{V,geom}$	0,878	b_V^2/S_V
VTP Span	b_V	1,81 m	Measurement
VTP Efficiency Factor	-	1,25	Fig. 4.21
VTP Sweep	Λ_V	36°	Measurement

A side note should be made at this point, also to be seen as a validation of the drag increments due to engine failure considered in the last two paragraphs. Comparing the overall drag force created by engine windmilling and asymmetrical flight conditions together, a drag coefficient at maximum differential thrust of $\Delta C_{D,OEI} = 0{,}0191$ is obtained.

At a speed of 70 m/s, this would lead to a total drag force due to engine failure of 1350,6 N, determined at ISA, MSL. At a speed of 110 m/s, the drag force would be 3335 N. Compared to the net thrust T_0 of 3500 lbs or 15870 N, the drag due to engine failure would amount to 8,5% of the engine net thrust at 70 m/s, or 21% of the engine net thrust at 110 m/s.

This can be compared to the assumption from **Scholz 1999** given in Section 4.4.2, stating that an engine creates roughly around 15% of the net thrust in drag force after failure for a low-bypass-ratio engine. It seems that this is just in middle of the values determined at high precision according to **Torenbeek 1982**.

Spoiler Deflection Drag Coefficient Increment

The spoiler deflection drag coefficient increment was determined according to Eq. 4.120. The parameters from Tab. 6.13 were used and yield:

$$\Delta C_{D,spoiler} = 0{,}0253$$

Table 6.13 Spoiler Deflection Condition Drag Coefficient Increment Calculation Parameters

Parameter	Symbol	Value	Equation/Source
Spoiler Deflection Angle	δ_S	40°	**PM 103, 1992**
Spoiler Efficiency Factor	K'_S	1,0	**LTH BM 21 600-01**
Spoiler Area, projected in flight direction	S_S	0,561	Measurement

Validation with GJE EXTGFD-003 Data

There is also an overall drag coefficient given in **GJE EXTGFD-003**. As was outlined, the calculation method employed by the latter does not match the approach chosen in this report. Since no forces and coefficients were calculated time-step-wise, average values had to be used. Consequently, the specific data derived for this report needs to be taken into perspective of the average drag coefficient calculation employed by **GJE EXTGFD-003**. The drag coefficients used by the latter are presented in Tab. 6.14.

Table 6.14 Drag Coefficients used in **GJE EXTGFD-003** Takeoff Performance Simulation

Parameter	Symbol	Value	Value used in Report
Overall Aircraft Drag Coefficient, AEO	$C_{D,G}$	-	0,0606
Overall Aircraft Drag Coefficient, Takeoff with OEI	$C_{D,TO}$	0,0682	0,0797
Overall Aircraft Drag Coefficient, Stop with OEI	$C_{D,AS}$	0,0965	0,0979
Zero Lift Drag Coefficient	$C_{D,0}$	0,0238	0,0249

The **GJE EXTGFD-003** drag coefficient for the OEI Takeoff is an average value and lies roughly the middle of the drag coefficient OEI and the drag coefficient AEO determined for this report. Furthermore, the drag coefficient in the stopping case, OEI, seems to match very closely as well. In comparison, the simulation parameters are to be seen slightly conservative.

Therefore, the assumptions taken within this report for the drag coefficients can be assumed as plausible input parameters to the takeoff performance simulation.

6.7 Lift-to-Drag Ratio and Aircraft Polar

The Lift-to-Drag Ratio or glide ratio is used to evaluate the drag coefficient and the Oswald factor chosen in Section 6.5. According to Eq. 4.68 and the parameters from Tab. 6.8, an Oswald factor in takeoff configuration of $e_{T/O} = 0{,}72$ has been determined by using the **Raymer 1989** data for the Gates Learjet given in Tab. 6.7. According to the **Raymer 1989** drag breakdown, the Learjet shows an Oswald factor of $e_{cruise} = 0{,}875$ in cruise.

The resulting glide ratio *E* is then determined from Eq. 4.75. A range of different configurations has been investigated in order to be able to evaluate the result and its order of magnitude, as shown in Tab. 6.15. The OEI conditions were not included, as this would lead to no

Table 6.15 Glide Ratio of Learjet 35A/36A as determined from Parameter Estimation, AEO

Parameter	Symbol	$C_{D,0}$	e	Glide Ratio *E*
Glide Ratio, Climb Config, No Gear, No Stores, $e_{T/O}$	E_{clean}	0,0249	0,72	11,38
Glide Ratio, Climb Config, No Gear, Stores, $e_{T/O}$	E_{clean}	0,0385	0,72	9,5
Glide Ratio, Takeoff ConFig., No Stores, $e_{T/O}$	E_{TO}	0,0445	0,72	8,51
Glide Ratio, Takeoff ConFig., Stores, $e_{T/O}$	E_{TO}	0,0581	0,72	7,45
Glide Ratio, Clean Aircraft, Cruise, e_{cruise}	E_{cruise}	0,0249	0,875	12,51

According to the **Learjet 30 Series Pilot Training Manual**, the aircraft is able to glide 2 nm per 1000 ft. This would yield a glide ratio of 12,15. Certainly, this is a simplified reference value, but it shows that the assumptions taken for the Learjet 35A/36A are in the correct order of magnitude.

Furthermore, the aircraft polar could be plotted with the parameters determined for this report. The aircraft polar is shown in Fig. 6.9.

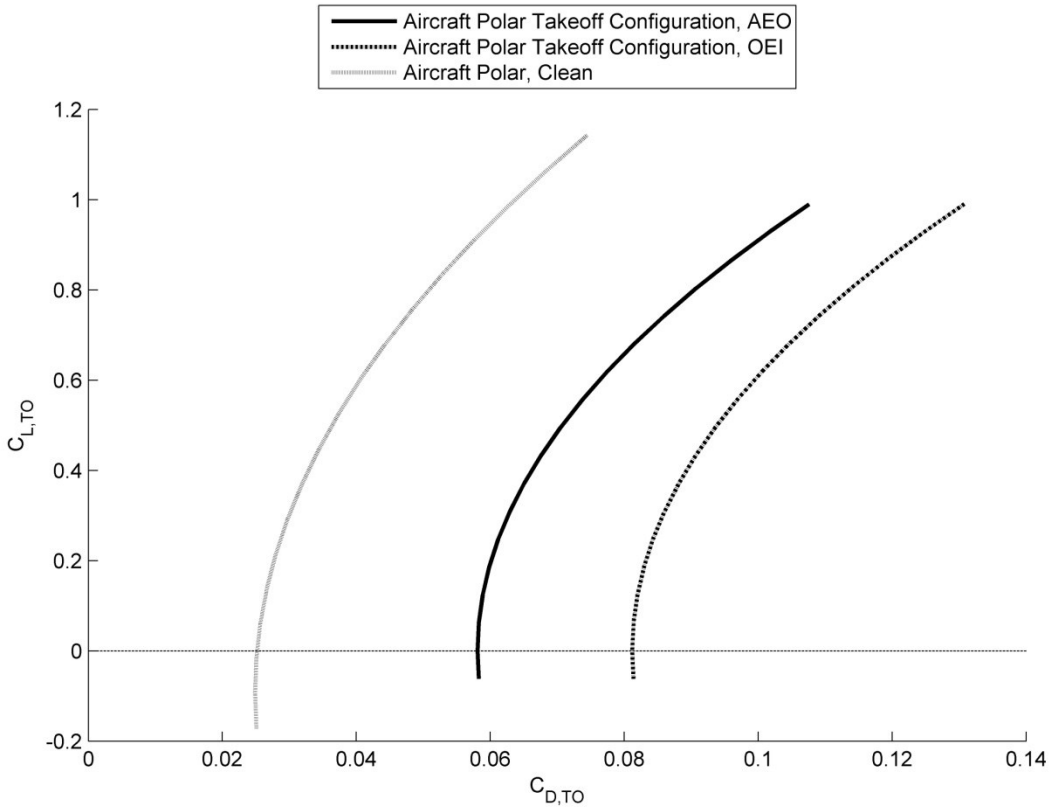

Fig. 6.9 Aircraft Polar, Learjet 35A/36A acc. to Parameter Estimations, Varied Configurations

As the aircraft polar is plotted, it becomes visible how large the impact of the drag increments due to the aircraft (with stores) at takeoff configuration is when compared to the clean aircraft. An engine inoperative configuration at full differential thrust is further degrading the performance strongly. This may explain the rather low glide ratios obtained for these configurations.

6.8 Braking Force

For the rolling friction, values determined by NASA have been provided in Fig. 4.17 and have been used for the simulation. In the deceleration case, the friction for a rolling tire is being replaced by the friction for a braking tire. For the simulation, the braking friction acc. to **CS-25.109** is being used, as presented in Tab. 4.2. An Anti-Skid efficiency factor of 0.8 was applied to the $\mu_{brake,wet,max}$ used at 200 psi tire pressure. This is an assumption including a conservatism.

The advantage of existing data was used to obtain a Maximum Brake Energy Chart from **GJE EXTGFD-003**. In this chart, the maximum achievable braking friction at various aircraft speeds on a dry runway with worn-down brakes as required by **CS-25.109** has been plotted. The original Maximum Brake Energy Chart is included in Appendix A. Due to poor quality, but also to produce a numerical relationship between the Learjet 35A/36A rolling speed and maximum achievable tire friction, the chart has been digitalized and a trend line added. The result is shown in Fig. 4.10. In order to convert aircraft speed into brake energy, Eq. 6.5 was used.

$$E_{brake} = m \cdot v_{aircraft}^2 \tag{6.5}$$

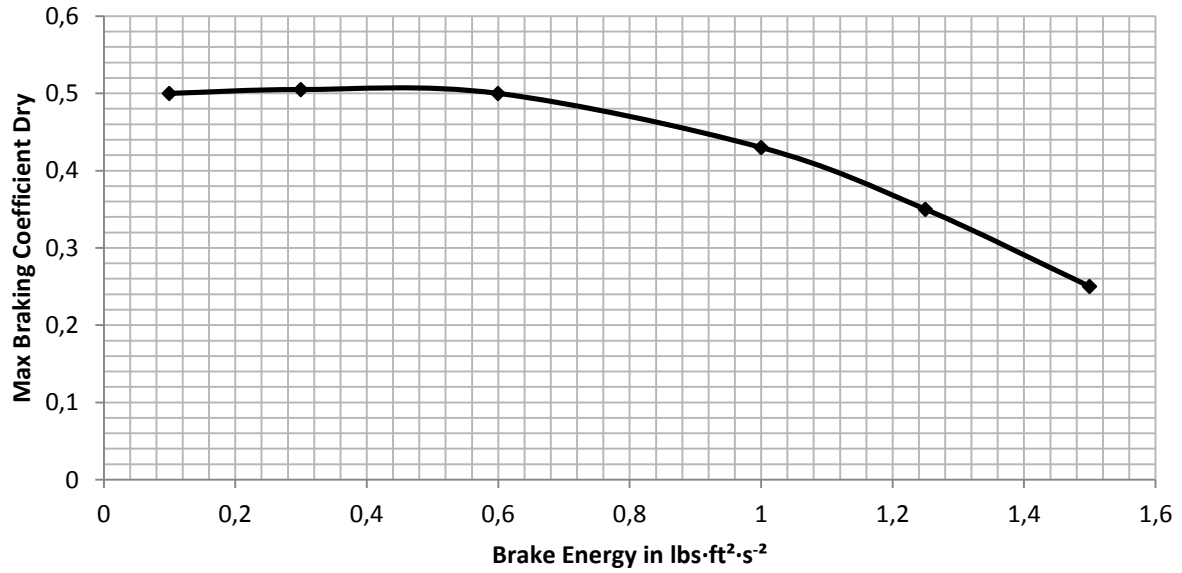

Fig. 6.10 Braking Friction Coefficient Dry Runway for a Learjet 35A/36A (**GJE EXTGFD-003**)

A trend line approximation of second polynomial order yields equation 6.6 used for the report to determine a speed dependent max. braking coefficient:

$$\mu_{brake\ max,dry} = -0.1992 \cdot E_{brake}^2 + 0.1421 \cdot E_{brake} + 0.4852 \tag{6.6}$$

The $\mu_{brake,dry,max}$ value is defined for $\mu_{brake,dry,max} \geq 0.05$. It will not drop below this value due to the fact that **EASA AMC 25.109** defined this as the lower boundary for $\mu_{brake,wet,max}$. This limitation conservatively then applies for a dry runway as well.

The data from Fig. 4.10 or Eq. 6.3 cannot directly be used as an input parameter to the simulation due to the fact that a wet runway shall be considered. However, it was pointed out that the braking friction can never be higher for a wet runway than for a dry runway. Therefore, $\mu_{brake,dry,max}$ is used as the upper boundary for the $\mu_{brake,wet,max}$ determined acc. to **CS-25.109**. This is of relevance for very low and high speeds, as can be seen in Fig. 6.11. In this figure, obtained from the takeoff performance simulation, the Anti-Skid Correction factor of 0,8 is already applied on the **CS-25.109** braking friction coefficients, because the Learjet 35A/36A operates with Anti-Skid ON.

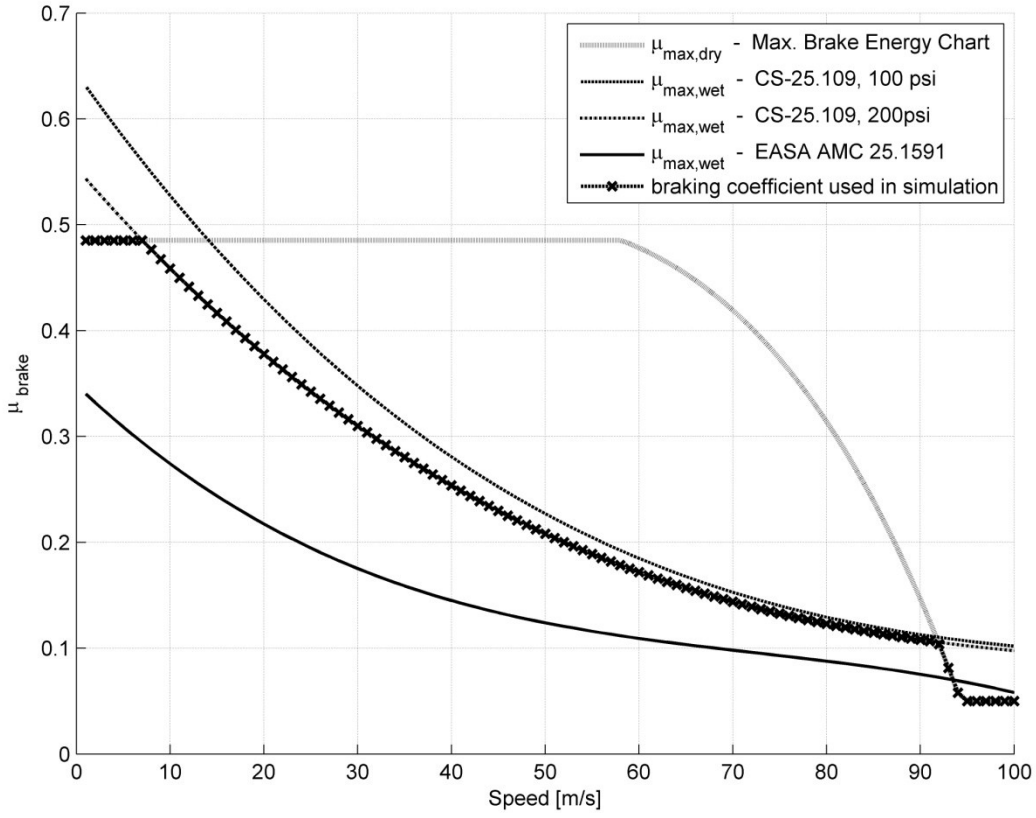

Fig. 6.11 Braking Coefficient used in Simulation for the Learjet 35A, 36A

Gear Load Factor

As pointed out in Sect. 4.5.1, the braking case brings with it a moment around the center of gravity of the aircraft, so that the load on each gear strut changes. Furthermore, only the main gear of the Learjet 35A/36A contributes with braking friction to decelerate the aircraft. The nose wheel rolling friction is insignificant in comparison. Therefore, the amount of normal load on the main gear struts had to be determined.

As the consideration of a momentum balance around the pitch axis of the aircraft should not be performed in order to simplify the calculations, a good reference to estimate the load factors was the Weight Sheet of the Learjet 35A/36A obtained from the operator. This chart is included in appendix G. It yielded a main-gear-to-nose-gear weight distribution ratio of 90%. This means, that at operating empty weight (excluding crew), 90% of the aircraft mass is acting on the four braked wheels of the main gear. With fuel and stores installed under the wings thus close to the center of gravity, this would further increase this ratio.

To assume a gear load factor $f_{load,gear} = 0{,}9$ in Eq. 4.115 for the braking case is therefore estimated to be a conservative value that may include the margin of load change due to pitch axis momentum.

6.9 Reaction Time Considerations

In the scope of this report, the certification requirements to take into account pilot reaction times for the activation of braking devices have been used. They have been agreed upon with the operator GFD. According to the **AFMS 9702-2**, the overall transition time from engine failure to full stopping configuration is 2,5 seconds. The reaction times used in the simulation have therefore been broken down into the following major phases after engine failure:

0,0 s	The critical engine fails, while the other engine sustains thrust at 100%
1,0 s	The pilot recognizes the engine failure, and needs another 0,5 seconds to react
1,5 s	The pilot applies the wheel brakes
2,0 s	The pilot reduces the thrust remaining on the healthy engine to idle
2,5 s	The pilot extends the spoilers of the aircraft influencing lift and drag

A plot of the acceleration experienced by the aircraft shortly after engine failure is shown in Fig.6.12. It can be seen that the acceleration of the aircraft decreases with each activation of a retardation device. It can also be seen that a single engine failure in a twin-engine jet has serious impacts on the acceleration performance of the aircraft caused by the loss of thrust and increase in drag.

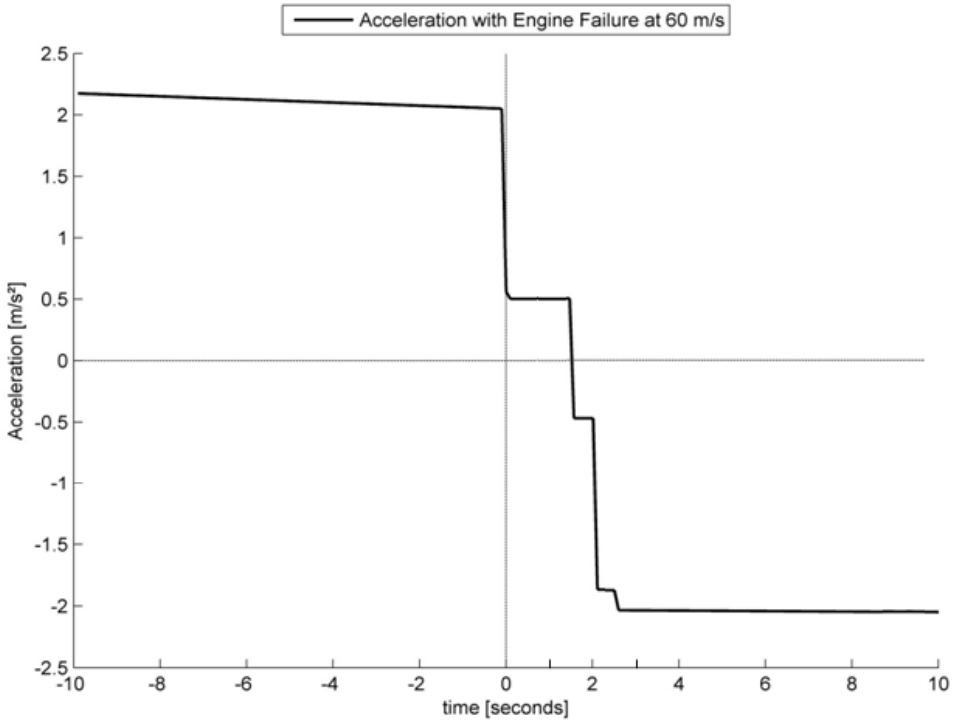

Fig. 6.12 Reaction Times and Aircraft Retardation with Engine Failure at t=0, Simplified

The distance margin equivalent to 2 seconds at V_1 speed according to **CS-25.109** has been considered.

6.10 Reference Speeds

The reference speeds are a very important factor for the calculation of the BFL, as they are the basis for all speed dependent calculations. The reference speeds for the Learjet 35A/36A have been extracted from the **AFMS 9702-2**. The figures 6.13, 6.14 and 6.15 shown in this section have been converted into numerical relationships between aircraft takeoff weight in lbs and the resulting reference speeds in order to use them in the performance simulation.

Stall Speeds

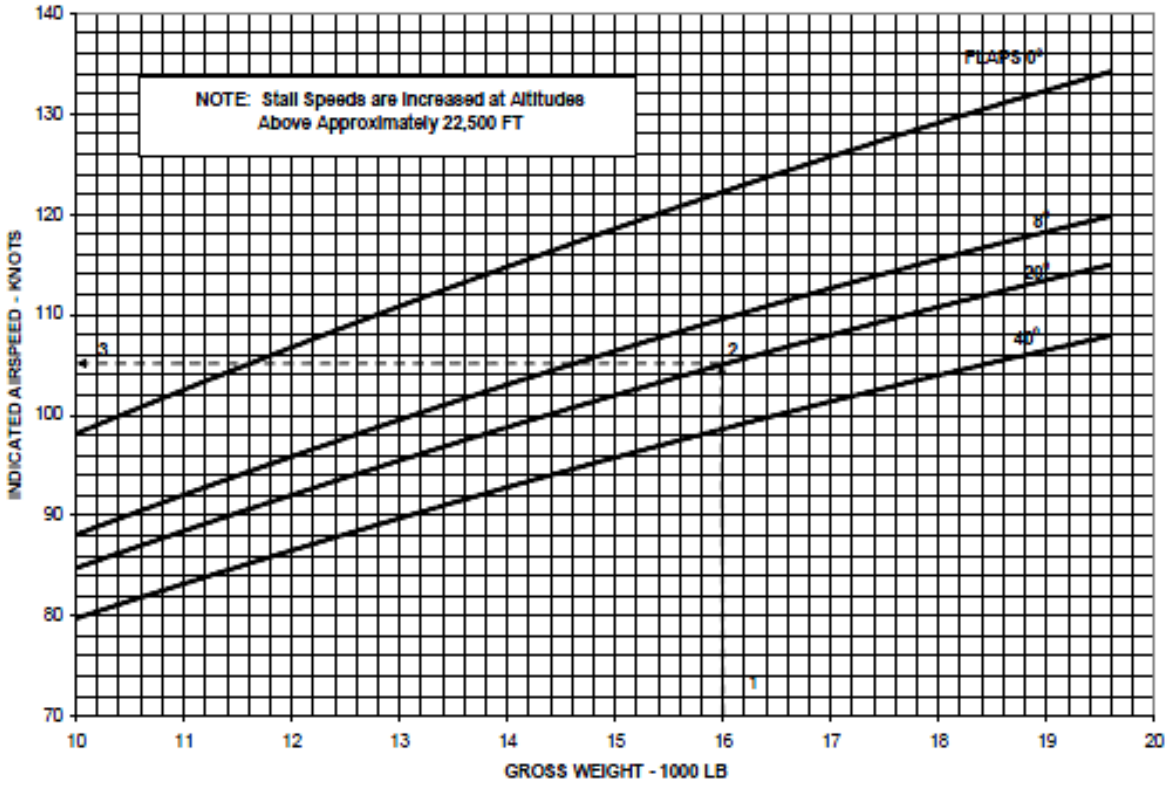

Fig. 6.13 Stall speeds with regard to Gross Weight and Flap Deflection (**AFMS 9702-2**)

Equation 6.7 has been obtained for the stall speed reference (IAS) with regard to gross weight at a flap deflection of 8°.

$$v_{s,IAS} = 88 + \left(\frac{118-88}{19000-10000}\right) \cdot (m_{lbs} - 10000) \text{ [kts]} \tag{6.7}$$

According to **AFMS 9702-2**, the stall speed (IAS) is increased by 6 knots with stores installed.

$$v_{s,stores,IAS} = v_s + 6 \text{ [kts]} \tag{6.8}$$

Rotation Speeds

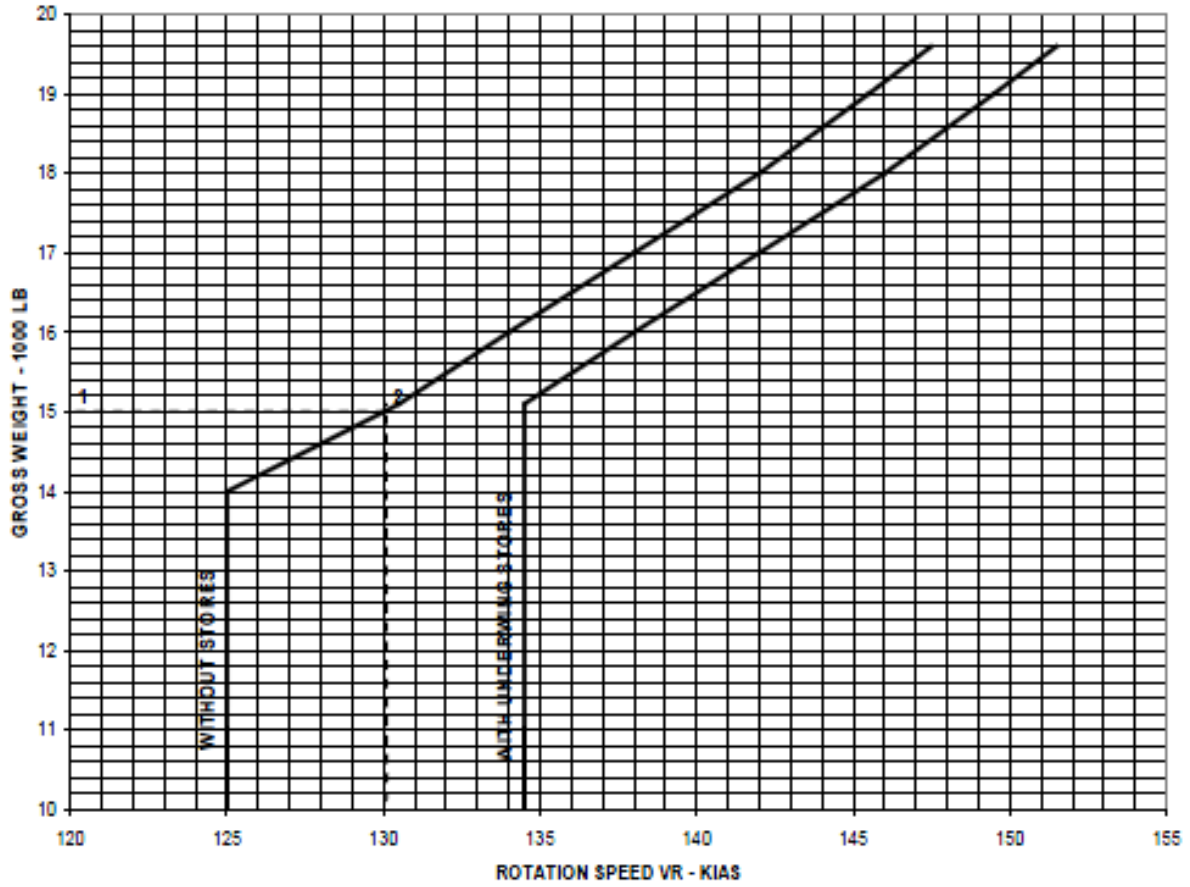

Fig. 6.14 Rotation Speeds with regard to Gross Weight and Store Installation (**AFMS 9702-2**)

For the *no-stores configuration*, the following equations for the rotation speed (IAS) could be derived:

$$v_{R,IAS} = 125 \text{ kts} \qquad m_{lbs} < 14000 \text{ lbs}$$

$$v_{R,IAS} = 125 + \left(\frac{145.5 - 125}{19000 - 14000}\right) \cdot (m_{lbs} - 14000) \text{ [kts]} \qquad m_{lbs} > 14000 \text{ lbs} \qquad \textbf{(6.9)}$$

For the *stores configuration*, the following equations could be derived:

$$v_R = 134.5 \text{ kts} \qquad m_{lbs} < 15100 \text{ lbs}$$

$$v_{R,IAS} = 134.5 + \left(\frac{149.5 - 134.5}{19000 - 15100}\right) \cdot (m_{lbs} - 15100) \text{ [kts]} \qquad m_{lbs} > 15100 \text{ lbs} \qquad \textbf{(6.10)}$$

V2 Speeds

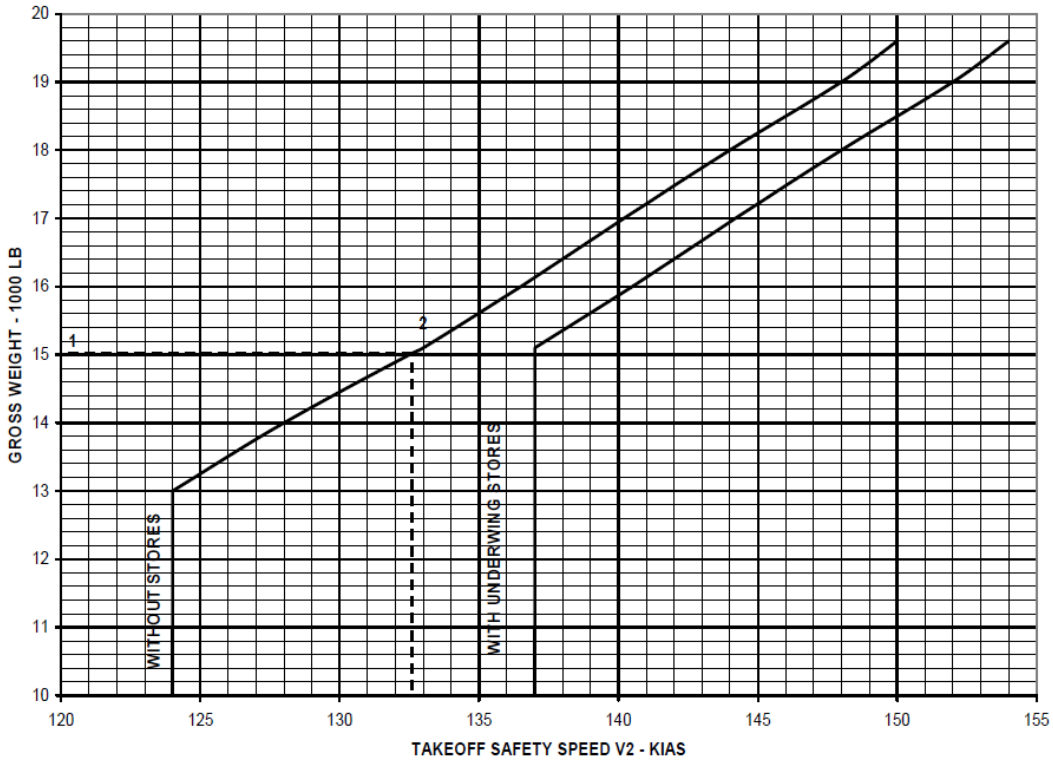

Fig. 6.15 Safe Climb speeds with regard to Gross Weight and Store Installation (**AFMS 9702-2**)

For the *no-stores configuration*, the following equations for the safe climb speeds (IAS) could be derived:

$$v_2 = 124 \text{ kts} \qquad m_{lbs}<13000\text{lbs}$$

$$v_{2,IAS} = 124 + \left(\frac{148-124}{19000-13000}\right)\cdot(\mathrm{m_{lbs}} - 13000)\ [\text{kts}] \qquad m_{lbs}> 13000 \text{ lbs} \qquad \textbf{(6.11)}$$

For the *stores configuration*, the following equations could be derived:

$$v_2 = 137 \text{ kts} \qquad m_{lbs}<15100\text{lbs}$$

$$v_{2,IAS} = 137 + \left(\frac{152-137}{19000-15100}\right)\cdot(\mathrm{m_{lbs}} - 15100)\ [\text{kts}] \qquad m_{lbs}> 15100 \text{ lbs} \qquad \textbf{(6.12)}$$

Minimum Control Speed Ground

The minimum control speed ground was selected from the **AFMS 9702-2**.

$$v_{MCG} = 109\ kts$$

The minimum control speed is the lower boundary for the decision speed V_1. Should a lower decision speed result from BFL calculations, it must be changed to at least V_{MCG}. The aircraft is not able to maintain directional stability in a continued takeoff below V_{MCG} in an engine failure case. The impact of an artificially increased V_1 on the BFL has been considered for the distance correction in the performance simulation.

Conversion of IAS into CAS

According to the **AFMS 9702-2**, the indicated air speed for which the reference speeds are given, need to be converted by the relation shown in Fig. 6.16.

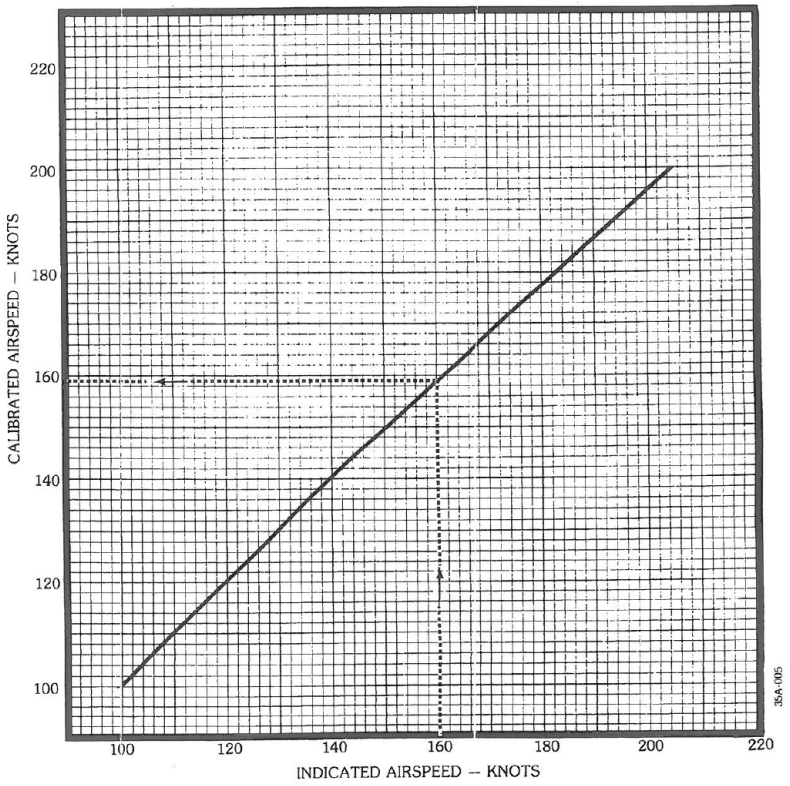

Fig. 6.16 Conversion of IAS into CAS for the Learjet 35A/36A (**AFM Learjet 35A/36A**) *Calibration for Takeoff Configuration, Normal System*

As can be seen, the difference between IAS and CAS amounts to 2 kts. Hence:

$$v_{i,CAS} = v_{i,IAS} - 1\ [\text{kts}] \qquad \textbf{(6.13)}$$

6.11 Data for Precipitation Drag Determination

As discussed in Section 4.1.10, the drag due to precipitation such as displacement, skin friction and impingement drag, is highly dependent on the aircraft tire properties. The Skin Friction Drag also requires knowledge of the wetted fuselage length. Therefore, this section shall summarize the parameters used for the Learjet 35A/36A calculation, as given in Tab. 6.16.

Applied for the wet runway calculations were the *displacement drag* according to Eq. 4.81, the *skin friction drag* according to Eq. 4.86 and the *spray impingement drag* according to Eq. 5.8.

Table 6.16 Calculation Parameters for Precipitation Drag, Learjet 35A/36A

Parameter	Symbol	Value	Source
Effective Tire Width Nose Wheel	d_{nose}	0,101 m	Eq. 4.83
Effective Tire Width Main Wheel	d_{main}	0,127 m	Eq. 4.83
Deflection Nose Wheel Tire	δ_{nose}	0,028 m	Eq. 4.85
Deflection Main Wheel Tire	δ_{main}	0,028 m	Eq. 4.85
Percental Tire Deflection	$d_{\%}$	32%	Eq. 4.84
Contaminant Depth	d_{cont}	0,003 m	Definition Wet RWY
Nose Wheel Number	n_{nose}	1	-
Main Wheel Number	n_{main}	4	-
Nose Wheel Pressure	p_{nose}	175 psi	Operator Information
Main Wheel Pressure	p_{main}	105 psi	Operator Information
Fuselage Length	$l_{fuselage}$	14,8 ft	Measurement

In order to calculate the percental deflection of the tire, the data from **Goodyear 2002** given in Tab. 6.17 has been used. The GFD operated Learjet 35A/36A use the following tire sizes:

- Nose Wheel: Goodyear 184 F10-2, chined "Rip DDT" 18x4,4 in
- Main Wheels: Goodyear 187 K43-1, "Flight Eagle" 17,5x5,75 in

Table 6.17 Learjet 35A/36A Tire Data, **Goodyear 2002**

Parameter	Symbol	Nose Wheel Tire	Main Wheel Tire
Static Load Radius	SLR	7,85 in	7,4 in
Mean Overall Tire Diameter	D_M	17,9 in	17,5 in
Rim Flange Outer Diameter	D_F	10,81 in	8,88 in

The validation and interpretation of the obtained precipitation drag forces is done in combination with other flight mechanical forces in Chapter 8.

7 Numerical Takeoff Simulation

The numerical takeoff simulation is the tool that integrates all assumptions, parameters and validated modeling of the Learjet 35A/36A. Its task is to determine a BFL and its associated V_1. For verification reasons, various other side parameters are also produced in a run of the simulation program. A very important aspect of the simulation is the concept of normalization or calibration of the results with reference to existing certification data. The choice of the calibration source data is outlined in Sect. 7.1.

As outlined in Section 4.1.4, the takeoff distances can be obtained by a numerical integration of the equation of motion. A simulation framework for the BFL determination based on a Runge-Kutta Integration Algorithm was developed in the Aero (Aircraft Design and Systems Group) at HAW Hamburg University. This baseline has been used and expanded in the aspects necessary in order to match the specifications set forth by the project objectives.

The approach to use a numerical takeoff performance simulation stands in contrast to usual methods to determine takeoff performance based on simplified equations with average speeds and force components. Simplified approaches are based on the equation of motion simplifications outlined in Sect. 4.1.2. It has already been shown in Sect. 6.5 that average drag coefficients were used for the averaged equation of motion integration method. The numerical integration is expected to produce data of a very high accuracy, as all force components are considered with a high level of detail and in their speed and time dependency. The determination of the decision speed V_1 and the BFL for the Stores+Wet case is performed at a range of combinations of takeoff weight, runway elevation and Delta-ISA temperature deviations in order to obtain a data matrix that can be used for flight operations.

Chapter 7 shall outline the general structure of the developed takeoff simulation program. It serves to understand how all equations and models described in the previous chapters have been integrated into a simulation that determines the BFL and V_1 from an array of given environmental parameters. The detailed functionality of the code is explained by comments inserted in the code, which is not included in the online version of this report. The following functions constitute the simulation when executed together, and shall be presented in this chapter:

Main Function	Main Program Steering File
Parameters_Learjet.m	Parameter Input File
Take_off_1Eng.m	Distance Integration Function: TOD, OEI
Take_off_AEO.m	Distance Integration Function: TOD, AEO
Take_off_Acc_Stop.m	Distance Integration Function: ASD, OEI
fsG_Learjet.m	Acceleration Function for OEI cond.
fsG_Learjet_AEO.m	Acceleration Function for AEO cond.
fsG_Learjet_Stop.m	Deceleration Function for OEI cond.

7.1 Simulation Concept

The general concept of the simulation is the numerical integration of two differential equations of motion, one for the Takeoff Distance (TOD) and one for the Accelerate Stop Distance (ASD). The equation of motion is solved for a number of different assumed engine failure speeds, yielding the two converging graphs shown in Fig. 3.8. The engine failure speed at which both ASD and TOD equations of motion yield the same distance is also the distance at which the decision to continue or abort the takeoff needs to be taken, thus V_1.

As no data is available for the aircraft configuration with installed under-wings on a wet runway, it is necessary to check the plausibility of the results and to correct the simulation results for possible error. Therefore, it is required to compare results of a configuration for which certified data is available with the simulation outputs for BFL and V_1 of the same configuration before calculating results for the new configuration.

It is always a considerable challenge to select the right parameters from a range of possible equations and approaches, where different assumptions are possible. A reasonable set of approaches was chosen for this report. However, the simulation can only model the effects and conditions that are considered within the equations used. The real aircraft might have still different parameters that are unknown to the simulation, and therefore a deviation of the simulation results compared to the real certification data that have been partly flight-tested is very likely.

This is why the calibration factor may be applied to the simulation results of the unknown case, as it covers general uncertainties within the simulation which can be eliminated by the calibration factor, given the fact that the reference data is of high enough precision.

7.2 Verification and Calibration

Certified performance data already exists for the aircraft operation *without stores* in both the *dry and wet runway* environments. This shall from now on be referred to as *Clean+Dry*, respectively the *Clean+Wet* configuration. Certified performance data also exists for operation *with under-wing stores* in the *dry runway* environment, the S*tores+Dry* configuration. Which data is governing the calibration is an important decision, as the significance and validity of the calibrated value depends directly from it.

The Clean+Dry performance data performance data was flight-tested and has been included in the **AFMS 9702-2**. With the application of the *Wet Data Addendum* for the GFD fleet, correction factors may be applied to the Clean+Dry data to yield Clean+Wet takeoff performance data. Certification of the Stores+Dry configuration was done with data from the **GJE EXTGFD-003** report that contains limited flight tested data, but is mostly based on an analytical approach. This data is also contained in the **AFMS 9702-2**. It would be possible to calibrate the simulation results from the Clean+Wet and the Stores+Dry configuration, as both include elements of the unknown configuration that shall be investigated.

The Four-Corner Sheet developed from the available data displays the configurations for which existing data is available, as shown in Fig. 7.1. It indicates the missing set of data required for *wet runway* operation *with under-wing stores* configuration.

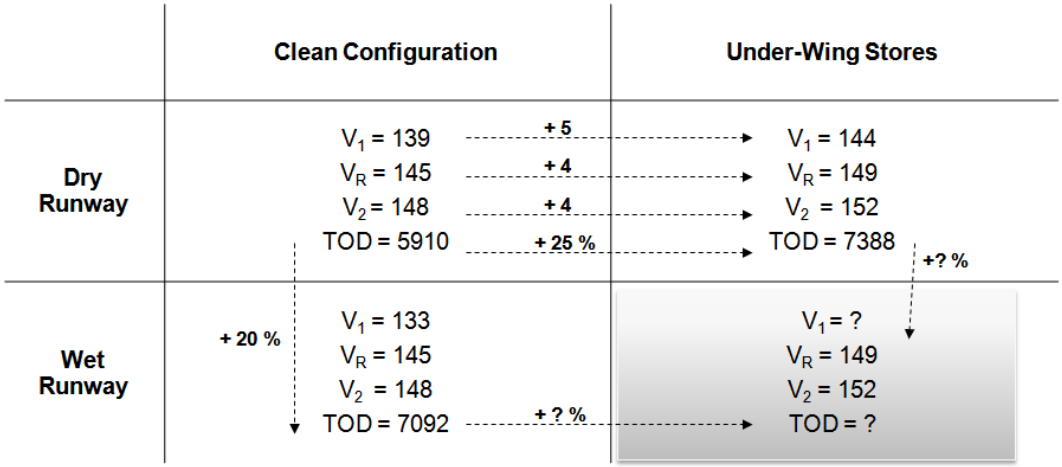

Fig.7.1 Four-Corner Sheet of existing certification data
Example: TOW = 19000 lbs, ISA, Stores (MTR-101), Units: knots, ft

The certification data of the clean configuration is seen to be the most accurate source of aircraft information, because it reflects the purest data for the basic aircraft. The certification for dry runways with under-wing stores was found to have certain assumptions taken that are not entirely conservative.

Therefore, the baseline for calibration of the simulation results was selected to be the Clean+Wet data from the **AFMS 9702-2** corrected for wet runway conditions with the *Wet Data Addendum*. Wet runway effects included in the simulation are comparable in this case, making it the best baseline for a validation also of the additional effects of the wet runway.

In order to have the highest degree of accuracy, the calibration is applied on the equations of motion individually for the TOD and the ASD, not on the final result of the simulated BFL and V_1. A target match for each of the two distance calculations is given by the BFL/V_1 pair provided by the AFMS certified data. This permits to calculate in fact two calibration factors – one for the TOD equation of motion, and one for the ASD equation of motion. This is shown in Fig. 7.2.

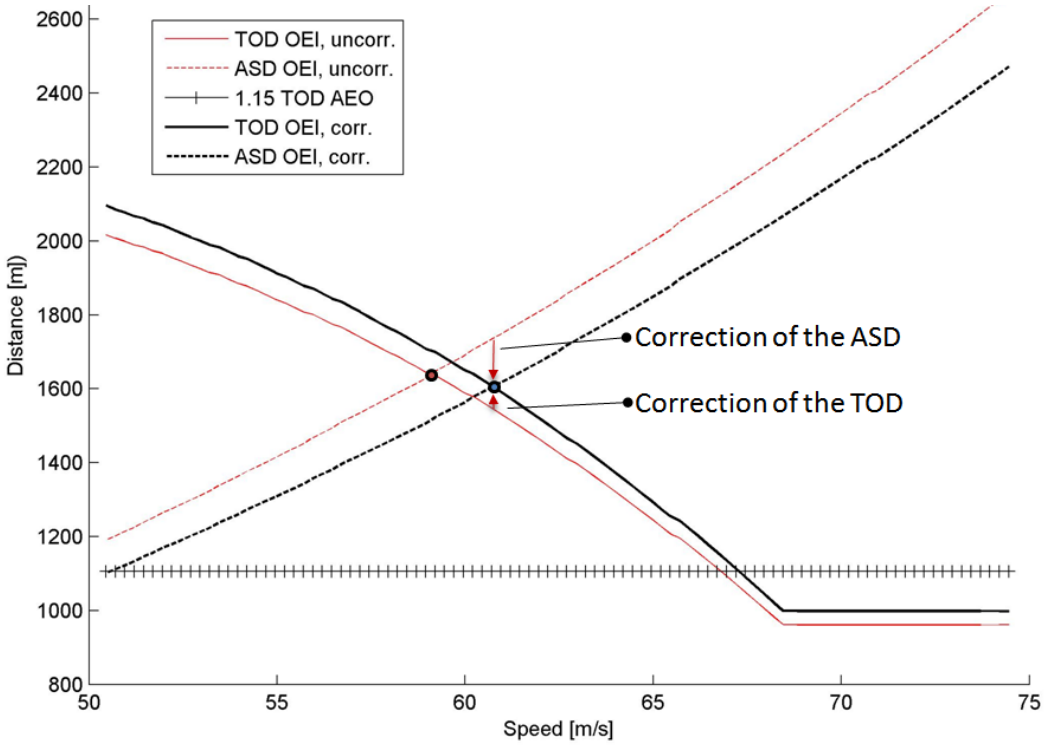

Fig. 7.2 Application of the Correction to the ASD and the TOD to match reference BFL/V_1

Matching of the target coordinate is done by linear scaling of the simulation result for the ASD/TOD distances; the ratio of scaling necessary determines the calibration factor. As this method permits individual evaluation of the possible errors made by either the TOD determination function, or the ASD determination function, it is more versatile than a simple correction of the final BFL/V_1 result.

The determination of two individual correction factors makes it possible to apply the correction factor determined for either distance to the Stores+Wet configuration, because the error made by each of the two necessary calculation function can be assumed constant. Together, both corrections then determine the actual intersection point for the corrected BFL/V_1 determination for the Stores+Wet configuration.

7.3 Simulation Architecture

The inclusion of a calibration mechanism results in the simulation architecture shown in Fig. 7.3. The color code will be reapplied in the detailed architecture discussion and the Nassi-Shneiderman Diagram of the program in Appendix C.

Fig. 7.3 Overall Simulation Architecture and Calibration Concept, Simplified

The general architectural outline shown in Fig. 7.3 is the architecture used in the main file.

The simulation is run for varying aircraft masses and varying outside air temperatures and varying pressure altitudes – the results of which are summarized in a chart of the same structure as existing matrices of BFL/V_1 for varying environmental parameters. This is done by cycling the architecture shown in Fig. 7.3 that through a number of different environmental variables and storing the results of each run into the specified field in an output file. That way, the simulation automatically develops a set of output files filled with the data created by each run of the Simulation.

7.4 Simulation in Octave and MATLAB

The simulation was developed in a mathematical programming environment. Both Octave and the common MATLAB® suite can read these input files.

The program consists of a main function which contains all structural elements of the program in accordance to the Simulation Architecture. Within the main function, further detailed functions are called in order to carry out specific integration tasks.

7.4.1 Main Function

The main goal of the main function is to obtain the intersection point of the TOD and ASD curves and thus obtain a BFL and a V_1. This is done twice within the simulation architecture due to the calibration concept. In order to obtain TOD and ASD curves in a numerical simulation, it is necessary to calculate specific TOD's and ASD's for specific engine failure speeds V_{EF} and then plot these distances as a function of V_{EF}. From these plots, the BFL/V_1 intersection point is determined.

In order to be able to determine TOD and ASD graphs, the main function is calling the distance integration functions in a loop for an increasing assumed engine failure. In the main function, the resulting distances of TOD and ASD are the stored in an array and the intersection point (BFL, V_1) determined. For cross-check reasons, the AEO TOD is also determined for each environmental condition in order to check whether it actually yields smaller distances than the BFL. No loop is required for the determination of the AEO TOD because no engine failure speed needs to be iterated.

7.4.2 Outer Loop - Distance Integration Functions

The TOD is determined in accordance to the flight path specifications as described in CS-25.113, which was outlined in Section 3.3. The Accelerate-Stop Distance is determined in accordance to the requirements set forth by CS-25.109 for wet runways outlined in Section 3.4.

In each loop within which distance functions are called from the main function, each distance function receives an assumed engine failure speed and puts out the resulting Takeoff- or Accelerate-Stop-Distance for that engine failure speed. The synthesis for numerical integration of the equation of motion was presented in Eq. 4.22. The Runge-Kutta integration algorithm designated “ode23” in the script language is used to determine the distance increments for each time step. At each time step, the velocity and acceleration experienced by the aircraft is evaluated and yields the distance increment obtained the respective time step.

Accelerate-Stop Distance

The ASD is increasing with increasing engine failure speed. The aircraft accelerates until V_{EF}, and decelerates again until it comes to a complete stop. Therefore, the Accelerate-Stop Distance determining function Take_off_Acc_Stop.m is composed purely from two equations of motion – a dedicated function solves the differential equation of motion for the acceleration, and another dedicated function solves it for the deceleration.

The code was translated into a written series of operations to ease the overview on the numerical ASD distance integration method, as shown in Fig. 7.4. Again, the color code is reemployed in the Nassi-Shneiderman Diagram in Appendix C.

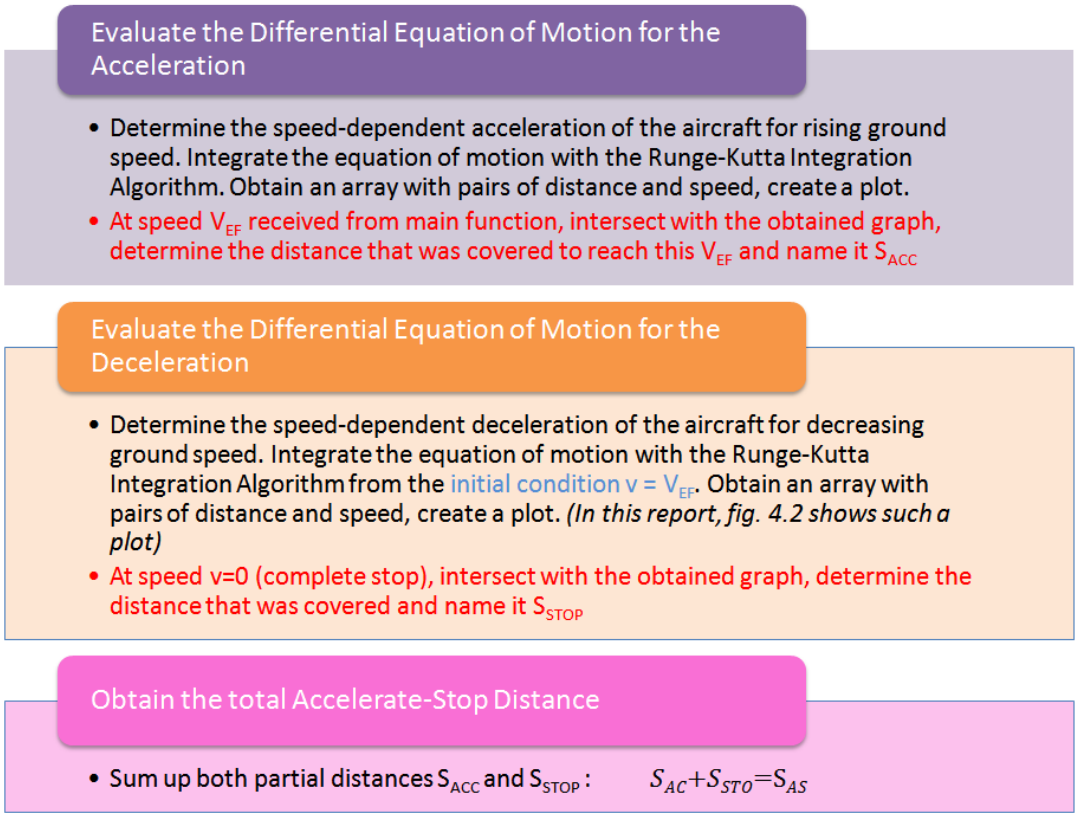

Fig. 7.4 Overall Accelerate-Stop Distance Function Architecture

The color code is applied to the function code section shown below as an example:

```
functions_AS = Take_off_Acc_Stop (vEF)

%Calculation of the acceleration distance (s_Acc)
y0=[0 0];
Parameters_Learjet

options = odeset('MaxStep',0.1);
[t,y]=ode23('fsG_Learjet',[0 250],y0,options);
s_Acc = interp1(y(:,1),y(:,2),vEF,'linear');

%Calculation of the stop distance (s_Stop)
y0=[vEF 0];

options = odeset('MaxStep',0.1);
[t,y]=ode23('fsG_Learjet_Stop',[0 250],y0,options);
vStop = 0.0;
s_Stop = interp1(y(:,1),y(:,2),vStop,'linear');

s_AS = s_Acc+s_Stop;
```

Takeoff Distance

The TOD consists of an acceleration phase very similar to the acceleration phase in the Accelerate-Stop-Case. However, after the V_{EF} speed has been reached, the aircraft in this case does not decelerate but instead accelerates further with reduced thrust until the liftoff speed V_{LOF} is reached. This V_{LOF} therefore represents the transition speed for the distance determination of the Liftoff Distance. After V_{LOF} is reached, the aircraft has to cover the Air Distance. This distance is calculated based on the principle outlined in Sect. 4.22.

The overall architecture of the TOD Integration Function Take_off_1Eng.m has been transcribed as shown in Fig. 7.5 and the color code been applied.

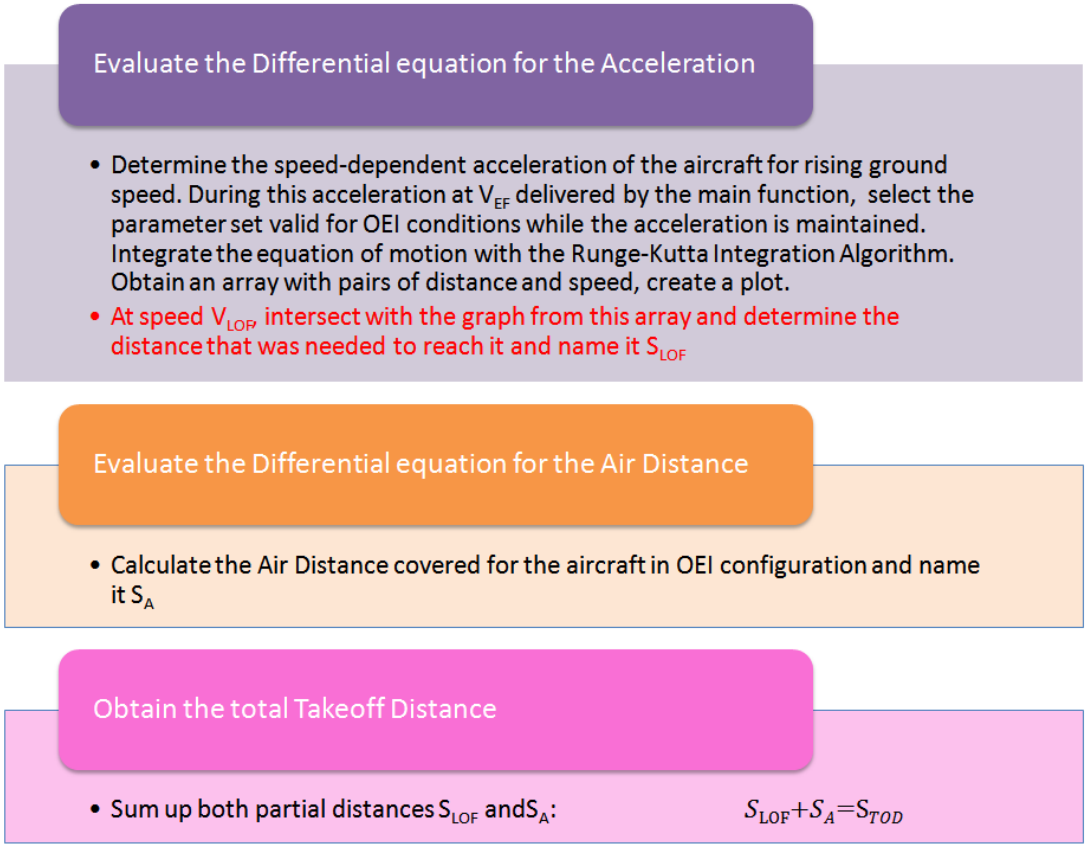

Fig. 7.5 Overall Takeoff Distance Function Architecture

7.4.3 Inner Loop –Acceleration and Deceleration Functions

As the distance integration functions need to evaluate an acceleration of a point mass at each time step, this requires another function calculating this acceleration as a function of the speed considered at the respective time step. Consequently, the acceleration acc. to Eq. 4.21 is determined in two different functions for acceleration and deceleration that are called by the distance integration functions within the Runge-Kutta Integration algorithm.

These functions are fsG_Learjet.m for the forces governing the TOD OEI, fsG_Learjet_AEO.m for the TOD AEO, and fsG_Learjet_Stop.m for the ASD OEI.

In order to determine the acceleration, all parameters determined for the Learjet 35A/36A are applied and determine the excess thrust or retardation forces in dependence of speed. The functions therefore receive the speed at the respective time step as an input. As ground speeds are used in the equations of motion, a conversion into equivalent air speeds is done for all aerodynamic forces.

Configuration changes as a function of the inputted time and velocity for each time step is possible. This way, the inner loop functions are also capable of distinguishing key time steps and key speeds such as the engine failure speed. Configuration parameters are selected as a function of the key parameter, e.g. the activation of the spoiler drag coefficient at 3 seconds after engine failure or engine failure drag activation and thrust reduction at V_{EF}.

This way the reaction time considerations have been accurately modeled inside the simulation. The distinction mechanism determines which forces are active and at which time step after V_{EF} they are activated. With regard to the aircraft configuration (e.g. spoilers deployed, brakes activated), a different acceleration is then obtained.

8 Simulation Results and Result Comparison

8.1 Simulation Results

The simulation described in Chapter 7 was used to determine the Balanced Field Length and associated decision speeds V_1 for a range of different takeoff weights, pressure altitudes and outside air temperatures (OAT).

An analysis with the Learjet 35A/36A operator GFD led to the selection of key environmental parameters that were selected as the set of environmental conditions for which simulation results will be presented. The parameter grids presented in this chapter show the following parameters in their combination:

- Takeoff Weight: 19600 lbs, 18500 lbs, 16000 lbs, 13000 lbs
- Pressure Altitude: MSL (0 ft), 2000 ft, 4000 ft
- Outside Air Temperature: OAT from 0°C to 30°C in steps of 5K

All results shown in this chapter have been calculated using a 0,1 seconds maximum time step width for the Runge-Kutta Integration. The time step width between each point at which the equation of motion is evaluated determines the precision of the simulation results, with 0,1 seconds time step width yielding more accurate results as a 1 second time step solution.

The error made by the simulation due to larger time steps than 0,1 seconds can be considerable, because the TOD/ASD graph intersection coordinates determining BFL and V_1 are dependent from the steadiness of these two graphs. The variation in steadiness of these graphs for different time step widths is a consequence of the Runge-Kutta integration algorithm performed in a loop that determines the TOD/ASD for different engine failure speeds.

If the Runge-Kutta integration is not precise enough between the different engine failure speed increments, neighboring increments for V_{EF} may be exhibiting inconsistent values. The intersection point of ASD and TOD can then not accurately be determined, as is shown exemplarily in Fig. 8.1.

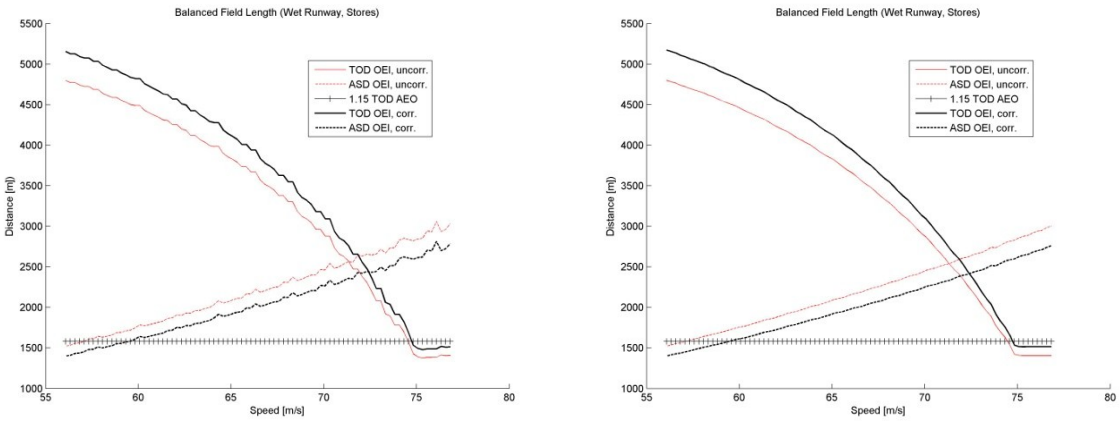

BFL at Time Step Width of 1 seconds

BFL at Time Step Width of 0,1 seconds

Fig. 8.1 Precision of the Simulation with regard to Time Step Width

Hence, the estimation of the error made by the simulation due to a deteriorated time step width is not a proportional function of the time step used, as the peaks on each graph may create intersection points with each other that are not predictable. This is shown in Tab. 8.1 for a range of time step widths. From Fig. 8.1, it becomes apparent why a time step width of 0,1 seconds had to be used for the final results determination presented in this report.

Table 8.1 Comparison of Time-Step-Width Resolution Deviations in Simulation Results
Test Case: 18500 lbs TOW, ISA, MSL

Value Name	Time Step Width 0,1 seconds	Time Step Width 0,5 seconds	Time Step Width 1 seconds
Clean + Wet: BFL, ft (rounded)	6663	6714	6703
Clean + Wet: V_1, KIAS (rounded)	127	127	127
Stores + Wet: BFL, ft (rounded)	8159	8160	8255
Stores + Wet: V_1, KIAS (rounded)	140	140	140

Since minor undulations remain at 0,1 seconds precision of integration, the reasonable result resolution of the simulation may be assumed to lie in the region of +/-1%, as can be seen in Tab. 8.1.

8.1.1 Useful Result Range

Within the grid of parameters shown in Table 8.1, not all combinations of parameters are leading to meaningful results. The aircraft performance may not be sufficient for a certain combinations of environmental variables. Section 4.8 defines the Climb Weight Limit and denotes the importance of its consideration in the takeoff calculation as a requirement. For the Learjet 35A/36A which is considered in the simulation, this requirement is reflected in a performance chart given in the aircraft flight manual (AFM).

For the aircraft with stores installed, the aircraft flight manual supplement **AFMS 9702-2** gives corrections that need to be applied to the original AFM values due to the resulting performance degradation. Resulting from both sources is the grid given in Table 8.2 and 8.3, containing the climb weight limits as a function of environmental parameters.

Table 8.2 Climb Weight Limit for Learjet 35A/36A in Extended Tip Tank Configuration (from **AFMS 9702-2**)

0	5	10	15	20	25	30	A/C Weight (lbs)	Pressure Altitude (ft)
19600	19600	19600	19600	19600	19600	19600	19600	0
19600	19600	19600	19600	19600	19600	19600	18500	
19600	19600	19600	19600	19500	19600	19600	16000	
19600	19600	19600	19600	19600	19600	19600	13000	
19600	19600	19600	19600	19600	19485	18630	19600	2000
19600	19600	19600	19600	19600	19485	18630	18500	
19600	19600	19600	19600	19600	19485	18630	16000	
19600	19600	19600	19600	19600	19485	18630	13000	
19600	19600	19600	19600	19350	18690	17620	19600	4000
19600	19600	19600	19600	19350	18690	17620	18500	
19600	19600	19600	19600	19350	18690	17620	16000	
19600	19600	19600	19600	19350	18690	17620	13000	

OAT(°C)

The climb weight limited chart for the aircraft with MTR-101 under-wing stores installed is given in Table 8.3.

Table 8.3 Climb Weight Limit for Learjet 35A/36A in Extended Tip Tank and Dual MTR-101 Stores Configuration (from **GFD Performance Outbound Chart**)

0	5	10	15	20	25	30	A/C Weight (lbs)	Pressure Altitude (ft)
19600	19600	19600	19600	19500	18750	17960	19600	0
19600	19600	19600	19600	19500	18750	17960	18500	
19600	19600	19600	19600	19500	18750	17960	16000	
19600	19600	19600	19600	19500	18750	17960	13000	
19600	19600	19600	19035	18350	17685	16830	19600	2000
19600	19600	19600	19035	18350	17685	16830	18500	
19600	19600	19600	19035	18350	17685	16830	16000	
19600	19600	19600	19035	18350	17685	16830	13000	
19600	19360	18850	18140	17550	16840	15820	19600	4000
19600	19360	18850	18140	17550	16840	15820	18500	
19600	19360	18850	18140	17550	16840	15820	16000	
19600	19360	18850	18140	17550	16840	15820	13000	

OAT(°C)

Grayed out values indicate that the climb weight limit lies below the aircraft takeoff weight. The aircraft would not be permitted to take off with this combination of parameters. As a consequence, all fields marked in tables 8.2 and 8.3 have been considered unusable results, and will therefore be excluded from the final result grids of takeoff performance data calculated by the simulation.

8.1.2 Simulation Results for Wet Runway, No Stores

It has been outlined that the simulation concept is based on the calculation of results for two configurations – the Clean+Wet configuration that known data exists for, and the Stores+Wet configuration that is currently not certified.

Table 8.4 and Table 8.5 therefore first present the results calculated by the simulation for the aircraft taking off on a wet runway in clean configuration, with no under-wing stores installed. For the integration, a time step width of 0,1 seconds has been used. In accordance to Section 8.1, the climb weight limited results have been removed. The results for Balanced Field Lengths from Table 8.8 are plotted in Appendix H.1 for easier visual representation of the trends of the simulation results with changing environmental parameters.

Table 8.4 Simulation Results for BFL Wet Runway, No Stores Configuration (ft)

0	5	10	15	20	25	30	A/C Weight (lbs)	Pressure Altitude (ft)
7243	7336	7482	7659	7830	8261	8890	19600	0
6314	6459	6528	6663	6801	7157	7704	18500	
4543	4635	4728	4823	4924	5155	5532	16000	
3978	4056	4131	4211	4288	4393	4520	13000	
8040	8142	8338	8510	9046	-	-	19600	2000
6982	7138	7297	7410	7874	8495	9209	18500	
5083	5192	5293	5402	5674	6065	6557	16000	
4385	4470	4550	4650	4771	4921	5079	13000	
9011	9203	9584	10431	-	-	-	19600	4000
7813	8007	8307	8957	9709	10655	-	18500	
5684	5798	6035	6424	6940	7450	8064	16000	
4861	4953	5081	5241	5410	5613	5817	13000	

OAT(°C)

Table 8.5 Simulation Results for V_1 Wet Runway, No Stores Configuration (KIAS)

0	5	10	15	20	25	30	A/C Weight (lbs)	Pressure Altitude (ft)
134	134	134	134	134	135	137	19600	0
128	128	127	127	128	129	131	18500	
113	113	113	113	113	114	116	16000	
109	109	109	109	109	109	109	13000	
134	134	134	134	135	-	-	19600	2000
128	128	128	127	129	131	133	18500	
113	114	114	114	115	116	118	16000	
109	109	109	109	109	109	109	13000	
134	134	134	137	-	-	-	19600	4000
127	127	128	130	132	134	-	18500	
114	114	114	116	117	119	121	16000	
109	109	109	109	109	109	109	13000	

OAT(°C)

The results for Balanced Field Lengths from Table 8.4 are plotted in Appendix I.1 for easier visual representation. As can be seen, the variation of BFL and V_1 values is showing expected behavior, with a tendency to higher values in the regions with decreasing air density.

The comparison with the reference data from the **AFMS 9702-2** adapted to wet runway conditions with the *Wet Data Addendum* for the GFD configuration is shown in tables 8.6 and 8.7.

The Wet Data Addendum is not applicable to takeoff weights below 15000 lbs due to minimum control speed limitations. At low takeoff weights, irregularities occur as the V_{MCG} becomes the lower boundary to V_1. As a result, the BFL must be increased artificially as well, which is not considered in the original Wet Data Addendum. In the simulation, the effect of the minimum control speed to increase the BFL is fully considered. An adjustment factor of 1,35 multiplied instead of the 1,2 wet runway adjustment factor for the clean aircraft to account for an increased BFL due to artificial increase in V_1 was estimated by the operator GFD. It is not part of the original *Wet Data Addendum*, and the artificial increase in BFL and V_1 is not instrumental to indicate the natural deviations between the simulation and the AFMS data.

Therefore, this data has been grayed out in tables 8.6 and 8.7. Furthermore, values that are excluded in the simulation results for the Stores+Wet configuration due to the climb weight limit of the aircraft with stores are also marked in grey.

Positive percentages indicate the simulation yielding higher results than the reference data.

Table 8.6 Deviation of BFL calculated by the Simulation to AFM Reference Data for Clean+Wet

3.9%	2.9%	1.5%	0.7%	-1.0%	0.5%	2.2%	19600	0
1.2%	1.6%	0.4%	0.4%	-2.3%	-2.2%	-2.0%	18500	
-2.9%	-2.5%	-1.7%	-1.0%	-3.4%	-3.9%	-4.0%	16000	
-3.4%	-3.1%	-2.5%	-1.9%	-4.3%	-6.8%	-6.5%	13000	
2.4%	0.8%	1.3%	1.5%	2.1%	-	-	19600	2000
2.3%	2.0%	1.3%	0.1%	0.0%	0.8%	-4.8%	18500	
1.6%	1.8%	0.5%	-0.6%	-1.9%	-1.9%	-3.6%	16000	
-0.4%	-0.3%	-1.7%	-2.7%	-5.3%	-7.5%	-7.6%	13000	
7.9%	7.7%	7.2%	11.7%	-	-	-	19600	4000
5.0%	4.9%	3.2%	5.9%	11.5%	-4.6%	-	18500	
3.9%	3.5%	2.4%	3.9%	2.2%	-0.5%	-6.9%	16000	
1.1%	0.8%	-0.7%	-1.5%	-0.1%	2.4%	0.2%	13000	
0	5	10	15	20	25	30	A/C Weight (lbs)	Pressure Altitude (ft)

OAT(°C)

Table 8.6 shows clearly that the simulation creates higher BFL results in most combinations of environmental parameters, which means it is generally conservative in comparison to the AFMS data with the *Wet Runway Addendum*.

Table 8.7 Deviation of V_1 calculated by the Simulation to AFM Reference Data for Clean+Wet

-1.2%	-1.5%	-1.5%	-1.5%	-2.2%	-2.1%	-2.1%	19600	0
-1.6%	-1.6%	-1.9%	-1.9%	-1.9%	-2.6%	-1.8%	18500	
-1.8%	-1.8%	-1.8%	-1.8%	-2.6%	-1.7%	-0.9%	16000	
0.0%	0.0%	0.0%	0.0%	0.0%	0.0%	0.0%	13000	
-1.5%	-1.8%	-2.5%	-2.4%	-1.4%	-	-	19600	2000
-1.9%	-1.9%	-1.9%	-2.9%	-2.5%	-1.8%	-1.7%	18500	
-1.3%	-1.3%	-1.3%	-2.1%	-1.3%	-0.8%	-0.8%	16000	
0.0%	0.0%	0.0%	0.0%	0.0%	0.0%	0.0%	13000	
-1.7%	-1.7%	-2.0%	-1.0%	-	-	-	19600	4000
-3.5%	-3.5%	-3.1%	-2.4%	-1.7%	-0.4%	-	18500	
-1.3%	-1.2%	-1.6%	-1.2%	-0.4%	-0.8%	-0.8%	16000	
0.0%	0.0%	0.0%	0.0%	0.0%	0.0%	0.0%	13000	
0	5	10	15	20	25	30	A/C Weight (lbs)	Pressure Altitude (ft)

OAT(°C)

It can be seen clearly from Table 8.7 that the V_1 speeds are deviating with an average of -1,3%, which means the simulation is calculating a decision speed that is 1,3% lower than the reference value. This deviation indicates that the braking distance calculated by the simulation is conservative in comparison with the AFMS data.

The change in percental deviation within a row of data does not appear to be steady; this is a result of the difference in calculation methods between the AFMS and the simulation data. Values for the AFMS have been derived through a simplified method, and the differences in calculation methods become visible in a direct comparison.

The correction factors for the individual Takeoff Distances and Accelerate-Stop Distances determined by the simulation in accordance to Fig. 7.2 are presented in Appendix I. However, only the absolute deviations presented in Tab. 8.7 and 8.7 are relevant for an assessment of the simulation precision, as outlined in Appendix I.

8.1.3 Simulation Results for Wet Runway, Stores, Uncalibrated

The simulation results for the new configuration with Stores+Wet are presented in Table 8.8 and Table 8.9. The results for Balanced Field Lengths from Table 8.8 are plotted in Appendix H.2 for easier visual representation of the trends of the simulation results with changing environmental parameters.

Table 8.8 Simulation Results for BFL Wet Runway, Stores Configuration (ft)

0	5	10	15	20	25	30	A/C Weight (lbs)	Pressure Altitude (ft)
8971	9086	9187	9429	-	-	-	19600	0
7744	7937	8083	8159	8327	8789	-	18500	
5593	5716	5832	5930	6035	6312	6788	16000	
3901	3986	4066	4140	4221	4317	4452	13000	
9825	9961	-	-	-	-	-	19600	2000
8545	8634	8840	9015	-	-	-	18500	
6168	6250	6381	6496	6908	7399	7979	16000	
4316	4392	4483	4570	4696	4858	5233	13000	
10951	-	-	-	-	-	-	19600	4000
9501	9659	10076	-	-	-	-	18500	
6886	7005	7268	7739	8343	9082	-	16000	
4784	4890	5006	5173	5485	5901	6391	13000	

OAT(°C)

Table 8.9 Simulation Results for V_1 Wet Runway, Stores Configuration (KIAS)

148	148	147	147	-	-	-	19600	0
141	141	141	140	140	141	-	18500	
125	125	125	125	125	126	128	16000	
109	109	109	109	109	109	109	13000	
147	146	-	-	-	-	-	19600	2000
140	139	139	139	-	-	-	18500	
125	124	124	124	126	127	129	16000	
109	109	109	109	109	109	112	13000	
146	-	-	-	-	-	-	19600	4000
139	139	140	-	-	-	-	18500	
125	124	125	126	128	130	-	16000	
109	109	109	109	111	112	115	13000	
0	5	10	15	20	25	30	A/C Weight (lbs)	Pressure Altitude (ft)

OAT(°C)

It can be seen that the trends expected for the BFL and V_1 towards higher values with lower air density are followed by the simulation in general. For certain V_1 speeds, at very low temperatures the trend is inversed for a limited number of environmental and weight combinations. This fact will need to be investigated in more detail in the validation of the results.

8.1.4 Simulation Results with Applied Calibration, Wet Runway, Stores

The simulation was set up in a specific way in order to offer the possibility to calculate calibration factors from the comparison of the Clean+Wet data of simulation results and AFMS. The correction factor was then to be applied on the new Stores+Wet configuration to account for the error made by the simulation. The results with applied calibration are presented in tables 8.10 and 8.11.

Table 8.10 Simulation Results for BFL Wet Runway, Stores Configuration (ft), Applied Calibration

8477	8660	8951	9163	-	-	-	19600	0
7602	7719	7885	8018	8424	8760	-	18500	
5702	5789	5865	5917	6172	6502	7041	16000	
4063	4150	4199	4258	4441	4661	4791	13000	
9408	9741	-	-	-	-	-	19600	2000
8180	8391	8589	8834	-	-	-	18500	
6060	6176	6384	6504	6981	7513	8258	16000	
4369	4430	4591	4734	4989	5297	5701	13000	
10052	-	-	-	-	-	-	19600	4000
8758	9016	9564	-	-	-	-	18500	
6598	6743	7020	7434	8229	9084	-	16000	
4759	4882	5071	5286	5526	5819	6436	13000	
0	5	10	15	20	25	30	A/C Weight (lbs)	Pressure Altitude (ft)

Table 8.11 Simulation Results for V_1 Wet Runway, Stores Configuration(KIAS), Appl. Calibration

0	5	10	15	20	25	30	A/C Weight (lbs)	Pressure Altitude (ft)
149	148	148	148	-	-	-	19600	0
142	142	142	142	142	143	-	18500	
127	127	127	127	127	127	129	16000	
109	109	109	109	109	109	109	13000	
148	148	-	-	-	-	-	19600	2000
141	141	141	142	-	-	-	18500	
126	126	126	127	127	128	130	16000	
109	109	109	109	109	109	112	13000	
148	-	-	-	-	-	-	19600	4000
142	142	143	-	-	-	-	18500	
126	126	126	128	129	131	-	16000	
109	109	109	109	111	112	115	13000	

OAT(°C)

In comparison to the original simulation results, the application of the calibration factor leads to slightly less conservative results in the lower OAT regions, while it leads to slightly higher results for the BFL in the higher OAT regions. For better comparison, this has been visualized in Fig. 8.2 for the BFL results at MSL.

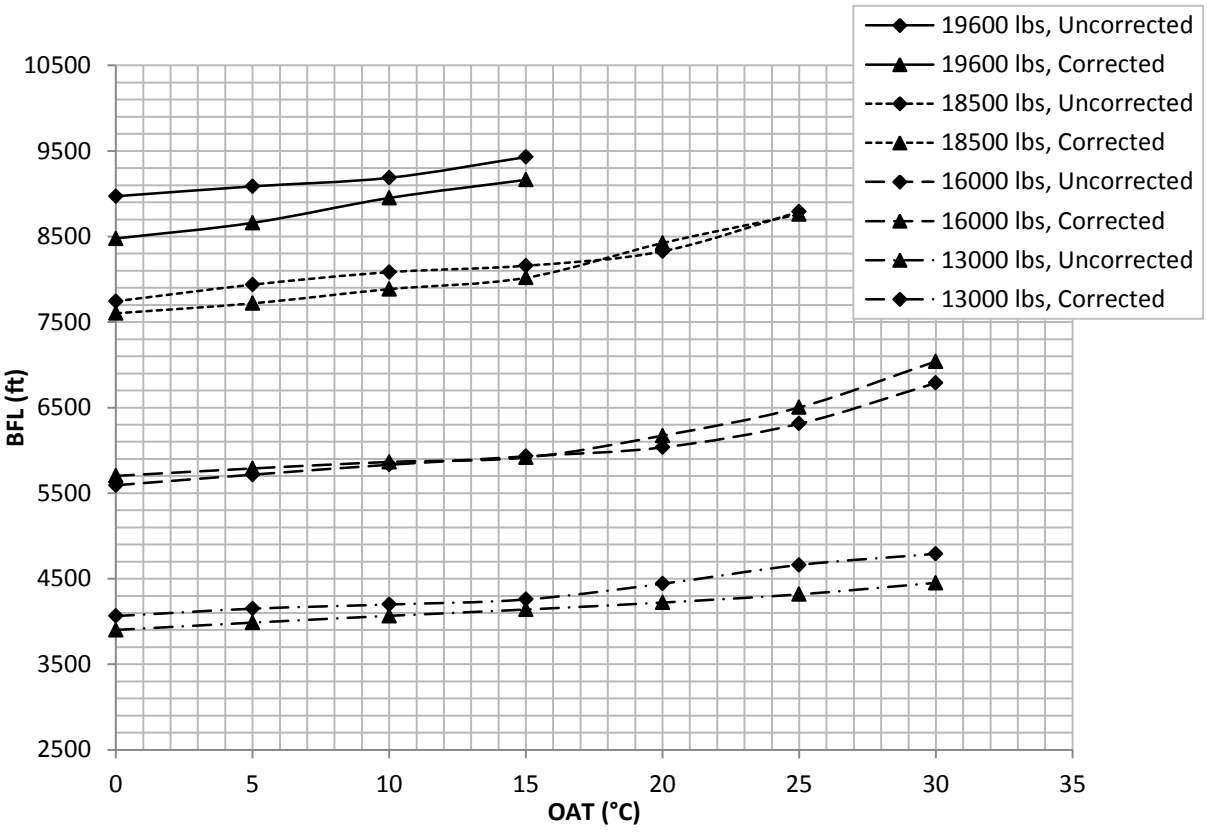

Fig. 8.2 Comparison of Simulation Results for BFL with and without Calibration, *Stores+Wet configuration, MSL*

It can be seen that the calibration leads to higher results than the original simulation data mostly for small TOW, while for higher TOW, the uncalibrated simulation results are higher. By a cross check with Table 8.6, this is coherent to the deviations calculated for the Clean+Wet aircraft between simulation and AFMS reference at MSL. The data from Table 8.6 also suggests that the simulation is becoming more conservative with regard to the AFMS data with rising pressure altitude.

It should be noted that for the further comparisons between simulation results and other references, the uncorrected results will be used, as this is the only means to directly evaluate the simulation results without interference through a calibration factor. Especially when comparing simulation results to other fields in the *Four Corner Sheet* which are all based on the AFMS data, it should be clear that the comparison must not be influenced through calibration with those same AFMS data.

8.2 Results Cross-Correlation

In order to assess the plausibility of the results calculated by the simulation, the results have to be correlated with other sources and methods that can serve as a reference. Certified references that are existent as outlined before describe the aircraft in three conditions:

- clean aircraft + dry runway configuration (Clean+Dry)
- clean aircraft + wet runway configuration (Clean+Wet)*(used for the calibration)*
- aircraft with stores + dry runway configuration (Stores+Dry)

Furthermore, a simplified calculation method shall be used as a basic reference to check whether the results are in the same order of magnitude as the simulation results.

8.2.1 Comparison of Simulation Results with existing Certified Data

Integration of Simulation Results into the Four Corner Sheet Concept

The Four Corner Sheet was introduced in Chapter 7 in order to show possible relationships between the three existing certified data sets and the expected simulation results. The relationships between each of the four fields shall now be presented, completed with the actual results and shown exemplarily at MSL in Tab. 8.12 and 8.13. Where the Climb Weight Limit becomes effective, the data field is left empty.

Table 8.12 Four Corner Sheet of BFL at SL with Simulation Results Stores+Wet (Time Step 0,1 s)

Clean + Dry (**AVCON STC ST00608WI** and **AFMS 9702-2**)							Stores + Dry (**AVCON STC ST00608WI** and **AFMS 9702-2**)							Weight (lbs)
5810	5940	6140	6340	6590	6850	7250	7260	7430	7680	7930	-	-	-	19600
5200	5300	5420	5530	5800	6100	6550	5980	6090	6230	6920	7250	7620	-	18500
3900	3960	4010	4060	4250	4470	4800	4490	4550	4610	4670	4890	5140	5520	16000
3050	3100	3140	3180	3320	3490	3580	3508	3565	3611	3657	3818	4014	4117	13000
6972	7128	7368	7608	7908	8220	8700	8971	9086	9187	9429	-	-	-	19600
6240	6360	6504	6636	6960	7320	7860	7744	7937	8083	8159	8327	8789	-	18500
4680	4752	4812	4872	5100	5364	5760	5593	5716	5832	5930	6035	6312	6788	16000
4118	4185	4239	4293	4482	4712	4833	3901	3986	4066	4140	4221	4317	4452	13000
Clean + Wet (**AVCON STC ST00608WI** and **AFMS 9702-2 + Wet Data Addendum** applied/adjusted)							Stores + Wet (Simulation)							
0	5	10	15	20	25	30	0	5	10	15	20	25	30	OAT (°C)

Table 8.13 Four Corner Sheet of V_1 at SL with Simulation Results (Time Step 0,1 s)

Clean + Dry (**AVCON STC ST00608WI** and **AFMS 9702-2**)							Stores + Dry (**AVCON STC ST00608WI** and **AFMS 9702-2**)							Weight (lbs)
142	142	142	142	143	144	145	147	147	147	147	-	-	-	19600
137	137	137	137	137	138	139	142	142	142	142	142	143	-	18500
122	122	122	122	123	124	125	127	127	127	127	128	129	130	16000
109	109	109	109	109	109	109	109	109	109	109	110	111	112	13000
136	136	136	136	137	138	140	148	148	147	147	-	-	-	19600
130	130	130	130	130	132	133	141	141	141	140	140	141	-	18500
115	115	115	115	116	116	117	125	125	125	125	125	126	128	16000
109	109	109	109	109	109	109	109	109	109	109	109	109	109	13000
Clean + Wet (**AVCON STC ST00608WI** and **AFMS 9702-2 + Wet Data Addendum** applied/adjusted)							Stores + Wet (Simulation)							
0	5	10	15	20	25	30	0	5	10	15	20	25	30	OAT (°C)

The takeoff weight of 18500 lbs was selected as a baseline for the test cases, because the same test case is used in the results validation performed in Chapter 9.

The trend of higher BFL for lower air density conditions is clearly shown in Fig. 8.3, where the results for MSL from the Four Corner Sheet are plotted.

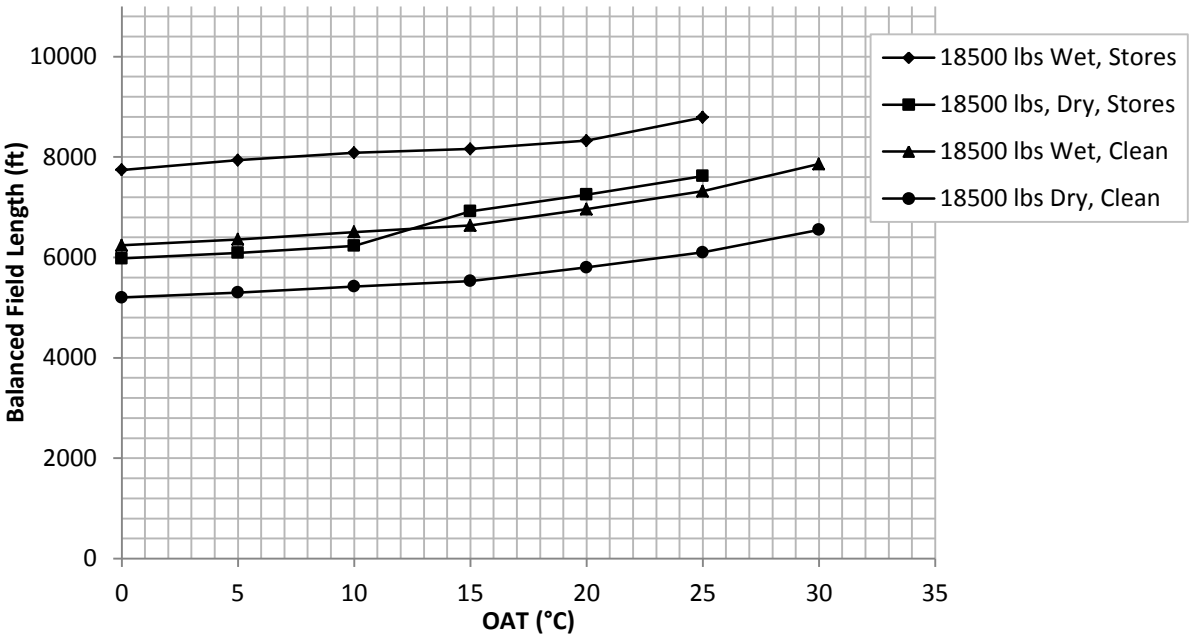

Fig. 8.3 Balanced Field Lengths for 18500 lbs TOW and MSL from Four Corner Sheet Data

As can be seen clearly from Figure 8.3, the slope of the graph of the simulation results for Stores+Wet is equal to the slope of the graphs of the other data from the AFMS. A rising OAT incurs a rising BFL.

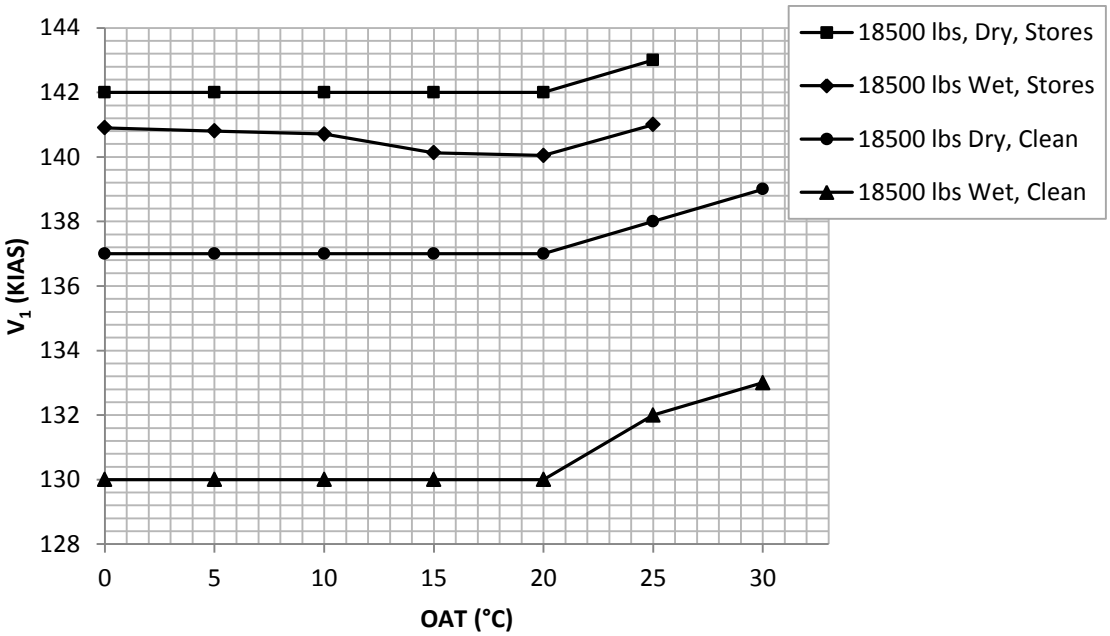

Fig. 8.4 Decision Speeds V_1 for 18500 lbs TOW and MSL from Four Corner Sheet Data

For the decision speed, Fig. 8.4 shows two remarkable characteristics. The kink of the graph at a temperature of 20°C OAT is present in all data. This is very likely due to the thrust reduction at the flat rate temperature of 22°C (compare Fig. 6.3) with a resulting increase in takeoff distance at constant braking distance.

This leads to an increasing decision speed, as the acceleration performance reduces considerably, at relatively constant deceleration performance.

The second effect clearly visible in Fig. 8.4 is the fact that the decision speed calculated by the simulation initially decreases at a constant rate with increasing OAT, while the other graphs remain constant at the level before the flat rating becomes active. This effect is another consequence of the flat rating behavior of the engine, and must be validated. This is done in Sect. 9.2.1.

Percental Relationships between Data in the Four Corner Sheet

The percental deviation between the values of the Four Corner Sheet shows the relationship of the four data corners to each other. The following percental data is given as calculated as the difference between neighboring fields of the Four Corner Sheets. Four neighboring relationships are present in a Four Corner Sheet, therefore four tables are presented in this paragraph. Fig. 8.5 summarizes the data presented in tables 8.14 to 8.17. This allows an important conclusion on the calculation method used to obtain the simulation results.

Table 8.14 Deviation of BFL from Clean+Dry towards Clean+Wet values

20%	20%	20%	20%	20%	20%	20%	19600 Weight (lbs)
20%	20%	20%	20%	20%	20%	20%	18500
20%	20%	20%	20%	20%	20%	20%	16000
35%	35%	35%	35%	35%	35%	35%	13000
0	5	10	15	20	25	30	OAT(°C)

In Table 8.14, the upper left hand corner of the Four Corner Sheet was compared to the lower left hand corner, it presents the deviation from the Clean+Dry data to the Clean+Wet data. Interestingly, the values for BFL of the wet runway are exactly 20% higher than the BFL values for the dry runway. An exception is the correction for 13000 lbs, for which the effect of the minimum control speed limit leading to higher BFL has already been discussed.

The simple relationship between the data for the Clean+Dry and the Clean+Wet values results from the simple scaling method of the **AFMS 9702-2** through the *Wet Data Addendum* to yield wet runway data from dry runway data. Individual differences between different takeoff weights and pressure altitudes are disregarded. The correction method must be evaluated accordingly in terms of precision.

Table 8.15 Deviation of BFL from Clean+Dry towards Stores+Dry values

25%	25%	25%	25%	-	-	-	19600 Weight (lbs)
15%	15%	15%	25%	25%	25%	-	18500
15%	15%	15%	15%	15%	15%	15%	16000
15%	15%	15%	15%	15%	15%	15%	13000
0	5	10	15	20	25	30	OAT(°C)

In Table 8.15, the upper left hand corner of the Four Corner Sheet was compared to the upper right hand corner. It presents the deviation from the Clean+Dry data to the Stores+Dry data. The BFL values for the aircraft with stores are either 15% or 25% higher than the values for the clean aircraft. From the **GJE EXTJFD-003**report it is known that a simplified calculation method has been the baseline for the calculation of the **AFMS 9702-2** data for the Stores+Dry configuration. Hence, it is not surprising that there are also simplified relationships between the performance data for these two aircraft configurations.

As the simulation however does not base on a simplified method but utilizes a completely different numerical integration method, it can be expected that the percental deviations between different configurations are not constant. This is clearly confirmed by the data in Tab. 8.16 and 8.17.

Table 8.16 Deviation of BFL from Stores+Dry towards Stores+Wet values

24%	22%	20%	19%	-	-	-	19600 Weight (lbs)
29%	30%	30%	18%	15%	15%	-	18500
25%	26%	27%	27%	23%	23%	23%	16000
11%	12%	13%	13%	11%	8%	8%	13000
0	5	10	15	20	25	30	OAT(°C)

Table 8.16 suggests that the simulation results for BFL in the Stores+Wet configuration are on average 23% higher than for the Stores+Dry configuration. This appears reasonable and may be even conservative, given that the BFL for the clean conditions rises by 20% from the Clean+Dry to the Clean+Wet configuration.

It should be noted that the cross check performed in Tab. 8.16 also satisfies the requirement of CS-25.113 b) for wet runways, as outlined in Section 3.2. It has been shown that the takeoff distances on a dry runway are lower than on a wet runway with the same aircraft configuration. Hence, the wet data becomes limiting for the Stores+Wet configuration.

Table 8.17 Deviation of BFL from Clean+Wet towards Stores+Wet values

29%	27%	25%	24%				19600 Weight (lbs)
24%	25%	24%	23%	20%	20%		18500
20%	20%	21%	22%	18%	18%	18%	16000
-9%	-8%	-8%	-7%	-9%	-12%	-11%	13000
0	5	10	15	20	25	30	OAT(°C)

Shifting from the bottom left to the bottom right hand corner of the Four Corner Sheet, it presents the deviation from the Clean+Wet data to the Stores+Wet data. The BFL rises by an average of 14%. This is comparable to the rise of 22% in BFL (excluding 13000 lbs TOW) when shifting from a Clean+Dry to a Stores+Dry configuration (top left to top right corner).

The 13000 lbs TOW data again is exhibiting a noticeable difference to the other data. This is a consequence of the artificial increase in V_1 to V_{MCG}. The BFL adjustment factor for the Clean+Wet aircraft was estimated to 1,35 (compared to 1,2 for other TOW). At a rejected takeoff from 109 KIAS, the aircraft with stores however is assisted in its braking performance due to the additional drag force – which yields to the decreased BFL in comparison to the clean aircraft. It is therefore not surprising that the deviation analysis yields even reduced distances in the Stores+Wet configuration, where the effect on the BFL of an artificial increase in V_1 has been considered accurately.

Figure 8.5 summarizes the deviation analysis performed and presents the average deviations calculated between all four neighboring data sets.

Fig. 8.5 Synthesis of Percental Deviations within the Four Corner Sheet

What can be seen clearly from the synthesis of percental deviations is that the simulation determines approximately the same deviations between its neighboring configurations in the Four Corner Sheet as the existing certification data. This must be seen as a strong support of the plausibility of the simulation results, as it integrates very well into the existing Four Corner Sheet data.

The analysis also showed that the remainder of the Four Corner Sheet is likely to represent only simplified relations, all data having been calculated in simplified methodology. This must be considered judging possible deviations between the simulation results and the AFMS.

8.2.2 Comparison of Takeoff Distance from Simulation with Simplified Method

For the comparison of the simulation results with a simplified method, the approach presented in Section 4.1.2 for hand calculations is used and further. The simplified approach presented in this section is comparable to the simplified approach used in the **GJE EXTGFD-003** report for the determination of the AFMS data.

The ground roll distance can be determined from the basic equation 8.1.

$$S_G = m \cdot \int_{v_i}^{v_f} \frac{v_G}{T - D - F_f - m \cdot g \cdot \sin\gamma} dv_G \tag{8.1}$$

With

v_f Final Speed

v_i Initial Speed

With the assumption of constant forces present during the ground roll, equation 8.1 can be simplified to yield:

$$S_G = \frac{m}{2} \cdot \left(\frac{v_f^2}{T - D - F_f - m \cdot g \cdot \sin\gamma} - \frac{v_i^2}{T - D - F_f - m \cdot g \cdot \sin\gamma} \right) \tag{8.2}$$

This is an extension of the equation 4.7, because it permits dividing the ground roll into different segments. The takeoff run is marked by the significant event of an engine failure. If no distinction between the segments was made along the entire takeoff run from brake release to liftoff speed, average drag coefficients and thrust values would have to be used to account for the loss in thrust and increase in drag due to OEI conditions. This was done in the **GJE EXTGFD-003** report.

As the hand calculation shall enable a comparison with the simulation results and the V_1 speed is known, this section shall employ the simplified method divided in two ground roll segments.

The first segment starts at brake release and covers a distance up to V_1, where an engine is assumed to fail, which is of course a simplified assumption. The second segment covers a distance from V_1 to V_{LOF}, where the aircraft lifts off. A third segment is the distance covered in the air until the screen height is passed, for which the approach presented in Section 4.2 is used.

The input parameters given in Table 8.18 are needed for the calculation. They are based on the parameters determined and presented in this report and have been validated in Chapter 6. As a test case, an aircraft of 18500 lbs takeoff weight at ISA conditions has been considered. Due to water on the runway, the friction force F_f contains also the displacement, impingement and skin friction drag forces. These have been calculated according to the equations provided in Section 4.1.9, respectively 5.5.

For the simplified method, this yields a total friction force of:

$$F_f = \mu \cdot (m \cdot g - L) + D_{Displ,av} + D_{Skin,av} + D_{imp,max} \tag{8.3}$$

With

$$D_{Displ,av} = 0{,}75 \cdot \frac{1}{2} \rho \cdot v_{av}^2 \cdot A_{tire,subm} \cdot n_{tire} \cdot f_{aquaplaning} \tag{8.4}$$

$$F_{W,Skin} = 8 \cdot L \cdot 0{,}0025 \cdot \frac{1}{2} \rho \cdot v_{av}^2 \cdot A_{tire,subm} \cdot f_{aquaplaning} \tag{8.5}$$

And

v_{av}	Average speed for considered segment
f_{aqua}	Average aquaplaning factor acc. to Eq. 1.2 at average speed
$A_{tire,subm}$	Submerged tire frontal area acc. to Eq. 4.82

Table 8.18 Input Parameters for the hand calculation

Variable	Name	Value	Source
m	Aircraft Mass	18500 lbs	Test Case
V_1	Decision Speed	132 kts	**AMFS 9702-2**
V_S	Stall Speed	116,33 kts	**AMFS 9702-2**
V_{LOF}	Liftoff Speed	139,6 kts	Calculated according to Eq. 4.13 from V_S
V_{AV1}	Average Speed 1	98,7 kts	Average Speed for Segment 1
V_{AV2}	Average Speed 2	136,2 kts	Average Speed for Segment 2
ρ_{Air}	Air Density	1,225 kg/m³	ISA Conditions
ρ_{Spray}	Water Density	1000 kg/m³	Simplified Conditions
$f_{aquaplaning}$	Aquaplaning Factor	1,0 @ V_{AV1}	Drag Reduction due to Aquaplaning
$f_{aquaplaning}$	Aquaplaning Factor	0,24 @ V_{AV2}	Drag Reduction due to Aquaplaning
g	Gravity	9,81 m/s²	Standard Value
S	Wing Area	23,53 m²	According to Section 6.2
$c_{D,AEO}$	Drag Coefficient	0,0606	Before Engine Failure, Stores installed
$c_{D,OEI}$	Drag Coefficient	0,0797	After Engine Failure, Stores installed
c_L	Lift Coefficient	0,243	Ground Roll Lift Coefficient
T_{av1}	Thrust per Engine at V_{AV1}	3024 lbs	from **GJE EXTGFD-003**, at $V_{A,V1}$
T_{av2}	Thrust per Engine at V_{AV2}	2880 lbs	from **GJE EXTGFD-003**, at $V_{A,V2}$
μ	Rolling Friction at V_{AV1}	0,0397	Acc. to Fig. 4.17, **NASA TP-2770**
μ	Rolling Friction at V_{AV2}	0,0443	Acc. to Fig. 4.17, **NASA TP-2770**
$A_{tire,subm}$	Submerged Tire Area	0,0003 m²	Simplified for all Wheels from Eq. 4.82
n_{tire}	Number or Tires	5	Learjet 35A/36A Basic Information
$D_{skin,av}$	Average Skin Friction Drag	46,8 N	Acc. to Eq. 4.86, at V_1
$D_{displ,av}$	Averg. Displacement Drag	2594 N	Acc. to Eq. 4.81, at V_1
$D_{imp,max}$	Store Impgmt. Drag	163,4 N	Refer to Section 5.4

First TOD Segment

The first segment of the Takeoff Distance is covered on the ground between zero initial speed at brake release and engine failure speed, assumed at V_1. Therefore, the simplified method from equation 8.2 reduces to:

$$S_{G1} = \frac{m}{2} \cdot \left(\frac{V_1^2}{T - D - F_f - m \cdot g \cdot \sin\gamma} \right) \tag{8.6}$$

For the calculation of the forces, the average speed V_{AV1} was used. As defined in Section 4.1.2, it amounts to 70,7% of the segment final speed.

$$V_{AV1} = 0{,}707\, V_1^2 \tag{8.7}$$

From this phase, the first segment distance S_{G1} was determined to be

$$S_{G1} = 3319\, ft$$

Second TOD Segment

The second segment of the Takeoff Distance is covered between the speeds V_1 and V_{LOF}. Therefore, equation 8.2 is adapted and yields:

$$S_{G2} = \frac{m}{2} \cdot \left(\frac{v_{LOF}^2}{T - D - F_f - m \cdot g \cdot \sin\gamma} - \frac{V_1^2}{T - D - F_f - m \cdot g \cdot \sin\gamma} \right) \tag{8.8}$$

However, in contrast to the first TOD Segment, the average speed for this part of this segment could not be 70,7% of the final speed V_{LOF}, as this value would be below the initial speed $V1$. Therefore, the average speed V_{AV2} was selected to be the mean of V_{LOF} and V_1. From this phase, the second segment distance S_{G2} was then determined to be

$$S_{G2} = 4199\, ft$$

The Liftoff Distance therefore amounts to

$$S_{LOF} = S_{G1} + S_{G2} \tag{8.9}$$

$$S_{LOF} = 7518\, ft$$

The Takeoff Distance is determined when the third segment, the air distance until clearance of the obstacle height, is added to the Liftoff Distance.

Third TOD Segment

The air distance is calculated from the equations provided in Section 4.2. All required parameters are given in Table 8.18. This leads to

$$S_{TR} = 550\ ft$$

$$h_{TR} = 4{,}02\ m = 13{,}2\ ft$$

$h_{TR} < 15\ ft$, therefore the climb distance also has to be calculated.

$$S_{CL} = 38\ ft$$

The total Air Distance is then determined from the sum of the rotation phase distance S_{TR} and the climb distance S_{CL}.

$$S_a = S_{TR} + S_{CL} = 588\ ft$$

Following these segmental calculations, the sum of all three segments determines the Takeoff Distance.

$$S_{TOD} = S_{G1} + S_{G2} + S_a \qquad \textbf{(8.10)}$$

It amounts to

$$S_{TOD} = 8106\ ft$$

The Balanced Field Length calculated by the simulation for the same test case of the wet aircraft with stores at 18500 lbs and ISA, SL amounted to 8159 ft.

This leads to a deviation of 0,6% with an indication for conservatism of the simulation. The deviation is in the same region and aligns with the deviation of 0,4% that was determined between the AFMS data and the simulation result for the same test case as shown in Tab. 8.6.

It is therefore a further reference point to the assumption that the simulation is producing consistent, and generally slightly higher results for the BFL as is determined with a simplified method, even if the simplified method precision has been augmented by dividing the Liftoff Distance in two segments in the above example.

The empirical equation from **Torenbeek 1982** could not be used for the validation of the simulation results for a wet runway, as it is applicable for dry runways only. An exemplary calculation of the test case presented in this section using the necessary input parameters which have been presented in this report, it yields a distance of 7432 ft for the BFL in Stores+Dry configuration. This is only 3,7% short of the AFMS value given for the same configuration.

8.3 Comparison of Main Forces during Takeoff Ground Roll with Simplified Calculation

Two plots created by the simulation representing the forces during the takeoff roll shall be presented to facilitate the assessment of the relations between the different forces. This will also make it easier to assess the impact of a variation of these parameters. The simulation has been programmed to plot all forces occurring during the takeoff roll for each condition considered. This makes it easy to track, evaluate and understand forces influencing the takeoff roll and see their variation with speed.

The forces plot will now also serve to validate many time-step-dependent effects that have been included in the simulation, notably the time reaction time between the activation of different retarding forces in the case of an aborted takeoff.

Figure 8.6 provides the forces in case of a continued takeoff with an engine failure occurring at V_{EF}. Figure 8.7 provides the forces in case of an aborted takeoff with engine failure at V_{EF}, its recognition at V_1, and the subsequent activation of retarding devices at a rate of one per second. Therefore, the x-axis of Figure 8.7 is reflecting time in seconds after V_{EF}.

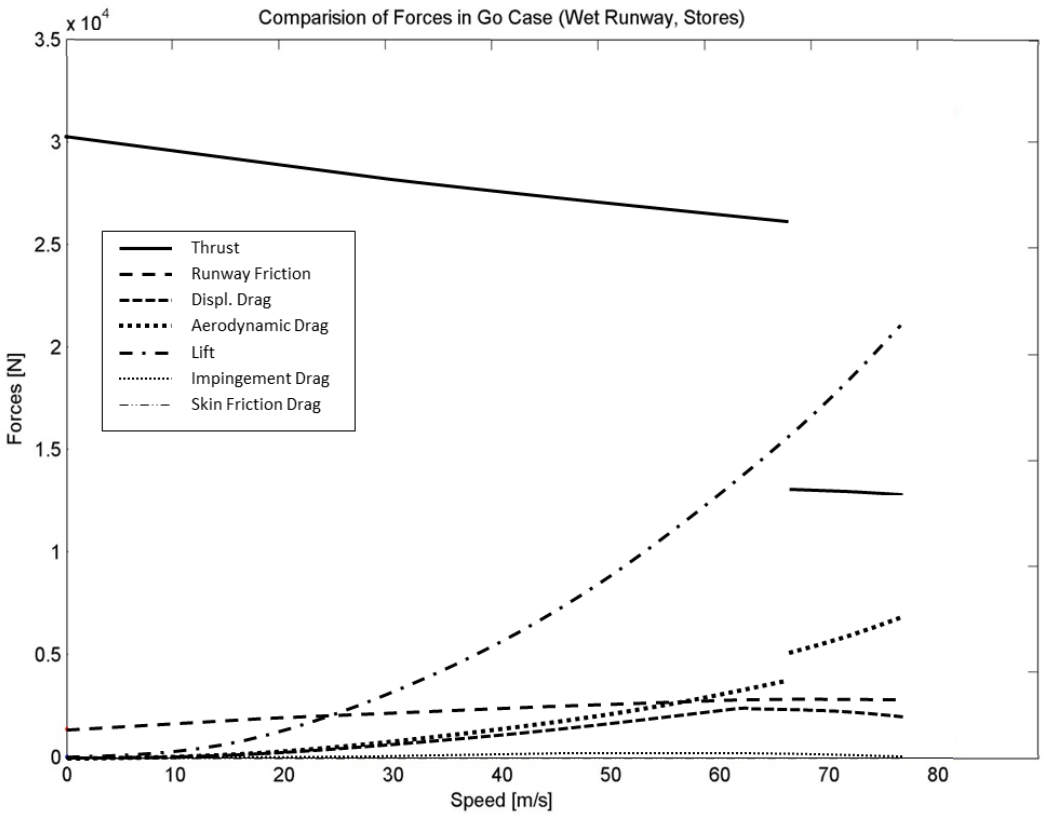

Fig. 8.6 Forces on the Aircraft during Acceleration with Engine Failure
18500 lbs TOW, ISA, SL, Stores+Wet

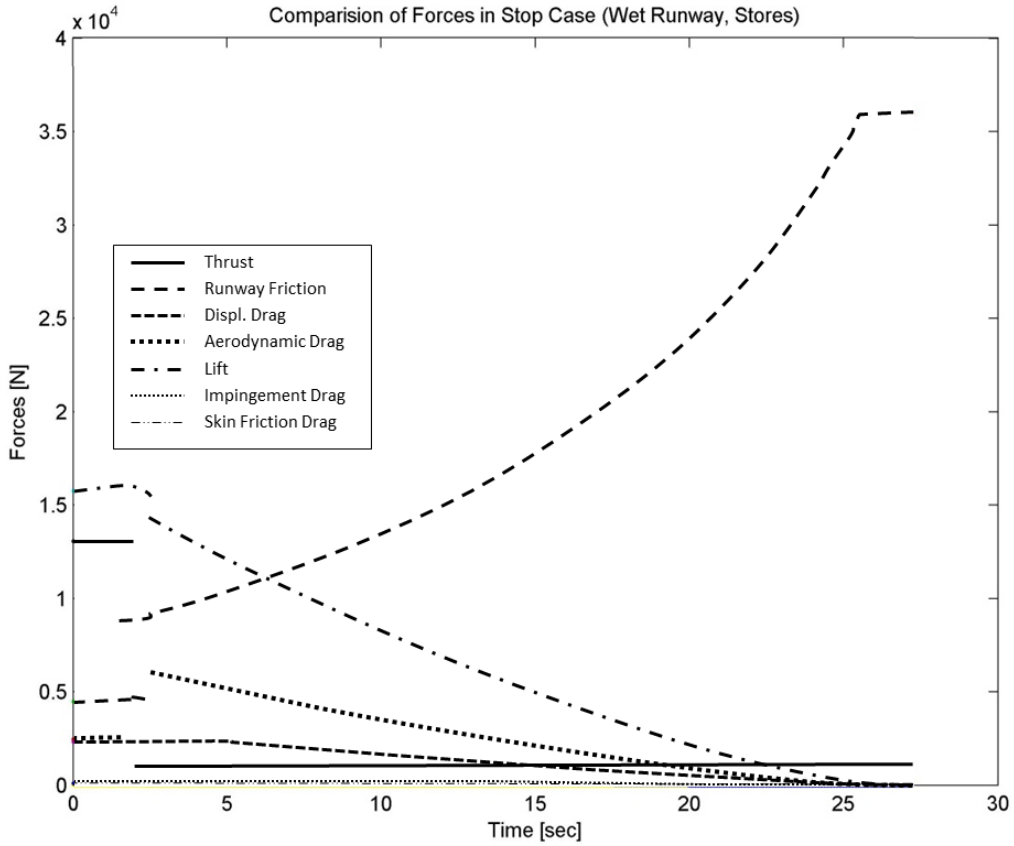

Fig. 8.7 Forces on the Aircraft during Deceleration after Engine Failure
18500 lbs TOW, ISA, SL, Stores+Wet

A very interesting fact that can be directly seen in Fig. 8.6 is the speed dependency of the Displacement Drag, which is marked in pink. It is calculated with regard to speed and the aquaplaning factor is considered. This means that the drag due to water displacement by the tires drops significantly after the aquaplaning speed has been reached. Other important effects that are visible in Fig. 8.6 are:

- The significant reduction in engine thrust at engine failure speed
- The considerable increase in aerodynamic drag due to engine failure
- The fact that Spray Impingement and Skin Friction drag forces are negligibly small

Fig. 8.7 is even more interesting in terms of evaluation of the different effects used in the set-up of the simulation. Visible in the forces plot are:

- The activation of wheel brakes two seconds after engine failure
- The thrust reduction 3 seconds after engine failure
- At thrust reduction, a small aerodynamic drag increment due to pilot input of rudder force to balance the idle engine thrust imbalance
- The reduction in lift force due to spoiler activation 4 seconds after engine failure
- The increase in aerodynamic drag due to spoiler activation
- The increase in braking friction due to lift depletion after spoiler activation
- The fact that before thrust reduction, excess thrust is produced by the remaining engine

A simplified calculation used to validate the forces acting on the aircraft as calculated by the simulation shows, that the simulation provides plausible magnitudes for the forces when compared to values determined for a single speed. Input data for the data in Table 8.19 bases on the parameters presented in Table 8.18 for the simplified calculation method.

At a speed of 67,91 m/s, the following forces have been calculated by hand based on the equations and input data provided in Section 8.2.2.

Table 8.19 Forces calculated with Simplified Method at 67,91 m/s for 18500 lbs, SL, ISA, Stores

Variable	Name	Value
T	Thrust	13451 N (after Engine Failure)
D	Aerodynamic Drag	5297 N
L	Lift	16151 N
F_f	Friction Force	2626 N
D_{displ}	Displacement Drag	2594 N

A comparison with Figure 8.5 shows a very good match with the forces calculated and plotted by the simulation. Also, special speed dependent effects such as the water drag reduction due to aquaplaning have been validated by the plots. The forces considered by the simulation for the Balanced Field Length calculation can be regarded as plausible.

9 Validation of the Simulation Results

9.1 Possible Error Sources and Rectification

9.1.1 Programming Errors

There are three general types of programming errors that need to be considered – Syntax, Semantic and Logic errors.

Syntax errors are relatively easy to discover, as the programming language usually detects them already during the writing process. These kinds of errors are usually discovered during the programming phase. Semantic errors occur and are detected during execution of the program when inconsistencies lead to impossibility to execute a code section, such as for example caused by a division by zero. These kinds of errors are then discovered during execution of the code. As the simulation has undergone rigid testing and been executed for a range of diverse input parameters, Syntax and Semantic errors have been progressively eliminated.

The most challenging types of errors though are Logic errors, as these errors do produce a program code that is executable and produces results. However, these kinds of errors occur, when the specification for the program has not been respected (for example procedures defined in certification documents), or simply when wrong equations or conversions have been used.

Logic errors therefore can only be found when understanding the expected results of the program (such as the direction of variation of results with parameter variation) and a cross-check of the results produced by the program with these expectations. Already the comparison of simulation results with other sources of data as performed in Chapter 8 has been a very important part of the elimination of programming errors and showed consistent results. Logic errors can also be discovered when unexpected unsteadiness or spikes are found in a consistent row of results over a range of consistent input parameter variations (e.g. a constant change of BFL with OAT increase).

As these kinds of errors are generally difficult to detect, a cross checking mechanism has already been built into the very structure of the simulation. This is the calculation of the calibration factors between simulation results for the known case, and the comparison to reference data, as described in Section 7.2. As this verification method is an integral component of the simulation and is always executed at each run of the simulation, it was possible to determine certain logic errors relatively early in the design process, because errors either in the Accelerate-Stop or the Takeoff case would directly be reflected by a large deviation of either of the two curves in the Balanced Field Length chart.

9.1.2 Model Inaccuracies

As for any computer simulation, the degree at which physical reality can be represented through equations and their interactions cannot be exhaustive. Model inaccuracies are, however, not unexpected, because models were selected and simplifications were made that have rendered analytical treatment of the physical problem possible in the first place. Therefore, listing the models used for the simulation and investigating their deviation to known values from test data or other references is an invaluable tool to gain trust and be able to validate the simulation results.

The general models used in this simulation describe the Thrust, the Lift, the Drag and the Friction model of the aircraft. For all of these models, it was necessary to assume certain simplifications in order to represent physical properties in the simulation.

As model inaccuracies can best be determined by validation with other sources, Chapter 6 (Aircraft Parameters) of this report validated data from the models used in the simulation with other references. Therefore, the model input parameters do not have to be re-examined in this section. However, an additional source of trust in the simulation is the analysis of parameter variation effects, as this shows whether the ensemble of all models used in interaction with each other produces consistent results.

9.1.3 Test Methods for Analysis

The previous two sections have already given some information on how certain types of errors and inaccuracies can be detected and assessed or rectified. The most important means discussed were the comparison of the models and the simulation results to known data.

For the execution of a parameter variation impact assessment to validate model accuracy, a test case needs to be selected. Subsequently, input parameters can be either increased or decreased by a certain percentage, variables made constants (from literature values), certain individual model effects be turned on or off for the test case run. A comparison with the baseline results then facilitates the impact assessment.

This analysis in turn allows for two major conclusions:

The first conclusion can be drawn on whether logic errors in the simulation are still present, or if the variation of the results with the variation of impact parameters produces results in accordance to the expected variation.

The second conclusion concerns an assessment on the need for precision in the models used by the program. Through deviation of a model parameter, it becomes clear by how much a change of this parameter impacts the final result. If a substantial variation of the final result is found, it should be considered to define the respective model in a more precise and detailed way in order to prevent larger deviations.

In practice, this was done for this simulation with the models for Thrust of the aircraft, by choosing the most detailed academic thrust model applicable to the scarce information available on the engine, and by further specifying special engine parameters such as thrust variation due to flat rating, as well as a correction factor application to match test data. As another example, also the rolling friction of the aircraft was reconsidered and the static friction coefficient from common aircraft preliminary design literature replaced by a speed dependent rolling friction coefficient from NASA flight test data.

9.2 Parameter Variation Effects and Influence on Simulation Results

For the analysis of the parameter deviation effects, it is very important to have an expectation towards the result after the parameter was varied. Therefore, Section 4.1.3 gave an overview on the expected deviations in Takeoff Distance due to parameter variation. Present section consequently verifies the correct behavior of the simulation with varying input parameters, and furthermore allows a conclusion on the impact of certain model assumptions.

When judging deviations to the AFMS data, the fact that this data also bases on a simplified calculation method must be taken into account, with respective accuracy. However, as certified material, the data may serve as a good reference for comparison with the simulation results during the parameter variation.

9.2.1 Variation of Aircraft Mass and Air Density

The variation of the two important parameters, aircraft mass and air density, is reflected in the parameter input grid for the simulation used throughout Chapter 8. Table 9.1 provides an overview on the parameter variation due to a change in OAT. With rising OAT, the air density decreases. An increase in BFL is therefore expected, and reflected by the data in Table 9.1.

Table 9.1 Impact on Simulation Results of Variation of OAT by 5K at MSL, with 18500 lbs TOW
Influenced by Flat Rating Characteristics, Anti-Ice off, Anti-Skid on, no wind, no slope

Value Name		OAT -5K	OAT 15°C	OAT +5K
Clean + Wet:	**BFL, ft** (rounded)	**6528**	**6663**	**6801**
Clean + Wet:	BFL Baseline Deviation	-2.03%	-	2.07%
Clean + Wet:	**V_1, KIAS** (rounded)	**127**	127	**128**
Clean + Wet:	V_1Baseline Deviation	0.00%	-	0.79%
Stores + Wet:	**BFL, ft** (rounded)	**8083**	**8159**	**8327**
Stores + Wet:	BFL Baseline Deviation	-0.93%	-	2.06%
Stores + Wet:	**V_1, KIAS** (rounded)	**141**	**140**	**140**
Stores + Wet:	V_1Baseline Deviation	0.71%	-	0.00%

Fig. 9.1 graphically presents the variation of the simulation results of the BFL with regard to air density and aircraft mass for MSL as presented in the Four Corner Sheet.

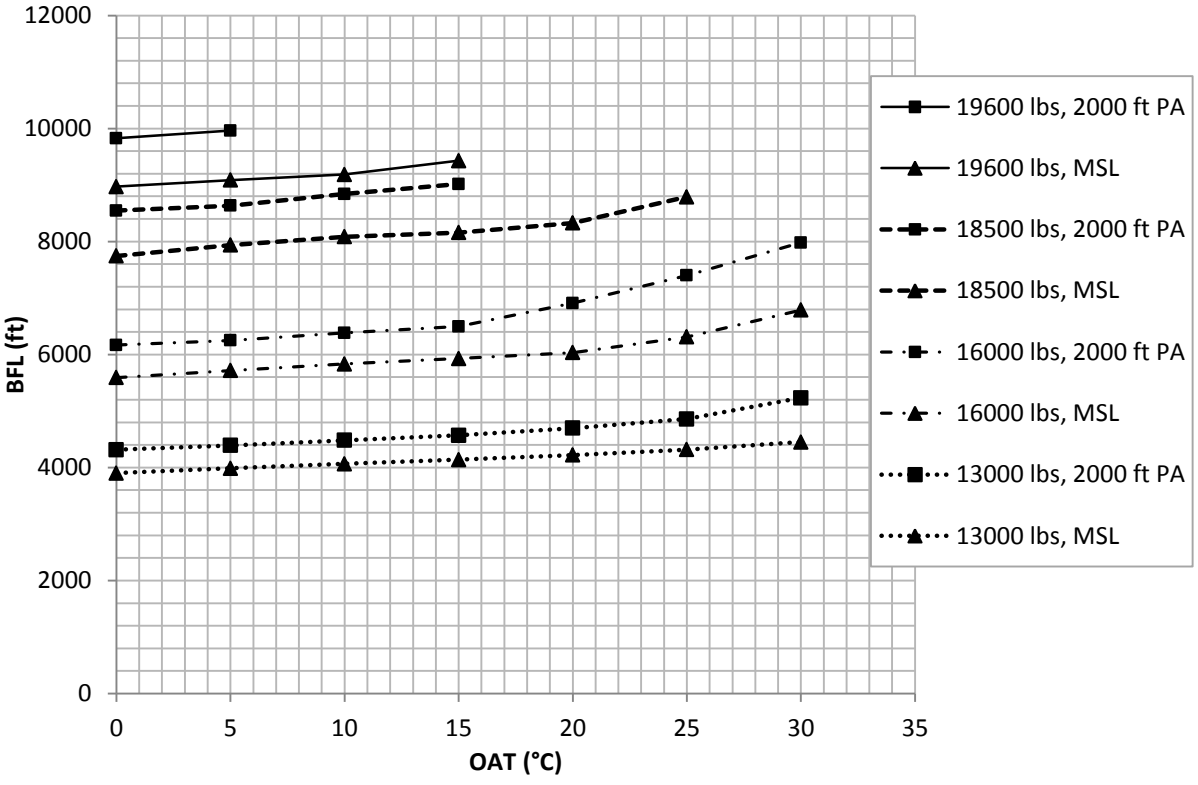

Fig. 9.1 Variation of Balanced Field Length with Density and Aircraft Weight

As can be seen, the variation of the graph as a function of increasing aircraft mass shows the expected behavior of an increased BFL with rising aircraft mass. Likewise, with rising temperature (decreasing density) and increasing pressure altitude (decreasing density) the BFL also rises.

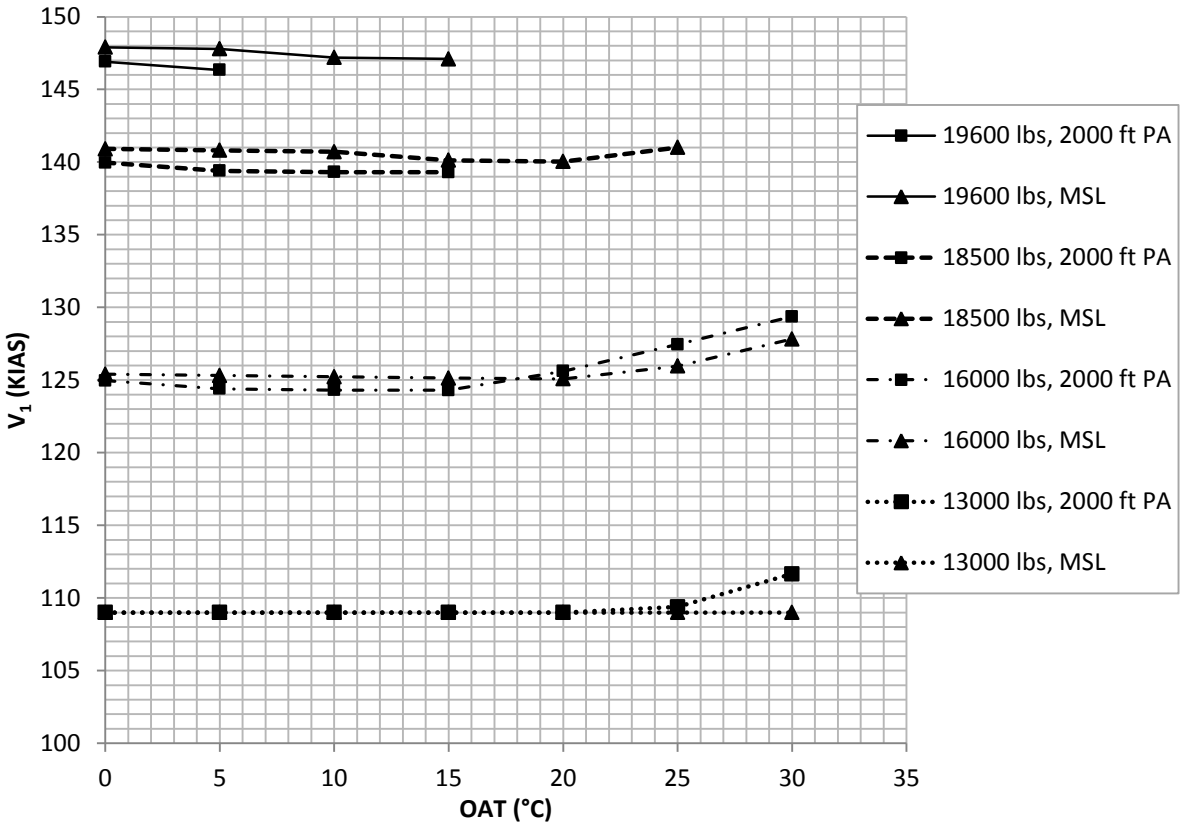

Fig. 9.2 Variation of V_1 with Density and Aircraft Weight

From the V_1 Decision Speed graphs presented in Fig. 9.2, it becomes apparent that the flat rate temperature limit plays a considerable role for the V_1 speed determination.

The first expectation for a linearly decreasing density would be a reflection of linear regularity in the graphs obtained for the Decision Speeds. However, the aircraft parameters with decreasing air density are behaving not linear, due to the flat rating of the engines.

If a flat rate limit of the engines exists and the environmental conditions are such that the flat rating becomes active, the thrust of the aircraft will vary only with speed and pressure altitude. The manufacturer refers to the thrust below flat rate limit temperature limit also as the maximum guaranteed thrust.

Consequently, the thrust below the flat rate limit temperature for a certain pressure altitude can be assumed constant. The limitations on engine performance through the engine control system are turned off and the engine reacts as predicted with regard to air density as soon as the OAT rises over the flat rate temperature limit. Consequently, a kink can be perceived in Figure 9.1 and Figure 9.2 at the respective flat rate temperature limits.

According to Fig. 6.3, the flat rate temperature limit at sea level is located at 22°C OAT, the flat rate limit at 2000 ft PA at 16°C OAT. Allowing a certain amount of tolerance, the described kink due to flat rating can also be recognized in the appropriate graphs of Figure 9.1 and Fig. 9.2. An exception is again the graph for 13000 lbs TOW due to the fact that V_1 was artificially increased to V_{MCG}.

According to Eq. 4.14, if the thrust is assumed constant below flat rate limit temperature, the only three remaining parameters varying with density are then the *liftoff ground speed* as well as the *drag* and *lift* forces of the aircraft.

The lift plays only a secondary role in the horizontal distance calculation, as its only impact is the impact on friction force. It will be shown in Section 9.2.2 that a decrease in Lift actually has a beneficial effect on Balanced Field Length due to increased braking performance. Consequently, the *drag force reduction* due to *decreasing air density* impacts the overall BFL much more with a flat-rated engine behavior than without.

As will be shown in Section 4.2.2, a reduced drag coefficient reduces the V_1 considerably due to the fact that the aircraft acceleration and takeoff performance improves while the braking performance deteriorates. Inversely, with decreased air density the liftoff ground speed increases, yielding higher Takeoff Distances.

Therefore, the takeoff distance is impacted by a reduction in drag and an increase in liftoff ground speed, while the deceleration distance is impacted only by the reduction in drag. Both effects lead to higher distances, but the relative impact on the ASD is higher than the impact on the TOD. Hence, the BFL becomes larger, while a slight decrease in V_1 may occur as long as the engine remains flat rated.

9.2.2 Variation of Aerodynamic Parameters

For impact assessment of aerodynamic parameters variation, a test case has been selected and variations been determined at a 0,1 seconds time step width resolution. This test case referred to as *Baseline* in all tables is the Learjet 35A/36A at 18500 lbs TOW on a wet runway, with MSL and ISA conditions.

For the evaluation of the BFL and V_1 results from a parameter variation, the simulation results for the Clean+Wet and the Stores+Wet aircraft are provided in this section. This is done in order to determine the consistency in the parameter deviation Impact. Furthermore, in analogy to the method described in Section 8.2.1, the percental deviation of the simulation values with regard to the certified data provided by the AFMS is shown. This will allow an assessment on the question whether a parameter variation will enhance or deteriorate the match between simulation and AFMS values.

Lift Variation

The ground lift coefficient $C_{L,G}$ variation was performed by a magnitude of +/-10%.

Table 9.2 Impact on Simulation Results of Variation of $C_{L,G}$ by 10%
ISA, MSL, 18500 lbs TOW, Anti-Ice off, Anti-Skid on, no wind, no slope

Value Name		$C_{L,TO}$ +10%	Baseline	$C_{L,TO}$ -10%
Deviation to AFMS Reference, BFL		0.74%	0.41%	0.98%
Deviation to AFMS Reference, V_1		-2.31%	-2.31%	-1.54%
Clean + Wet:	**BFL, ft** (rounded)	**6685**	**6663**	**6701**
Clean + Wet:	BFL Baseline Deviation	0.33%	-	0.57%
Clean + Wet:	**V_1, KIAS** (rounded)	**127**	**127**	**128**
Clean + Wet:	V_1 Baseline Deviation	0.00%	-	0.79%
Stores + Wet:	**BFL, ft** (rounded)	**8183**	**8159**	**8190**
Stores + Wet:	BFL Baseline Deviation	0.29%	-	0.38%
Stores + Wet:	**V_1, KIAS** (rounded)	**140**	**140**	**141**
Stores + Wet:	V_1 Baseline Deviation	0.00%	-	0.71%

The effect of the ground lift coefficient is only indirectly a part of the equation of motion – through the normal force component on the wheels that determine rolling and braking friction. A decreased lift coefficient should increase both the rolling and the braking friction. For the ASD, these effects are antagonist with regard to the overall distance due to decreased acceleration and increased braking performance. Consequently, the impact of the lift model variation on the overall simulation results in terms of BFL is very small. The simulation assessment shows that the overall distances are varying by a rather small amount below the 1% range of precision of the simulation results. This is the reason why the results do not show a consistent behavior – expected was the BFL distance to rise with increased lift coefficient, while a decreased lift coefficient should lead to a lower Balanced Field Length. Hence, due to the small effect smaller than 1% with regard to BFL, the simulation is not capable of measuring the variation, which leads to the results shown in Tab. 9.2.

The simulation provides the same type of results for both aircraft configurations shown.

Drag Variation

For the drag coefficient $C_{D,TO}$, a variation was performed by +/-10%. Also, a variation of the drag coefficient increment due to the failed engine $\Delta C_{D,OEI}$ was performed by +/- 20%. The value $\Delta C_{D,OEI}$ comprises both the drag due to engine windmilling as well as the increased drag due to the asymmetrical flight condition.

Table 9.3 Impact on Simulation Results of Variation of C_D
ISA, MSL, 18500 lbs TOW, Anti-Ice off, Anti-Skid on, no wind, no slope

Value Name		**Baseline**	**$C_{D,TO}$ +10%**	**$C_{D,TO}$ -10%**	**$\Delta C_{D,OEI}$ +20%**	**$\Delta C_{D,OEI}$ -20%**
Deviation to AFMS Reference, BFL		0.41%	3.12%	-1.31%	1.96%	-0.87%
Deviation to AFMS Reference, V_1		-2.31%	-0.77%	-3.08%	-1.54%	-2.31%
Clean + Wet:	**BFL, ft** (rounded)	**6663**	**6843**	**6549**	**6766**	**6578**
Clean + Wet:	BFL Baseline Deviation	-	2.70%	-1.71%	1.55%	-1.28%
Clean + Wet:	V_1, KIAS (rounded)	**127**	**129**	**126**	**128**	**127**
Clean + Wet:	V_1 Baseline Deviation	-	1.57%	-0.79%	0.79%	0.00%
Stores + Wet:	**BFL, ft** (rounded)	**8159**	**8538**	**7922**	**8315**	**8056**
Stores + Wet:	BFL Baseline Deviation	-	4.65%	-2.90%	1.91%	-1.26%
Stores + Wet:	**V_1, KIAS** (rounded)	**140**	**144**	**138**	**142**	**139**
Stores + Wet:	V_1 Baseline Deviation	-	2.86%	-1.43%	1.43%	-0.71%

The unfavorable impact of a 10% *higher drag coefficient* leads to a 4,65% *increase in Balanced Field Length* for the aircraft with stores, the beneficial effect of a decreased drag coefficient leads to a respective decrease of the BFL by -2,90%. The simulation shows consistent behavior for both configurations selected, for the overall drag coefficient as well as for the drag due to engine failure.

A *higher drag coefficient increases the decision speed V_1*, as the braking performance of the aircraft is assisted by higher drag, so the takeoff acceleration can be aborted at a later point during the takeoff. The inverse is true for the decreased drag coefficient.

While increasing the drag coefficient by 10% leads the V_1 deviation compared to AFMS reference data to be smaller, it actually increases the error for the BFL made by the simulation. Both effects are opposing each other, which leaves the original drag coefficient seem a good compromise between both possible variations.

9.2.3 Variation of Thrust Parameters

The thrust is the only force actually creating excessive thrust that accelerates the aircraft. As shown in Section 4.1.3, its variation can have significant impact on the actual Takeoff Distance.

For impact assessment of thrust parameters variation, the same test case as for the aerodynamic parameter variation has been selected.

Table 9.4 Impact on Simulation Results of Variation of Installed Thrust
ISA, MSL, 18500 lbs TOW, Anti-Ice off, Anti-Skid on, no wind, no slope

Value Name		T+10%	Baseline	T -10%
Deviation to AFMS Reference, BFL		-10.52%	0.41%	16.15%
Deviation to AFMS Reference, V_1		-5.38%	-2.31%	2.31%
Clean + Wet:	**BFL, ft** (rounded)	**5938**	**6663**	**7708**
Clean + Wet:	BFL Baseline Deviation	-10.88%	-	15.68%
Clean + Wet:	**V_1, KIAS** (rounded)	**123**	**127**	**133**
Clean + Wet:	V_1 Baseline Deviation	-3.15%	-	4.72%
Stores + Wet:	**BFL, ft** (rounded)	**7194**	**8159**	**9414**
Stores + Wet:	BFL Baseline Deviation	-11.83%	-	15.38%
Stores + Wet:	**V_1, KIAS** (rounded)	**135**	**140**	**146**
Stores + Wet:	V_1 Baseline Deviation	-3.57%	-	4.29%

The analysis of the thrust variation shows expected behavior. An increase in thrust by 10% shortens the BFL by ca. 965 ft; a decrease by 10% lengthens it by ca. 1225 ft.

The V_1 speed decreases with an increase in thrust, as the aircraft is higher performing and can perform a takeoff with OEI from a lower speed, while the braking performance remains constant. This appears consistent and the representation of this relationship in the results produced by the simulation supports the credibility of the simulation model.

The relatively large deviations in BFL due to thrust variation have been expected before, so they are not surprising. This motivated the correction of the thrust model based on test data in order to yield realistic values.

As a result of the comparison of the deviations to the AFMS reference data, the value chosen for the net thrust in the simulation according to the academic model can be seen as reliable, slightly conservative and of consistent behavior.

9.2.4 Variation of Precipitation Drag Force

The water drag force determination due to store installation has played an important role in the analysis of the Learjet 35A/36A wet runway takeoff performance. A considerable effort has been invested into the calculation of the drag force created through impingement of water particles on the exposed areas of the aircraft, notably the under-wing stores.

Therefore, this force component was validated and compared through a parameter variation. Deactivating the spray impingement drag component for the analysis does not incur any change to the aerodynamic characteristics of the aircraft. It impacts only the spray impingement drag force on the under-wing store.

Table 9.5 Impact on Simulation Results of Variation of Spray Impingement Drag
ISA, MSL, 18500 lbs TOW, Anti-Ice off, Anti-Skid on, no wind, no slope

Value Name	**Store Impingement Drag off**	**Baseline**
Deviation to AFMS Reference, BFL	0.41%	0.41%
Deviation to AFMS Reference, V_1	-2.31%	-2.31%
Clean + Wet: BFL, ft (rounded)	**6663**	**6663**
Clean + Wet: BFL Baseline Deviation	-	-
Clean + Wet: V_1, KIAS (rounded)	**127**	**127**
Clean + Wet: V_1 Baseline Deviation	-	-
Stores + Wet: BFL, ft (rounded)	**8158**	**8159**
Stores + Wet: BFL Baseline Deviation	0.01%	-
Stores + Wet: V_1, KIAS (rounded)	**140**	**140**
Stores + Wet: V_1 Baseline Deviation	0.00%	-

The calculation of percental deviations to the AFMS data does not change, because the aircraft without stores does not change. Consequently, the calculation results for the clean aircraft are equal to the baseline.

For the store impingement drag, no influence on the V_1 can be determined, and the BFL almost neither changes. This has two major reasons – the first, and causal reason is the small magnitude of the spray impingement drag force. The aquaplaning factor and speed dependency further reduce the impact on the excess thrust balance. The resultant drag force is so small that a variation does not produce any significant changes to the overall takeoff performance of the aircraft. The second reason for this variation not being measured is the simulation useful result precision. Due to the drag force being very minor, the estimated 1% precision of the simulation results for the BFL is clearly undershot by the effect the variation creates, considering an average spray impingement drag force of 80 N, compared to 13451 N of thrust force. Therefore, the total impingement drag effect is so small that it is not reasonably measureable in a parameter variation.

The direct conclusion from this result is that the increase in Balanced Field Length on a wet runway due to stores installation can be attributed almost entirely to the increase in aerodynamic drag. This appears only consequent, considering that each store adds 6,8 drag counts to the zero lift drag coefficient of the aircraft. In a dual store configuration, aerodynamic drag is therefore increased by almost 20% in AEO conditions. The precision set forth in the determination of the spray impingement drag in view of these Figures seems disproportionate to the effect that is produced at small water depths.

However, the spray impingement drag force is not the only force that has been considered by applying the **EASA AMC-25.1591** to the wet runway conditions. While the skin friction drag is even smaller than the spray impingement drag due to under-wing stores installation as shown in Tab. 8.19, a large drag force is created by the displacement of the tires. Hence, the variation of the displacement drag D_{disp} with regard to the overall simulation result was also investigated.

Table 9.6 Impact on Simulation Results of Variation of Precipitation Displacement Drag
ISA, MSL, 18500 lbs TOW, Anti-Ice off, Anti-Skid on, no wind, no slope

Value Name		**Baseline**	**D_{disp} +5%**	**D_{disp} -5%**
Deviation to AFMS Reference, BFL		0.41%	1.34%	-0.20%
Deviation to AFMS Reference, V_1		-2.31%	-1.54%	-2.31%
Clean + Wet:	**BFL, ft** (rounded)	**6663**	**6725**	**6623**
Clean + Wet:	BFL Baseline Deviation	-	0.93%	-0.60%
Clean + Wet:	**V_1, KIAS** (rounded)	**127**	**128**	**127**
Clean + Wet:	V_1 Baseline Deviation	-	0.79%	0.00%
Stores + Wet:	**BFL, ft** (rounded)	**8159**	**8223**	**8096**
Stores + Wet:	BFL Baseline Deviation	-	0.78%	-0.77%
Stores + Wet:	**V_1, KIAS** (rounded)	**140**	**141**	**140**
Stores + Wet:	V_1 Baseline Deviation	-	0.71%	0.00%

It can be seen that an increased displacement drag leads to an increased BFL and V_1. The impact of a displacement drag component variation on the overall BFL is in the region of 0,8% for the aircraft with stores. It becomes apparent that the choice of considering the displacement drag on a wet runway was a decision that leads the simulation to producing conservative results.

9.2.5 Variation of the Runway Friction Coefficient

The runway friction coefficient for the rolling and braking aircraft tire is very important for the accurate determination of the takeoff performance. It has been shown in Sect. 4.1.3. that the runway friction coefficient is an important component of the excessive thrust.

Possible deviations of the runway friction coefficients for rolling and braking that would influence the takeoff performance were investigated. Additionally, a (conservative) static rolling coefficient as commonly used in literature has been tested. This static rolling coefficient was also used in the **GJE EXTGFD-003** report.

Table 9.7 Impact on Simulation Results of Variation of Rolling and Braking Coefficients
ISA, MSL, 18500 lbs TOW, Anti-Ice off, Anti-Skid on, no wind, no slope

Value Name		**Baseline**	**$\mu_{friction,wet}$ 0,05**	**$\mu_{friction,wet}$ +10%**	**$\mu_{max,wet}$ +10%**
Deviation to AFMS Reference, BFL		0.41%	5.24%	2.70%	-1.45%
Deviation to AFMS Reference, V_1		-2.31%	-0.77%	-1.54%	-1.54%
Clean + Wet:	**BFL, ft** (rounded)	**6663**	**6984**	**6815**	**6540**
Clean + Wet:	BFL Baseline Deviation	-	4.82%	2.28%	-1.85%
Clean + Wet:	**V_1, KIAS (rounded)**	**127**	**129**	**128**	**128**
Clean + Wet:	V_1 Baseline Deviation	-	1.57%	0.79%	0.79%
Stores + Wet:	**BFL, ft** (rounded)	**8159**	**8523**	**8391**	**7984**
Stores + Wet:	BFL Baseline Deviation	-	4.46%	2.84%	-2.14%
Stores + Wet:	**V_1, KIAS** (rounded)	**140**	**142**	**142**	**141**
Stores + Wet:	V_1 Baseline Deviation	-	1.43%	1.43%	0.71%

The presented values indicate that any of the suggested variations of the runway rolling friction coefficient $\mu_{friction,wet}$ increases the balanced field length, while the decision speed remains at the same level. This is coherent with the assumptions from Section 4.1.3 of an increased rolling friction force increasing the rolling distance in an acceleration motion. Also, no impact on V_1 is seen due to the fact that the rolling friction coefficient impacts the acceleration performance for both the ASD and the TOD.

For the Accelerate-Stop Distance, an increased braking coefficient $\mu_{max,wet}$ leads to non-conservative results for the BFL. The increased match with the AFMS data when using an increased braking coefficient indicates that the braking coefficient determination used for the simulation based on **CS-25.109** is conservative.

9.2.6 Variation of the Wind and Runway Slope

According to **CS-25.105** d), the takeoff data for an aircraft must include corrections for runway gradients. Therefore a parameter variation was performed. The given values are only test cases and do not constitute limitations.

The impact of a runway slope γ or runway gradient variation on the Liftoff Distance has been shown analytically. An uphill slope increases the acceleration distance, while a negative slope lengthens the acceleration distance. Factors that are positive for the Liftoff Distance have an inverted effect on the Accelerate Stop Distance. Because a downhill slope decreases the braking force or negative excessive thrust of the aircraft due to the aircraft weight component, while an uphill sloped runway helps in braking performance, a runway slope clearly has an antagonist effect on the two distances assessed in the Balanced Field Length consideration.

The impact of the wind force V_W has been discussed in Section 4.1.2. A headwind is beneficial for the takeoff performance, as the necessary liftoff ground speed decreases, while a tailwind is having an inverse impact on the takeoff performance. However, the expected performance benefit or penalty is not proportional to the nominal wind speed due to **CS-25.105** implications.

Only 50% of the headwind component of the nominal speed wind may be considered for the estimation of a takeoff performance benefit, while 150% of the tailwind component of the nominal wind speed must be considered for a takeoff performance penalty.

According to this requirement, a nominal (measured) headwind speed $\mathbf{v_{W,Head}}$ of 10 kts reduces to 5 kts for consideration in the simulation, while a tail wind speed $\mathbf{v_{W,Tail}}$ of 2,5 kts increases to 3,75 kts for consideration in the simulation.

The data presented in Tab. 9.8 represents the maximum variations for which reasonable simulation results could be obtained, which was relevant for the tailwind and uphill conditions.

Table 9.8 Impact on Simulation Results of Variation of Wind Speed and Runway Slope,18500lbs
ISA, MSL, 18500 lbs TOW, Anti-Ice off, Anti-Skid on

Value Name		**Baseline**	**$v_{W,Head}$ 10 kts**	**$v_{W,Tail}$ 2,5 kts**	**gradient +0,5%** (uphill)	**gradient -2%** (downhill)
Clean + Wet:	**BFL, ft** (rounded)	**6663**	**6054**	**7125**	**7015**	**5642**
Clean+ Wet:	BFL Baseline Deviation	-	-9.14%	6.93%	5.28%	-15.32%
Clean + Wet:	V_1, KIAS (rounded)	**127**	**122**	**131**	**131**	**115**
Clean+ Wet:	V_1 Baseline Deviation	-	-3.94%	3.15%	3.15%	-9.45%
Stores + Wet:	**BFL, ft** (rounded)	**8159**	**7469**	**8754**	**8698**	**6810**
Stores + Wet:	BFL Baseline Deviation	-	-8.46%	7.29%	6.61%	-16.53%
Stores + Wet:	**V_1, KIAS** (rounded)	**140**	**135**	**145**	**144**	**126**
Stores + Wet:	V_1 Baseline Deviation	-	-3.57%	3.57%	2.86%	-10.00%

As expected, the BFL for the headwind case was reduced for both the aircraft with stores and the clean aircraft. A reduction in V_1 indicates that the aircraft is supported in its takeoff performance through the wind component and can sustain a takeoff from a lower engine failure speed.

The inverse is true for the tailwind component consideration. As 150% of the wind component have to be considered as a penalty, the performance degradation due to tail wind are very large, and the BFL is increased by 7,28% even at a nominal tailwind component of only 2,5 kts. As the tailwind component impacts takeoff performance negatively, while the braking performance remains quasi constant, the increase in V_1 is consistent.

For the runway slope considerations, the expectations following the analysis of the impact of a sloped runway from Sect. 4.1.3 have been met. The antagonist influence on the BFL appears to be smaller with regard to the Accelerate-Stop Distance than on the Takeoff Distance, as the BFL increases by 6,61% at an uphill gradient of 0,5%, while it decreases by 16,5% at a downhill gradient of 2%.

As the Accelerate-Stop Distance contains an acceleration segment that is influenced in the same way as the Takeoff Distance by a sloping runway, the ASD is in part also adversely influenced by an uphill slope, which explains the above relations.

As the variation of wind and slope proved to be rather restrictive for the 18500 lbs TOW test case, a variation for a 16000 lbs TOW was also performed, as shown in Tab. 9.9. The given data do not represent limitations, but a common scenario at the GFD operations homebase on the airfield Hohn. Coherent results to the data from Tab. 9.8 were obtained.

Table 9.9 Impact on Simulation Results of Variation of Wind Speed and Runway Slope,16000lbs
ISA, MSL, 16000 lbs TOW, Anti-Ice off, Anti-Skid on

Value Name		**Baseline**	**$v_{W,Head}$ 10 kts**	**$v_{W,Tail}$ 10 kts**	**gradient +0,5%** (uphill)	**gradient -0,5%** (downhill)
Clean + Wet:	**BFL, ft** (rounded)	**4823**	**4479**	**6377**	**5032**	**4681**
Clean+ Wet:	BFL Baseline Deviation	-	-7.13%	32.22%	4.33%	-2.94%
Clean + Wet:	V_1, KIAS (rounded)	**113**	**109**	**129**	**116**	**111**
Clean+ Wet:	V_1 Baseline Deviation	-	-3.54%	14.16%	2.65%	-1.77%
Stores + Wet:	**BFL, ft** (rounded)	**5930**	**5336**	**7657**	**6172**	**5644**
Stores + Wet:	BFL Baseline Deviation	-	-10.02%	29.12%	4.08%	-4.82%
Stores + Wet:	**V_1, KIAS** (rounded)	**125**	**119**	**141**	**128**	**122**
Stores + Wet:	V_1 Baseline Deviation	-	-4.80%	12.80%	2.40%	-2.40%

9.2.7 Variation of Reaction and Transition Times

As the reaction times have been discussed intensively in this report, two significant variations were investigated.

The first variation evaluates the impact on the simulation results if the distance equivalent to 2 seconds at V_1 according to **CS-25.109** had not been considered. The second test case shows the impact of one second additional lapse in reaction time. This is an interesting investigation, as the pilot reaction times depend on many factors, and a delayed reaction by just one second may have a large impact on the overall BFL.

Table 9.10 Impact on Simulation Results of Variation of Reaction and Transition Time
ISA, MSL, 18500 lbs TOW, Anti-Ice off, Anti-Skid on, no wind, no slope

Value Name	**Baseline**	**React. Time +1 second**	**No 2 second margin at V_1 considered**
Deviation to AFMS Reference, BFL	0.41%	3.10%	-3.27%
Deviation to AFMS Reference, V_1	-2.31%	-2.31%	-0.77%
Clean + Wet: BFL, ft (rounded)	**6663**	**6842**	**6419**
Clean+ Wet: BFL Baseline Deviation	-	2.69%	-3.66%
Clean + Wet: V_1, KIAS (rounded)	**127**	**127**	**129**
Clean+ Wet: V_1 Baseline Deviation	-	0.00%	1.57%
Stores + Wet: BFL, ft (rounded)	**8159**	**8353**	**7831**
Stores + Wet: BFL Baseline Deviation	-	2.38%	-4.02%
Stores + Wet: V_1, KIAS (rounded)	**140**	**140**	**141**
Stores + Wet: V_1 Baseline Deviation	-	0.00%	0.71%

It can be concluded that the reaction time of the pilot at V_1 has a larger impact on the BFL than most of the parameter variations performed beforehand. The aircraft during the delayed reaction does not remain at constant speed, but accelerates further with one engine remaining at full thrust. This results in the BFL increment of 2,38% or 194 ft in case the pilot reacts one second late.

Due to the **CS-25.109** requirement to consider a distance equivalent to *two seconds at V_1 speed* to be added to the ASD, the overall BFL becomes smaller by 4,02% when this increment is not considered.

10 Conclusions

10.1 Conclusion on Modeling Precision

The calculations performed by the simulation appear to be consistent with the expectations an analytical assessment of the equations of motion has produced. Trust in the simulation approach and plausibility could be gained due to the behavior of the simulation as predicted.

A synthesis of model input parameter variation impact on the overall simulation result is given in Table 10.1. The parameters that have been varied to validate the overall Lift, Drag, Thrust and Friction Model, are shown with their degree of variation. The impact of the indicated deviation on the BFL and V_1 is shown in columns 3 and 4. The qualitative impact assessment performed in column 5 is based on the deviation the parameter variation creates with respect to the original simulation result.

Table 10.1 Synthesis of Input Parameter Variation Impact on Simulation Results based on a test case; *185000 lbs TOW, ISA, SL, Stores+Wet*

Parameter	Variation	Deviation Impact on BFL,Store	Deviation Impact on V_1,Store	Relative Impact of Parameter
$C_{L,TO}$	+10%	0,29 %	0 %	Small
$C_{L,TO}$	-10%	0,38 %	0,71 %	Small
$C_{D,TO}$	**+10%**	**4,65 %**	**2,86 %**	**Large**
$C_{D,TO}$	**-10%**	**-2,90 %**	**-1,43 %**	**Large**
$\Delta C_{D,OEI}$	**+20%**	1,91 %	1,43 %	Medium
$\Delta C_{D,OEI}$	**-20%**	-1,26 %	-0,71 %	Medium
T	+10%	**-11,83 %**	**-3,57 %**	**Large**
T	-10%	**15,38 %**	**4,29 %**	**Large**
Store Impingement Drag	**off**	0,01 %	0 %	Small
D_{disp}	+5%	0,78 %	0,71 %	Small
D_{disp}	-5%	-0,77 %	0 %	Small
$\mu_{friction,wet}$	0,05 static	**4,46 %**	**1,43 %**	**Large**
$\mu_{friction,wet}$	+10%	**2,84 %**	**4,43 %**	**Large**
$\mu_{max,wet}$	+10%	**-2,14 %**	**0,71 %**	**Large**
React. Time	+1 second	**2,38 %**	**0 %**	**Large**
No 2 second margin at V_1 considered	-	**-4,02 %**	**0,71 %**	**Large**

From this analysis, it becomes obvious that deviations in the Drag, Thrust and the ground roll friction model have the highest impact on the simulation results. Furthermore, in comparison with the impact of a 1 second lapse in pilot reaction, most other variation impacts appear comparatively small. The Thrust, Drag, Friction and Reaction time models should therefore have the highest amount of precision, as a deviation in these models would influence the final simulation result most. Other models used in the simulation, such as the lift model, have only a relatively marginal impact on the overall simulation results.

10.2 Correlation of Expected and Actual Results

It has been shown in Section 9.2 that the behavior of the simulation with variation of essential parameters reflects closely the expectations which were developed from analysis of the equation of motion. The individual models and input parameters that were used for the simulation were verified with other sources and checked for individual plausibility. This establishes trust in the plausibility of the results obtained by the simulation for a range of varying input parameters.

A comparison of the simulation results with the AFMS values needs to be done with caution, as a simplified method has been used for the calculation of the AFMS values. In the case of the **GJE EXTGFD-003**, it was shown that assumptions taken were in some cases simplified or not conservative enough.

As this data however is the only source that could be used to validate the simulation results, the simulation results for the BFL and V_1 have been compared to existing data. This comparison revealed that the simulation results are generally conservative, and a very small deviation to the AFMS values is obtained for the BFL results of the simulation depending on the TOW and OAT considered. V_1 results obtained by the simulation are generally smaller than the reference data.

A simplified calculation method has been used to evaluate simulation results for BFL and forces acting on the aircraft. It was a comparable approach to the one used in **GJE EXTGFD-003**. This simplified calculation has shown that the simulation creates reasonable results and is conservative.

A comparison of the steadiness of the graphs of the AFMS values and the simulation results showed that the simulation creates graphs with a higher variability in slope. The overall run and inclination of theses graphs however is comparable. The variation of the simulation results with varying air density has been explained and been determined to result primarily from the thrust flat rate model.

10.3 Calculation Approach Validation

A calculation method for a Balanced Field Length and its associated decision speed V_1 was developed for the takeoff performance determination of a Learjet 35A/36A, impacted especially through the wet runway conditions and the presence of under-wing stores.

The modeling approach differs to other standard calculation methods for Balanced Field Lengths that are based on a simplification of speed dependent variables for the integration process. The approach that was chosen in this report to model the aircraft performance is providing the remarkable benefit that any parameter of the aircraft can be considered precisely in its speed and time dependency. Hence, given that the precision of the models used in this integration process is high enough, the approach chosen for the simulation presented in this report is capable of producing performance results of a very high accuracy.

Furthermore, the numerical simulation provides another very remarkable benefit. Due to the creation of Balanced Field Lengths graphs, as shown in Appendix H, it is now possible for the operator to consider stop- and clearways as a performance benefit. This is not possible with the data currently available to the operator. By going off-balance to either side of the ASD/TOD intersection, a higher ASDA or TODA due to stop- or clearway may be considered. In conclusion, the operation at higher Takeoff Weights from previously limited conditions is possible. This extension of the takeoff operation envelope comes in addition to the performance data creation for the Stores+Wet conditions.

All models used by the simulation have been validated by a cross-check with existing data from reference documents, and by cross checking the internal models and deviations on the overall simulation result.

By all the means employed for checking the plausibility and reliability of the simulation, no significant contradictions have been found, even though the simulation approach varies significantly from the calculation approach used in other sources for BFL and V_1 data, such as the **GJE EXTGFD-003** report. This shows that the approach for the calculation of pairs of BFL and V_1 that was chosen in this report is producing valid results.

An additional conservatism of the simulation is owed to the fact that the equations from **AMC 25.1591** normally applicable for contaminated runways have been applied to the wet runway conditions by request of the operator. As the data derived by the simulation shall be used in actual flight operations, such conservatism must be seen as a beneficial safety factor.

A final method of testing and validating the simulation results would be the conduct of flight tests and subsequent parameter capturing. By measuring the horizontal acceleration experienced by the aircraft, this test data could be used to validate the acceleration considered time-step-wise by the simulation.

11 Recommendations

11.1 Instrumental Decisions for Increased Simulation Precision

As has been shown in Section 10.1, not all model data that were developed for the simulation required the level of detail that was applied in their determination. The most striking example is the estimation of the impingement drag, which was determined in a highly detailed way, but the final impact on the overall Balanced Field Length calculation was small.

Other model data was only discovered during the development process to be of high importance. An example is the rolling friction coefficient. The analysis of parameter variation showed clearly in which way the use of a detailed rolling friction model with regard to aircraft speed was beneficial to increase the precision of the simulation.

The calculation of a calibration factor from the simulation results to match the AFMS values for known results (Wet+Clean) was initially thought to compensate any inaccuracies in the models used. Application of the calibration to the Stores+Wet conditions however showed that not always conservative results were obtained by the simulation. The investigation showed also that the basis for the calibration, the AFMS reference data, based on simplified assumptions and may not be seen to be of significantly higher precision than the detailed numerical integration based calculation applied by the simulation.

Consequently, the intent of eliminating any model inaccuracies through the application of a calibration factor must be cautiously regarded, due to the limited precision of the reference data. However, the concept of the calibration factor determination was very beneficial during the development of the simulation. Especially the application of two individual correction factors allowed tracking the quality of the models used by the simulation for the TOD and ASD determination individually. This was a very efficient means to identify needs where to augment model precision in order to match the AFMS reference values more precisely, and is the only reason why the simulation is now presented with such a high number of detailed model data.

As a consequence of the final simulation to contain so many detailed sub-models with various interdependent parameters, the simulation creates very accurate results even without the application of a general correction factor.

11.2 Adaption for use in other Applications

The simulation approach can be applied to assess the takeoff performance of any other aircraft, given that the Learjet specific input parameters are changed. By comparing the takeoff performance data of another aircraft to the simulation results with adapted input parameters, this could be used as another means to validate the calculation approach chosen in the simulation.

The following parameters applying to the Learjet 35A/36A need to be adapted to match the data of another airplane:

- Airplane Geometry
- Airplane Takeoff Configuration
- Aerodynamic Speeds and Speed Corrections
- Lift Coefficient (Profile, Wing, Overall Airplane, and Lift Coefficient Increments)
- Drag Coefficient (AEO and OEI conditions)
- Engine Data and Flat Rating Behavior
- Maximum Brake Energy Data
- Tire and Wheel Data
- Operator-specific Reaction Times
- Water Spray Geometry

If more precise data is available for the new airplane, an optimization of the important model data used by the simulation should be attempted. The important model data that have a high impact on the overall simulation results are the Thrust Model, the Drag Model and the Friction Force Model.

Additional model data that could be developed for a further gain in precision could concern the motion around more axes. An investigation of the motion around the pitch axis with regard to the center of gravity may yield higher precision in the individual wheel loads with changing acceleration. An analysis of the moment around the yaw axis should provide further details on the OEI conditions, especially due to asymmetric flight. In addition to the consideration of the longitudinal motion of the aircraft along the runway, sideway forces due to OEI conditions and cross wind may lead to stability and control questions that can be solved by the investigation of the moments around the bank and the yaw axis. Lastly, the acceleration of the aircraft to V_2 after liftoff should be considered, especially if dry runway conditions are to be evaluated.

11.3 Variation of Takeoff Performance with Pilot Technique

The results for BFL and V_1 that have been obtained through analytical methods are veritable data for the planning of the aircraft takeoff performance. However, it should not be forgotten that human factors also have a great influence on the takeoff performance. The influence of a time delay of only 1 second in recognition to an engine failure has already been discussed.

Also the pilot technique, especially during the rotation phase, has a very large impact on the overall Takeoff Distance. When the pilot over-rotates during liftoff, the aircraft might reach the maximum lift coefficient, which in turn increases the aerodynamic drag beyond the optimum, so that the Takeoff Performance is impacted.

The rationale of providing V_1 speeds with a precision of 1 knot is clearly a result of the analytical method used. In theory though, with vibration in the cockpit and on an analog air speed indicator with a small resolution such as the one installed in the Learjet 35A/36A, it must be clear that the speed cannot always be read out at a 1 knot resolution. If during acceleration, the V_1 speed was erroneously missed by only 1 knot due to readout error by the pilot, the Takeoff Distance may rise by approx. 200 ft.

Herrington 1966 states the following:

> *"Even with highly trained pilots, it is difficult to make the aircraft take off at the same value of lift coefficient each time. As this is the rule rather than the exception, a rigorous mathematical treatment of reducing observed take-off data to standard conditions is not warranted; therefore, no mathematically exact solutions will be given for reducing data."*

The mentioned data reduction refers to the Flight Test Engineering task of validating the analytical takeoff performance calculations through flight test data.

This final statement shall not challenge the analytical precision that was used to determine the takeoff performance of the Learjet presented by this report. It shall demonstrate that with all mathematical precision that can be applied, the human factor side in the takeoff performance estimation must not be forgotten, because it plays a crucially important role in the concrete takeoff performance behavior of the aircraft.

List of References

AFM Learjet 35A/36A — GATES LEARJET CORPORATION: *Gates Learjet35A/36A withFC-200 Autopilot, FAA Approved Airplane Flight Manual.* Wichita, Kansas : 1981

AFMS 9702-2 — AVCON INDUSTRIES, INC.: *FAA Approved Airplane Flight Manual Supplement. AFMS 9702-2.* Newton, Kansas: 1997

Airbus 1998 — AIRBUS OPERATIONS SAS: *Getting to Grips with ETOPS.* Blagnac : 1998. – Customer Services

Airbus 2002 — AIRBUS OPERATIONS SAS: *Getting to Grips with Aircraft Performance.* Blagnac : 2002. – Customer Services

Anderson 2007 — ANDERSON, John D.: *Fundamentals of Aerodynamics.* New York : McGraw Hill, 2007

Barrett 1970 — BARRETT, R.V.: *Research into Slush Drag, Wheel Spray and Aquaplaning at Bristol University using Small Pneumatic Tyres.* London : Her Majesty's Stationery Office, 1970 – Ministry of Defence, R & M No. 3682

Bartel & Young 2007 — BARTEL, Matthias; YOUNG, Trevor.: *Simplified Thrust and Fuel Consumption Models for Modern Two-Shaft Turbofan Engines.* AIAA ATIO Conference, and CEIAT International Conference on Innovation and Integration in Aerospace Sciences No7, Belfast : AIAA 2007

Bräunling 2004 — BRÄUNLING, Willy J.G.: *Flugzeugtriebwerke: Grundlagen, Aero-Thermodynamik, Kreisprozesse, Thermische Turbomaschinen, Komponenten- und Emissionen.* Berlin-Heidelberg : Springer-Verlag, 2004

Brüning, Hafer, Sachs 1993 — BRÜNING, G.; HAFER, X., SACHS, G.: *Flugleistungen.* Berlin-Heidelberg : Springer-Verlag, 1993

CS-25 — EUROPEAN AVIATION SAFETY AGENCY: *Certification Specifications and Acceptable Means of Compliance for Large Aeroplanes CS-25.* Köln : EASA, 2012. – Amendment 12

DATCOM 1965 HOAK, D.E.; ELLISON, D.E.: *USAF Stability and Control Datcom.* Wright-Patterson Air Force Base, Ohio : Flight Control Division, Air Force Flight Dynamics Laboratory, 1965

DATCOM 1978 HOAK, D.E.; ELLISON, D.E.: *USAF Stability and Control Datcom.* Wright-Patterson Air Force Base, Ohio : Flight Control Division, Air Force Flight Dynamics Laboratory, 1978

ESDU 83042 ENGINEERING SCIENCE DATA UNIT: *Estimation of spray patterns generated from the sides of aircraft tyres running in water or slush. Item No. 83042.*London : ESDU, 1983

EU-OPS 1 EUROPEAN AVIATION SAFETY AGENCY: *Commercial Air Transportation. Commission Regulation EC No 859/2008.* Köln : EASA, 2008

EUROCONTROL 2009 EUROCONTROL: *Base of Aircraft Data (BADA) Aircraft Performance Modeling Report, EEC Technical/Scientific Report No. 2009-009.* Brussels : EUROCONTROL, 2009

FAA AC 25-7B FEDERAL AVIATION ADMINISTRATION: *Flight Test Guide for Certification of Transport Category Airplanes.* Washington, D.C. : FAA, 2011

Flightglobal FLIGHTGLOBAL: *Learjet 35A/36A Cutaway,* URL:http://www.flightglobal.com/airspace/media/businessaircraftcutaways/gates-learjet-35-36-cutaway-5694.aspx (09.08.2012)

Goodyear 2002 GOODYEAR, GLOBAL AVIATION TIRES: *Aircraft Tire Data Book.* Akron, Ohio : Goodyear, 2002

GJE EXTGFD-003 G.J. ENTERPRIZES. INC.: *Performance Substantiation Learjet 35A/36A with AVCON Delta Fins, External Tip Tanks, Increased TOW and Underwing Stores.* Prepared by C. Gene Voorhees. FAA-Project No. ST 1413WI-T, G.J. Enterprizes, 1997

Herrington 1966 HERRINGTON, Russell M.: *Flight Test Engineering Handbook.* Edwards Air Force Base : AFFTC, 1966. – AF Technical Report 6273

Hoerner 1965 HOERNER, Sighard F.: *Fluid-Dynamic Drag.* Bakersfield : Hoerner Fluid Dynamics, 1965

Janes 1999 JACKSON, Paul (Editor): *Jane's All the Worlds Aircraft Edition 1999-2000.* Couldson : Janes Information Group, 1999

Learjet 30 Series Pilot Training Manual FLIGHT SAFETY INTERNATIONAL, INC.: *Learjet 30 Series Pilot Training Manual.* Flushing, New York : Flight Safety, 1986

Loftin 1980 LOFTIN, Laurence K.: *Subsonic aircraft: Evolution and the matching of size to performance.* Hampton, VA : NASA Langley Research Center, 1980

LTH AT21000.06 BIEHL, H.: *Rechnerische Ermittlung der installierten Leistungen von Turbostrahltriebwerken.* MBB-UFE (Messerschmitt-Bolkow-Blohm), 1989. –AT 21 000-05. – Distribution: LTH

LTH BM 21 600-01 GRIESER, SCHOERNACK: *Luftkräfte auf Bremsklappen, Spoiler und Spreizklappen.* Dornier GmbH/IABG, 1976. - Reference Number BM 21 600-01. – Distribution: LTH

NACA Report 903 LOFTIN, Laurence K.: *Theoretical and Experimental Data for a number of NACA 6A-Series Airfoil Sections.* Langley Field : National Advisory Committee for Aeronautics (NACA), 1948

NASA TM-X-72650 HORNE, Walter B.: *Technical Memorandum: Wet Runways.* Hampton, VA : NASA Langley Research Center, 1975

NASA TN D-6573 SODERMAN, Paul T.; AIKEN, Thomas N.: *Full-Scale Wind-Tunnel Tests of a Small Unpowered Jet Aircraft with a T-Tail.* Washington, D.C. : NASA, 1971

NASA TP2718 DAUGHERTY, Robert H.; STUBBS, Sandy M.: *Measurements of Flow Rate and Trajectory of Aircraft Tire-Generated Water Spray.* Hampton, VA : NASA Langley Research Center, 1987

NASA-TN-D-2056 HORNE, Walter B.; DREHER, Robert C.: *Phenomena of Pneumatic Tire Hydroplaning.* Hampton, VA : NASA Langley Research Center, 1963

Nita, Scholz 2012 NIȚĂ, Mihaela; SCHOLZ, Dieter: *Estimating the Oswald Factor from Basic Aircraft Geometrical Parameters.* From: DGLR: Deutscher Luft- und Raumfahrtkongress 2012 : Tagungsband - Manuskripte (DLRK, Hamburg, 10. - 12. September 2012). - Download: http://OPerA.ProfScholz.de

NLR-TP-2001-204 GOODEN, J.H.M.: *CRspray - Impingement drag calculation of aircraft on water-contaminated runways.* Amsterdam : National Aerospace Laboratory of the Netherlands, 2001

NLR-TP-2001-216 VAN ES, G.W.H.; ROELEN, A.L.C.; KRUIJSEN, E.A.C.: *Safety aspects of aircraft performance on wet and contaminated runways.* Amsterdam : National Aerospace Laboratory of the Netherlands, 2001

NLR-TP-2001-490 GIESBERTS, M.K.H.: *Test and evaluation of precipitation drag on an aircraft caused by snow and standing water on a runway.* Amsterdam : National Aerospace Laboratory of the Netherlands, 2001

Raymer 1989 RAYMER, Daniel P.: *Aircraft Design: A Conceptual Approach.* Washington, D.C. : AIAA, 1989

Roskam I ROSKAM, Jan: *Airplane Design I: Preliminary Sizing of Airplanes.* Lawrence, KS : DARcorporation, 1985

Roskam III ROSKAM, Jan: *Airplane Design III: Layout Design of Cockpit, Fuselage, Wing and Empennage: Cutaways and Inboard Profiles.* Lawrence, KS : DARcorporation, 1986

Roskam VI ROSKAM, Jan: *Airplane Design VI: Preliminary Calculation of Aerodynamic, Thrust and Power Characteristics.* Lawrence, KS : DARcorporation, 1987

Roskam VII ROSKAM, Jan: *Airplane Design VII: Determination of Stability, Control and Performance Characteristics: FAR and Military Requirements.* Lawrence, KS : DARcorporation, 1986

Roskam, Lan 1997 ROSKAM, Jan; LAN, C.T.E.: *Airplane Aerodynamics and Performance.* Lawrence, KS : DARcorporation, 1997

Scholz 1997 SCHOLZ, Dieter: *Entwicklung eines CAE- Werkzeuges zum Entwurf von Flugsteuerungs- und Hydrauliksystemen*. Fortschritt-Berichte VDI, Reihe 20, Nr. 262, Düsseldorf : VDI, 1997

Scholz 1999 SCHOLZ, Dieter: *Skript zur Vorlesung Flugzeugentwurf.* Hamburg, Universität für Angewandte Wissenschaften Hamburg, Fachbereich Fahrzeugtechnik und Flugzeugbau, Vorlesungsskript, 1999

Torenbeek 1982 TORENBEEK, Egbert: *Synthesis of Subsonic Airplane Design.* London : Kluwer Academic Publishers, 1982

Yechout 2003 YECHOUT, Thomas R.: *Introduction to Aircraft Flight Mechanics: Performance, Static Stability, Dynamic Stability and Classical Feedback Control.* Reston, VA : AIAA, 2003

Young 2001 YOUNG, Trevor: *Flight Mechanics.* Limerick, University of Limerick, Department of Mechanical and Aeronautical Engineering, Lecture Notes, 2001

Appendix A
Maximum Brake Energy Chart

The data was presented in **GJE EXTGFD-003** at present quality.

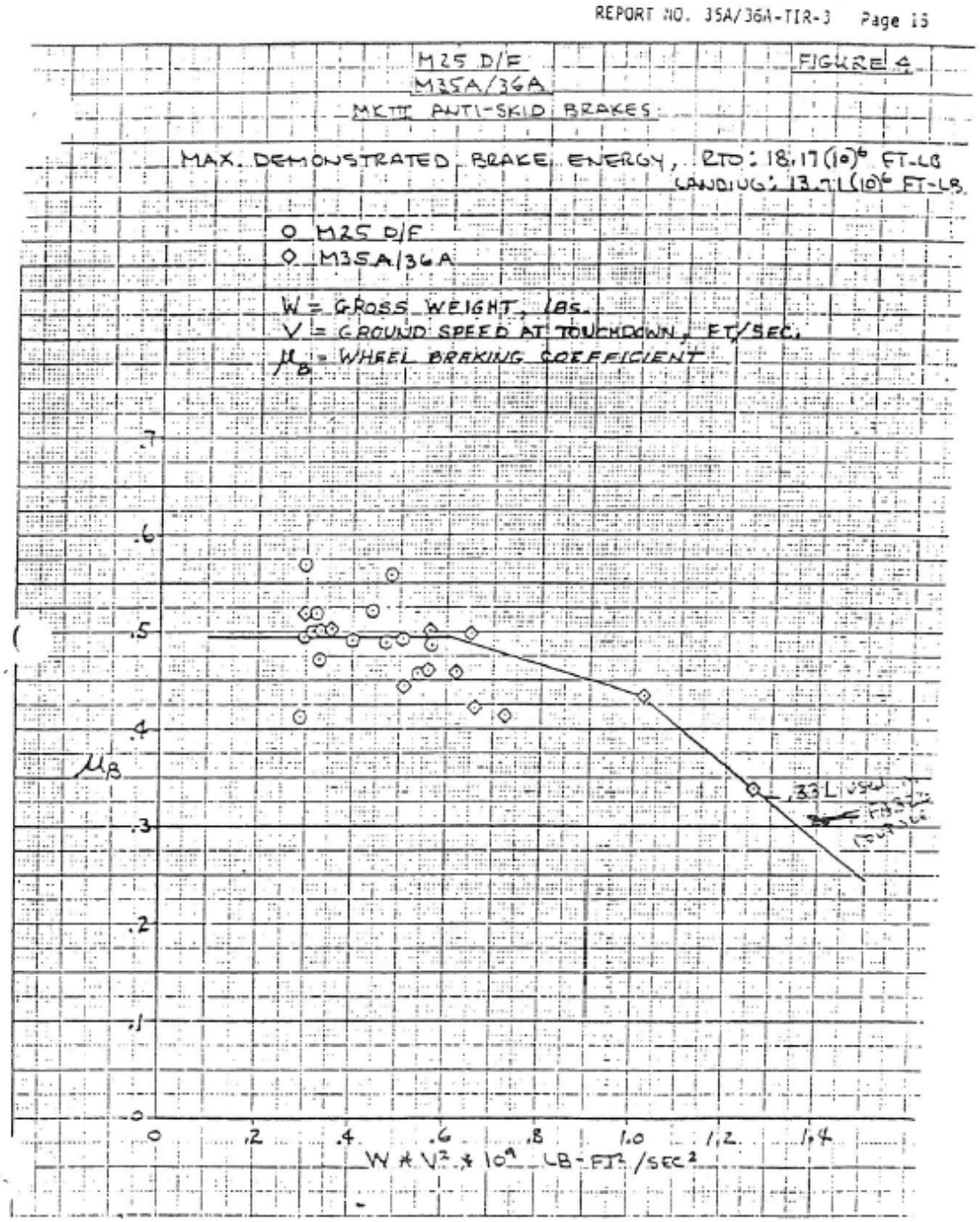

Fig. A.1 Maximum Brake Energy Chart (**GJE EXTGFD-003**)

Appendix B
Engine Thrust Validation

The test data obtained from **GJE EXTGFD-003** is presented in comparison with the corrected and uncorrected thrust from the academic approach as presented in Sect. 6.4.

Validation for MSL, ISA

No corrections of the academic thrust model were necessary for MSL, ISA. The installed net thrust of 3400 lbs is matched by the extrapolation of the test data as well as the academic approach.

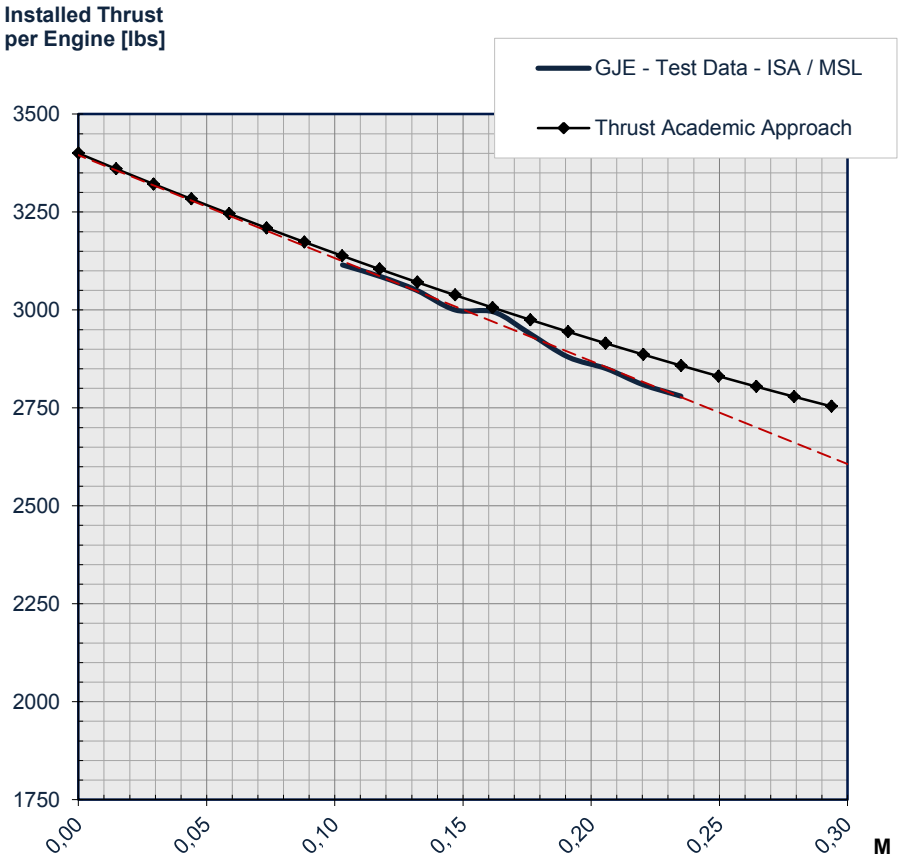

Fig. B.1 Validation of GJE Test Data with Academic Thrust Model for MSL, ISA

Validation for MSL, ISA+20

Corrections applied: $G = 0{,}7$ $f_{corr,A} = 1{,}0$

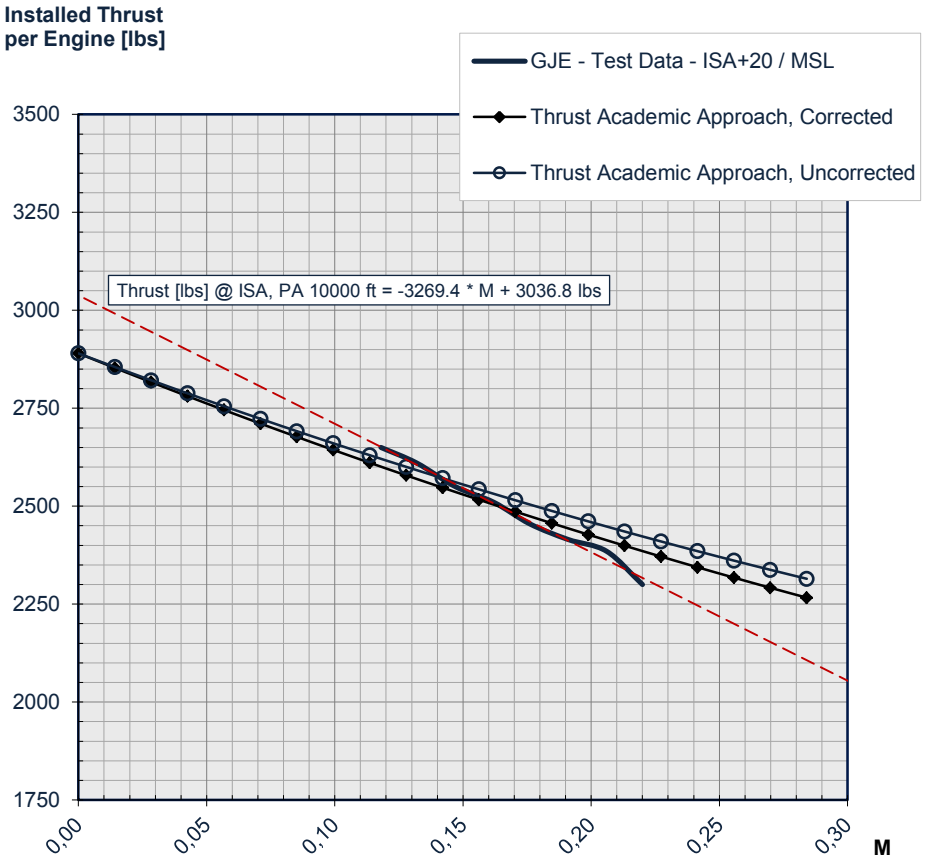

Fig. B.2 Validation of GJE Test Data with Academic Thrust Model for MSL, ISA+20

The corrected thrust decay slope matches the test data slope indicated by the red extrapolation.

Validation for 5000 ft PA, ISA

Corrections applied: $G = 0{,}9$ $f_{corr,A} = 1{,}04$

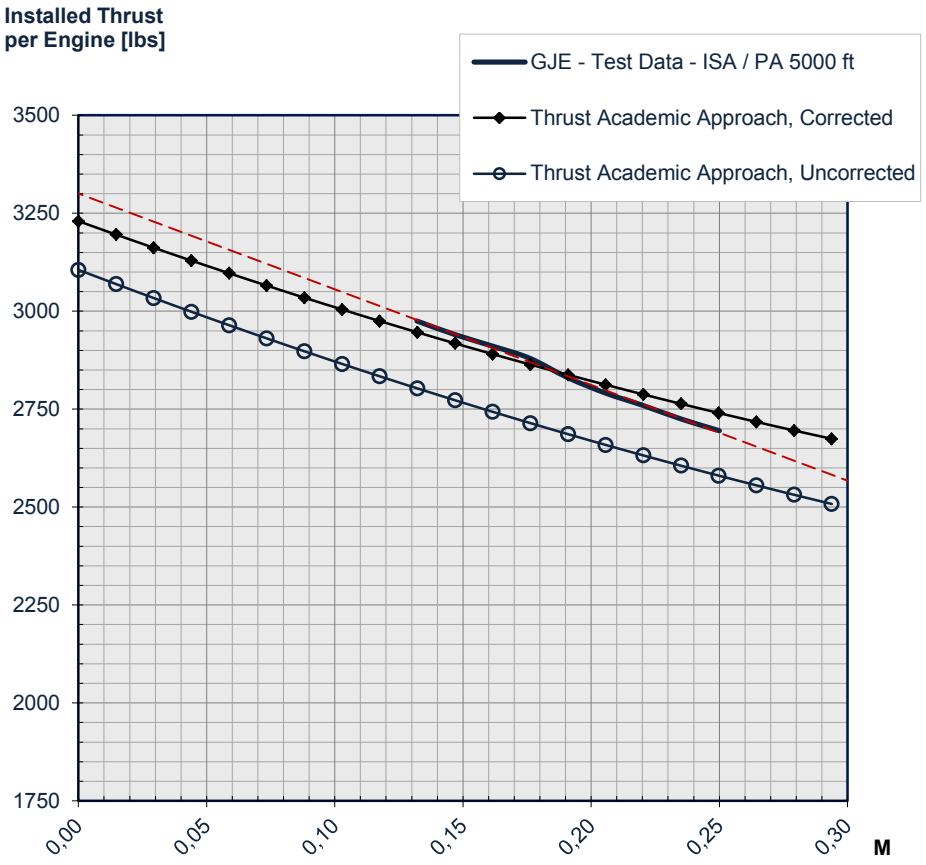

Fig. B.3 Validation of GJE Test Data with Academic Thrust Model for 5000 ft PA, ISA

Validation for 5000 ft PA, ISA+20K

Corrections applied: $G = 0{,}7$ $f_{corr,A} = 1{,}04$

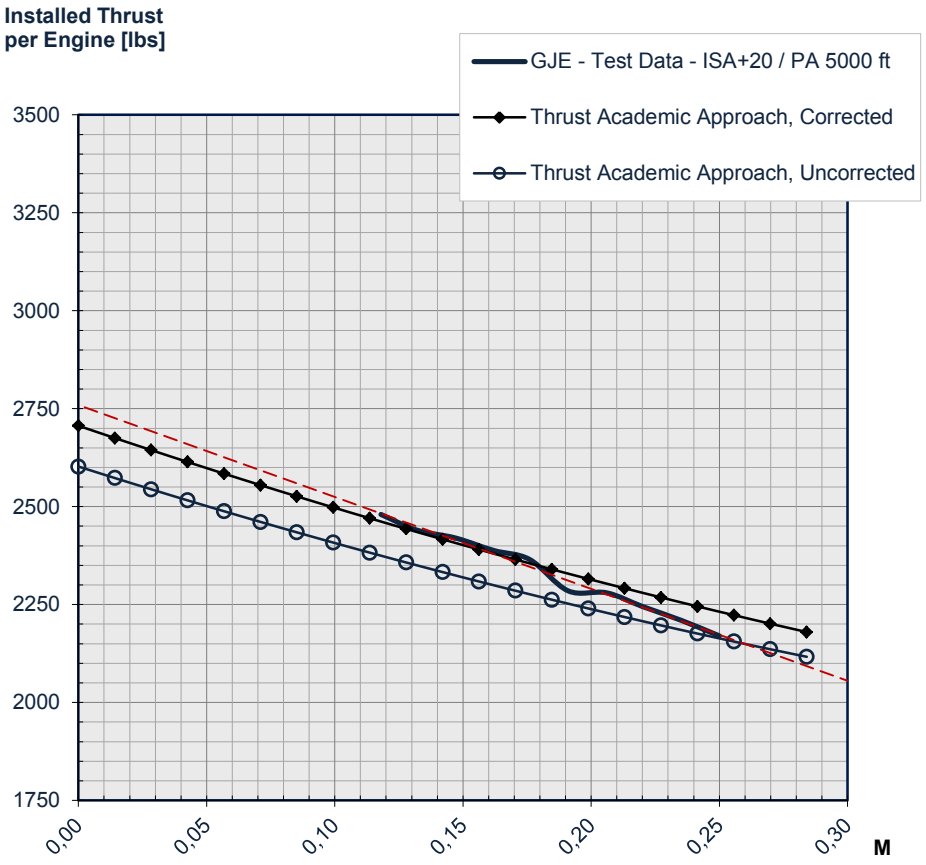

Fig. B.4 Validation of GJE Test Data with Academic Thrust Model for 5000 ft PA, ISA+20

Validation for 10000 ft PA, ISA

Corrections applied: $G = 0{,}9$ $f_{corr,A} = 1{,}08$

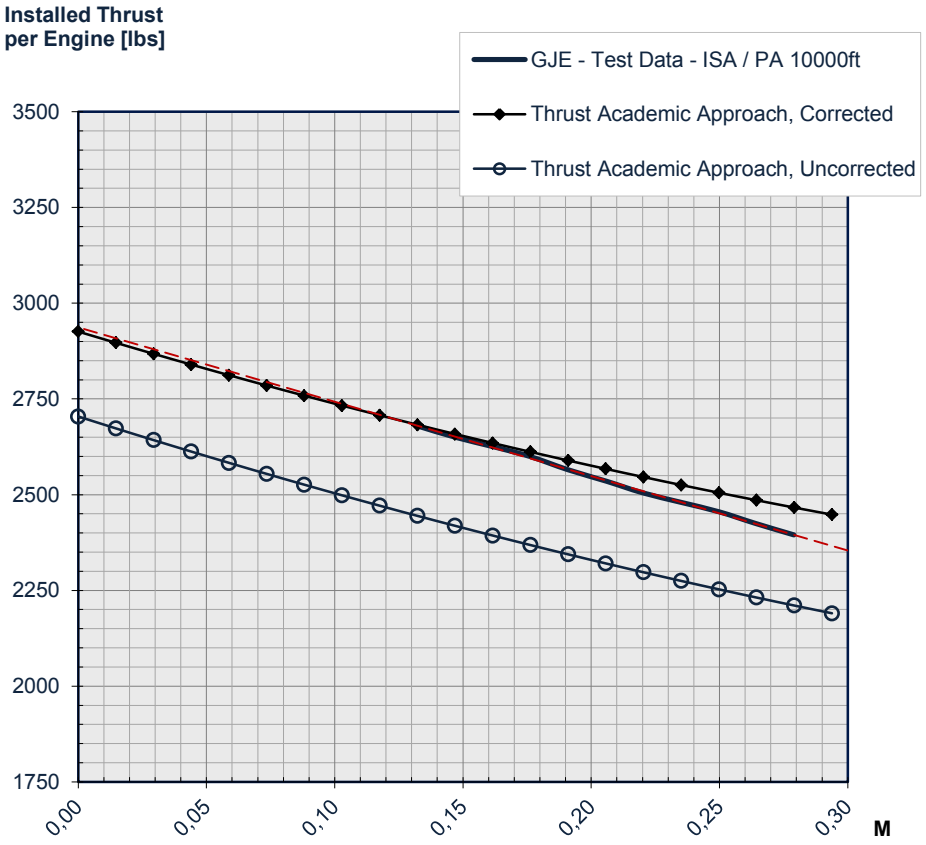

Fig. B.5 Validation of GJE Test Data with Academic Thrust Model for 10000 ft PA, ISA

Estimation of $f_{corr,A}$ for the correction of 'A' in Academic Thrust Model

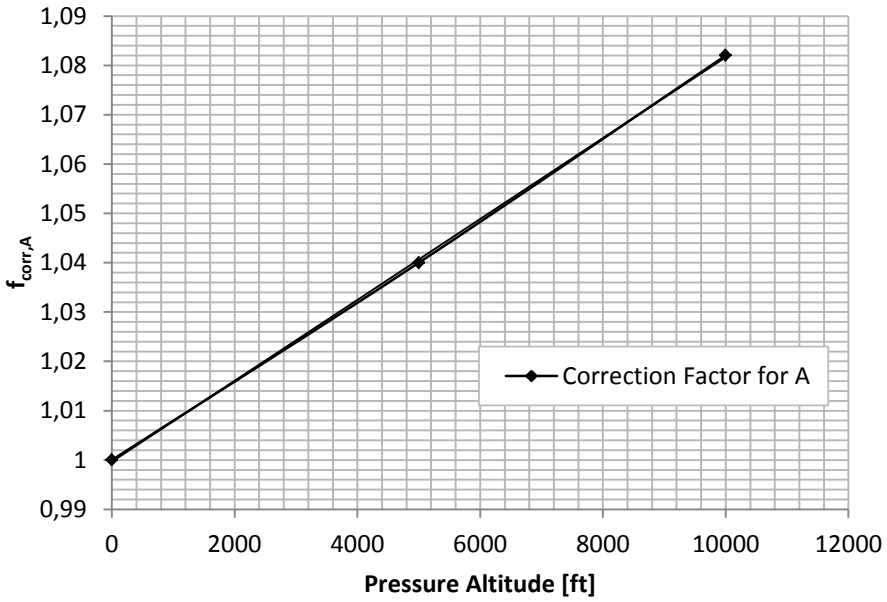

Fig. B.6 Estimation of a Correction Factor for 'A' in the Academic Thrust Model

As can be seen in Fig. B.6, the correction factor necessary to scale the thrust obtained in the academic approach to the test data by a correction factor to the 'A' term is a function of the pressure altitude.

The three data points available from the test data indicate a linear relationship. Hence, Eq. 6.2 is the approximation of a linear function through all three data points shown in Fig. B.6.

Appendix C
Nassi-Shneiderman Diagram of the Simulation

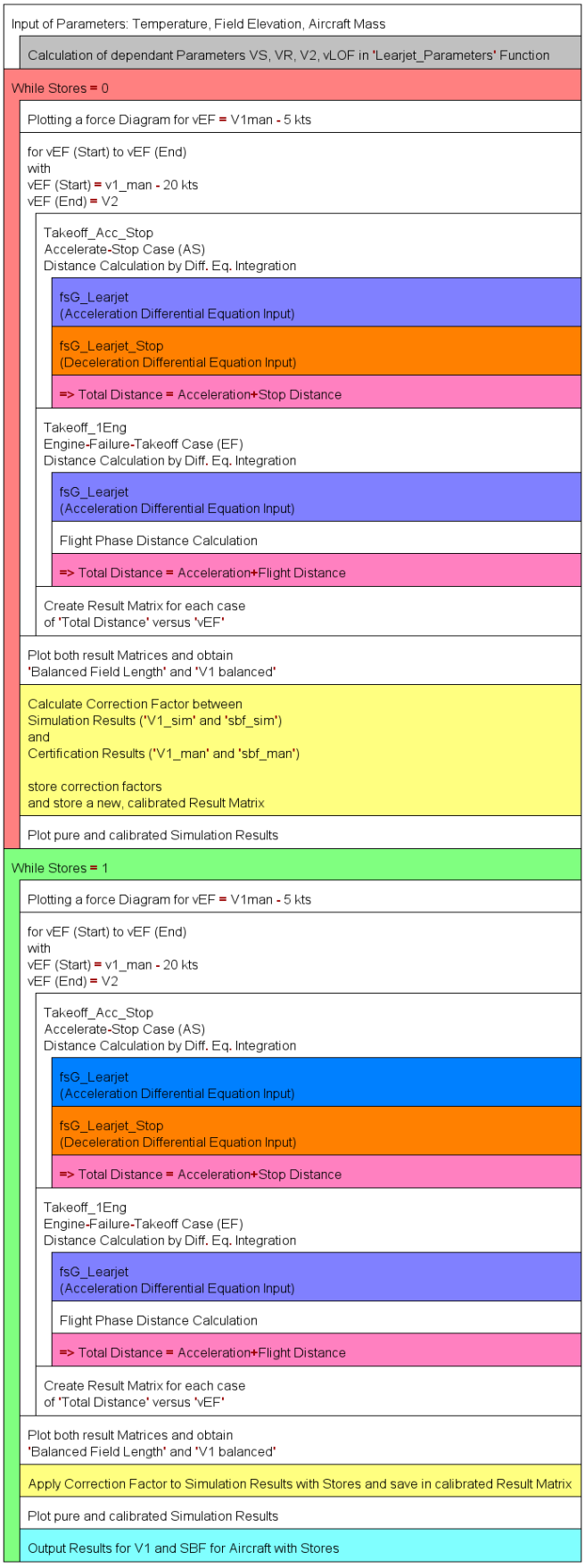

Compare Color coding to Fig. 7.3

Red – Clean Aircraft Calculation
Green – Stores Aircraft Calculation
Yellow – Calibration Appliance
Ocean – Final Result Determination

Compare Color coding to Fig. 7.4

Dark Blue – Acceleration Diff. Eq.
Orange – Deceleration Diff. Eq.
Pink – Total Distance Calculation

Fig. C.1
Nassi-Shneiderman Diagram of the Simulation

Appendix D
Honeywell TFE-731-2 Thrust Setting Chart

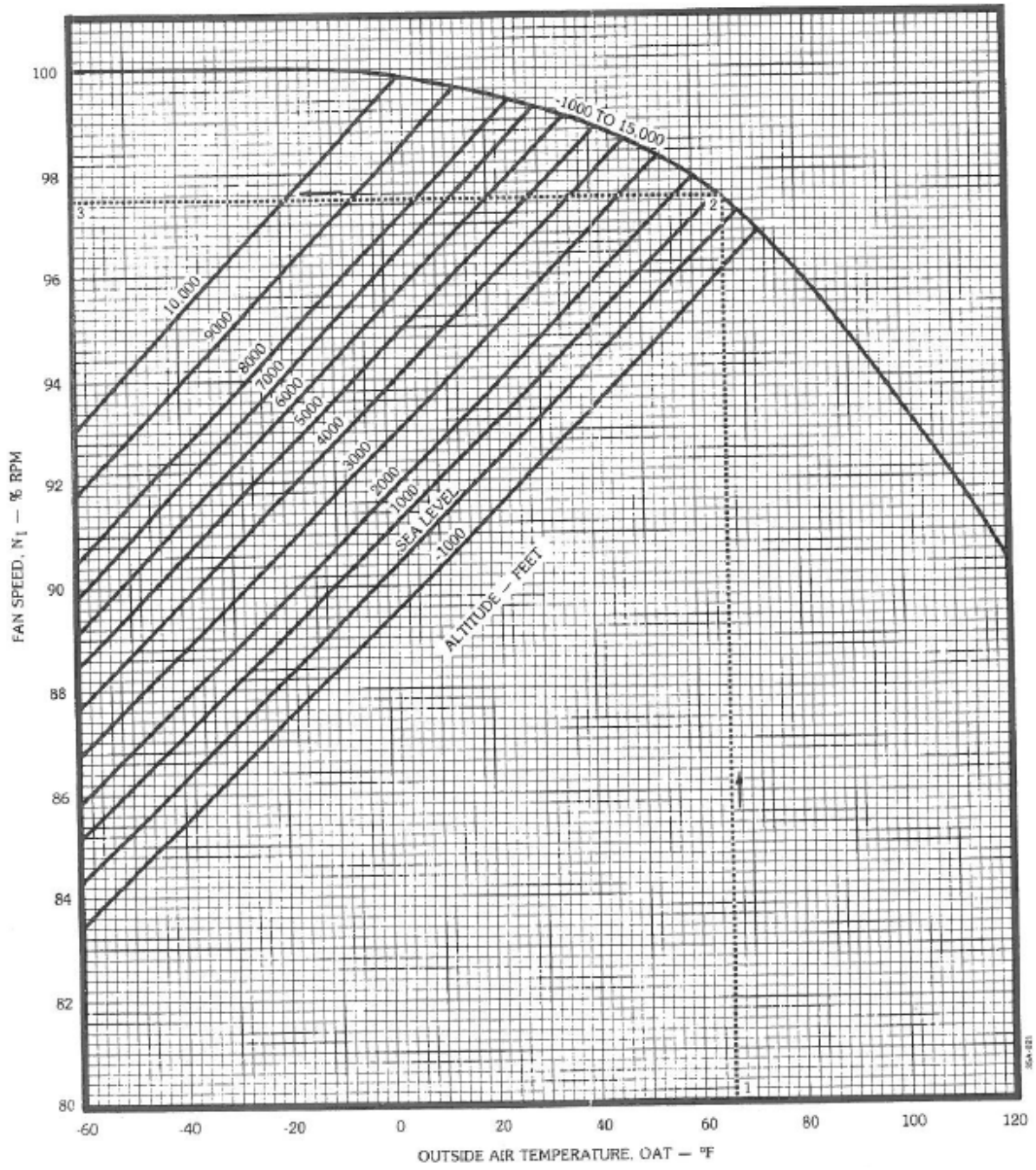

Fig. D1 Learjet TFE-731-2 Thrust Setting Chart (**Learjet 35A/36A Flight Manual**)

Appendix E
Aircraft Wetted Area Equations

The following equations have been used to determine the wetted area of the aircraft.

Wing (Torenbeek 1982):

$$S_{wet,W} = 2 \cdot S_{\exp} \cdot \left(1 + 0.25 \cdot \left(\frac{t}{c}\right)_r \frac{1 + \tau \cdot \lambda}{1 + \lambda}\right) \quad \textbf{(E.1)}$$

With

S_{exp}	Exposed wing area
τ	Ratio of relative airfoil thicknesses acc. to Eq. E.2
λ	Taper Ratio acc. to Eq. E.3

$$\tau = \frac{\left(\frac{t}{c}\right)_t}{\left(\frac{t}{c}\right)_{r,F}} \quad \textbf{(E.2)}$$

According to **Torenbeek 1982**, in this case the root section is not taken at the wing centerline as usual, but at the wing-fuselage intersection.

$$\lambda = \frac{c_t}{c_{r,F}} \quad \textbf{(E.3)}$$

Horizontal and Vertical Empennage:

The same equation as for the wing is used.

$$S_{wet,H} = 2 \cdot S_{\exp,H} \cdot \left(1 + 0.25 \cdot \left(\frac{t}{c}\right)_{r,H}\right) \quad \textbf{(E.4)}$$

$$S_{wet,V} = 2 \cdot S_{\exp,V} \cdot \left(1 + 0.25 \cdot \left(\frac{t}{c}\right)_{r,V}\right) \quad \textbf{(E.5)}$$

Assumptions:

- Relative thicknesses is constant, τ =1
- t/c_H is 10% less than for the wing

Dorsal, Ventral Fin, Tip Tank Fin and Pylons:

The same equation as for the wing is used for the dorsal and ventral fin.

$$S_{wet,VF} = 2 \cdot S_{\exp,VF} \cdot \left(1 + 0.25 \cdot \left(\frac{t}{c}\right)_{r,VF}\right) \quad \textbf{(E.6)}$$

$$S_{wet,DF} = 2 \cdot S_{\exp,DF} \cdot \left(1 + 0.25 \cdot \left(\frac{t}{c}\right)_{r,DF}\right) \quad \textbf{(E.7)}$$

$$S_{wet,TipTankF} = 2 \cdot S_{\exp,TipTankF} \quad \textbf{(E.8)}$$

$$S_{wet,pylons} = 2 \cdot S_{\exp,pylons} \quad \textbf{(E.9)}$$

Assumptions:

- Relative thicknesses is constant ->τ =1

Fuselage (F) (when $\lambda F \geq 4.5$, Torenbeek 1982):

$$S_{wet,F} = \pi \cdot d_F \cdot l_F \cdot \left(1 - \frac{2}{\lambda_F}\right)^{2/3} \cdot \left(1 + \frac{1}{\lambda_F{}^2}\right) \quad \textbf{(E.10)}$$

With

d_F	Fuselage diameter
l_F	Fuselage length
λF	Fuselage fineness ratio, $\lambda F = lF / dF$

Tiptanks (when $\lambda F \geq 4.5$, Torenbeek 1982):

The same equation as for the fuselage is used.

$$S_{wet,TipTank} = \pi \cdot d_{TipTank} \cdot l_{TipTank} \cdot \left(1 - \frac{2}{\lambda_{TipTank}}\right)^{2/3} \cdot \left(1 + \frac{1}{\lambda_{TipTank}{}^2}\right) \quad \textbf{(E.11)}$$

With

$D_{TipTank}$	Tip Tank diameter
$l_{TipTank}$	Tip Tank length
$\lambda_{TipTank}$	Tip Tank fineness ratio,
$\lambda_{TipTank}$	$l_{TipTank} / d_{TipTank}$

Nacelles:

$$S_{wet,N} = S_{wet,fan} + S_{wet,gas} \quad \textbf{(E.12)}$$

$$S_{wet,fan} = l_n \cdot D_n \cdot \left(2 + 0.35 \cdot \frac{l_l}{l_n} + 0.8 \cdot \frac{l_l \cdot D_{hl}}{l_n \cdot D_n} + 1.15 \cdot \left(1 - \frac{l_l}{l_n}\right) \cdot \frac{D_{ef}}{D_n}\right) \quad \textbf{(E.13)}$$

$$S_{wet,gas} = \pi \cdot l_g \cdot D_g \quad \textbf{(E.14)}$$

With geometrical parameters acc. to Fig. F.1

Appendix F
Specific Learjet 35A/36A Geometry

F.1 Schematic Drawings of Learjet 35A/36A

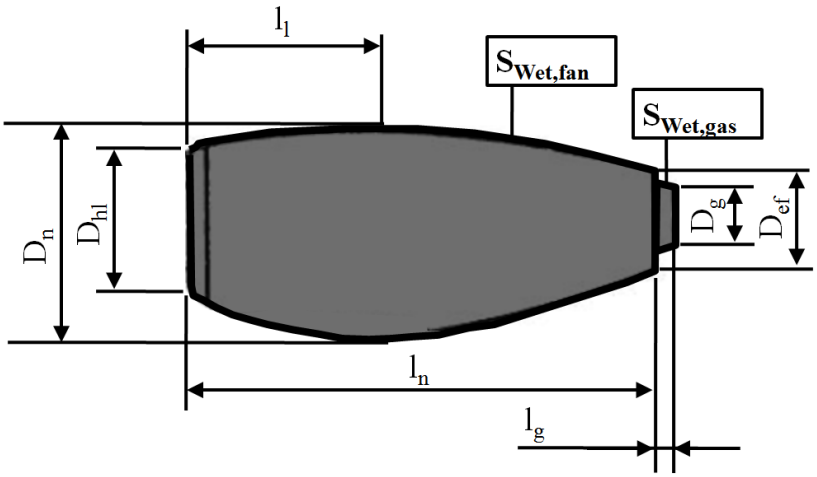

Fig. F.1 Learjet 35A/36A Engine Nacelle Geometry for a TFE-731-2B-2 Engine

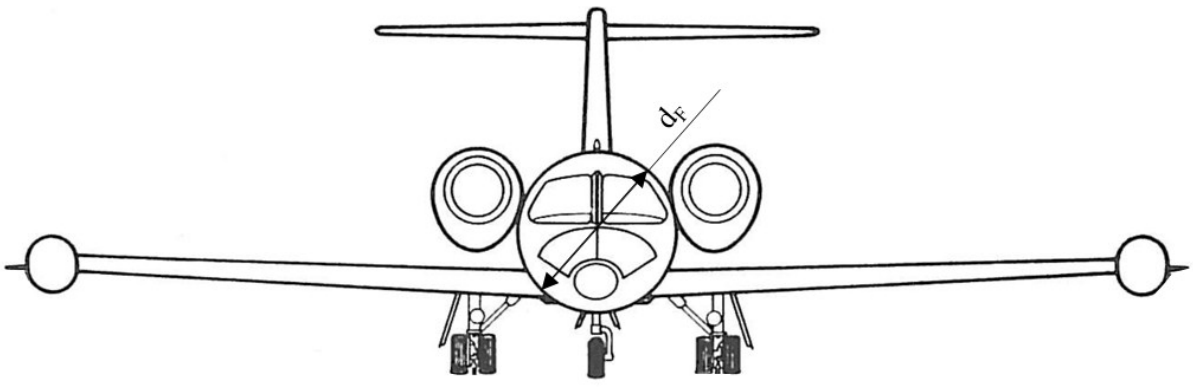

Fig. F.2 Learjet 35A/36A Fuselage Diameter and Frontal View

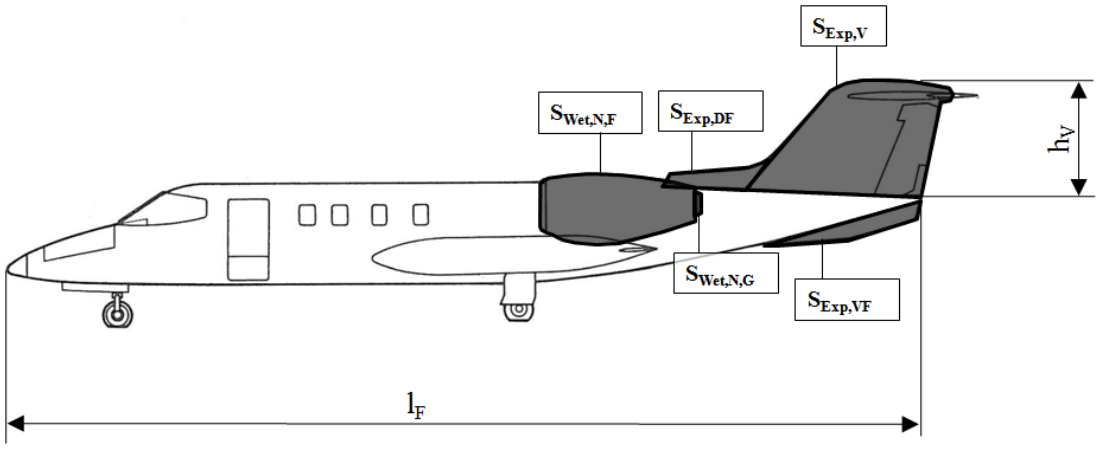

Fig. F.3 Learjet 35A/36A Side View, with Wetted Areas of Nacelle, VTP and Fins

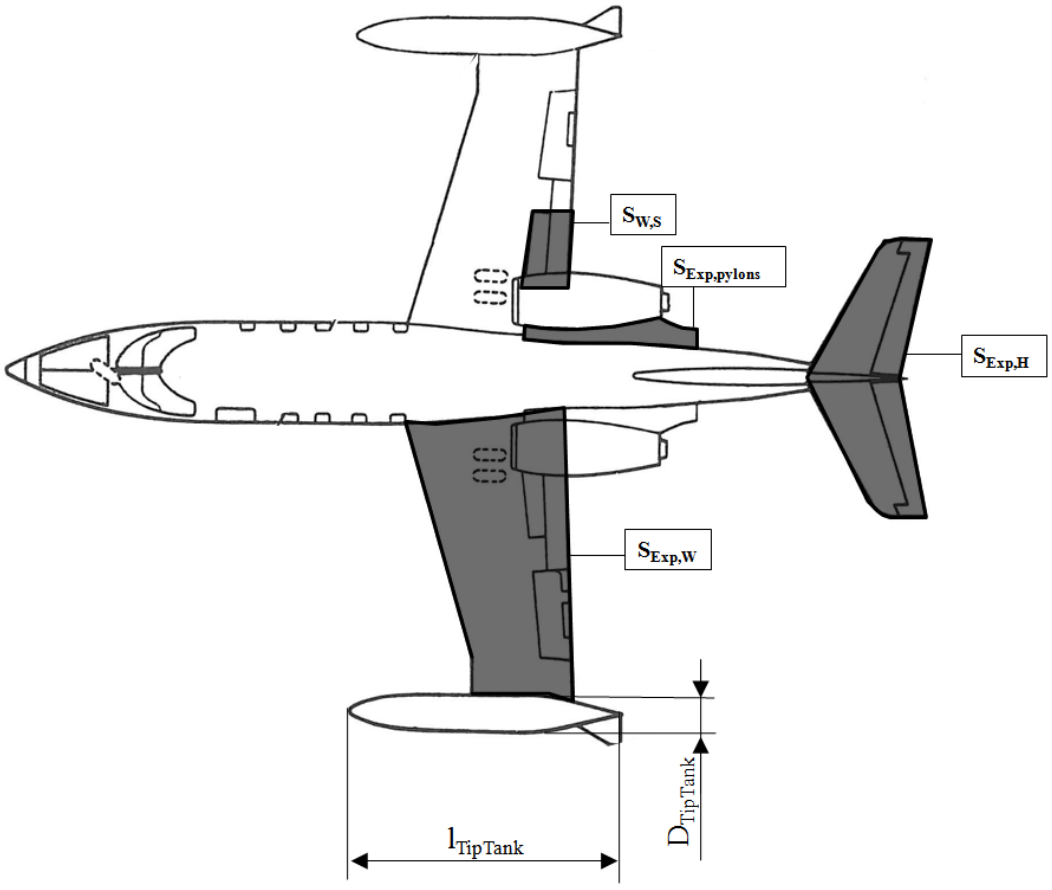

Fig. F.4 Learjet 35A/36A Top View, with Wetted Areas Pylon, HTP, Exposed Wing Area

F.2 List of Geometrical Parameters for the Learjet 35A/36A

Parameters shown in this section have been determined in a previous investigation conducted in the Aero Group of the Hamburg University of Applied Science under the lead of Prof. Dr. Dieter Scholz, MSME. They have been determined based on actual measurements taken on the Learjet 35A/36A by an assistant to the Aero Group.

Table F.1 Measurements taken from the Learjet 35A/36A

Parameter Name	Symbol	Value	Unit
Fuselage Length	l_F	13,900	m
Fuselage Diameter	d_F	1,580	m
Wing Area	S_W	23,530	m²
Thickness Ratio Wing Tip	t/c_t	0,090	-
Chord Length Wing Tip	c_t	1,550	m
Thickness Wing Tip	t_t	0,140	m
Thickness Ratio Wing Root, Assumption: t/c constant	t/c_r	0,090	-
Chord Length Wing Root	c_r	2,740	m
Chord Length at Intersection of Wing and Fuselage	c_{rF}	2,600	m
Thickness Wing Root	t_r	0,247	m
Thickness at the intersection Wing-Fuselage	t_{rF}	0,234	m
Projected Area of extended Spoiler in Windstream	S_S	0,516	m²
Horizontal tailplane span	b_H	4,470	m
Chord at tip for the HTP	c_{tH}	0,740	m
Chord at root for the HTP	c_{rH}	1,580	m
Thickness Ratio HTP, Assumption: t/c_H = 10% t/c_r	t/c_{rH}	0,081	-
Vertical Empennage height	h_V	1,810	m
Chord at tip for the VTP	$c_{r,V}$	2,720	m
Chord at root for the VTP	$c_{t,V}$	1,600	m
Thickness at root for the VTP	$t_{r,V}$	0,280	m
Thickness Ratio VTP	$t/c_{r,V}$	0,103	-
Number of Engines	n_E	2,000	-
Thickness Ventral Fin and Dorsal Fin, Estimate	t_{VF}	0,100	m
Chord Length Ventral Fin and Dorsal Fin, Estimate	c_{VF}	2,400	m
Number of Tip Tanks	$n_{TipTank}$	2,000	-
Tip Tank Length	$l_{TipTank}$	4,200	m
Tip Tank Diameter	$D_{TipTank}$	0,600	m

Table F.2 Exposed areas of the Learjet 35A/36A as shown in Appendix E

Parameter Name	Symbol	Value	Unit
Exposed Wing Area	S_{exp}	18,826	m²
Exposed Area of Horizontal Empennage	S_{expH}	4,100	m²
Exposed Area of vertical Empennage	$S_{exp,V}$	3,730	m²
Exposed Area AVCON Dorsal Fin	$S_{exp,DF}$	1,500	m²
Exposed Area Ventral Fin	$S_{exp,VF}$	0,325	m²
Exposed Area Pylons	$S_{exp,pylon}$	0,973	m²
Exposed Area Tip Tank	$S_{exp,TipTank}$	0,164	m²

F.3 Wetted Area Determination acc. to Appendix E

The wetted areas determined with the parameters from Appendix F.2 are a result of the investigations and measurements performed at Aero. They have been applied for this report.

Table F.3 Wetted Areas for the Learjet 35A/36A based on the Exposed Area Calculation Method

Parameter Name, Location		Symbol	Value	Unit
Fuselage				
	Fuselage Fineness Ratio	λ_F	8,797	m²
	Wetted Area Fuselage	$S_{Wet,Fuselage}$	58,847	m²
Wing				
	Taper Ratio Wing	λ_W	0,596	
	Thickness Wing	τ_W	1,000	
	Wetted Area Wings	$S_{Wet,W}$	38,499	m²
Horizontal Empennage				
	Wetted Area HTP	$S_{Wet,H}$	8,366	m²
Vertical Empennage				
	Wetted Area VTP	$S_{Wet,V}$	7,652	m²
Nacelle				
	Wetted Area Fan Nacelle	$S_{Wet,Fan}$	6,577	m²
	Wetted Area Exhaust Nozzle	$S_{Wet,Gas}$	0,123	m²
	Wetted Area Nacelle, total	$S_{Wet,N}$	6,699	m²
Pylon				
	Wetted Area Pylons	$S_{Wet,Pylons}$	1,946	m²
Tip Tank				
	Fineness Ratio Tip Tank (basic)	$\lambda_{TipTank}$	7,000	
	Wetted Area Tip Tank	$S_{Wet,TipTanks}$	6,455	m²
Tip Tank Fin				
	Wetted Area Tip Tank Fin	$S_{Wet,TipTankFin}$	0,328	m²
Dorsal Fin				
	Wetted Area Dorsal Fin	$S_{Wet,DF}$	3,000	m²
Ventral Fin				
	Wetted Area Ventral Fin	$S_{Wet,VF}$	0,657	m²
Base Wetted Area				
	Wetted Area, Sum	$S_{Wet,Total}$	150,878	m²
Wetted Area Final Result (incl. 2,5% margin)				
	Wetted Area Learjet 35A/36A	S_{Wet}	154,650	m²

The resulting wetted area includes a factor of 2,5% which accounts for additional measurement / scaling inaccuracies and elements not being accounted for such as antennas etc.

Appendix G Weight Record for Learjet 35A/36A

GFD

Gesellschaft für Flugzieldarstellung

Formblatt : GFD-IHB 010
Seite : 1/1
Datum : 01.12.2010
Änderung : 0

Weight Record

Aircraft Reg.:	D-CGFB	Model:	Lear 35A	Operator:	G F D
Aircraft S/N.:	35A-268	T A T:	11579:24	Date:	08. Feb 11

Reaction	Scale Reading	Tare	Net Weight	ARM	MOMENT
Left Jack	4429	---	4429		
Right Jack	4522	---	4522		
Sub Total	8951	---	8951	414,85	3713322
Nose Jack	1325	---	1325	170,53	225952
Total (as weighted)		---	10276		3939275
Total items Column 1					
Total items Column 2			119,5		44000
Basic Airplane	(includes unusable fuel)		10395,5	383,17	3983275

COLUMN 1 (-)				COLUMN 2 (+)			
Item	Weight	Arm	Moment	Item	Weight	Arm	Moment
				Unusable fuel	119,5	368,2	44000
Total				Total	119,5	368,2	44000

Remarks: Aircraft weighted i/a/w Aircraft Weight Configuration, Formblatt GFD-IHB 014 and current Equipment List after installation of EASA Minor Change 10032053 "Removal/Re-Installation of Drag Chute Assembly" (Drag Chute Dummy installed) and installation of "structure reinforcement for fwd and aft COMJAM Antenna" (Part of EASA STC 10032056 "COMJAM System").

Inspector: Stamp: LBA D-2163 C Certifying Staff

Fig. G.1 Weight Record for Learjet 35A/36A in GFD Configuration

Appendix H
Graphical Representation of BFL Results

H.1 BFL Trend with OAT and TOW, Wet Runway, No Stores

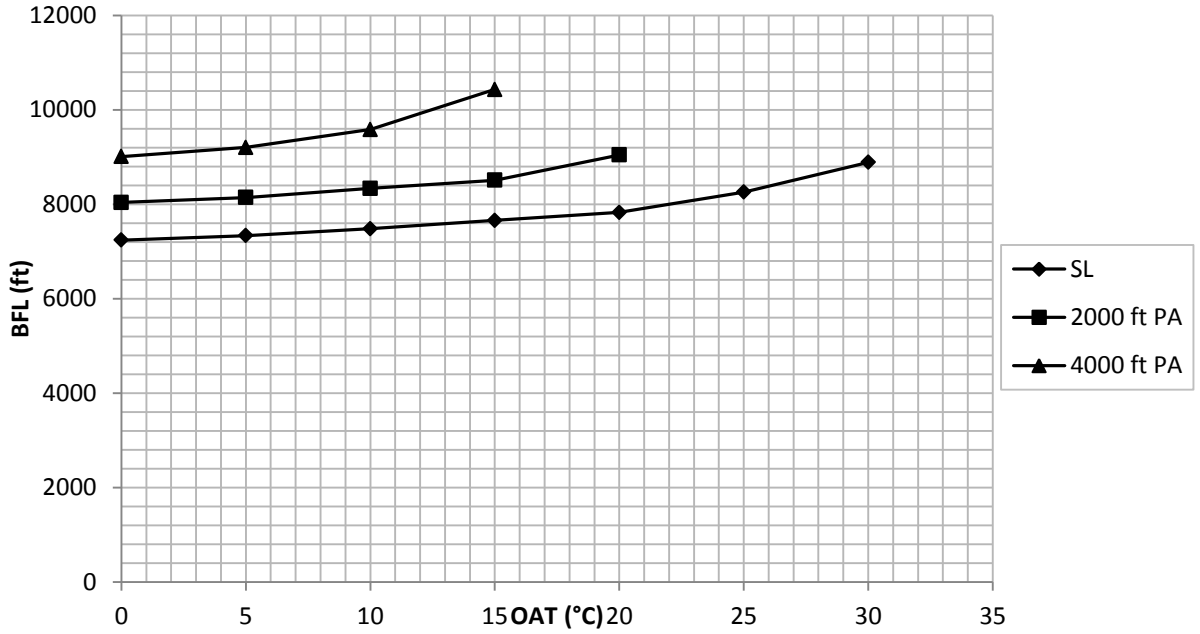

Fig. H.1 Simulation Results for BFL, Wet Runway, No Stores, 19600 lbs TOW

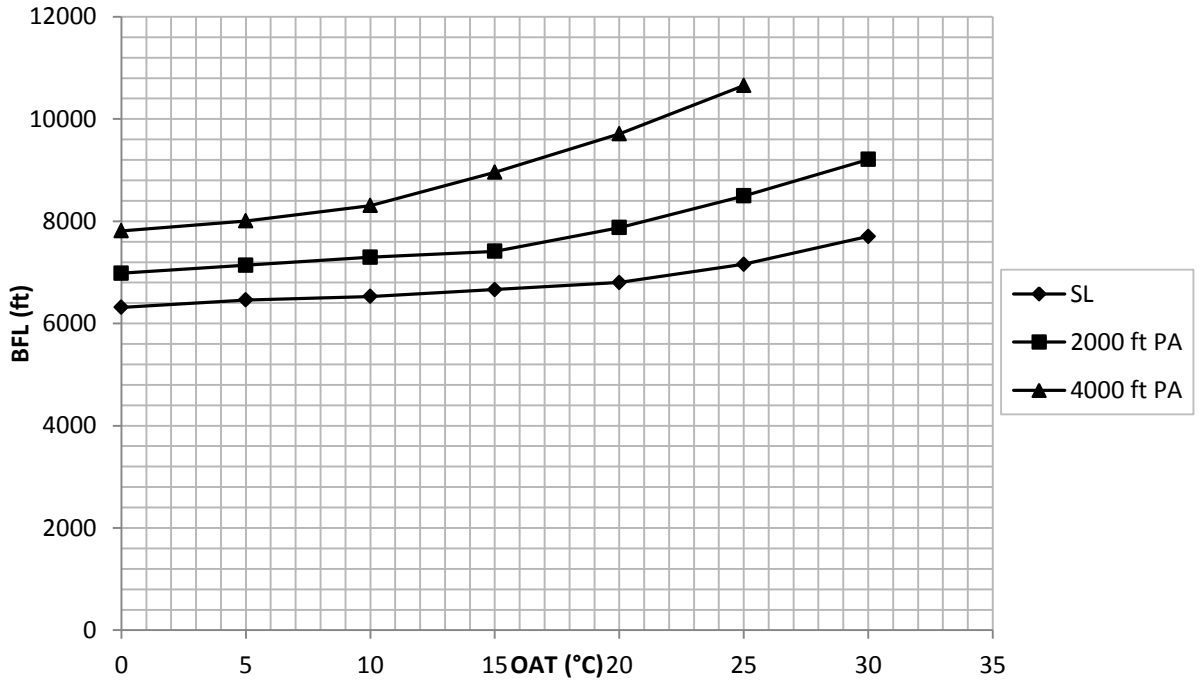

Fig. H.2 Simulation Results for BFL, Wet Runway, No Stores, 18500 lbs TOW

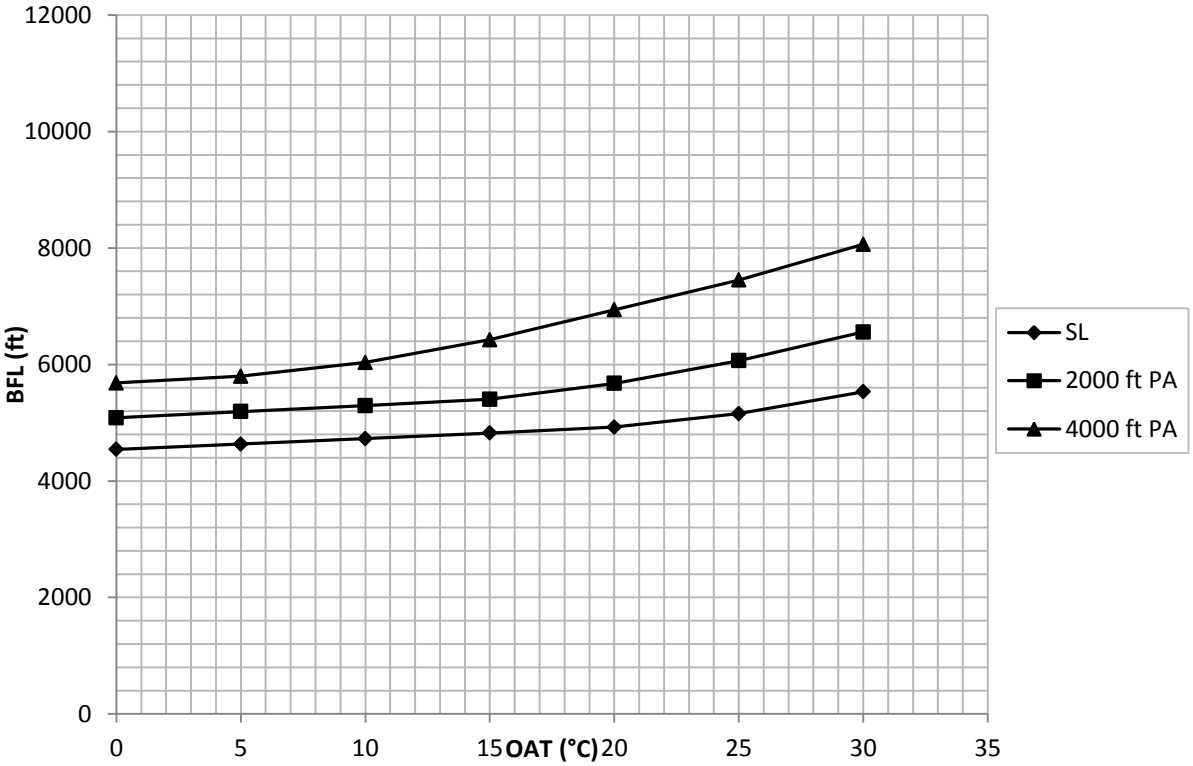

Fig. H.3 Simulation Results for BFL, Wet Runway, No Stores, 16000 lbs TOW

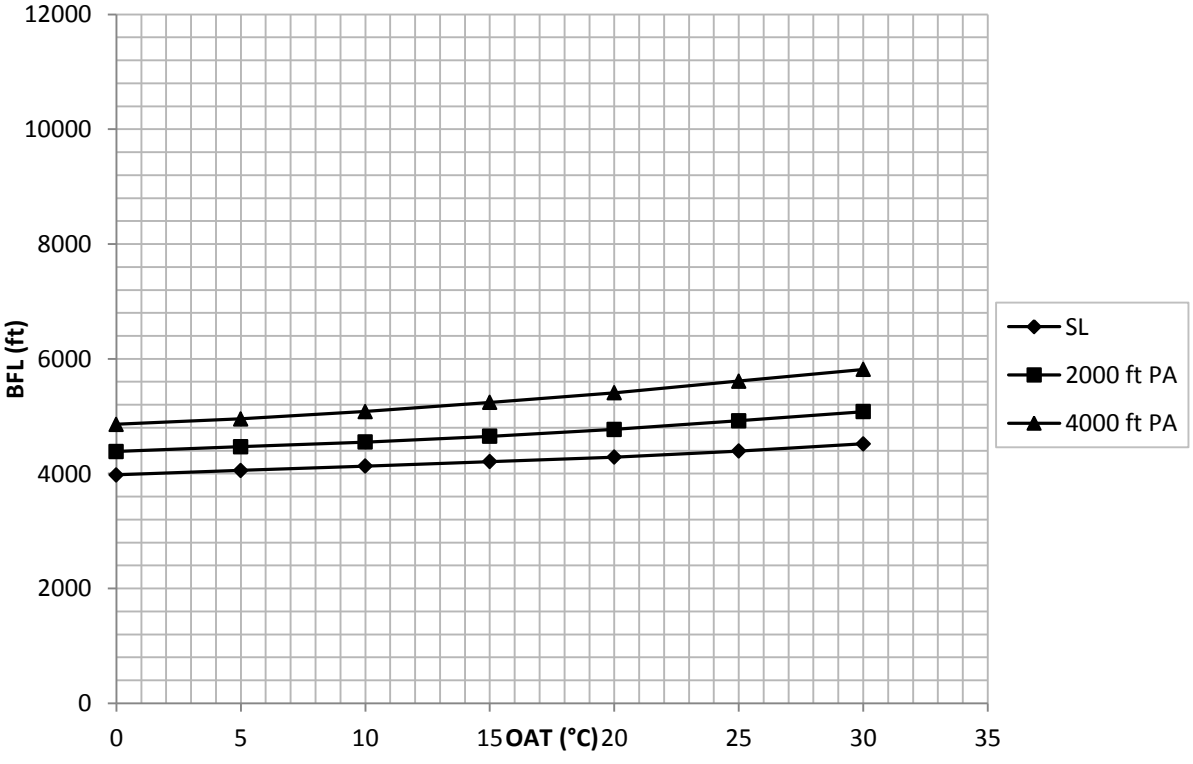

Fig. H.4 Simulation Results for BFL, Wet Runway, No Stores, 13000 lbs TOW

H.2 BFL Trend with OAT and TOW, Wet Runway, Stores

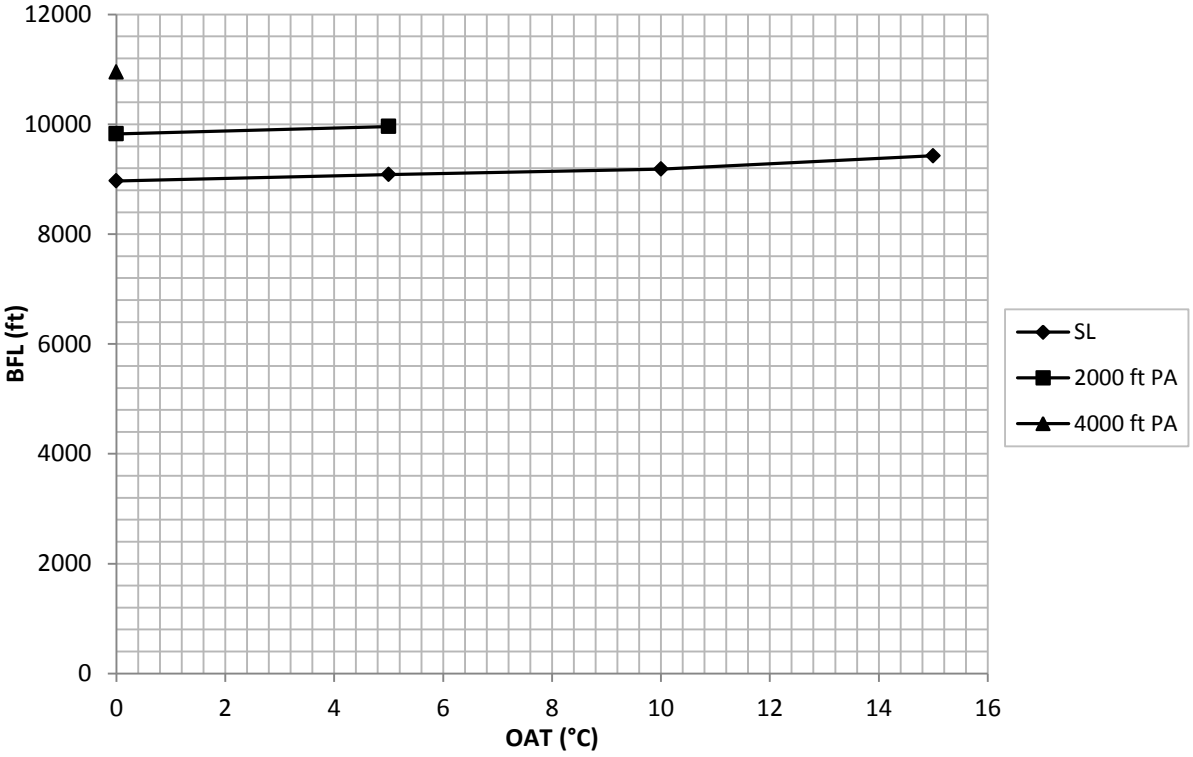

Fig. H.5 Simulation Results for BFL, Wet Runway, Stores, 19600 lbs TOW

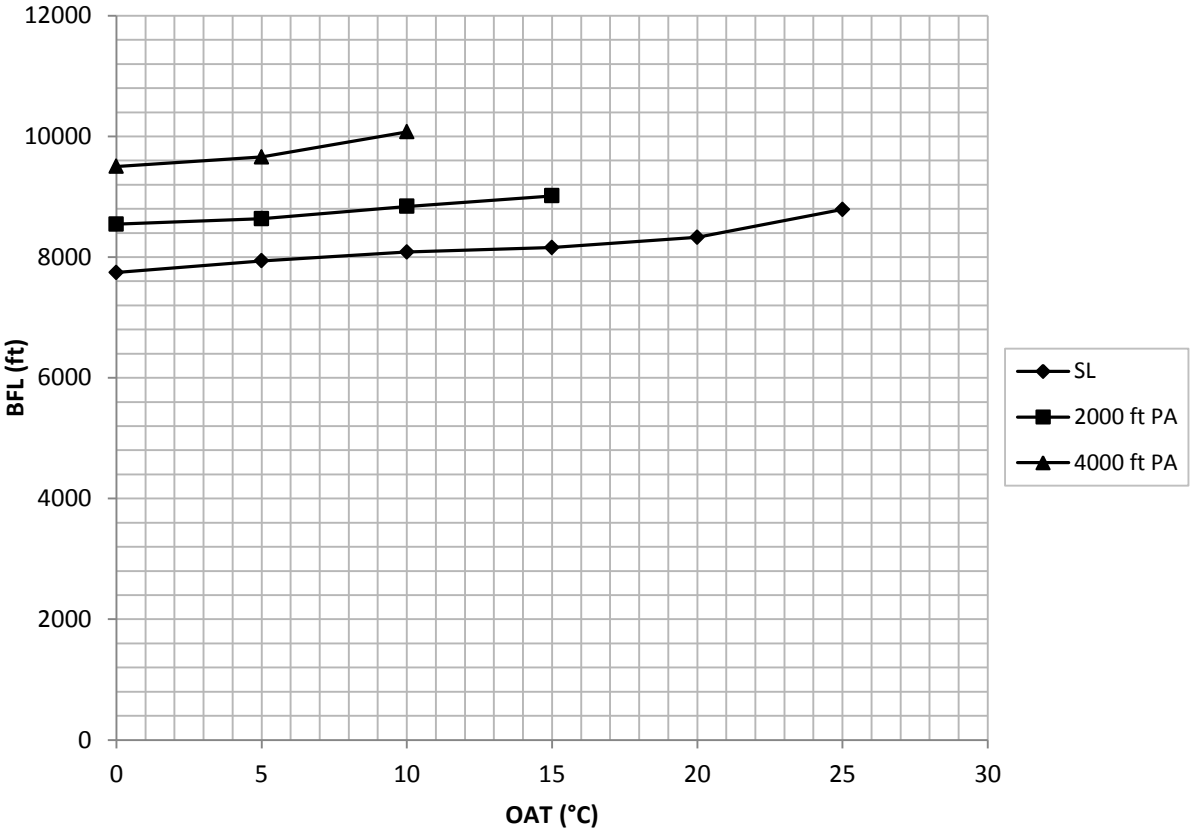

Fig. H.6 Simulation Results for BFL, Wet Runway, Stores, 18500 lbs TOW

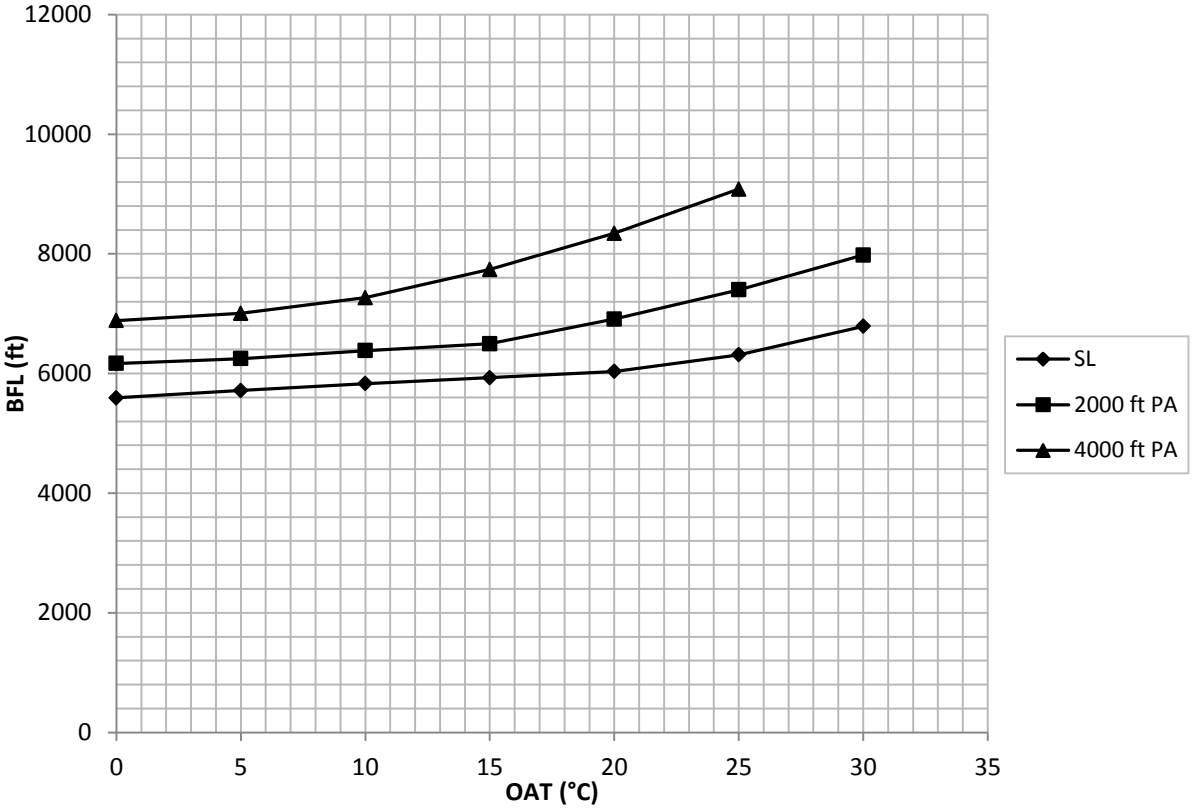

Fig. H.7 Simulation Results for BFL, Wet Runway, Stores, 16000 lbs TOW

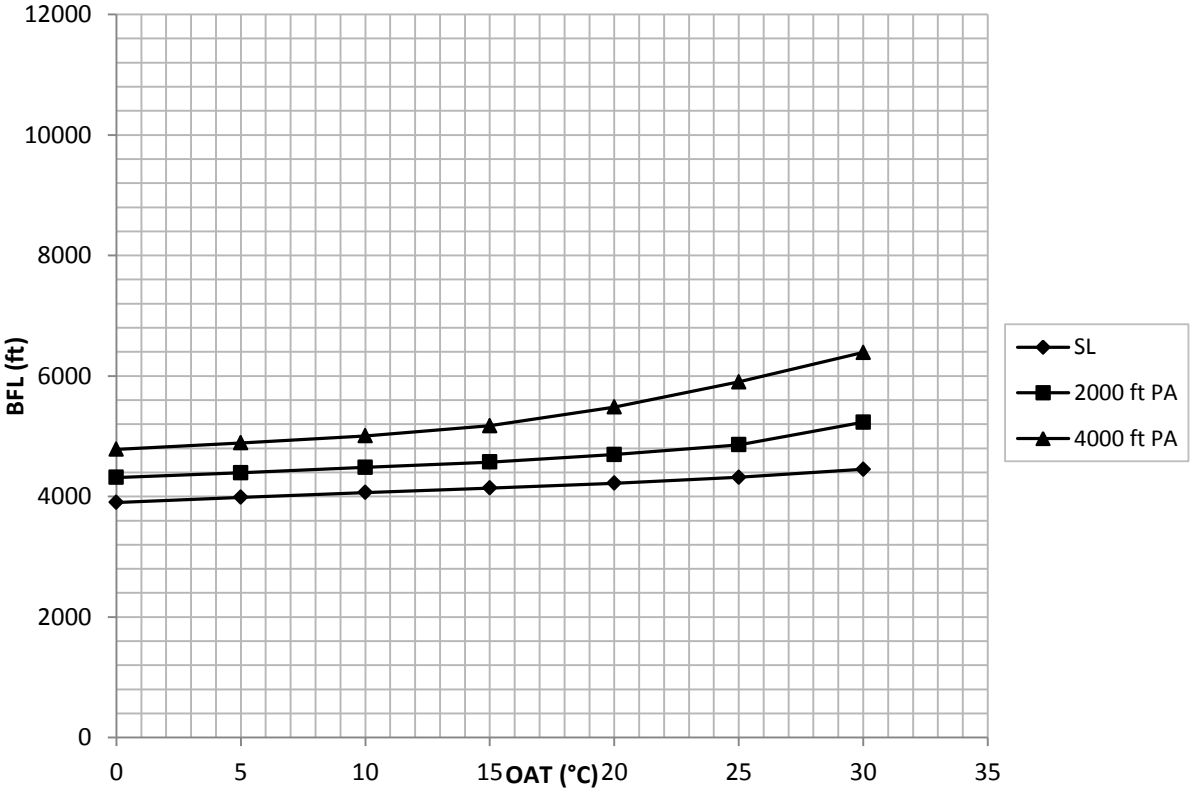

Fig. H.8 Simulation Results for BFL, Wet Runway, Stores, 13000 lbs TOW

H.3 BFL Plots for Wet Runway, No Stores

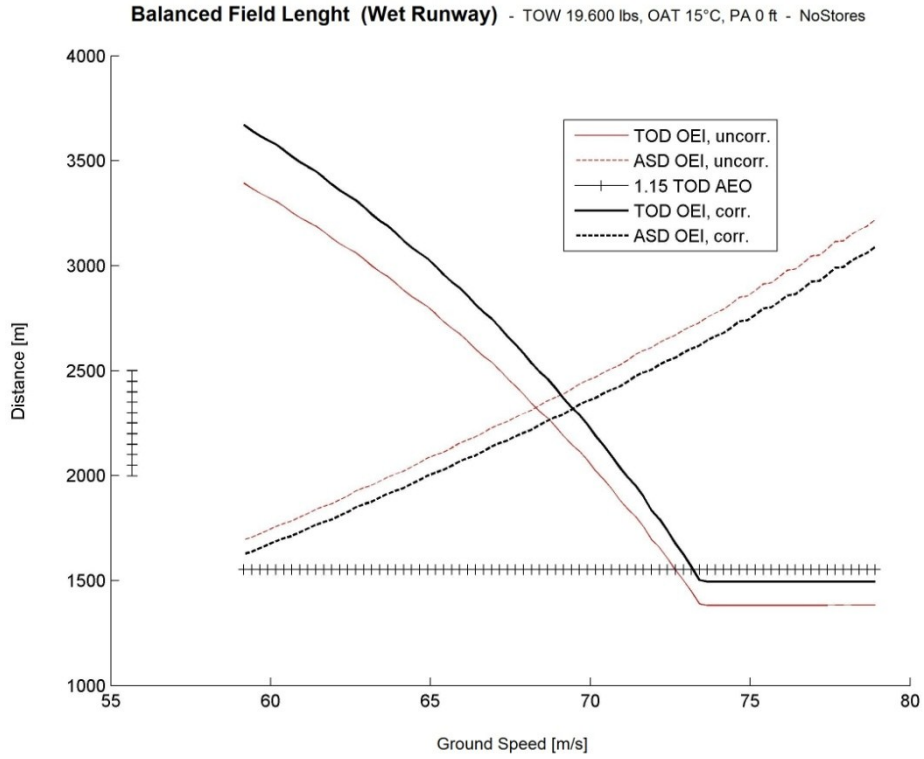

Fig. H.9 Balanced Field Length Plot 15°C OAT, MSL, 19600 lbs TOW, NoStores

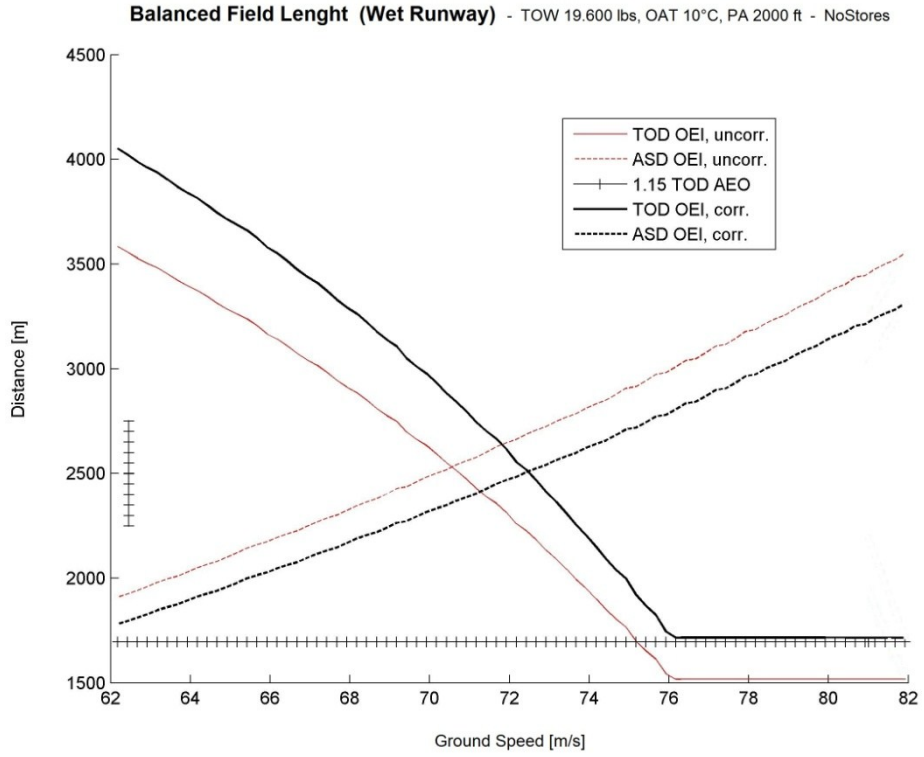

Fig. H.10 Balanced Field Length Plot 10°C OAT, 2000 ft PA, 19600 lbs TOW, NoStores

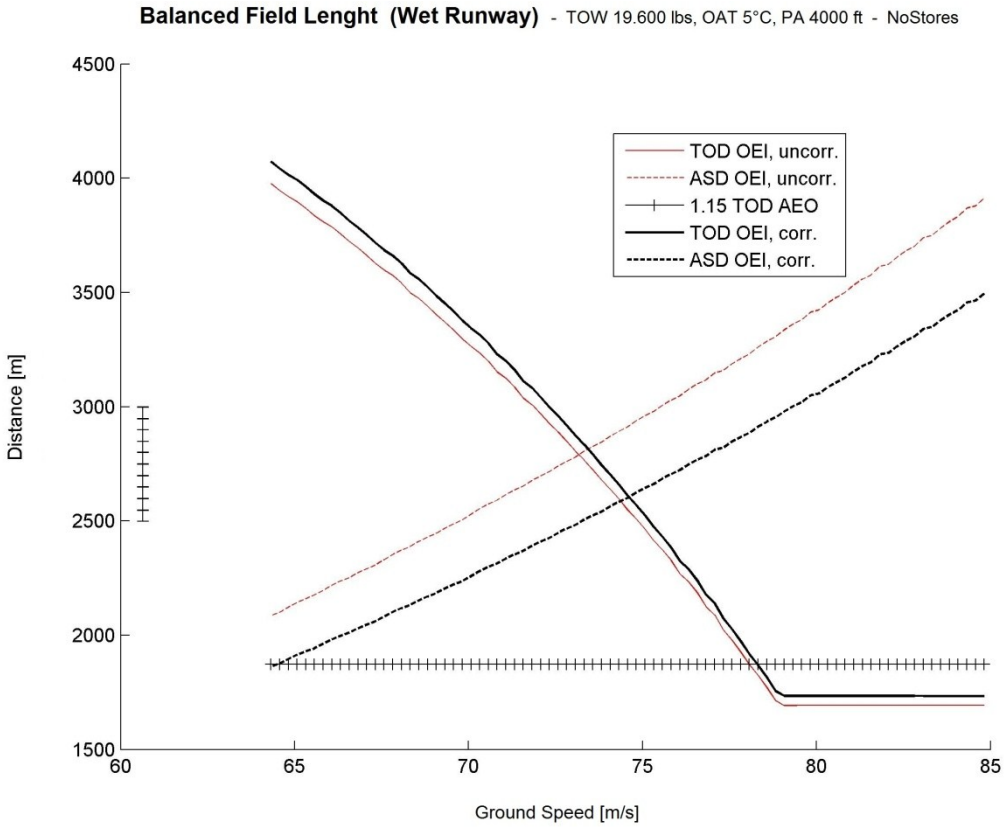

Fig. H.11 Balanced Field Length Plot 5°C OAT, 4000 ft PA, 19600 lbs TOW, NoStores

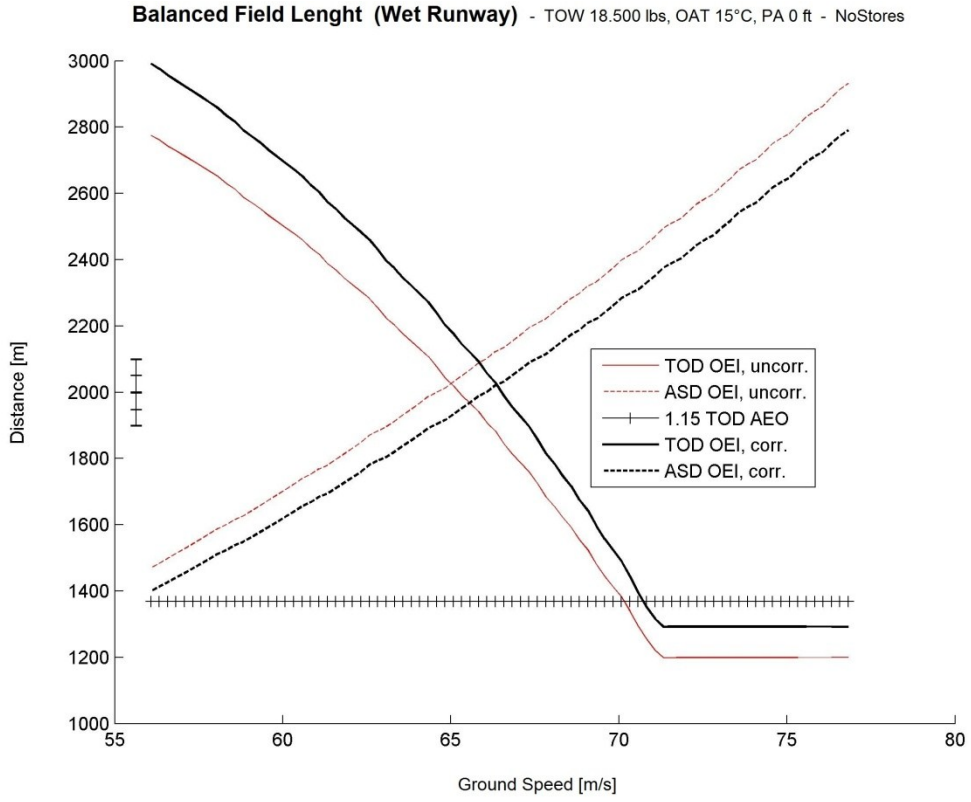

Fig. H.12 Balanced Field Length Plot 15°C OAT, MSL, 18500 lbs TOW, NoStores

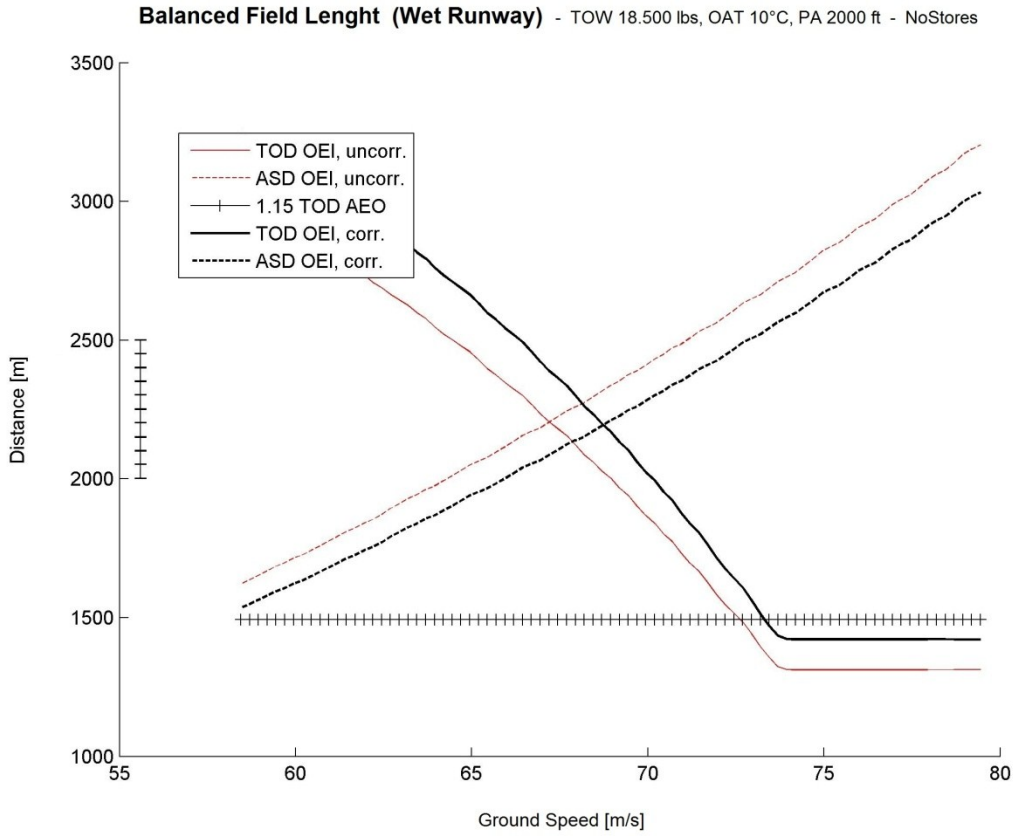

Fig. H.13 Balanced Field Length Plot 10°C OAT, 2000 ft PA, 18500 lbs TOW, NoStores

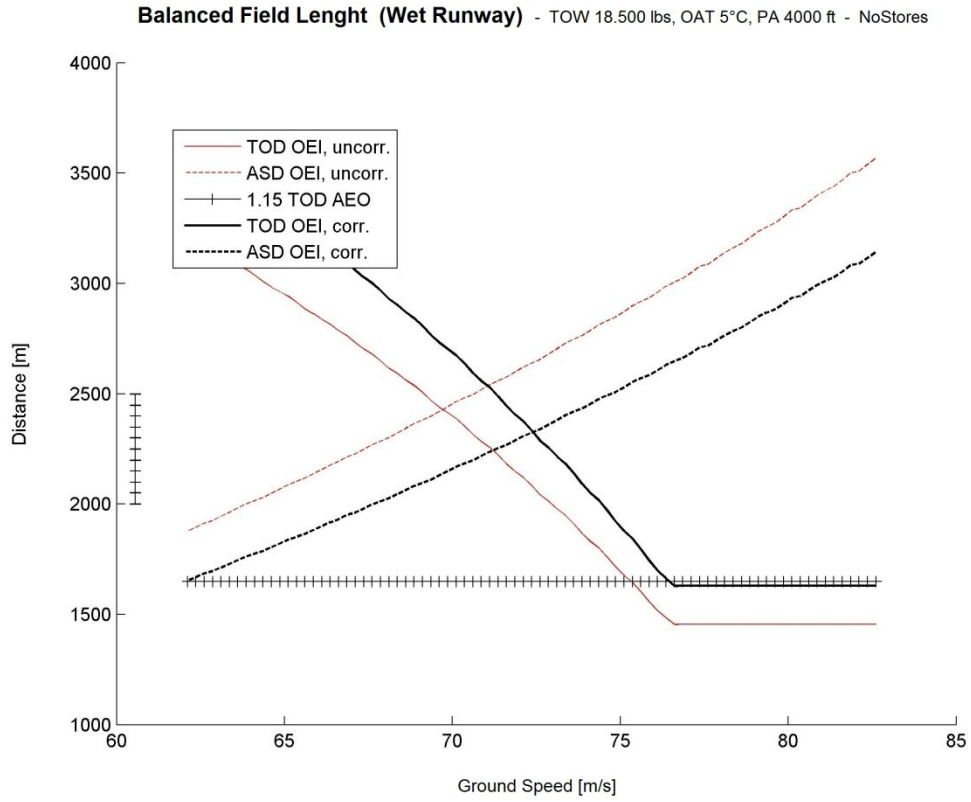

Fig. H.14 Balanced Field Length Plot 5°C OAT, 4000 ft PA, 18500 lbs TOW, NoStores

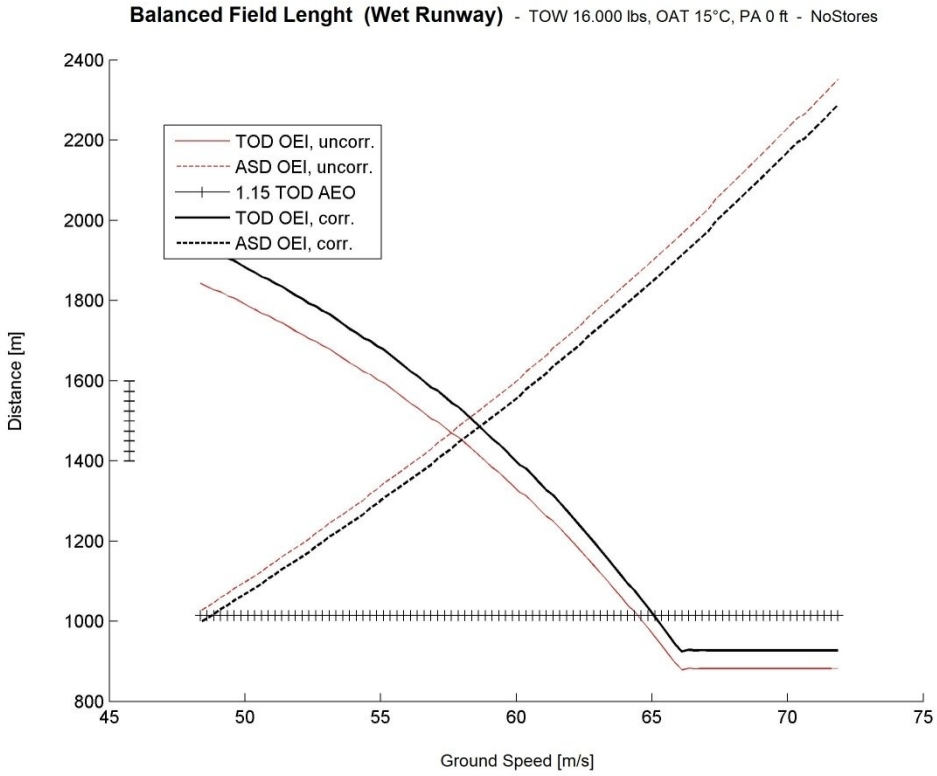

Fig. H.15 Balanced Field Length Plot 15°C OAT, MSL, 16000 lbs TOW, NoStores

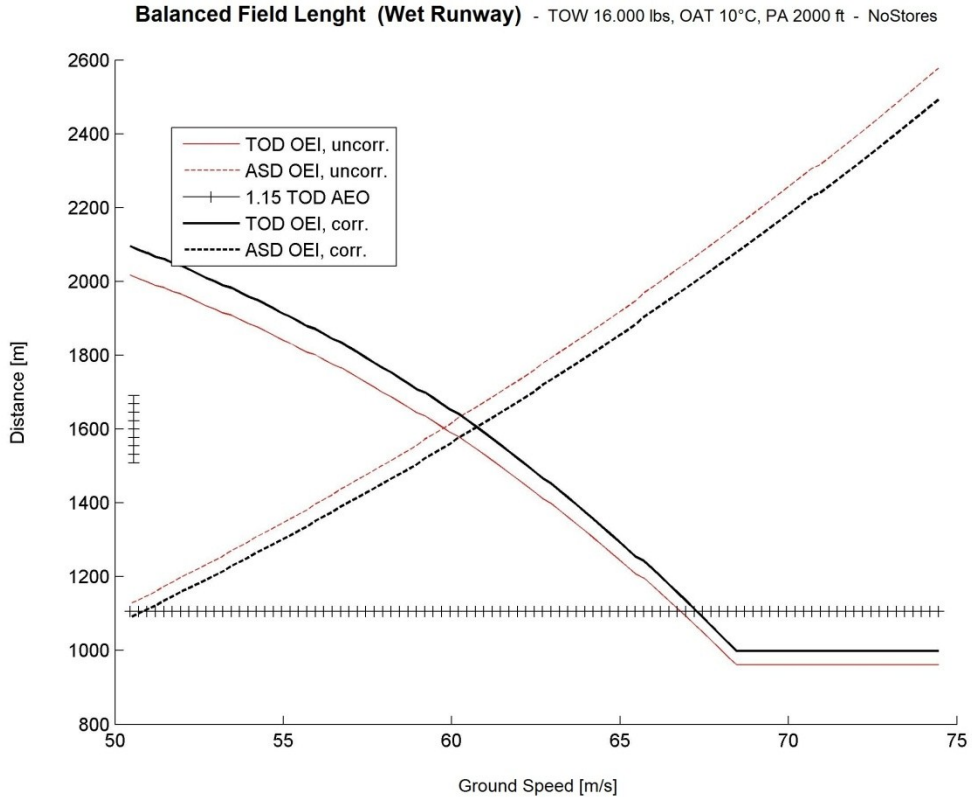

Fig. H.16 Balanced Field Length Plot 10°C OAT, 2000 ft PA, 16000 lbs TOW, NoStores

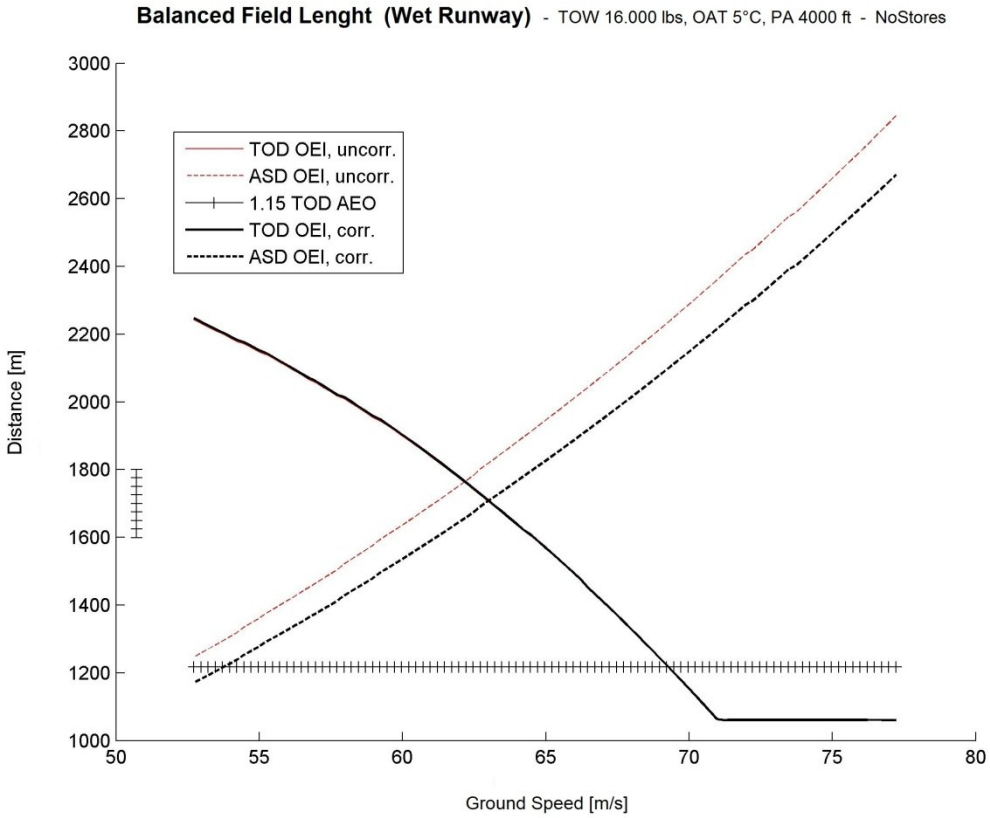

Fig. H.17 Balanced Field Length Plot 5°C OAT, 4000 ft PA, 16000 lbs TOW, NoStores

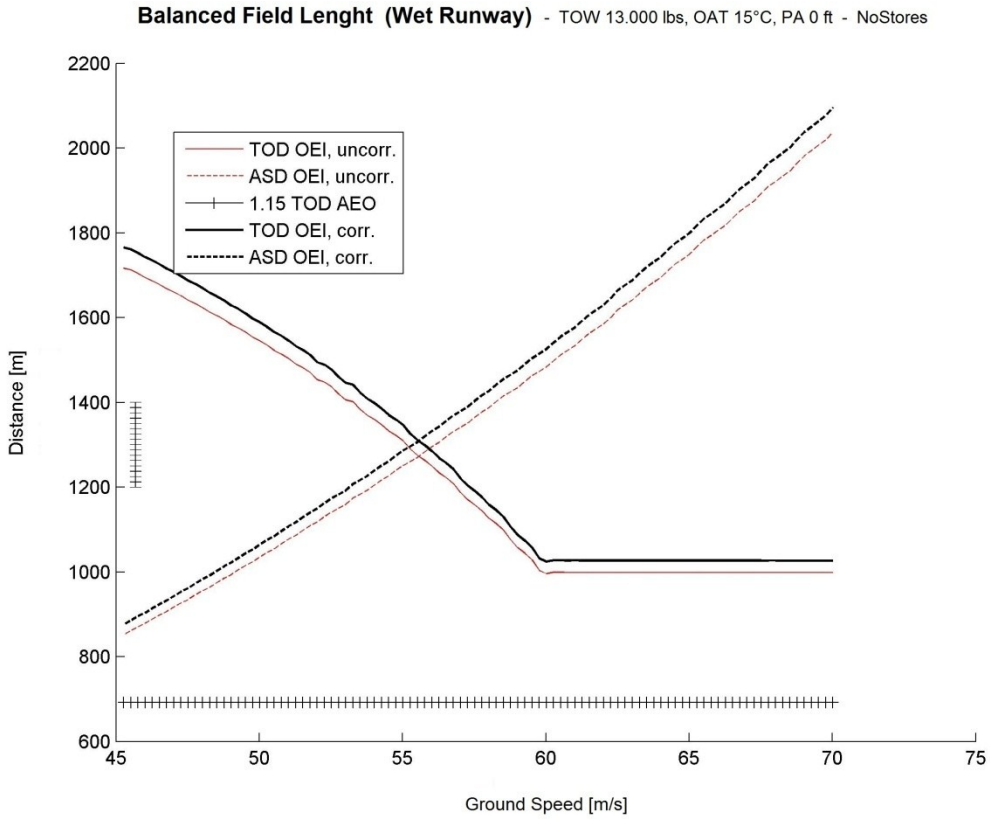

Fig. H.18 Balanced Field Length Plot 15°C OAT, MSL, 13000 lbs TOW, NoStores

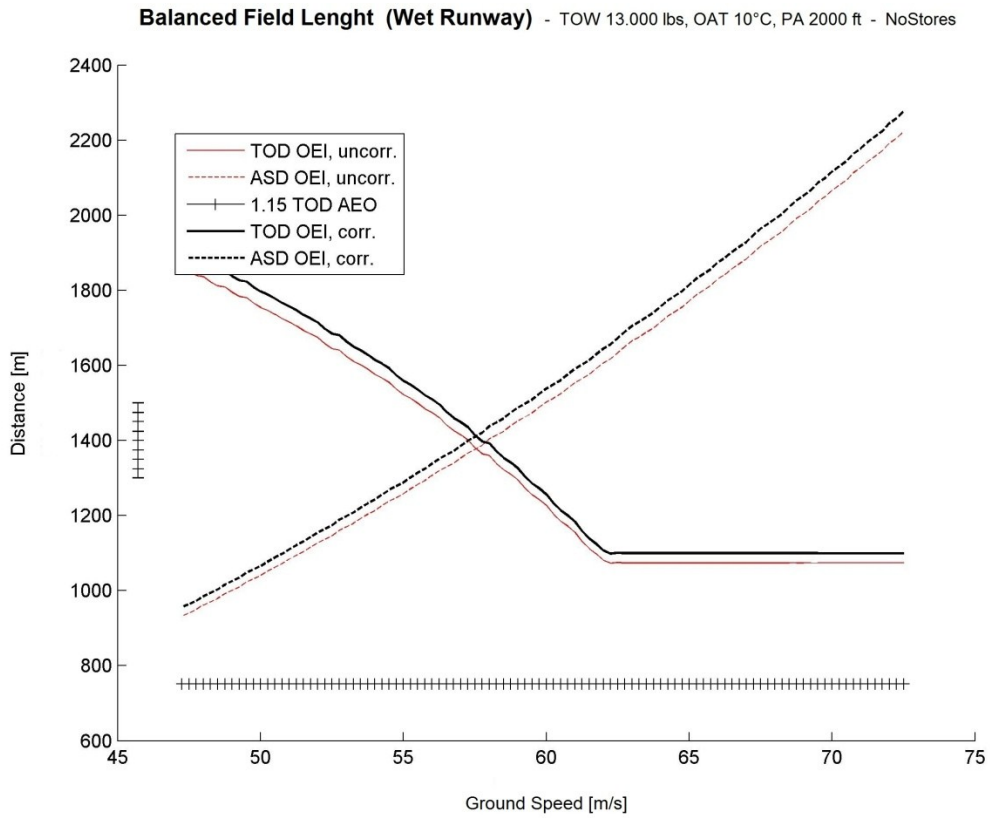

Fig. H.19 Balanced Field Length Plot 10°C OAT, 2000 ft PA, 13000 lbs TOW, NoStores

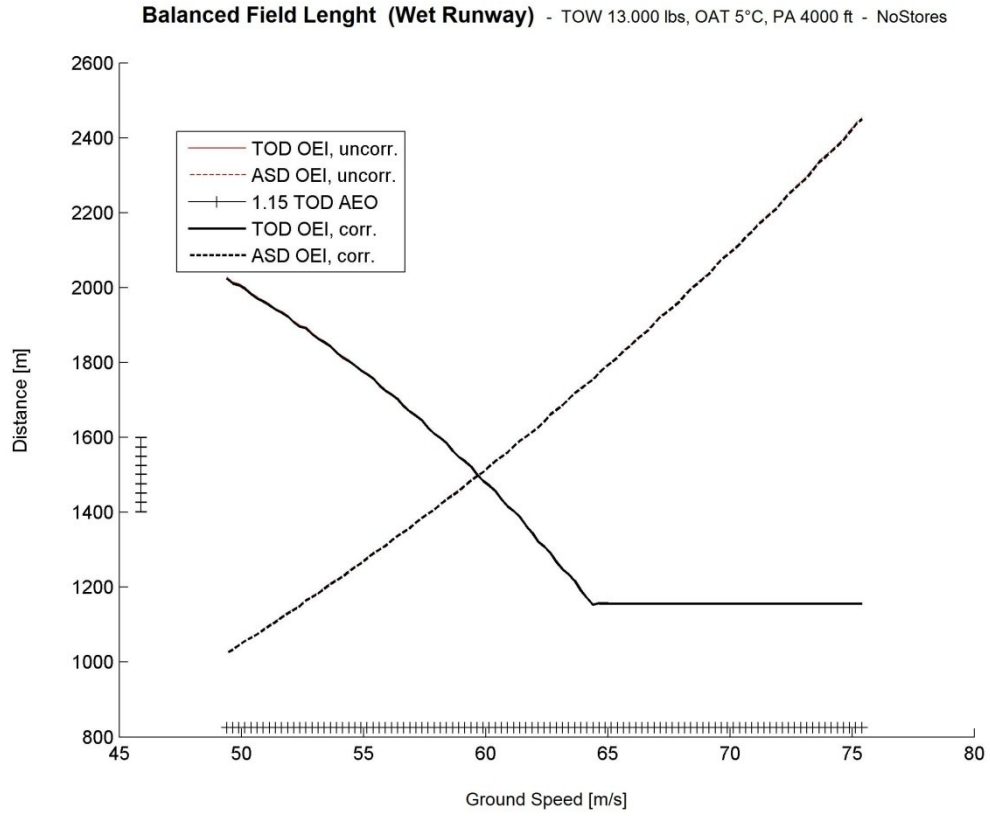

Fig. H.20 Balanced Field Length Plot 5°C OAT, 4000 ft PA, 13000 lbs TOW, NoStores

H.4 BFL Plots for Wet Runway, Stores

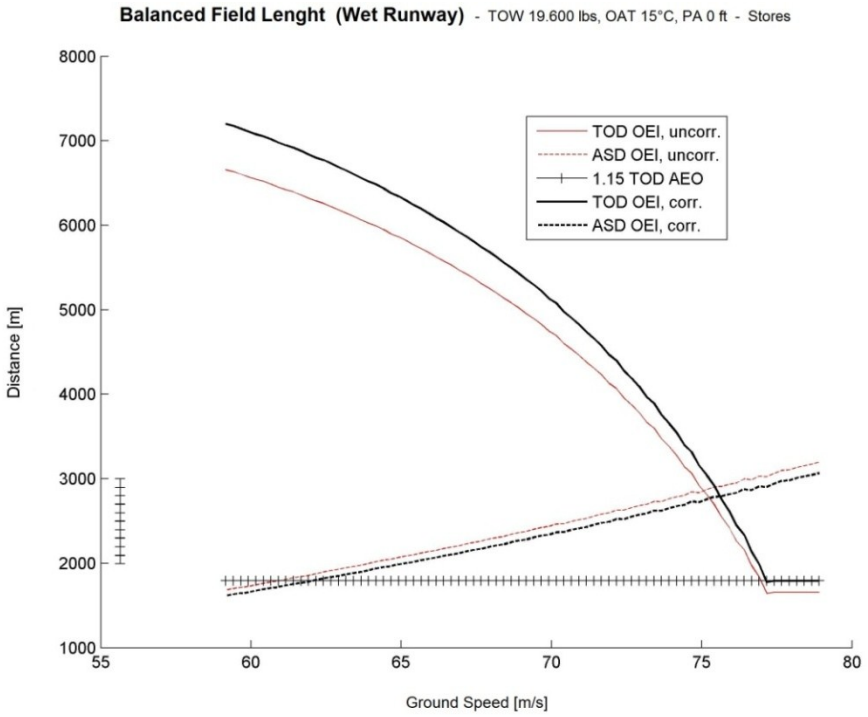

Fig. H.21 Balanced Field Length Plot 15°C OAT, MSL, 19600 lbs TOW, Stores

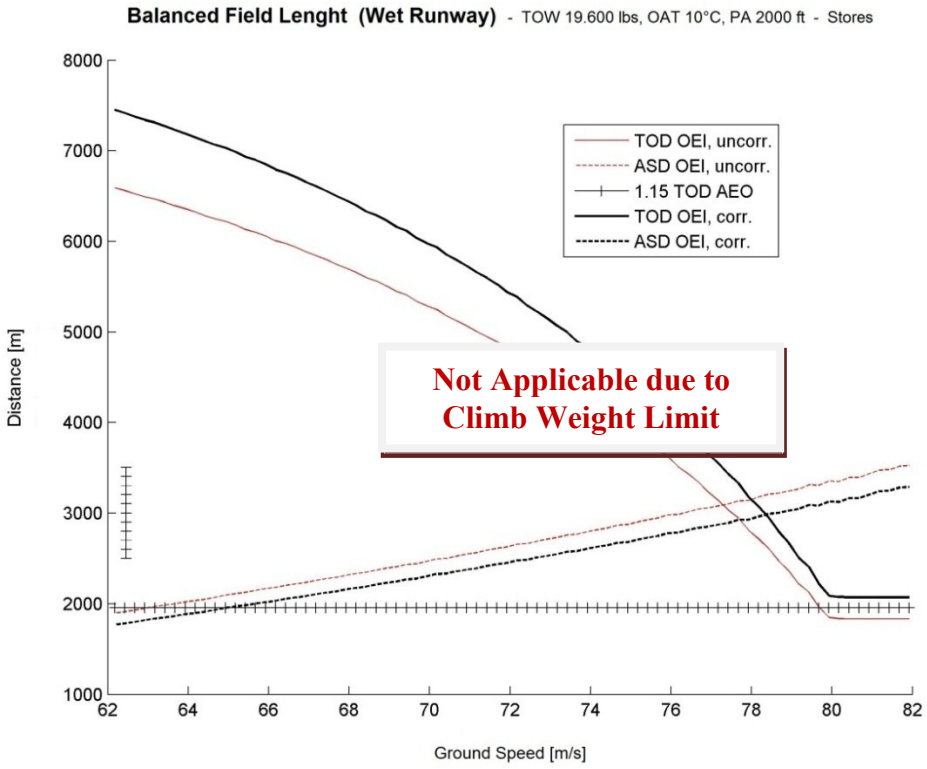

Fig. H.22 Balanced Field Length Plot 10°C OAT, 2000 ft PA, 19600 lbs TOW, Stores

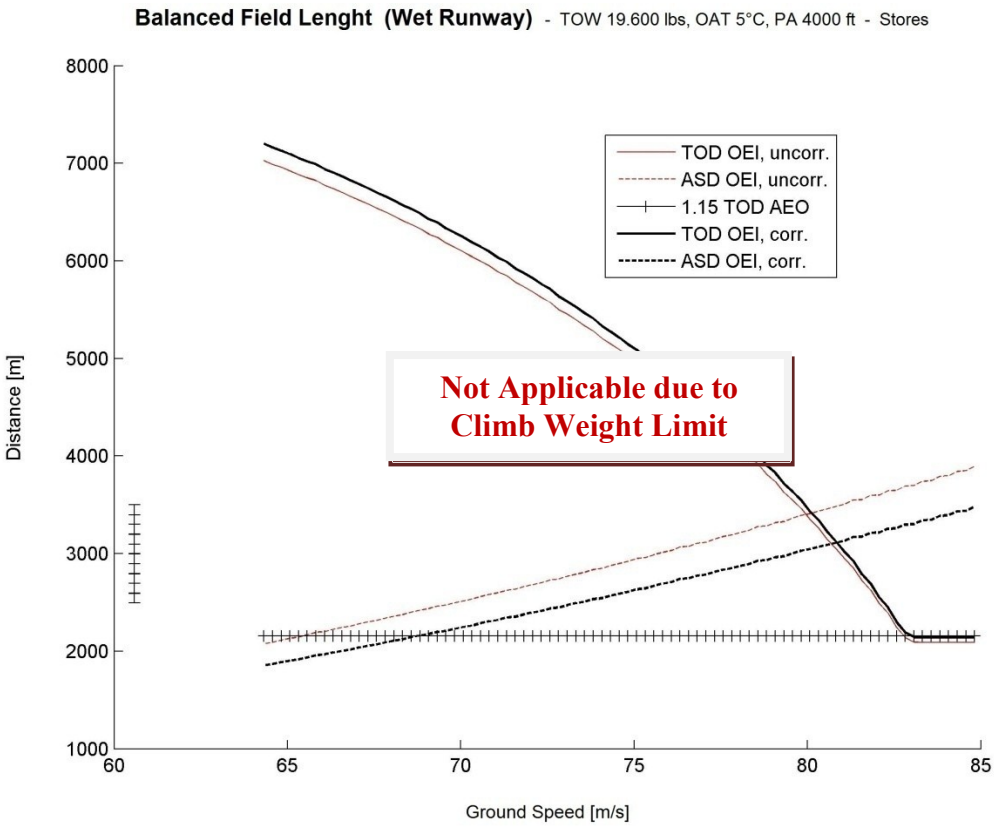

Fig. H.23 Balanced Field Length Plot 5°C OAT, 4000 ft PA, 19600 lbs TOW, Stores

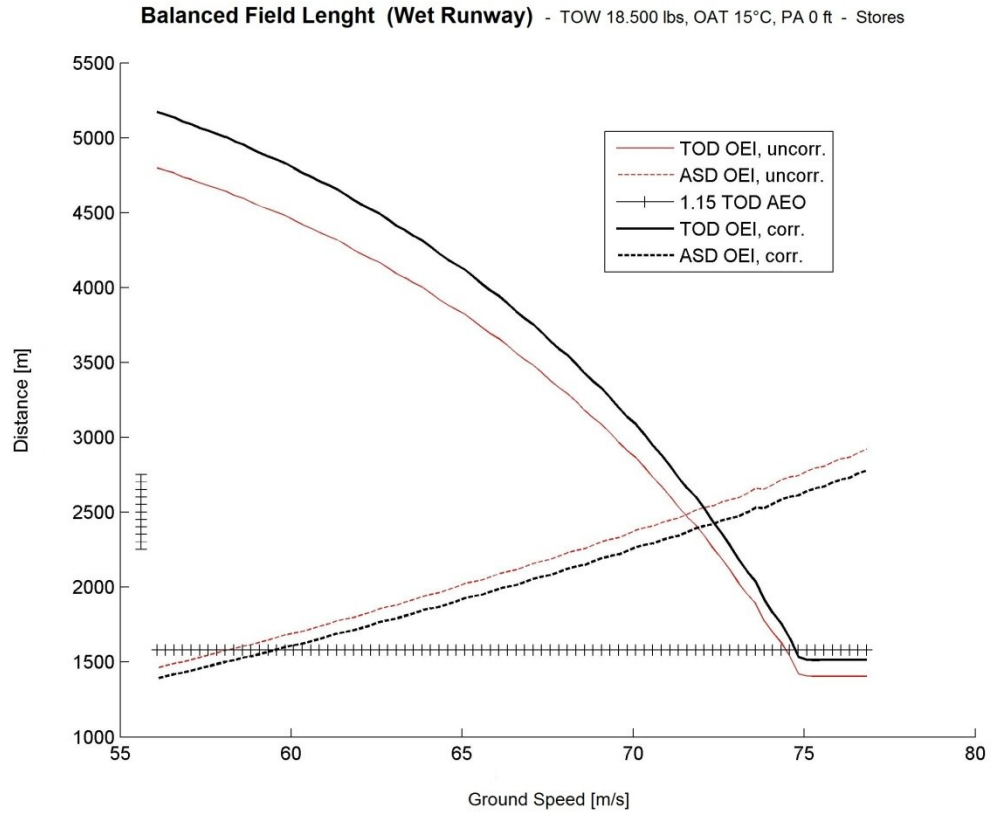

Fig. H.24 Balanced Field Length Plot 15°C OAT, MSL, 18500 lbs TOW, Stores

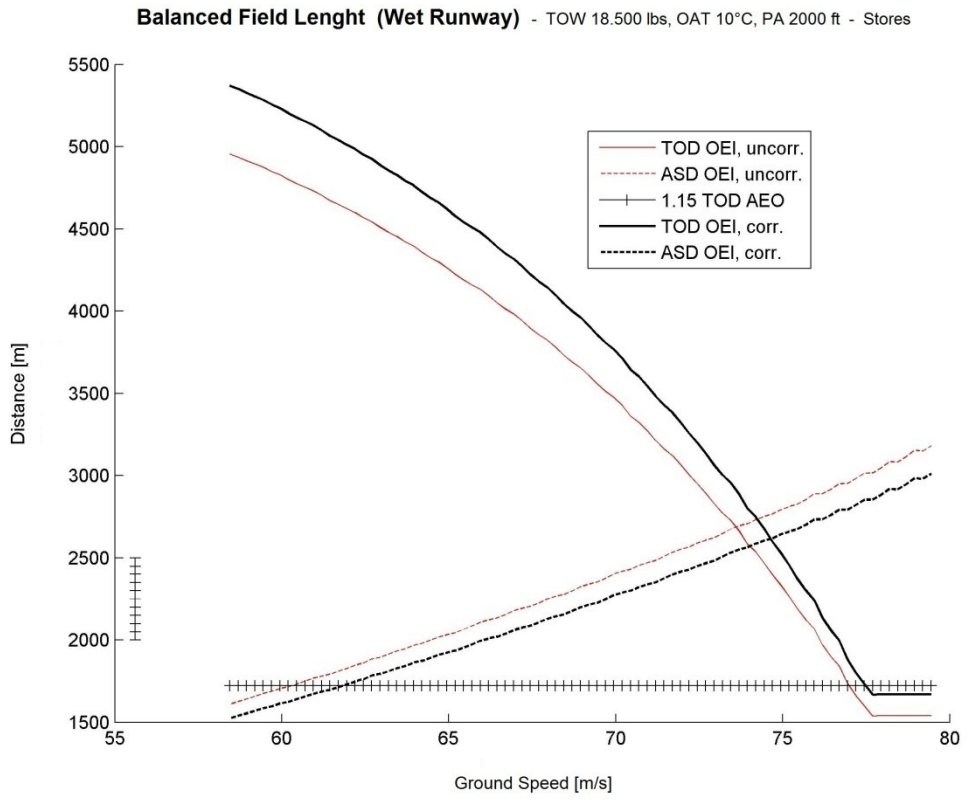

Fig. H.25 Balanced Field Length Plot 10°C OAT, 2000 ft PA, 18500 lbs TOW, Stores

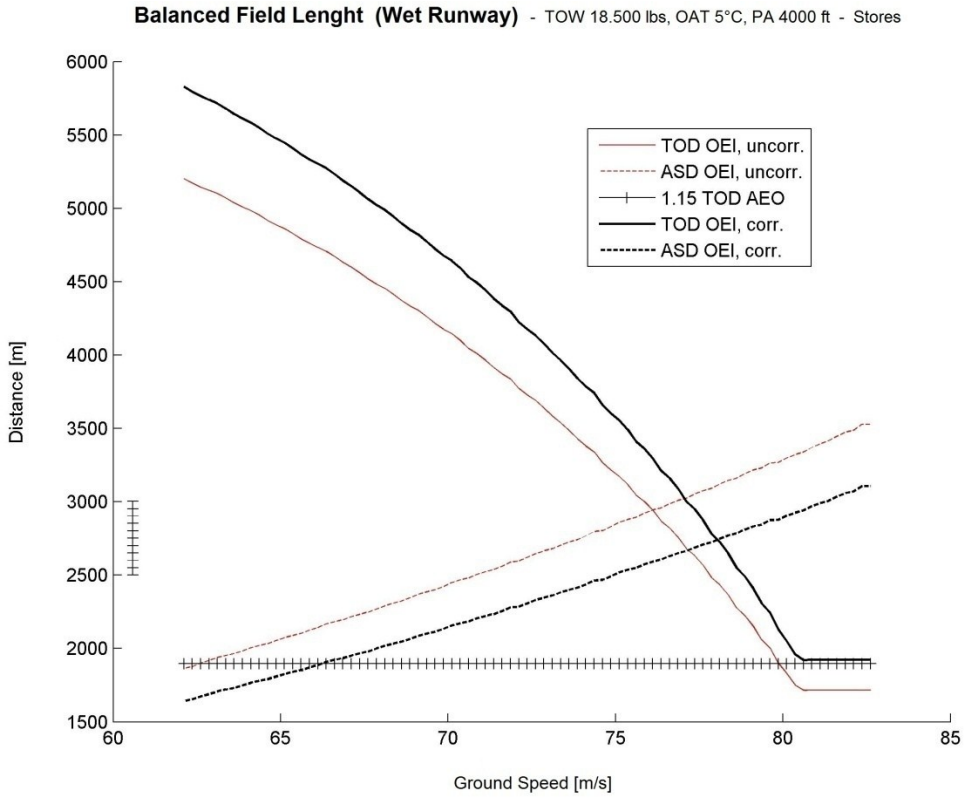

Fig. H.26 Balanced Field Length Plot 5°C OAT, 4000 ft PA, 18500 lbs TOW, Stores

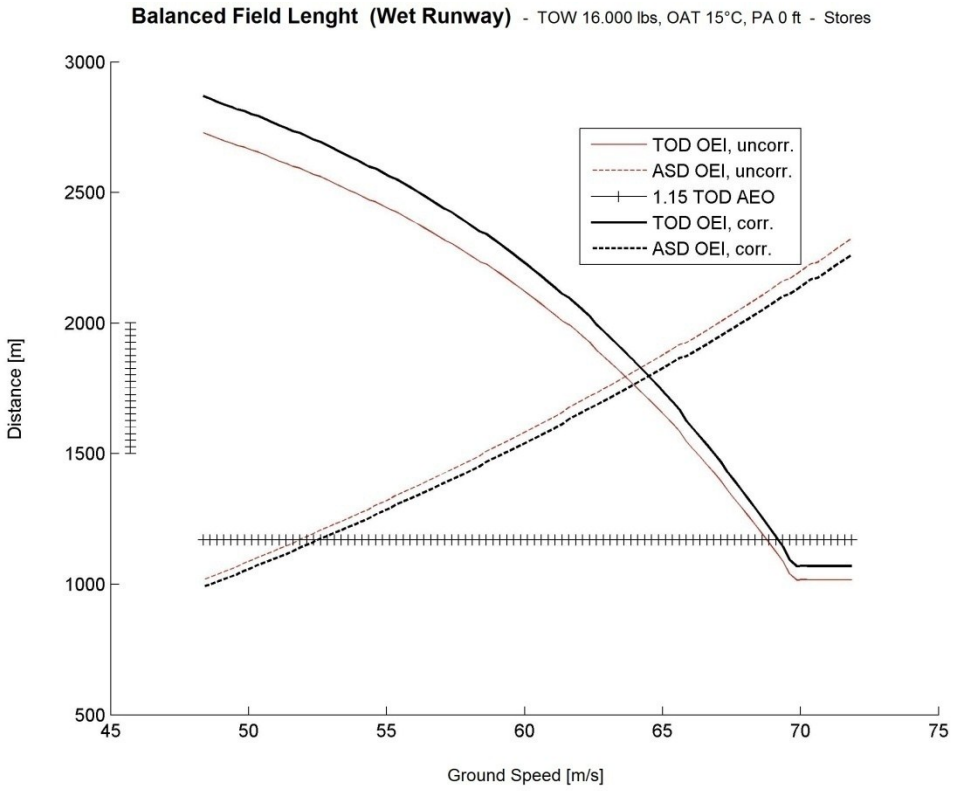

Fig. H.27 Balanced Field Length Plot 15°C OAT, MSL, 16000 lbs TOW, Stores

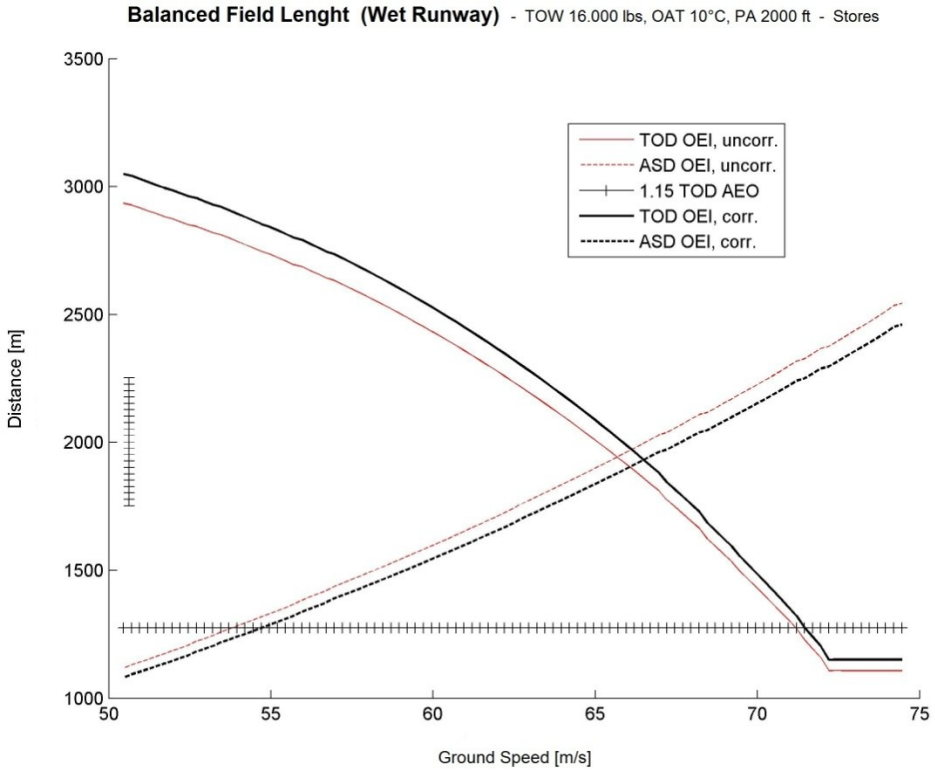

Fig. H.28 Balanced Field Length Plot 10°C OAT, 2000 ft PA, 16000 lbs TOW, Stores

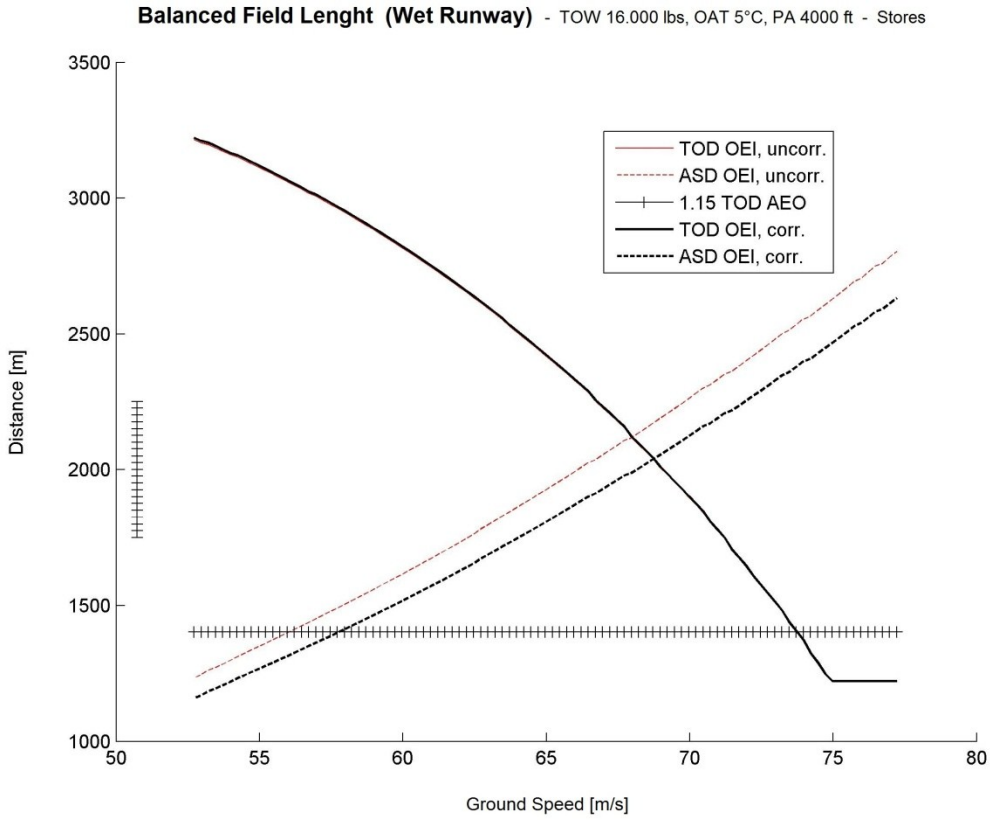

Fig. H.29 Balanced Field Length Plot 5°C OAT, 4000 ft PA, 16000 lbs TOW, Stores

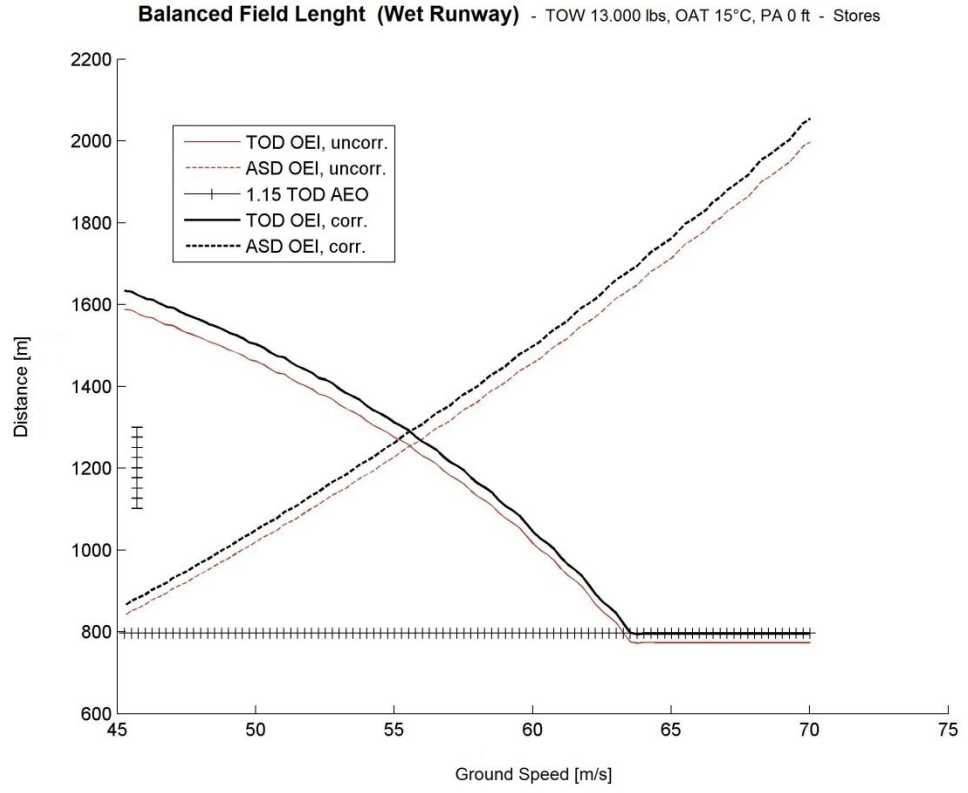

Fig. H.30 Balanced Field Length Plot 15°C OAT, MSL, 13000 lbs TOW, Stores

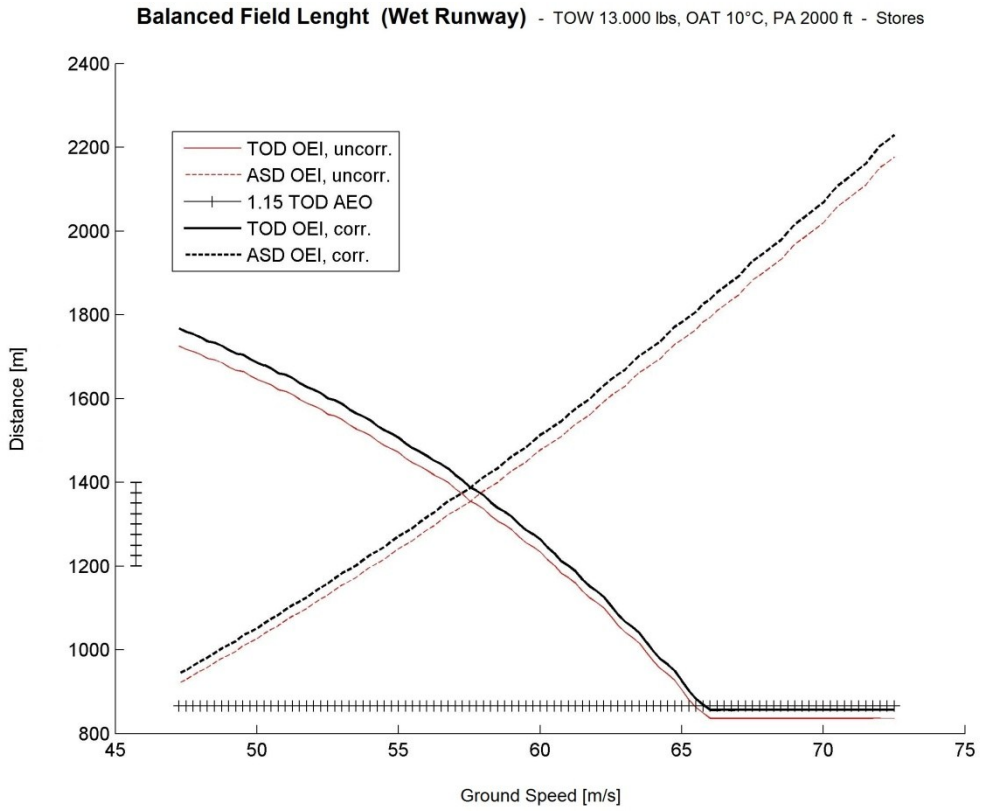

Fig. H.31 Balanced Field Length Plot 10°C OAT, 2000 ft PA, 13000 lbs TOW, Stores

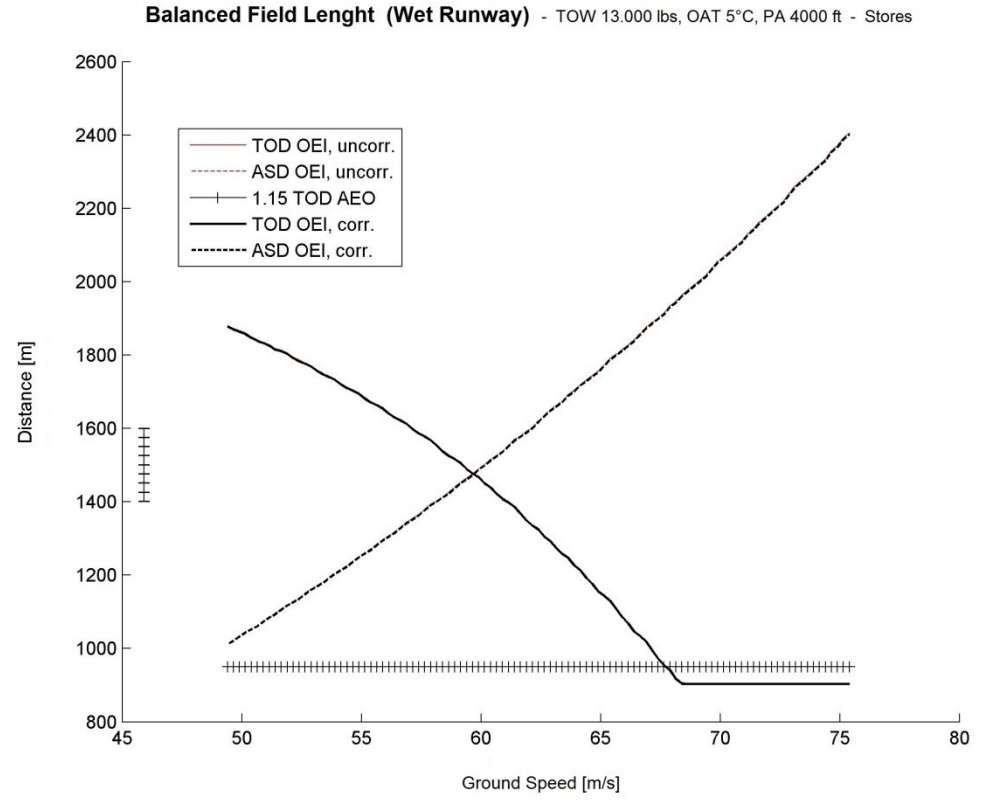

Fig. H.32 Balanced Field Length Plot 5°C OAT, 4000 ft PA, 13000 lbs TOW, Stores

Appendix I
Calibration Factors for individual TOD/ASD

In Section 7.2, the concept of calibration of the individual Accelerate-Stop and Takeoff Curves has been discussed. The calibration concept is used in order to match the Accelerate-Stop and the Takeoff Distances to certified data. This concept therefore provides an individual correction factor for each of the two distances.

Tables I.1 and I.2 present the calibration factors obtained by comparison of the Clean+Wet configuration.

Table I.1 Calibration Factor on the TOD, Comparison of Simulation Result to AFMS Data

-3.9%	-4.9%	-6.9%	-8.2%	-14.8%	-14.6%	-16.4%	19600	0
-7.1%	-7.6%	-8.1%	-7.8%	-10.9%	-16.0%	-14.4%	18500	
-7.3%	-6.8%	-6.0%	-5.2%	-10.2%	-8.8%	-7.9%	16000	
-4.1%	-4.1%	-3.3%	-2.8%	-5.2%	-8.0%	-7.6%	13000	
-7.3%	-8.5%	-13.1%	-13.2%	-6.9%	-	-	19600	2000
-6.7%	-7.4%	-8.4%	-13.2%	-13.6%	-10.8%	-20.2%	18500	
-3.0%	-2.8%	-3.9%	-7.5%	-6.0%	-4.6%	-8.2%	16000	
-1.2%	-0.9%	-2.4%	-3.6%	-6.2%	-9.0%	-8.9%	13000	
-2.1%	-2.4%	-4.6%	2.0%	-	-	-	19600	4000
-11.2%	-12.0%	-11.6%	-8.0%	-0.3%	-9.0%	-	18500	
0.5%	-0.2%	-2.4%	0.1%	-0.8%	-4.4%	-12.2%	16000	
0.5%	0.2%	-1.3%	-2.2%	-0.7%	1.4%	-0.7%	13000	
0	5	10	15	20	25	30	A/C Weight (lbs)	Pressure Altitude (ft)

OAT(°C)

Table I.2 Calibration Factor on the ASD, Comparison of Simulation Result to AFMS Data

6.3%	6.1%	4.8%	4.0%	4.0%	4.9%	6.8%	19600	0
4.6%	4.7%	4.5%	4.8%	2.2%	3.6%	2.2%	18500	
0.8%	1.3%	2.0%	2.7%	1.9%	-0.4%	-2.1%	16000	
-4.1%	-4.1%	-3.3%	-2.8%	-5.2%	-8.0%	-7.6%	13000	
5.4%	4.8%	6.7%	6.9%	5.5%	-	-	19600	2000
6.2%	6.0%	5.4%	6.3%	5.5%	4.9%	-0.9%	18500	
4.2%	4.4%	3.3%	4.0%	0.9%	0.0%	-2.0%	16000	
-1.2%	-0.9%	-2.4%	-3.6%	-6.2%	-9.0%	-8.9%	13000	
10.7%	10.7%	10.9%	12.3%	-	-	-	19600	4000
12.3%	11.9%	9.9%	10.9%	13.6%	-3.8%	-	18500	
6.3%	6.1%	5.8%	6.4%	2.9%	1.0%	-5.5%	16000	
0.5%	0.2%	-1.3%	-2.2%	-0.7%	1.4%	-0.7%	13000	
0	5	10	15	20	25	30	A/C Weight (lbs)	Pressure Altitude (ft)

OAT(°C)

Despite the corrections needed to scale the individual distances appear to be quite high, they do not represent the absolute deviation between the AFMS reference data and the simulation results for BFL and V_1. The absolute deviation to the reference as presented in Tab. 8.6 and 8.7. is much smaller.

The intersection point of the two TOD/ASD graphs determines the final BFL result, and the intersection point location is a function of both individual calibration factors. Hence, the final deviation of BFL and V_1 can be much smaller than the individual calibration factors would suggest.

Figure I.1 shall illustrate this fact. Two arbitrarily selected Balanced Field Length Intersection Charts have been selected to show that the final intersection point of two graphs can be creating conservative final results even if individual calibration factors appear to be not conservative. The original simulation results are shown by the *red graphs*, corrected results are shown by the *black graphs*. When the red graph lies below the black graph, it means that the individual distance had to be scaled up in order to match the AFMS reference value.

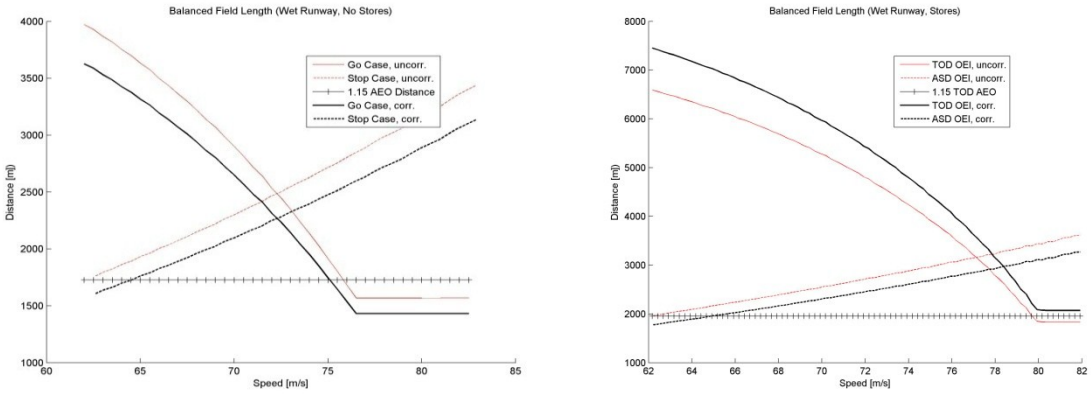

Fig. I.1 Balanced Field Length and V_1 in dependence of individual Correction Factors

No conclusion on the conservatism of the final simulation result can therefore be made when regarding the individual calibration factors alone. Consequently, the analysis of the simulation final results must be based on the absolute deviations to AFMS data, as presented in Tab. 8.6 and 8.7.

Appendix J
Simulation Program Code

The Simulation presented is executable by OCTAVE or MATLAB®. It is necessary to name the functions according to the subtitles used in this Appendix. All functions need to be contained in the same storage location. Furthermore, it is required to provide two Excel files containing the reference BFL and V_1 data. The data must be arranged in a 7x12 matrix as shown in table 8.1. The Excel files must be named as follows:

- Takeoff_Speed_Chart.xls
- Takeoff_Distance_Chart.xls

Upon successful execution, the storage folder will contain a number of output files in .dat format. These are text files that can be imported into common spreadsheet software.
When run for a test case, the simulation produces the following textual output in the workspace.

```
-------------------------------------------

Select one of the following weights from the List, type
1 for: 19600 lbs
2 for: 18500 lbs
3 for: 16000 lbs
4 for: 13000 lbs
Select one of the following Temperature conditions from the List, type
1 for: 0 deg C conditions
2 for: 5 deg C conditions
3 for: 10 deg C conditions
4 for: 15 deg C conditions
5 for: 20 deg C conditions
6 for: 25 deg C conditions
7 for: 30 deg C conditions
Select one of the following altitude conditions from the List, type
1 for: pressure altitude of 0 feet
2 for: pressure altitude of 2000 feet
3 for: pressure altitude of 4000 feet

TOM selected [lbs]: 18500
Temperature conditions selected : 15deg C
Altitude conditions selected : 0 feet pressure altitude

All speeds shown in Matlab Execution File are TAS, all speeds stored in Excel are EAS
Reference v1 speed from GFD handbook (wet) : 130 knots
Reference T/O distance from GFD handbook (wet) : 6636 feet

vEF for the forces graphics [m/s] to verify with the graphs: 66.3633

vEF at which the iteration loop will start [kts]: 109
```

New Simulation (wet)
vs (kts): 115.3333
vR (kts): 146.5769
v2 (kts): 149.0769
Check vEFmax=V2 of vEF= 149.3348
reached after increment 84

Results without stores and wet runway [kts](uncorrected):
v1: 127,4946
s: 6662.5529

Correction factor EF: 1.0779
Correction factor AS: 0.95195

Results without stores and wet runway [kts](corrected):
v1: 129.4104
s: 6638.1091

Correction accuracy: 0.99683

vs (kts): 121.3333
vR (kts): 146.5769
v2 (kts): 149.0769
Check vEFmax = V2 ?: 149.3348
reached after increment 84

With stores and wet runway [kts](uncorrected):
v1: 140.1296
s: 8158.8166
Correction Factor Go-Case considered: 1.0779
Correction Factor Stop-Case considered: 0.95195

Results with stores and wet runway [kts](corrected):
v1: 142.0734
s: 8017.8775
Simulation Performed

J.1 Main Function

```
% Takeoff_BFL
%Florian Ehrig, HAW Hamburg
%Main Function for the Takeoff Performance Calculation
%Basic Input User Interface provisions included in the code

clear all
 disp ('  ')
disp ('-------------------------------------------')
disp ('  ')

%Input of Reference Data
v1_man_vector = xlsread('Takeoff_Speed_Chart.xls');
sbf_man_vector = xlsread('Takeoff_Distance_Chart.xls');

%Preparation of storage variables
thrustsetting_vector = zeros(12,7);
delta_isa_vector = zeros(12,7);
theta_isa_vector = zeros(12,7);
sigma_isa_vector = zeros(12,7);
delta_density_vector = zeros(12,7);
NoIntersectionGraphsNoStores = zeros(12,7);
sbf_nostores_sim_vector_un = zeros(12,7);
v1_nostores_sim_vector_un = zeros(12,7);
NoIntersectionGraphsStores = zeros(12,7);
sbf_sim_vector_un = zeros(12,7);
v1_sim_vector_un = zeros(12,7);
NoIntersectionGraphsStores = zeros(12,7);
sbf_sim_vector = zeros(12,7);
v1_sim_vector = zeros(12,7);
AS_sim_correctionvector = zeros(12,7);
EF_sim_correctionvector = zeros(12,7);


%Definition of a set of global variables
global wet;
global v1;
global makeplots;

%Configuration Options
global stores;
global graphics

%Output Options
global ploter;
global makeplots
global plot_s;
global isa_selection; %The OAT in C
global alt_selection;  %the pressure altitude in ft
global isa_selection_variable; %the selection variable for temperature con-
ditions from a grid
global alt_selection_variable; %the selection variable for pressure alt
from a grid
global weight_selection_variable
global m_lbs; %Aircraft mass in lbs
global thrustsetting
```

```
% USER INTERFACE
%Was programmed if the program should be used in flight operations by
%non-trained personnel
%These lines must be activated before they are useable

% Use 1 for Yes, 0 for No

%DEFINITION OF WET OR DRY CASE
%wet = input('Calculate wet case? Then type in 1, else type 0 for dry case
:  ');

 wet = 1; %default setting

 disp ('  ')


%makeplots = input ('Would you like to create Force and Distance Plots?
Y=1, N=0  :');
 makeplots = 1; %default setting


keepfigures = 0; %used to close plots automatically after each loop, set 0
to close figures automatically

calculatenostores=1; %Set '1' to calculate results also for the aircraft
without under-wing stores

%makemanualinputs = input ('Would you like to select environmental parame-
ters manually? Y=1, N=0 :');
makemanualinputs = 0; %default setting, a loop is used to cycle environmen-
tal variables
%IF MANUAL INPUT SHALL BE USED, THIS VARIABLE MUST BE SET TO 1 AND THE
%VARIABLES LOOP BE DEACTIVATED

%Manual Selection of the Envioronmental Parameters if selected
if makemanualinputs ==1
    disp (' ')
disp ('Ensure the Automatic Variables Cycling has been outcommented in the
source code')
   disp (' ')
end

%Definition of the TOW variables vector, data is in lbs
m_lbs_vector = [19600 ; 18500 ; 16000 ; 13000];
disp ('Select one of the following weights from the List, type ')

    disp(['1 for: ', num2str(m_lbs_vector (1)), ' lbs'])
    disp(['2 for: ', num2str(m_lbs_vector (2)), ' lbs'])
    disp(['3 for: ', num2str(m_lbs_vector (3)), ' lbs'])
    disp(['4 for: ', num2str(m_lbs_vector (4)), ' lbs'])

if makemanualinputs ==1
    weight_selection_variable = input ('Your Input for weight selection va-
riable: ');
end

%Definition of the OAT variables vector, data is in degress Celsius
isa_vector = [0 ; 5; 10; 15; 20 ; 25; 30];
```

```
  disp ('Select one of the following Temperature conditions from the List,
type ')

    disp(['1 for: ', num2str(isa_vector (1)), ' deg C conditions'])
    disp(['2 for: ', num2str(isa_vector (2)), ' deg C conditions'])
    disp(['3 for: ', num2str(isa_vector (3)), ' deg C conditions'])
    disp(['4 for: ', num2str(isa_vector (4)), ' deg C conditions'])
    disp(['5 for: ', num2str(isa_vector (5)), ' deg C conditions'])
    disp(['6 for: ', num2str(isa_vector (6)), ' deg C conditions'])
    disp(['7 for: ', num2str(isa_vector (7)), ' deg C conditions'])

if makemanualinputs ==1
    isa_selection_variable = input ('Your Input for ISA selection variable:
');
end

%Definition of the PA variables vector, data is in ft
alt_vector = [0 ; 2000 ; 4000];
  disp ('Select one of the following altitude conditions from the List,
type ')

    disp(['1 for: pressure altitude of ', num2str(alt_vector (1)), '
feet'])
    disp(['2 for: pressure altitude of ', num2str(alt_vector (2)), '
feet'])
    disp(['3 for: pressure altitude of ', num2str(alt_vector (3)), '
feet'])
if makemanualinputs ==1
    alt_selection_variable = input ('Your Input for altitude selection va-
riable: ');
end

%Automatic Cycling of the Environmental Parameters
for weight_selection_variable = 1:4;
for alt_selection_variable = 1:3;
for isa_selection_variable = 1:7;



disp (' ')
disp (' ')
disp (' ')



%Selecting input variables for the simulation

%A/C Mass definition

    m_lbs = m_lbs_vector (weight_selection_variable);

    disp(['TOM selected [lbs]: ', num2str(m_lbs)])
  disp ('  ')


% Temperature OAT conditions
% The isa_vector contains absolute temperatures - OAT
```

```
    isa_selection = isa_vector (isa_selection_variable);
    disp(['Temperature conditions selected : ', num2str(isa_selection),
'deg C'])
  disp ('  ')


% Altitude selection

    alt_selection = alt_vector (alt_selection_variable);
    disp(['Altitude conditions selected : ', num2str(alt_selection), ' feet
pressure altitude'])
  disp ('  ')


disp ('All speeds shown in Matlab Execution File are TAS, all speeds stored
in Excel are EAS')

%Parameter Definition Function is called with the Environmental Variables
defined
Parameters_Learjet %input of parameters

%Cross Check of Relative Ratio Parameters
delta_isa_vector ((weight_selection_variable+(alt_selection_variable-
1)*4),isa_selection_variable) = delta_p_isa;
theta_isa_vector ((weight_selection_variable+(alt_selection_variable-
1)*4),isa_selection_variable) = theta_isa;
sigma_isa_vector ((weight_selection_variable+(alt_selection_variable-
1)*4),isa_selection_variable) = sigma_isa;

%Reference V1 Speed Selection
v1_man = v1_man_vector ((weight_selection_variable+(alt_selection_variable-
1)*4),isa_selection_variable);

if wet == 0
    v1_man = v1_man+7; %approximation to match the corerction chart GFD
reference page 4
end

if v1_man < 109
    v1_man = 109; %minimum control speed is 109 kts
end


if wet ==1
    disp(['Reference v1 speed from GFD handbook (wet) : ', num2str(v1_man),
' knots'])
else
    disp(['Reference v1 speed from GFD handbook (dry) : ', num2str(v1_man),
' knots'])
end

%CAS-IAS Correction
v1_man = v1_man-ias_cas_correction;


v1_man_EAS = v1_man*0.514444444; %Conversion into m/s
v1_man = v1_man_EAS/sqrt(sigma_isa); %CONVERSION INTO TAS used by the simu-
lation
```

```
%Reference BFL selection, Data stored in the Excel File must be wet BFL da-
ta
sbf_man = sbf_man_vector
((weight_selection_variable+(alt_selection_variable-
1)*4),isa_selection_variable);

disp(['Reference T/O distance from GFD handbook (wet) : ',
num2str(sbf_man), ' feet'])

%wet correction factors acc. to Wet Data Addendum

wet_corr_fact_dist_vector = [1.2 ; 1.2 ; 1.2 ; 1.35]; %Applied Wet Data Ad-
dendum Data (adjusted for V1_min = 109 KIAS @ TOW 13.000lbs)
wet_korr_fact_dist = wet_corr_fact_dist_vector(weight_selection_variable);

%Correction of the Wet Data from the Excel file to Dry Data acc. to Wet
%Data Addendum, if necessary
if wet ==0
sbf_man = sbf_man/wet_korr_fact_dist;
disp(['Reference T/O distance from GFD handbook (dry) : ',
num2str(sbf_man), ' feet'])
end

sbf_man = sbf_man*0.3048; %conversion to m

%A plot of various forces is performed at the V1 speed from the Handbook
graphics=1; %defines the identifier for a graphics plot test run

%The speed at which the engine should fail for a graphic output of the
forces during the takeoff run
 disp ('  ')
vEF_graphics = v1_man; %m/s
disp(['vEF for the forces graphics [m/s] to verify with the graphs: ',
num2str(vEF_graphics)])

disp ('  ')

%The speed at which the iteration begin with the iteration for the simula-
tion is 20 knots below the manual v1
vEF_simulation_start = v1_man/0.514444444-20; %kts
disp(['vEF at which the iteration loop will start [kts]: ',
num2str(vEF_simulation_start)])

disp ('  ')



%-------------------------------------------------------------------------
%Calculation of Results for the Aircraft in Clean Configuration (no
%under-wing stores) to obtain the correction factors



if calculatenostores ==1
```

```
stores = 0;
disp(' ')

if wet == 1
disp('New Simulation (wet)')
else
disp('New Simulation (dry)')
end

%Plotting Information for the Simulation, if plots shall be created
if makeplots == 1
 ploter = 0;
 plot_s = 0;
end

assignin('base','t_Dec',120)

if makeplots == 1
ploter = 1;
h=figure('Visible','off');
end

%The Takeoff Distance Function is called to plot the forces acting on the
%aircraft
vEF = vEF_graphics; % Speed selected to display the engine failure in the
forces plot
Take_off_1Eng(vEF_graphics);

if makeplots == 1
legend('Impingement Drag','Thrust', 'Runway Friction', 'Displ.
Drag','Aerodynamic Drag', 'Lift', 'Skin Friction Drag', 'Location','Best')
xlabel('Speed [m/s]')
ylabel('Forces [N]')

if wet == 1
    title('Comparision of Forces in Go Case (Wet Runway, No Stores)')
else
    title('Comparision of Forces in Go Case (Dry Runway, No Stores)')
end
filename = (['Forces_TO_at_Weight(lbs)-', num2str(m_lbs),'-Temp(C)-',
num2str(isa_selection),'-Alt(ft)-', num2str(alt_selection), 'no_stores']);
print('-djpeg',  '-r300', filename);
ploter = 0;
plot_s = 1;


end
v1 = 0;
if makeplots ==1
       h=figure('Visible','off');
end

%The Accelerate-Stop Distance Function is called to plot the forces acting
on the
%aircraft
Take_off_Acc_Stop(vEF_graphics); %Function called for a single value, vEF

if makeplots == 1
```

```
legend('Impingement Drag','Thrust', 'Runway Friction',  'Displ.
Drag','Aerodynamic Drag', 'Lift',  'Skin Friction Drag','Location','Best')
xlabel('Time [sec]')
ylabel('Forces [N]')

if wet == 1
    title('Comparision of Forces in Stop Case (Wet Runway, No Stores)')
else
    title('Comparision of Forces in Stop Case (Dry Runway, No Stores)')
end

filename = (['Forces_AS_at_Weight(lbs)-', num2str(m_lbs),'-Temp(C)-',
num2str(isa_selection),'-Alt(ft)-', num2str(alt_selection), 'no_stores']);
print('-djpeg',  '-r300', filename);
plot_s = 0;
end

graphics=0;
%-------------------------------------------------------------------------
%CALCULATION OF THE BFL FOR THE CLEAN AIRCRAFT

vEF =vEF_simulation_start*0.514444444; % sets the start speed for the fol-
lowing vEF iteration loop [m/s]

if makeplots == 1
h=figure('Visible','off');
hold on
end

s_TO_temp = 0;

%Displaying the reference speeds for the selected conditions
disp(['vs (kts): ', num2str(vs_kts)])
 disp(['vR (kts): ', num2str(vR_kts)])
 disp(['v2 (kts): ', num2str(v2_kts)])


%calculation of V1 and TOD/ASD (pure simulation) in a loop
%The vEF is incrementally increased and the resulting TOD/ASD stored in the
%EF/ASD Array

for i=1:200
    assignin('base','t_Dec',120)

    s_TO = Take_off_1Eng (vEF); %Determination of the TOD
    s_TO_temp = s_TO;

if s_TO<0
        s_TO = 0;
end

    EF(1,i) = s_TO; %first row in EF array: distances at the respective the
vEF per iteration pair (i)


if s_TO>EF(1,1)
        s_TO=0;
```

```
         EF(1,i) = s_TO;
         disp (['maximum reached'])
end

    EF(2,i) = vEF;  %second row in EF array: speeds

    v1 = 0;

    s_AS = Take_off_Acc_Stop (vEF); %Determination of the ASD

%Plus 2 seconds at V1 increment for ASD
    s_AS = s_AS+cs_transitiontime*vEF;

    AS(1,i) = s_AS; %first row in AS vector: distances needed for the vEF
per iteration pair (i)
    AS(2,i) = vEF; %second row in EF array: speeds

%increasing the vEF incrementally for 0.25 m/s each loop until V2 is
reached
if vEF < v2
        vEF = vEF+0.25;
else
          disp(['Check vEFmax=V2 of vEF= ', num2str(vEF/0.514444444)])
          disp(['reached after increment ', num2str(i)])
break%vEF in this consideration can only be smaller than v2
end
end

% Calculate balanced V1 of simulation

for i=1:length(AS) %the loop will run for as many steps as have been
created in the previous loop

    diff = EF(1,i) - AS(1,i);
if diff < 0
        step = i; %this is the step at which (slowly before) the AS and EF
graphs intersected
break
elseif diff > 0
        step = 1;
end
end

if step == 1;
   disp ('The curves are not intersecting (or another error)')
%The combination of external variables leading to no graph intersection
%shall be marked with a 1 in an outputted table

NoIntersectionGraphsNoStores
((weight_selection_variable+(alt_selection_variable-
1)*4),isa_selection_variable) = 1;

end



%Determination of the function values at the intersection point for BFL and
V1
v1_sim = EF(2, step);
```

```
sbf_sim = AS(1, step);


%Due to Minimum Control Speed at 109 kts EAS, the v1 cannot be lower than
109 kts EAS
%This has an impact on the Accelerate-Go-Distance, as v1 is artificially
increased to a minimum of 109 kts EAS

v_min_ctrl = (((109-ias_cas_correction)*0.514444444)/sqrt(sigma_isa)); %TAS
in m/s

if v1_sim < v_min_ctrl %if minimum control speed is undershot, V1 is set to
minimum control speed and the complete plot rescaled for an accurate BFL
calculation

%An adaption of the respective TOD for the artificially increased ASD
%yields the new BFL for the condition V1=V_min_ctrl

     EF_v1_min_ctrl = interp1(EF(2,:),EF(1,:),v_min_ctrl);
     AS_v1_min_ctrl = interp1(AS(2,:),AS(1,:),v_min_ctrl);
     EF_korr_min_ctrl = AS_v1_min_ctrl/EF_v1_min_ctrl;

%the EF vector distances are multiplied with the correction
%factors
     EF(1,:) = EF(1,:) * EF_korr_min_ctrl;

% Calculate balanced V1 of simulation with V1 = v_min_ctrl
for i=1:length(AS) %the loop will run for as many steps as have been
created in the previous loop

    diff = EF(1,i) - AS(1,i);
if diff < 0
        step = i; %this is the step at which (slowly before) the AS and EF
graphs intersected
break
elseif diff > 0
        step = 1;
end
end

if step == 1;
   disp ('The curves are not intersecting (or another error)')
%The combination of external variables leading to no graph intersection
%shall be marked with a 1 in a table
NoIntersectionGraphsStores
((weight_selection_variable+(alt_selection_variable-
1)*4),isa_selection_variable) = 1;
end

%Determination of the function values at the intersection point for BFL and
%V1
v1_sim = v_min_ctrl;
sbf_sim = AS(1, step);

end
```

```
if makeplots == 1
%Plotting pure simulation results in red
plot (EF(2,:),EF(1,:),'-r')
plot (AS(2,:),AS(1,:),'--r')

end

%storage of the results for clean+wet uncorrected results in two arrays

sbf_nostores_sim_vector_un
((weight_selection_variable+(alt_selection_variable-
1)*4),isa_selection_variable) = sbf_sim/0.3048;
v1_nostores_sim_vector_un
((weight_selection_variable+(alt_selection_variable-
1)*4),isa_selection_variable) =
((v1_sim/0.514444444)*sqrt(sigma_isa)+ias_cas_correction); %CONVERTED INTO
KTS AND EAS

disp(' ')
if wet == 1
        disp('Results without stores and wet runway [kts](uncorrected):')
else
        disp('Results without stores and dry runway [kts](uncorrected):')
end
    disp(['v1: ', num2str(v1_sim/0.514444444)])
    disp(['s: ', num2str(sbf_sim/0.3048)])

%Calculation of the 1.15 AEO Takeoff Distance

graphics =1;
s_TO_AEO = Take_off_AEO(v1_sim); %The all engines operating Distance (1,15
factor included)
plottingscale = length(EF(2,:)); %defines the boundaries of the vector to
be plotted, to fit into the figure
s_TO_AEO_vector = rand (plottingscale,1); %random vector of correct size
for c=1:plottingscale
    s_TO_AEO_vector(c)=s_TO_AEO; %random vector gets filled with static
distance value
end

if makeplots ==1
plot (EF(2,:), s_TO_AEO_vector, '-+k')
end

graphics =0;

% Calculate simulation correction by interpolation between the results con-
tained
%in the AS and EF array to obtain a factor that scales each graph towards
% the reference manual (handbook) values for the distance

EF_v1_man = interp1(EF(2,:),EF(1,:),v1_man);
     EF_korr = sbf_man/EF_v1_man;
AS_v1_man = interp1(AS(2,:),AS(1,:),v1_man);
     AS_korr = sbf_man/AS_v1_man;

%the EF and AS vector distances are multiplied with the correction
%factors to yield the corrected graps
```

```
     EF(1,:) = EF(1,:) * EF_korr;
     AS(1,:) = AS(1,:) * AS_korr;
if makeplots == 1
     plot (EF(2,:),EF(1,:),'-k','LineWidth',1.2)
     plot (AS(2,:),AS(1,:),'--k','LineWidth',1.2)
end

    disp(' ')
    disp(['Correction factor EF: ', num2str(EF_korr)])
    disp(['Correction factor AS: ', num2str(AS_korr)])

%calculating the v1 again based on the scaled-to-distance AS/EF vecors
% balanced V1 of corrected simulation vector results

for i=1:length(AS) %the loop will run for as many steps as have been
created in the previous loop

    diff = EF(1,i) - AS(1,i);
if diff < 0
        step = i; %this is the step at which (slowly before) the AS and EF
graphs intersected
break
elseif diff > 0
        step = 1;
end
end

if step == 1;
   disp ('The curves are not intersecting (or another error)')

%The combination of external variables leading to no graph intersection
%shall be marked with a 1 in a table
NoIntersectionGraphsStores
((weight_selection_variable+(alt_selection_variable-
1)*4),isa_selection_variable) = 1;
end

v1_sim = EF(2, step);
sbf_sim = AS(1, step);

disp(' ')
if wet == 1
        disp('Results without stores and wet runway [kts](corrected):')
else
        disp('Results without stores and dry runway [kts](corrected):')
end
    disp(['v1: ', num2str(v1_sim/0.514444444)])
    disp(['s: ', num2str(sbf_sim/0.3048)])

%the correction of the distances is now cross checked
%by comparing the simulation result after the correction to the AFMS refer-
ence data

wet_korr = v1_man/v1_sim;
disp(' ')
    disp(['Correction accuracy: ', num2str(wet_korr)])

disp(' ')
```

```
if makeplots == 1
legend('TOD OEI, uncorr.','ASD OEI, uncorr.', '1.15 TOD AEO', 'TOD OEI,
corr.', 'ASD OEI, corr.', 'Location','Best')
xlabel('Speed [m/s]')
ylabel('Distance [m])')


if wet == 1
    title('Balanced Field Length (Wet Runway, No Stores)')
else
    title('Balanced Field Length (Dry Runway, No Stores)')
end
filename = (['BFL_at_Weight(lbs)-', num2str(m_lbs),'-Temp(C)-',
num2str(isa_selection),'-Alt(ft)-', num2str(alt_selection), 'no_stores']);
print('-djpeg',  '-r300', filename);
end


 clear EF
 clear AS
 clear s_TO_AEO
 clear vEF

 v1_sim = 0;
sbf_sim = 0;
end
%-------------------------------------------------------------------------

%If no-stores case has not been calculated, there are no correction factors
if calculatenostores ==0
    EF_korr=1;
    AS_korr=1;
end
%-------------------------------------------------------------------------
%Consideration of the aircraft WITH STORES
%Not all comments made in the first section of the code are repeated, when
%the calculations are performed in the way that was used for the clean
%aircraft

graphics = 1;
if makeplots == 1

hold on
end

stores = 1;
Parameters_Learjet

 disp(['vs (kts): ', num2str(vs_kts)])
disp(['vR (kts): ', num2str(vR_kts)])
 disp(['v2 (kts): ', num2str(v2_kts)])


%Plot of the Forces
if makeplots == 1
 ploter = 0;
 plot_s = 0;
end
```

```
assignin('base','t_Dec',120)
if makeplots == 1
ploter = 1;

h=figure('Visible','off');
hold on
end
vEF=vEF_graphics; %VEF at which the engine failure is displayed

%For Forces plot, the forces of an engine stop at vEF_graphics m/s are con-
sidered
Take_off_1Eng(vEF_graphics); %Acceleration Case

if makeplots == 1
legend('Thrust', 'Runway Friction','Displ. Drag', 'Aerodynamic Drag',
'Lift', 'Impingement Drag',  'Skin Friction Drag','Location','Best')
xlabel('Speed [m/s]')
ylabel('Forces [N]')

if wet == 1
    title('Comparision of Forces in Go Case (Wet Runway, Stores)')
else
    title('Comparision of Forces in Go Case (Dry Runway, Stores)')
end
filename = (['Forces_TO_at_Weight(lbs)-', num2str(m_lbs),'-Temp(C)-',
num2str(isa_selection),'-Alt(ft)-', num2str(alt_selection), 'stores']);
print('-djpeg',  '-r300', filename);

%Configuration of the Graphics Engine
ploter = 0;
plot_s = 1;

h=figure('Visible','off');
end
v1 = 0;
Take_off_Acc_Stop(vEF_graphics); %Deceleration Case

if makeplots == 1
legend('Impingement Drag','Thrust', 'Runway Friction','Displ.
Drag','Aerodynamic Drag', 'Lift', 'Skin Friction Drag', 'Location','Best')
xlabel('Time [sec]')
ylabel('Forces [N]')

if wet == 1
    title('Comparision of Forces in Stop Case (Wet Runway, Stores)')
else
    title('Comparision of Forces in Stop Case (Dry Runway, Stores)')
end

filename = (['Forces_AS_at_Weight(lbs)-', num2str(m_lbs),'-Temp(C)-',
num2str(isa_selection),'-Alt(ft)-', num2str(alt_selection), 'stores']);
print('-djpeg',  '-r300', filename);

plot_s = 0;
graphics = 0;
h=figure('Visible','off');
hold on
end
```

```
s_TO_temp = 0;

 clear EF
 clear AS

vEF =vEF_simulation_start*0.514444444; % Inital vEF speed for iteration of
TOD and ASD [m/s]

%calculation of v and s (pure simulation)
for i=1:200
    assignin('base','t_Dec',120)
    s_TO = Take_off_1Eng (vEF);%starts with vEF initial, see above
    s_TO_temp = s_TO;
if s_TO<0
        s_TO = 0;
end

    EF(1,i) = s_TO;%first row in EF vector: distances needed for the vEF
per iteration pair (i)
    EF(2,i) = vEF; %second row in EF vector: speeds

    v1 = 0;
    s_AS = Take_off_Acc_Stop (vEF);

%Plus 2 seconds at V1 increment
    s_AS = s_AS+cs_transitiontime*vEF;

    AS(1,i) = s_AS;%first row in AS vector: distances needed for the vEF
per iteration pair (i)
    AS(2,i) = vEF; %second row in AS vector: speeds

if vEF < v2
        vEF = vEF+0.25; %increasing the vEF incrementally for 0.25 m/s each
loop
else
       disp(['Check vEFmax = V2 ?: ', num2str(vEF/0.514444444)])
       disp(['reached after increment ', num2str(i)])
break%vEF in this consideration can only be smaller than v2
end
end

%Calculate balanced V1 of simulation
for i=1:length(AS) %the loop will run for as many steps as have been
created in the previous loop

    diff = EF(1,i) - AS(1,i);
if diff < 0
        step = i; %this is the step at which (slowly before) the AS and EF
graphs intersected
break
elseif diff > 0
        step = 1;
end
end

if step == 1;
   disp ('The curves are not intersecting (or another error)')
%The combination of external variables leading to no graph intersection
```

```
%shall be marked with a 1 in a table
NoIntersectionGraphsStores
((weight_selection_variable+(alt_selection_variable-
1)*4),isa_selection_variable) = 1;
end

v1_sim = EF(2, step);
sbf_sim = AS(1, step);


%Correction of the BFL in case of V1<Minimum Control Speed
v_min_ctrl = (((109-ias_cas_correction)*0.514444444)/sqrt(sigma_isa)); %TAS
in m/s
if v1_sim < v_min_ctrl

     EF_v1_min_ctrl = interp1(EF(2,:),EF(1,:),v_min_ctrl);
     AS_v1_min_ctrl = interp1(AS(2,:),AS(1,:),v_min_ctrl);
     EF_korr_min_ctrl = AS_v1_min_ctrl/EF_v1_min_ctrl;

%the EF vector distances are multiplied with the correction
%factors
     EF(1,:) = EF(1,:) * EF_korr_min_ctrl;

% Calculate balanced V1 of simulation with V1 = v_min_ctrl
for i=1:length(AS) %the loop will run for as many steps as have been
created in the previous loop

    diff = EF(1,i) - AS(1,i);
if diff < 0
        step = i; %this is the step at which (slowly before) the AS and EF
graphs intersected
break
elseif diff > 0
        step = 1;
end
end

if step == 1;
   disp ('The curves are not intersecting (or another error)')
NoIntersectionGraphsStores
((weight_selection_variable+(alt_selection_variable-
1)*4),isa_selection_variable) = 1;
end

v1_sim = v_min_ctrl;
sbf_sim = AS(1, step);
end

%Plotting pure simulation results in red
if makeplots == 1
 plot (EF(2,:),EF(1,:),'-r')
 plot (AS(2,:),AS(1,:),'--r')
end

%Storage of the Simulation Results in two Arrays
sbf_sim_vector_un ((weight_selection_variable+(alt_selection_variable-
1)*4),isa_selection_variable) = sbf_sim/0.3048;
```

```
v1_sim_vector_un ((weight_selection_variable+(alt_selection_variable-
1)*4),isa_selection_variable) =
((v1_sim/0.514444444)*sqrt(sigma_isa)+ias_cas_correction);

%Calculation of the 1.15 AEO Takeoff Distance
graphics =1;
s_TO_AEO = Take_off_AEO(v1_sim); %The all engines operating Distance (1,15
factor included)
plottingscale = length(EF(2,:)); %defines the boundaries of the vector to
be plotted, to fit into the figure
s_TO_AEO_vector = rand (plottingscale,1); %random vector of correct size
for c=1:plottingscale
    s_TO_AEO_vector(c)=s_TO_AEO; %random vector gets filled with static
distance value
end

if makeplots ==1
plot (EF(2,:), s_TO_AEO_vector, '-+k')
end
graphics=0;


disp(' ')
if wet == 1
        disp('With stores and wet runway [kts](uncorrected):')
else
        disp('With stores and dry runway [kts](uncorrected):')
end
    disp(['v1: ', num2str(v1_sim/0.514444444)])
    disp(['s: ', num2str(sbf_sim/0.3048)])



%Correction Factors calculated from the CLEAN Aircraft are now applied to
%the aircraft with STORES

     EF(1,:) = EF(1,:) * EF_korr;
     AS(1,:) = AS(1,:) * AS_korr;
disp(['Correction Factor Go-Case considered: ', num2str(EF_korr)])
disp(['Correction Factor Stop-Case considered: ', num2str(AS_korr)])

%Plotting corrected simulation results
if makeplots == 1
     plot (EF(2,:),EF(1,:),'-k','LineWidth',1.2)
     plot (AS(2,:),AS(1,:),'--k','LineWidth',1.2)
end

%Calculating balanced V1 of corrected simulation
for i=1:length(AS) %the loop will run for as many steps as have been
created in the previous loop

    diff = EF(1,i) - AS(1,i);
if diff < 0
        step = i; %this is the step at which (slowly before) the AS and EF
graphs intersected
break
elseif diff > 0
        step = 1;
end
```

```
end

if step == 1;
   disp ('The curves are not intersecting (or another error)')
NoIntersectionGraphsStores
((weight_selection_variable+(alt_selection_variable-
1)*4),isa_selection_variable) = 1;
end
  disp(' ')
if wet == 1
        disp('Results with stores and wet runway [kts](corrected):')
else
        disp('Results with stores and dry runway [kts](corrected):')
end


v1_sim = EF(2, step);
sbf_sim = AS(1, step);

    disp(['v1: ', num2str(v1_sim/0.514444444)])
    disp(['s: ', num2str(sbf_sim/0.3048)])


%storage of the corrected results for stores+wet in two arrays

sbf_sim_vector ((weight_selection_variable+(alt_selection_variable-
1)*4),isa_selection_variable) = sbf_sim/0.3048;
v1_sim_vector ((weight_selection_variable+(alt_selection_variable-
1)*4),isa_selection_variable) =
((v1_sim/0.514444444)*sqrt(sigma_isa)+ias_cas_correction);


AS_sim_correctionvector
((weight_selection_variable+(alt_selection_variable-
1)*4),isa_selection_variable) = AS_korr;
EF_sim_correctionvector
((weight_selection_variable+(alt_selection_variable-
1)*4),isa_selection_variable) = EF_korr;

if makeplots == 1
legend('TOD OEI, uncorr.','ASD OEI, uncorr.', '1.15 TOD AEO', 'TOD OEI,
corr.', 'ASD OEI, corr.', 'Location','Best')
xlabel('Speed [m/s]')
ylabel('Distance [m])')

if wet == 1
    title('Balanced Field Length (Wet Runway, Stores)')
else
    title('Balanced Field Length (Dry Runway, Stores)')
end
filename = (['BFL_at_Weight(lbs)-', num2str(m_lbs),'-Temp(C)-',
num2str(isa_selection),'-Alt(ft)-', num2str(alt_selection), 'stores']);
print('-djpeg',  '-r300', filename);
end

if keepfigures == 0;
close all
end
```

```
end
end
end


%Calculation of the Deviations in percent

simulation_result_vector_distance = sbf_nostores_sim_vector_un;
refererence_result_vector_distance = sbf_man_vector;
simulation_result_vector_speed = v1_nostores_sim_vector_un;
refererence_result_vector_speed = v1_man_vector;

simulation_result_distance = simulation_result_vector_distance ([1 2 3 4 5
6 7 8 9 10 11 12], [1 2 3 4 5 6 7]);
refererence_result_distance = refererence_result_vector_distance ([1 2 3 4
5 6 7 8 9 10 11 12], [1 2 3 4 5 6 7]);
simulation_result_speed = simulation_result_vector_speed ([1 2 3 4 5 6 7 8
9 10 11 12], [1 2 3 4 5 6 7]);
refererence_result_speed = refererence_result_vector_speed ([1 2 3 4 5 6 7
8 9 10 11 12], [1 2 3 4 5 6 7]);

Percentual_Deviation_Distances = zeros(12,7);
Percentual_Deviation_Speeds = zeros(12,7);

Percentual_Deviation_Distances = (simulation_result_distance - refere-
rence_result_distance)./refererence_result_distance;
Percentual_Deviation_Speeds = (simulation_result_speed - refere-
rence_result_speed)./refererence_result_speed;


%Storage of the results

fid = fopen('isa_delta.dat', 'wt');
fprintf(fid, '%f %f %f %f %f %f %f \n', delta_isa_vector(:,:)');
fclose(fid);

fid = fopen('isa_theta.dat', 'wt');
fprintf(fid, '%f %f %f %f %f %f %f \n', theta_isa_vector(:,:)');
fclose(fid);

fid = fopen('isa_sigma.dat', 'wt');
fprintf(fid, '%f %f %f %f %f %f %f \n', sigma_isa_vector(:,:)');
fclose(fid);

fid = fopen('NoIntersectionGraphsNoStores.dat', 'wt');
fprintf(fid, '%f %f %f %f %f %f %f \n', NoIntersectionGraphsNoS-
tores(:,:)');
fclose(fid);

fid = fopen('Takeoff_Speed_Chart.dat', 'wt');
fprintf(fid, '%f %f %f %f %f %f %f \n', v1_man_vector(:,:)');
fclose(fid);

fid = fopen('Takeoff_Distance_Chart.dat', 'wt');
fprintf(fid, '%f %f %f %f %f %f %f \n', sbf_man_vector(:,:)');
fclose(fid);
```

```
fid = fopen('Takeoff_Distance_Chart_NoStores_Results_uncorrected.dat',
'wt');
fprintf(fid, '%f %f %f %f %f %f %f \n', sbf_nostores_sim_vector_un(:,:)');
fclose(fid);

fid = fopen('Takeoff_Speed_Chart_NoStores_Results_uncorrected.dat', 'wt');
fprintf(fid, '%f %f %f %f %f %f %f \n', v1_nostores_sim_vector_un(:,:)');
fclose(fid);

fid = fopen('NoIntersectionGraphsStores.dat', 'wt');
fprintf(fid, '%f %f %f %f %f %f %f \n', NoIntersectionGraphsStores(:,:)');
fclose(fid);

fid = fopen('Takeoff_Distance_Chart_Stores_Results_uncorrected.dat', 'wt');
fprintf(fid, '%f %f %f %f %f %f %f \n', sbf_sim_vector_un(:,:)');
fclose(fid);

fid = fopen('Takeoff_Speed_Chart_Stores_Results_uncorrected.dat', 'wt');
fprintf(fid, '%f %f %f %f %f %f %f \n', v1_sim_vector_un(:,:)');
fclose(fid);

fid = fopen('Takeoff_Distance_Chart_Stores_Results.dat', 'wt');
fprintf(fid, '%f %f %f %f %f %f %f \n', sbf_sim_vector(:,:)');
fclose(fid);

fid = fopen('Takeoff_Speed_Chart_Stores_Results.dat', 'wt');
fprintf(fid, '%f %f %f %f %f %f %f \n', v1_sim_vector(:,:)');
fclose(fid);

fid = fopen('Takeoff_AS_CorrectionFactors.dat', 'wt');
fprintf(fid, '%f %f %f %f %f %f %f \n', AS_sim_correctionvector(:,:)');
fclose(fid);


fid = fopen('Takeoff_EF_CorrectionFactors.dat', 'wt');
fprintf(fid, '%f %f %f %f %f %f %f \n', EF_sim_correctionvector(:,:)');
fclose(fid);


fid = fopen('Percentual_Deviation_Distances.dat', 'wt');
fprintf(fid, '%f %f %f %f %f %f %f \n', Percen-
tual_Deviation_Distances(:,:)');
fclose(fid);

fid = fopen('Percentual_Deviation_Speeds.dat', 'wt');
fprintf(fid, '%f %f %f %f %f %f %f \n', Percentual_Deviation_Speeds(:,:)');
fclose(fid);

disp(' ')
disp('Simulation Performed')
```

J.2 Parameters_Learjet.m

```
%Parameter Function, Contains the Data for all Functions based on
%Learjet 35A/36A Extended Tiptanks Data

global stores;
global wet;
global m_lbs;
global isa_selection; %Input of total temperature in Degrees
global isa_selection_variable;
global alt_selection; %Input of total pressure altitude in feet
global alt_selection_variable;

%SETTING THE MAXIMUM TIME STEP FOR THE RUNGE-KUTTA INTEGRATION

max_step = 0.1; %Maximum time step in s used for time steps of diff. inte-
gration

%Correction variable to convert KIAS to KCAS
ias_cas_correction=1; %kts, conversion from IAS to CAS is defined positive

%REACTION AND TRANSITION TIME VARIABLES_____________________________________

reactiontime=1; %reaction time [seconds] acc. to operator transition time
cs_transitiontime=2; %transition time acc. to CS-25.109

%AIRCRAFT WEIGHT____________________________________________________________
m = m_lbs*0.45359237; % TOW [kg]
g = 9.81; % gravity
W = m*g; % Take-off weight [N]

%ATMOSPHERIC CONDITIONS ISA_________________________________________________

%Temperature
L_temp = 1.9812*10^-3; %Temperature Gradient [K/ft]
T_0 = 288.15 - L_temp * alt_selection; %ISA standard temperature [K]
T_test = isa_selection + 273.15; %the true outside temperature
theta_isa = T_test/T_0; %The temperature ratio
delta_ISA = T_test - T_0; %Delta-ISA temperature differerence

delta_p_isa = (1-(L_temp/T_0)*alt_selection)^5.25588; %pressure ratio ac-
tual conditions

P_amb_0 = 101325; % Standard Pressure at SL, ISA
P_amb = P_amb_0*delta_p_isa; %Ambient Pressure at actual conditions

%Speed of Sound
a_0 = 340.294; % Speed of Sound at ISA, SL [m/s]
a = a_0 * sqrt ( theta_isa); %Speed of Sound at actual conditions [m/s]

%Density
rho_0 = 1.225; % Density at ISA, SL [kg/m^3]
rho = (delta_p_isa/theta_isa) * rho_0; %densitiy at actual conditions
[kg/m^3]
sigma_isa = rho/rho_0; %relative density ratio

h_density = (T_0/L_temp)*(1-sigma_isa^(1/4.25588)); %density altitude at
present conditions
```

```
%AIRPORT ENVIRONMENTAL FACTORS_____________________________________________

gamma_RW = 0;    % Slope of the Runway [°], uphill defined positive
% 2% grade equals 1.1458 °
gammaRad = gamma_RW*pi/180; %conversion to radiants

vW = 0*0.514444444; % Wind Speed [m/s], Headwind defined positive

%AIRCRAFT REFERENCE SPEEDS_____________________________________________
%Aircraft V-speeds all dry values from AVCON AFMS 9702-2 Figure 5.1

%Stall Speeds
vs_kts = 88 + ((118-88)/(19000-10000))*(m_lbs-10000) ;
if stores == 1
    vs_kts = vs_kts + 6;
end

%Rotation Speeds
if stores == 0 %no stores installed
if m_lbs <= 14000
         vR_kts = 125 ;
else ((m_lbs > 14000) && (m_lbs < 19600));
        vR_kts = 125 + ((145.5-125)/(19000-14000))*(m_lbs-14000); %linear
from 14000 to 19000 and extrapolated
end

else%if stores installed
if m_lbs <= 15100
         vR_kts = 134.5 ;
else ((m_lbs > 15100) && (m_lbs < 19600));
        vR_kts = 134.5 + ((149.5-134.5)/(19000-15100))*(m_lbs-15100); %li-
near from 15100 to 19000 and extrapolated
end

end

%V2 Speeds
if stores == 0 %no stores installed
if m_lbs <= 13000
         v2_kts = 124 ;
else ((m_lbs > 13000) && (m_lbs < 19600));
        v2_kts = 124 + ((148-124)/(19000-13000))*(m_lbs-13000); %linear
from 13000 to 19000 and extrapolated
end

else%if stores installed
if m_lbs <= 15100
         v2_kts = 137 ;
else ((m_lbs > 15100) && (m_lbs < 19600));
        v2_kts = 137 + ((152-137)/(19000-15100))*(m_lbs-15100); %linear
from 15100 to 19000 and extrapolated
end

end

%IAS-CAS Conversion
vR_kts=vR_kts-ias_cas_correction;
v2_kts=v2_kts-ias_cas_correction;
```

```
vs_kts=vs_kts-ias_cas_correction;

vR_EAS = vR_kts*0.514444444; % m/s
v2_EAS = v2_kts*0.514444444; % m/s
vs_EAS = vs_kts*0.514444444; % m/s

% Conversion of the CAS/EAS (no compress) reference speeds into TAS and
%Calculation of Ground Speeds GS from TAS and wind correction
vR = (vR_EAS/sqrt(sigma_isa))-vW;
v2 = v2_EAS/sqrt(sigma_isa); %in the air, a relative difference between TAS
and GS due to wind is not relevant
vs = (vs_EAS/sqrt(sigma_isa))-vW;
%As headwind is defined as positive - its presence reduces the Ground Speed
%necessary for stall

vLOF=1.2*vs; %acc. to Scholz 1999

% JET ENGINE
PARAMETERS_____________________________________________________________
BPR = 2.51; % BPR By Pass Ratio
T0 = 3400*4.448222; % Initial (installed) Thrust (Value from GFD Data) in N

T0_Idle = 250*4.448222; %Idle Thrust from TFE HONEYWELL REPORT (no thrust
setting correction) in N

%Thrust Lapse acc. to Bartel and Young 2007
%G = 0.9; % Gas Generator Function Standard Reference Value
G=-0.01*delta_ISA+0.9; %Adapted G for Learjet 35A/36A Test Data from GJE-
EXTGFD-003
A_Thrust_BY = -0.4327*(P_amb/P_amb_0)^2+1.3855*(P_amb/P_amb_0)+0.0472;
%Standard A_Thrust from B. and Y. 2007
A_Thrust_corr = 8*0.000001*alt_selection+1; %Empirical Correction factor
based on GJE EXTGFD-003 for Learjet35A/36A
A_Thrust = A_Thrust_BY*A_Thrust_corr; %Application of the correction factor

%Further input variables for Bartel and Young 2007 approach
X = 0.1377*(P_amb/P_amb_0)^2-0.4374*(P_amb/P_amb_0)+1.3003;
Z = 0.9106*(P_amb/P_amb_0)^2-1.7736*(P_amb/P_amb_0)+1.8697;
k1 = 0.377*(1+BPR)*Z*(P_amb/P_amb_0)/sqrt((1+0.82*BPR)*G);
k2 = (0.23+0.19*sqrt(BPR))*X*(P_amb/P_amb_0);

%Flat Rating Characteristics
t_flat_rate_vector = [22; 16; 8]; %Flat Rate OAT Temperatures for [0; 2000;
4000] ft pressure alt
t_flat_rate = t_flat_rate_vector (alt_selection_variable); %selection of
the applicable flat rate temp.

if isa_selection > t_flat_rate
T0 = T0-0.0075*T0*(isa_selection-t_flat_rate); %Thrust Decay acc. to Raymer
1989
end

%SCREEN HEIGHT_____________________________________________________________
% 35ft for dry runway and 15 ft for wet runway in meters

hsc=35*0.3048;
if (wet == 1)
    hsc=15*0.3048; %Case of wet Runway
end
```

```
n_climb = 1.15; %load factor during rotation acc. to Scholz 1999

%Precipitation_____________________________________________________________
rhoCont = 1000; % Water density at 3,98 °C

contDepth = 0; %Case of Dry Runway
if (wet == 1) %Case of wet Runway
    contDepth = 0.003; %Contamination Depth in [m]

end


% LEARJET 35A/36A GEOMETRY___________________________________________________
%Validation and Sources, See Report chapter 6
b = 11.61; % b wing span over tip tank (not over vane) [m]
b_s = 1*cos(7*pi/180)*2; % Spoilers distance extended in the spanwise di-
rection
c_t = 1.55; % Chord at wing tip [m]
c_r = 2.74; % Chord at wing root [m]
c_s = 0.3; % Chord of the spoiler [m]
h = 1.0; % h Distance of the Wing to the Ground [m]
SW = 23.53; % S Wing Surface [m^2]
SW_Exp = 18.826; %Exposed Wing Area
S_Exp_H = 4.1; %Exposed Horizontal Tailplane Area
SW_F = 8.86; % Wing surface with Flaps [m^2] "Flapped"
SW_S = 1.3; % Wing surface affected by Spoilers [m^2]
SW_Stores = 0.811; %[m^2], launcher up config.
S_S = 0.516;   % Spoiler projected area extended into the windstream
A = b*b/SW; %=5.7 (thus corresponding to JANES reference)
phi_25 = 13.0; % Sweep Angle [°]
phi_25Rad = phi_25*pi/180; %Conversion to radians
alpha_0 = -3.0; %Zero Lift Angle, profile
alpha = 1.0; % Angle of Attack at rolling configuration [°]
alpha_H = -5.0; %Horizontal Stabilizer AOA, incl. Takeoff Trim Setting and
Downwash from Wing
alphaRad = alpha*pi/180; %Conversion to radians
twist_W = -3.0; %Twist Angle of the Wing [°]
lambda = c_t/c_r; %Taper
delta_FRad = 8*pi/180; %Deflexion angle of the flap [rad]
Lwet = 0.75*14.8*0.3048; %Wetted fuselage length in feet

%GEOMETRIC RELATIONS FOR AERODYNAMIC EQUATIONS_____________________________
phi_50Rad = atan(tan(phi_25Rad)-(4/A)*((50-25)*pi/180/100*(1-
lambda)/(1+lambda))); % [rad] Sweep at 50% Chord
alpha_0_W = alpha_0+(-0.40752)*twist_W*1; % [°] Zero Lift Angle
alpha_0_WRad = alpha_0_W*pi/180; % [rad]
alpha_delta = 0.38; % Lift-effectiveness parameter [-]
K_delta = 0.98; % Flap Effectiveness Factor
phi = (16*h/b)^2/(1+(16*h/b)^2); % Factor of the ground effect [-]

% AERODYNAMIC DRAG___________________________________________________________
e = 0.72; %Oswald Factor in Takeoff Configuration, See Chapter 6 for vali-
dation
CD_ExtTiptanks=0.0007; %Drag Increment due to extended Tip Tanks
CD0 = 0.0242+CD_ExtTiptanks; %Zero Lift Drag Coefficient Learjet 35A/36A
CD0_base = CD0; %Storage of the Zero Lift Drag combined for reference

if (stores == 1)
    CD_Stores = 0.0136; %Stores drag acc. to GJE EXTGFD-003
```

```
else
    CD_Stores = 0;
end

CD0_Gear = 0.0190; %Estimated acc. to Hoerner 1965
CD_Windmill = 0.0100; %Failed Engine Drag, with reference to Wing Area,
Based on Torenbeek 1982
CD_Asym_toga = 0.0091; %Asymmetrical Drag, Estimation acc. to Torenbeek,
Averaged, at TOGA thrust
CD_Asym_idle = 0.0020; %Asymmetrical Drag, Estimation acc. to Torenbeek,
Averaged, at IDLE thrust

% TIRES_____________________________________________________

Tyre_P_Main = 175; % Tire pressure Main Wheel (4x)[psi]
Tyre_P_Nose = 105; % Tire pressure Nose Wheel (1x)[psi]
Anti_Skid = 0.8; % Anti-Skid system efficient value FAR 25 paragraph
25.109. Fully modulating AntiSkid system, only for plotting FAR braking
coefficients

%Effective tire width
beff_Nose = 0.101; %[m]   Data measured by operator b_Nose = 0.091 m
beff_Main = 0.127; %[m]   Data measured by operator b_Main = 0.122 m

%Gear load factor considers shift of weight around CG in braking case
gear_load_factor = 0.9;
```

J.3 Take_off_1Eng.m

```
%Calculation of the Take-off distance

function s_TO = Take_off_1Eng (vEF)
global alt_selection
global weight_selection_variable
global alt_selection_variable
global isa_selection
global graphics
global makeplots
global thrustsetting
%Calculation of the Take-off ground roll (sG)
y0=[0 0];
Parameters_Learjet
options = odeset('MaxStep',max_step);
[t,y]=ode23('fsG_Learjet',[0 120],y0,options);

%Extraction of two data points for the plots
sG = interp1(y(:,1),y(:,2),vLOF,'spline'); %Liftoff Distance
sEF = interp1(y(:,1),y(:,2),vEF,'spline'); %Engine Failure Distance

if graphics == 1;
h=figure('Visible','off');
distancesvector=y(:,1);
speedsvector=y(:,2);
ind = (distancesvector > vLOF);
distancesvector(ind)= vLOF;
speedsvector(ind)=sG;
hold on
plot (speedsvector, distancesvector,'LineWidth',1.2)
plot(sEF,vEF,'bp')
plot(sG, vLOF, 'bo')
hold off
legend('Acceleration Curve', 'Engine Failure Point', 'Lift Off Point',
'Location','Best')
xlabel('Distance [m]')
ylabel('Speed [m/s]')
if stores ==0
 title(['Acceleration Curve Takeoff Plot, No Stores, TOM: ',
num2str(m_lbs),'lbs, Temp(C): ', num2str(isa_selection),', Alt(ft): ',
num2str(alt_selection), ' '])
filename = (['Curve Acceleration Takeoff Plot-', num2str(m_lbs),'-Temp(C)-
', num2str(isa_selection),'-Alt(ft)-', num2str(alt_selection),
'no_stores']);

else
  title(['Acceleration Curve ASD Plot, Stores, TOM: ', num2str(m_lbs),'lbs,
Temp(C): ', num2str(isa_selection),', Alt(ft): ', num2str(alt_selection), '
'])
filename = (['Curve Acceleration Takeoff Plot-', num2str(m_lbs),'-Temp(C)-
', num2str(isa_selection),'-Alt(ft)-', num2str(alt_selection), 'stores']);

end
print('-djpeg', '-r300', filename);
close
end

%Calculation of the Air Distance
```

```
M = vLOF/a;

%CL_TO for flight at v2 (EAS) (L=m*g=0.5*rho*v2*CL_TO(=CL2)*SW
CL_TO = (2*m*g)/(v2_EAS^2*SW);

% Flap Drag increment acc. to Loftin 1980
if CL_TO < 1.1
    CD0_Flaps = 0;
else
    CD0_Flaps = 0.05*CL_TO-0.055;
end

%total drag Coefficient OEI

CD0_TO = CD0+CD0_Flaps+CD_Stores+CD0_Gear+ CD_Windmill + CD_Asym_toga;
%Windmilling/Asymm. Drag is always present in this case
CD_TO = CD0_TO+phi*CL_TO^2/(pi*e*A);

E_TO = CL_TO/CD_TO;

%Takeoff Thrust OEI
T = T0*(A_Thrust-k1*M+k2*M*M);

%Determination of the Air Distance Acc. to Scholz 1999
gamma_climb=asin(T/W-1/E_TO);
R = vLOF*vLOF/(g*(n_climb-1));
htr=R-R*cos(gamma_climb);
if hsc <= htr               % Case a) hsc <= htr
sa=sqrt(R*R-(R-hsc)^2);
else% Case b) hsc > htr
    str=R*sin(gamma_climb);
scl=(hsc-htr)/tan(gamma_climb);
sa=str+scl;
end

%Total TOD
s_TO = sG+sa;
```

J.4 Take_off_AEO.m

```
%Calculation of the Take-off distance AOE, Sub-Function

function s_TO_AEO = Take_off_AEO (vEF)
global alt_selection
global weight_selection_variable
global alt_selection_variable
global isa_selection
global graphics
global makeplots
global thrustsetting

%Calculation of the Take-off ground roll (sG)
y0=[0 0];
Parameters_Learjet
options = odeset('MaxStep',max_step);
[t,y]=ode23('fsG_Learjet_AEO',[0 120],y0,options);

%Extraction of two data points for the plots
sG = interp1(y(:,1),y(:,2),vLOF,'spline'); %Liftoff Distance
sEF = interp1(y(:,1),y(:,2),vEF,'spline'); %Engine Failure Distance

if graphics == 1;
h=figure('Visible','off');
distancesvector=y(:,1);
speedsvector=y(:,2);
ind = (distancesvector > vLOF);
distancesvector(ind)= vLOF;
speedsvector(ind)=sG;
hold on
plot (speedsvector, distancesvector,'LineWidth',1.2)
plot(sG, vLOF, 'bo')
hold off
legend('Acceleration Curve', 'Lift Off Point', 'Location','Best')
xlabel('Distance [m]')
ylabel('Speed [kts]')
if stores ==0
 title(['Acceleration Curve Takeoff Plot AEO, No Stores, TOM: ',
num2str(m_lbs),'lbs, Temp(C): ', num2str(isa_selection),', Alt(ft): ',
num2str(alt_selection), ' '])
filename = (['Curve Acceleration Takeoff Plot AEO-', num2str(m_lbs),'-
Temp(C)-', num2str(isa_selection),'-Alt(ft)-', num2str(alt_selection),
'no_stores']);

else
  title(['Acceleration Curve ASD Plot, Stores, TOM: ', num2str(m_lbs),'lbs,
Temp(C): ', num2str(isa_selection),', Alt(ft): ', num2str(alt_selection), '
'])
filename = (['Curve Acceleration Takeoff Plot AEO-', num2str(m_lbs),'-
Temp(C)-', num2str(isa_selection),'-Alt(ft)-', num2str(alt_selection),
'stores']);

end
print('-djpeg', '-r300', filename);
close
end

%Calculation of the Air Distance
```

```
M = vLOF/a;

%CL_TO for flight at v2 (EAS) (L=m*g=0.5*rho*v2*CL_TO(=CL2)*SW
CL_TO = (2*m*g)/(v2_EAS^2*SW);

% Flap Drag increment acc. to Loftin 1980
if CL_TO < 1.1
    CD0_Flaps = 0;
else
    CD0_Flaps = 0.05*CL_TO-0.055;
end

%total drag coefficient AEO

CD0_TO = CD0+CD0_Flaps+CD0_Gear+CD_Stores; % no Windmilling/Asymm. Drag
present in this case
CD_TO = CD0_TO+phi*CL_TO^2/(pi*e*A);

E_TO = CL_TO/CD_TO;

%Takeoff Thrust AEO
T = 2*T0*(A_Thrust-k1*M+k2*M*M); %Full Thrust

%Determination of the Air Distance Acc. to Scholz 1999
gamma_climb=asin(T/W-1/E_TO);
R = vLOF*vLOF/(g*(n_climb-1));
htr=R-R*cos(gamma_climb);
if hsc <= htr               % Case a) hsc <= htr
sa=sqrt(R*R-(R-hsc)^2);
else% Case b) hsc > htr
    str=R*sin(gamma_climb);
scl=(hsc-htr)/tan(gamma_climb);
sa=str+scl;
end

%Total TOD
s_TO_AEO = 1.15*(sG+sa);
```

J.5 Take_off_Acc_Stop.m

```
function s_AS = Take_off_Acc_Stop (vEF)

global graphics
global makeplots

%Calculation of the acceleration distance (s_Acc)
y0=[0 0];
Parameters_Learjet
options = odeset('MaxStep',max_step);
%[t,y]=ode23('fsG_Learjet',[0 120],y0,options);
[t,y]=ode23('fsG_Learjet',[0 120],y0,options);
s_Acc = interp1(y(:,1),y(:,2),vEF,'spline'); %Acceleration Distance reached
at vEF

if graphics == 1;
h=figure('Visible','off');
distancesvector=y(:,1);
speedsvector=y(:,2);
ind = (distancesvector > vEF);
distancesvector(ind)= vEF;
speedsvector(ind)=s_Acc;
hold on
plot (speedsvector, distancesvector,'LineWidth',1.2)
plot(s_Acc,vEF,'bp')
hold off
legend('Acceleration Curve', 'Engine Failure Point', 'Location','Best')
xlabel('Distance [m]')
ylabel('Speed [m/s]')
if stores ==0
 title(['Acceleration Curve ASD Plot, No Stores, TOM: ',
num2str(m_lbs),'lbs, Temp(C): ', num2str(isa_selection),', Alt(ft): ',
num2str(alt_selection), ' '])
filename = (['Curve Acceleration ASD Plot-', num2str(m_lbs),'-Temp(C)-',
num2str(isa_selection),'-Alt(ft)-', num2str(alt_selection), 'no_stores']);

else
  title(['Acceleration Curve ASD Plot, Stores, TOM: ', num2str(m_lbs),'lbs,
Temp(C): ', num2str(isa_selection),', Alt(ft): ', num2str(alt_selection), '
'])
filename = (['Curve Acceleration ASD Plot-', num2str(m_lbs),'-Temp(C)-',
num2str(isa_selection),'-Alt(ft)-', num2str(alt_selection), 'stores']);

end
print('-djpeg', '-r300', filename);
close
end

%Calculation of the stop distance (s_Stop)
y0=[vEF 0];
options = odeset('MaxStep',max_step);
%[t,y]=ode23('fsG_Learjet_Stop',[0 100],y0,options);
[t,y]=ode23('fsG_Learjet_Stop',[0 120],y0,options);
vStop = 0.0;
s_Stop = interp1(y(:,1),y(:,2),vStop,'spline'); %Deceleration Distance be-
gins at vEF, reaction times considered in fsG_Learjet_Stop

if graphics == 1;
```

```
h=figure('Visible','off');
distancesvector=y(:,1);
speedsvector=y(:,2);
ind = (distancesvector < 0);
distancesvector(ind)= 0;
speedsvector(ind)=s_Stop;
hold on
plot (speedsvector, distancesvector,'LineWidth',1.2)
plot(0,vEF,'bp')
hold off
legend('Stopping Curve', 'Engine Failure Point',  'Location','Best')
xlabel('Distance [m]')
ylabel('Speed [m/s]')
if stores ==0
 title(['Stopping Curve ASD Plot, No Stores, TOM: ', num2str(m_lbs),'lbs,
Temp(C): ', num2str(isa_selection),', Alt(ft): ', num2str(alt_selection), '
'])
filename = (['Curve Stopping ASD Plot -', num2str(m_lbs),'-Temp(C)-',
num2str(isa_selection),'-Alt(ft)-', num2str(alt_selection), 'no_stores']);

else
  title(['Stopping Curve Plot, Stores, TOM: ', num2str(m_lbs),'lbs,
Temp(C): ', num2str(isa_selection),', Alt(ft): ', num2str(alt_selection), '
'])
filename = (['Curve Stopping ASD Plot -', num2str(m_lbs),'-Temp(C)-',
num2str(isa_selection),'-Alt(ft)-', num2str(alt_selection), 'stores']);

end
 print('-djpeg', '-r300', filename);
close
end


% Total ASD
s_AS = s_Acc+s_Stop;
```

J.6 fsG_Learjet.m

```
function [ydot] = fsG_Learjet(t,y)

global ploter;
global plot_s;
global alt_selection
global weight_selection_variable
global alt_selection_variable
global isa_selection
global thrustsetting

Parameters_Learjet
vG = y(1);
v = vG; %v refers to GS
M = (v+vW)/a;

%relating engine failure speed to time step
vDec = evalin ('base', 'vEF');

if v >= vDec
assignin('base','t_Dec',t)
end


%relating engine failure speed to time step
vDec = evalin ('base', 'vEF');
if v >= vDec
assignin('base','t_Dec',t)
end
t_Dec = evalin ('base', 't_Dec');


%Thrust of a Jet Engine
if t >= t_Dec
    T = T0*(A_Thrust-k1*M+k2*M*M); % Full thrust OEI
    CD0 = CD0_base + CD_Windmill+ CD_Asym_toga;  %Failed Engine produces
drag, Rudder force produces drag
else
    T = 2*T0*(A_Thrust-k1*M+k2*M*M);  % Full thrust AEO
end

% Lift L
CL_alpha = 2*pi*A/(2+sqrt(A^2*(1+tan(phi_50Rad)^2-M^2)+4)); %Lift Curve
Slope
CL_0 = -CL_alpha*alpha_0_WRad; %Zero AOA Lift Coefficient
CL_0_F=(1/3)*(2/(1+lambda))*(1.60/b)*CL_0; %Fuselage Carryover Increment
cL_F = CL_alpha*alpha_delta*delta_FRad; %Single Slotted Flap Increment,
airfoil
CL_F = cL_F*K_delta*SW_F/SW; % Flap Increment, Wing
CL_TO = (CL_0 + CL_alpha*alphaRad + CL_F + CL_0_F)*(SW_Exp/SW); %Aircraft
Lift Coefficient with Fuselage Effect, vertical tailplane effects assumed
to cancel out

%Lift
L = rho/2*(v*sqrt(sigma_isa)+vW)^2*CL_TO*SW; %Aerodynamic Force needs EAS
to be correct
```

```
% CD_TO acc. to Loftin 1980
if CL_TO < 1.1
    CD0_Flaps = 0;
else
    CD0_Flaps = 0.05*CL_TO-0.055;
end

%Total Drag Coefficient
CD0_TO = CD0+CD0_Flaps+CD0_Gear+CD_Stores; %contains CD0 drag increment due
to engine failure at condition, see above
CD_TO = CD0_TO+phi*CL_TO^2/(pi*e*A);


% Drag D
D = rho/2*(v*sqrt(sigma_isa)+vW)^2*CD_TO*SW; %Aerodynamic Force needs EAS
to be correct

%Rolling Friction Coefficient
%Taken from NASA TN-D2770
v_knots = v/0.514444444; %conversion from m/s
if wet == 1
    mu_ground_roll = 0.0002*v_knots+0.0165;
else mu_ground_roll = 0.0002*v_knots+0.0135;
end


% Rolling Friction Ff
Ff = mu_ground_roll*(m*g*cos(gammaRad)-L)+m*g*sin(gammaRad);

%Aquaplaning Speed Nose Wheel
vap_Nose = 9 * sqrt(Tyre_P_Nose);
vap_Nose = vap_Nose*0.514444444; %conversion to m/s

%Aquaplaning Speed Main Wheel
vap_Main = 9 * sqrt(Tyre_P_Main);
vap_Main = vap_Main*0.514444444; %conversion to m/s

%Drag reduction due to aquaplaning Nose Wheel
k_vap_Nose = 0;
if v/vap_Nose < 1
    k_vap_Nose = 1;
end
if ((v/vap_Nose > 1) && (v/vap_Nose < 1.6))
k_vap_Nose = 1 - (1/0.6) * ((v/vap_Nose)-1);
end

%Drag reduction due to aquaplaning Main Wheel
k_vap_Main = 0;
if v/vap_Main < 1
    k_vap_Main = 1;
end
if ((v/vap_Main > 1) && (v/vap_Main < 1.6))
k_vap_Main = 1 - (1/0.6) * ((v/vap_Main)-1);
end

Dd = 0;
Ds = 0;
D_store_wet = 0;
```

```
if wet == 1;

%Frontal area of tyre_Nose
S_Nose = beff_Nose * contDepth;

%Frontal area of tyre_Main
S_Main = beff_Main * contDepth;

%Displacement Drag Nose
cD_Nose = 0.75 * k_vap_Nose; %Drag coefficient
Dd_Nose = cD_Nose * 0.5 * rhoCont * v^2 * S_Nose;

%Displacement Drag Main
cD_Main = 0.75 * k_vap_Main; %Drag coefficient
Dd_Main = cD_Main * 0.5 * rhoCont * v^2 * S_Main * 4; %4 wheels main gear

Dd = Dd_Nose + Dd_Main; %Total Displacement drag

D_dis = Dd; %Total Displacement Drag for Plot

%Skin friction drag
cDSpray = (8 * Lwet * 0.0025) * k_vap_Nose; %Drag coefficient through Nose
Spray
Ds = cDSpray * 0.5 * rhoCont * v^2 * S_Nose;
Ds = 1 * Ds; %One wheels

rho_spray = rhoCont; %[kg/m^3] (=Water density)

%Spray Impingement Drag
if stores == 1
%Drag reduction due to aquaplaning Nose Wheel
        k_vap_Nose = 0;
if v/vap_Nose < 1
%k_vap_Nose = 1;
          k_vap_Nose = v/vap_Nose; %accounts for the spray plume rising
gradually up to max. intensity at vap
end
if ((v/vap_Nose > 1) && (v/vap_Nose < 1.6))
k_vap_Nose = 1 - (1/0.6) * ((v/vap_Nose)-1);
end

    VolumeFlow = v * S_Nose; %aircraft speed*frontal area tire
    MassFlow = VolumeFlow * rho_spray;
    MassFlow = MassFlow * 0.3; %considering 30% absorption (max) of stores
    D_store_wet = (1-0.2)* MassFlow * v * k_vap_Nose; %restitution coeffi-
cient e=0.2, and considering the drag reduction coefficient
    Dd = Dd + D_store_wet; %adding impingement drag due to collision drag
on the stores to the displacement drag variable only for calculation

end

end

% Acceleration calculated from all forces determined in this function
ydot(1) = 1/m*(T-D-Dd-Ds-Ff)-g*sin(gammaRad);

if ydot (1) == 0;
```

```
    disp ('The acceleration was zero in this run at t = ', num2str(t))
end

% Speed storage in ydot(2)
ydot(2) = y(1);

%Transposition for Input in the Runge-Kutta-Integration Method
ydot=ydot';

if v > v2
return
end

if ploter == 1

 plot (vG, T, '.k', 'LineWidth',3)
if wet ==1
 plot (vG, D_dis, '.m', 'LineWidth',3)
 plot (vG, Ff, '.r', 'LineWidth',3)
end
 plot (vG, D, '.g', 'LineWidth',3)
 plot (vG, L, '.c', 'LineWidth',3)
if wet==1
 plot (vG, Ds, '.y', 'LineWidth',3)
 plot(vG, D_store_wet,'.b', 'LineWidth',3)
end
 hold on

end
```

J.7 fsG_Learjet_AEO.m

```
function [ydot] = fsG_Learjet_AEO(t,y)

global ploter;
global plot_s;
global alt_selection
global weight_selection_variable
global alt_selection_variable
global isa_selection
global thrustsetting

Parameters_Learjet
vG = y(1);
v = vG; %v refers to GS
M = (v+vW)/a;

%relating engine failure speed to time step
vDec = evalin ('base', 'vEF');
if v >= vDec
assignin('base','t_Dec',t)
end
t_Dec = evalin ('base', 't_Dec');


%Thrust of a Jet Engine
%Full Thrust remains until engine failure time is reached
if t >= t_Dec
    T = 2*T0*(A_Thrust-k1*M+k2*M*M); % Full thrust AEO
else
    T = 2*T0*(A_Thrust-k1*M+k2*M*M);  %Full thrust AEO
end


% Lift L
CL_alpha = 2*pi*A/(2+sqrt(A^2*(1+tan(phi_50Rad)^2-M^2)+4)); %Lift Curve
Slope
CL_0 = -CL_alpha*alpha_0_WRad; %Zero AOA Lift Coefficient
CL_0_F=(1/3)*(2/(1+lambda))*(1.60/b)*CL_0; %Fuselage Carryover Increment
cL_F = CL_alpha*alpha_delta*delta_FRad; %Single Slotted Flap Increment,
airfoil
CL_F = cL_F*K_delta*SW_F/SW; % Flap Increment, Wing
CL_TO = (CL_0 + CL_alpha*alphaRad + CL_F + CL_0_F)*(SW_Exp/SW); %Aircraft
Lift Coefficient with Fuselage Effect, vertical tailplane effects assumed
to cancel out

%Lift
L = rho/2*(v*sqrt(sigma_isa)+vW)^2*CL_TO*SW; %Aerodynamic Force needs EAS
to be correct

% CD_TO acc. to Loftin 1980
if CL_TO < 1.1
    CD0_Flaps = 0;
else
    CD0_Flaps = 0.05*CL_TO-0.055;
end

%Total Drag Coefficient
```

```
CD0_TO = CD0+CD0_Flaps+CD0_Gear+CD_Stores; %contains CD0 drag increment due
to engine failure at condition, see above
CD_TO = CD0_TO+phi*CL_TO^2/(pi*e*A);

% Drag D
D = rho/2*(v*sqrt(sigma_isa)+vW)^2*CD_TO*SW; %Aerodynamic Force needs EAS
to be correct

%Rolling Friction Coefficient
%Taken from NASA TN-D2770
v_knots = v/0.514444444; %conversion from m/s
if wet == 1
    mu_ground_roll = 0.0002*v_knots+0.0165;
else mu_ground_roll = 0.0002*v_knots+0.0135;
end

% Rolling Friction Ff
Ff = mu_ground_roll*(m*g*cos(gammaRad)-L)+m*g*sin(gammaRad);

%Aquaplaning Speed Nose Wheel
vap_Nose = 9 * sqrt(Tyre_P_Nose);
vap_Nose = vap_Nose*0.514444444; %conversion to m/s

%Aquaplaning Speed Main Wheel
vap_Main = 9 * sqrt(Tyre_P_Main);
vap_Main = vap_Main*0.514444444; %conversion to m/s

%Drag reduction due to aquaplaning Nose Wheel
k_vap_Nose = 0;
if v/vap_Nose < 1
    k_vap_Nose = 1;
end
if ((v/vap_Nose > 1) && (v/vap_Nose < 1.6))
k_vap_Nose = 1 - (1/0.6) * ((v/vap_Nose)-1);
end

%Drag reduction due to aquaplaning Main Wheel
k_vap_Main = 0;
if v/vap_Main < 1
    k_vap_Main = 1;
end
if ((v/vap_Main > 1) && (v/vap_Main < 1.6))
k_vap_Main = 1 - (1/0.6) * ((v/vap_Main)-1);
end


Dd = 0;
Ds = 0;
D_store_wet = 0;


if wet == 1;

%Frontal area of tyre_Nose
S_Nose = beff_Nose * contDepth;

%Frontal area of tyre_Main
S_Main = beff_Main * contDepth;
```

```
%Displacement Drag Nose
cD_Nose = 0.75 * k_vap_Nose; %Drag coefficient
Dd_Nose = cD_Nose * 0.5 * rhoCont * v^2 * S_Nose;

%Displacement Drag Main
cD_Main = 0.75 * k_vap_Main; %Drag coefficient
Dd_Main = cD_Main * 0.5 * rhoCont * v^2 * S_Main * 4; %4 wheels main gear

Dd = Dd_Nose + Dd_Main; %Total Displacement drag

D_dis = Dd; %Total Displacement Drag for Plot

%Skin friction drag
cDSpray = (8 * Lwet * 0.0025) * k_vap_Nose; %Drag coefficient through Nose
Spray
Ds = cDSpray * 0.5 * rhoCont * v^2 * S_Nose;
Ds = 1 * Ds; %One wheels

rho_spray = rhoCont; %[kg/m^3] (=Water density)


%Spray Impingement Drag
if stores == 1
%Drag reduction due to aquaplaning Nose Wheel
        k_vap_Nose = 0;
if v/vap_Nose < 1
%k_vap_Nose = 1;
          k_vap_Nose = v/vap_Nose; %accounts for the spray plume rising
gradually up to max. intensity at vap
end
if ((v/vap_Nose > 1) && (v/vap_Nose < 1.6))
k_vap_Nose = 1 - (1/0.6) * ((v/vap_Nose)-1);
end

    VolumeFlow = v * S_Nose; %aircraft speed*frontal area tire
    MassFlow = VolumeFlow * rho_spray;
    MassFlow = MassFlow * 0.3; %considering 30% absorption (max) of stores
    D_store_wet = (1-0.2)* MassFlow * v * k_vap_Nose; %restitution coeffi-
cient e=0.2, and considering the drag reduction coefficient
    Dd = Dd + D_store_wet; %adding impingement drag due to collision drag
on the stores to the displacement drag variable only for calculation

end

end

% Acceleration calculated from all forces determined in this function
ydot(1) = 1/m*(T-D-Dd-Ds-Ff)-g*sin(gammaRad);

if ydot (1) == 0;
    disp ('The acceleration was zero in this run at t = ', num2str(t))
end

% Speed storage in ydot(2)
ydot(2) = y(1);

%Transposition for Input in the Runge-Kutta-Integration Method
ydot=ydot';
```

```
if v > v2
return
end

if ploter == 1

 plot (vG, T, '-b')
 plot (vG, D_dis, '-m')
 plot (vG, Ff, '-r')
 plot (vG, D, '-g')
 plot (vG, L, '-c')
 plot(vG, D_store_wet,'-k')

 hold on

end
```

J.8 fsG_Learjet_Stop.m

```
function [ydot] = fsG_Learjet_Stop(t,y)

global wet;
global plot_s;
global ploter;
global weight_selection_variable
global alt_selection_variable
global isa_selection
global thrustsetting

global v1;
Parameters_Learjet
vG = y(1);
v = vG; %v refers to Ground Speed
M = (v+vW)/a;
t_par = t;

%1 second after Engine Failure Recognition, the Thrust is reduced
if t_par >= (1+reactiontime)
    T = T0_Idle*(A_Thrust-k1*M+k2*M*M); %Remaining Engine reduced to Idle 2
Seconds after Engine failure
    CD_Asym = CD_Asym_idle; %Asymm. Drag at engine idle
else
%T = T0*(A_Thrust-k1*M+k2*M*M)-0.15*T0; %0.15 is the Drag coming from the
failed engine
    T = T0*(A_Thrust-k1*M+k2*M*M); %Remaining Engine running at full thrust
    CD_Asym = 0; %no Asymmetrical Drag Considered
end



% Lift L
CL_alpha = 2*pi*A/(2+sqrt(A^2*(1+tan(phi_50Rad)^2-M^2)+4)); %Lift Curve
Slope
CL_0 = -CL_alpha*alpha_0_WRad; %Zero AOA Lift Coefficient
CL_0_F=(1/3)*(2/(1+lambda))*(1.60/b)*CL_0; %Fuselage Carryover Increment
cL_F = CL_alpha*alpha_delta*delta_FRad; %Single Slotted Flap Increment,
airfoil
CL_F = cL_F*K_delta*SW_F/SW; % Flap Increment, Wing

%Spoiler activation 1.5 seconds after engine failure recognition
if t_par >= (1.5+reactiontime)
    CL_TO = (CL_0 + CL_alpha*alphaRad + CL_F )*(1-SW_S/SW)*(SW_Exp/SW); %No
Lift Carry Over Increment due to Spoiler Extension, Fuselage acts like a
void in the wing

else
    CL_TO = (CL_0 + CL_alpha*alphaRad + CL_F +
CL_0_F)*(SW_Exp/SW);%Aircraft Lift Coefficient with Fuselage Effect, ver-
tical tailplane effects assumed to cancel out

end

%Lift
L = rho/2*(v*sqrt(sigma_isa)+vW)^2*CL_TO*SW; %Aerodynamic Force needs EAS
to be correct
```

```
% Flap Drag increment acc. to Loftin 1980
if CL_TO < 1.1
    CD0_Flaps = 0;
else
    CD0_Flaps = 0.05*CL_TO-0.055;
end

%Total Drag Coefficient w/o Spoiler
CD0_TO = CD0+CD0_Flaps+CD0_Gear+CD_Stores+CD_Windmill+CD_Asym; %Function is
active as soon as engine fails => Windmilling Drag  included

%Spoiler activation 1.5 seconds after engine failure recognition
if t_par >= (1.5+reactiontime)
    CD_S = 1.8*sin(40*(pi/180))*S_S/SW; %acc: to Scholz and LTH BM 21 600-
01
%1.8 is the literature value flat plate, deployed 60°, => cos(60)=0.5, 1.3
is the efficiency factor for upper wing flow
    CD_TO = CD0_TO+phi*CL_TO^2/(pi*e*A)+CD_S; %Total Drag Coefficient is
increased by the Spoiler Drag
else
    CD_TO = CD0_TO+phi*CL_TO^2/(pi*e*A);
end

% Drag D
D = rho/2*(v*sqrt(sigma_isa)+vW)^2*CD_TO*SW; %Aerodynamic Force needs EAS
to be correct

%Save v1
if ((t_par >= 1) && (v1 == 0))
    v1 = v;
end

%Aquaplaning Speed Nose Wheel
vap_Nose = 9 * sqrt(Tyre_P_Nose);
vap_Nose = vap_Nose*0.514444444; %conversion to m/s

%Aquaplaning Speed Main Wheel
vap_Main = 9 * sqrt(Tyre_P_Main);
vap_Main = vap_Main*0.514444444; %conversion to m/s

%Drag reduction due to aquaplaning Nose Wheel
k_vap_Nose = 0;
if v/vap_Nose < 1
    k_vap_Nose = 1;
end
if ((v/vap_Nose > 1) && (v/vap_Nose < 1.6))
k_vap_Nose = 1 - (1/0.6) * ((v/vap_Nose)-1);
end

%Drag reduction due to aquaplaning Main Wheel
k_vap_Main = 0;
if v/vap_Main < 1
    k_vap_Main = 1;
end
if ((v/vap_Main > 1) && (v/vap_Main < 1.6))
k_vap_Main = 1 - (1/0.6) * ((v/vap_Main)-1);
end

%Rolling Friction Coefficient
%Taken from NASA TN-D2770
```

```
v_knots = v/0.514444444; %conversion from knots
if wet == 1
    mu_ground_roll = 0.0002*v_knots+0.0165;
else mu_ground_roll = 0.0002*v_knots+0.0135;
end

%Before the Brakes are set, the mu_ground is the mu_ground_roll
mu_ground = mu_ground_roll;

%When the brakes are set, a new breaking coefficient is selected

%Brakes are activated 0.5 sec after engine failure recognition
if t_par >= (0.5+reactiontime)

% Determination of the Braking Coefficient in Case of Dry Runway
%Based on Flight Test Data Maximum Break Energy Chart, 1 m/s = 3.2808 fps
v_fps = 3.2808*v; %speed in feet/second
E_break = m_lbs*(v_fps^2)/(10^9); %Energy of the Aircraft * e-9 (to match
the approximation formula)
mu_ground = -0.1992*(E_break^2) + 0.1421*E_break + 0.4852; %Approximated
Ground Friction Breaking coefficient

if mu_ground < 0.05 %cannot drop below this value (AMC-25.1591)
    mu_ground = 0.05;
end

if v<0
    mu_ground = 0.4852;
end
if mu_ground > 0.4852 %value for v=0, braking coefficient cannot rise above
that value
    mu_ground = 0.4852;
end

mu_ground_dry = mu_ground; %saving the dry braking coefficient for refer-
ence

% Case of Wet Runway

%The CS 25.109 Method is applied

if (wet == 1)
       v_knots = v/0.514444444; % v in knots
if v < 0
            mu_ground_far100 = 0.804;
            mu_ground_far200 = 0.692;
else
            mu_ground_far100 = Anti_Skid*(-
0.0437*(v_knots/100)^3+0.320*(v_knots/100)^2-0.805*(v_knots/100)+0.804);
            mu_ground_far200 = Anti_Skid*(-
0.0331*(v_knots/100)^3+0.252*(v_knots/100)^2-0.658*(v_knots/100)+0.692);

end
end



%Cross Check that the braking friction is not higher than on a dry runway
if wet ==1
```

```
mu_ground = mu_ground_far200;
if mu_ground > mu_ground_dry
    mu_ground = mu_ground_dry;
end

end
end


% Braking Friction Ff
Ff = mu_ground*(m*g*cos(gammaRad)*gear_load_factor-L)+m*g*sin(gammaRad);

%Frontal submerged area of tyre_Nose
S_Nose = beff_Nose * contDepth;

%Frontal submerged area of tyre_Main
S_Main = beff_Main * contDepth;

if stores == 0
D_store_wet = 0;
end

Dd=0;
Ds=0;
D_store_wet=0;

if wet == 1;

%Displacement Drag Nose
cD_Nose = 0.75 * k_vap_Nose; %Drag coefficient
Dd_Nose = cD_Nose * 0.5 * rhoCont * v^2 * S_Nose;

%Displacement Drag Main
cD_Main = 0.75 * k_vap_Main; %Drag coefficient
Dd_Main = cD_Main * 0.5 * rhoCont * v^2 * S_Main * 4; %4 wheels main gear

Dd = Dd_Nose + Dd_Main; %Total Displacement drag

D_dis = Dd; %Total Displacement Drag for Plotting

rho_spray = rhoCont; %[kg/m^3] (=Water density), this line allows for cor-
rection of the spray density if desired

%Spray Impingement Drag
if stores == 1
%Drag reduction due to aquaplaning Nose Wheel
        k_vap_Nose = 0;
if v/vap_Nose < 1
          k_vap_Nose = v/vap_Nose; %accounts for the spray plume rising
gradually up to max. intensity at aquaplaning speed
end
if ((v/vap_Nose > 1) && (v/vap_Nose < 1.6))
k_vap_Nose = 1 - (1/0.6) * ((v/vap_Nose)-1);
end
    VolumeFlow = v * S_Nose; %aircraft speed*frontal area tire
    MassFlow = VolumeFlow  * rho_spray;
    MassFlow = MassFlow * 0.3; %considering 30% absorption (max) of the
aircaft (stores+wingsection+gear) at exposed areas
```

```
    D_store_wet = (1-0.2)* MassFlow * v * k_vap_Nose; %restitution coeffi-
cient e=0.2, and considering the drag reduction coefficient

    Dd = Dd + D_store_wet; %adding impingement drag due to collision drag
on the stores to the displacement drag variable only for calculation

end

%Skin friction drag
cDSpray = (8 * Lwet * 0.0025) * k_vap_Nose; %Drag coefficient
Ds = cDSpray * 0.5 * rhoCont * v^2 * S_Nose;
Ds = 1 * Ds; %Nose Wheel is considered

end

% Acceleration calculated from all forces determined in this function
ydot(1) = 1/m*(T-D-Dd-Ds-Ff)-g*sin(gammaRad);

% Speed storage in ydot(2)
ydot(2) = y(1);

%Transposition for Input in the Runge-Kutta-Integration Method
ydot = ydot';

%Aircraft may not roll backwards after stopping
if v<0;
return
end

if plot_s == 1

plot (t, T, '.k', 'LineWidth',3)
if wet==1
 plot (t, Ff, '.r', 'LineWidth',3)
 plot (t, D_dis, '.m', 'LineWidth',3)
end

 plot (t, D, '.g', 'LineWidth',3)
 plot (t, L, '.c', 'LineWidth',3)

if wet==1
 plot (t, Ds, '.y', 'LineWidth',3)
 plot(t, D_store_wet,'.b', 'LineWidth',3)
end

 hold on

end
```